INFORMATION TO USERS

This manuscript has been reproduced from the microfilm master. UMI films the text directly from the original or copy submitted. Thus, some thesis and dissertation copies are in typewriter face, while others may be from any type of computer printer.

The quality of this reproduction is dependent upon the quality of the copy submitted. Broken or indistinct print, colored or poor quality illustrations and photographs, print bleedthrough, substandard margins, and improper alignment can adversely affect reproduction.

In the unlikely event that the author did not send UMI a complete manuscript and there are missing pages, these will be noted. Also, if unauthorized copyright material had to be removed, a note will indicate the deletion.

Oversize materials (e.g., maps, drawings, charts) are reproduced by sectioning the original, beginning at the upper left-hand corner and continuing from left to right in equal sections with small overlaps. Each original is also photographed in one exposure and is included in reduced form at the back of the book.

Photographs included in the original manuscript have been reproduced xerographically in this copy. Higher quality 6" x 9" black and white photographic prints are available for any photographs or illustrations appearing in this copy for an additional charge. Contact UMI directly to order.

UMI

A Bell & Howell Information Company
300 North Zeeb Road, Ann Arbor MI 48106-1346 USA
313/761-4700 800/521-0600

Université d'Ottawa · University of Ottawa

ASPECTS OF VISION-BASED SENSING AND CONTROL FOR SPACE ROBOTS

by

Michael E. Stieber

Thesis submitted to the
School of Graduate Studies and Research
in partial fulfillment of the requirements for the degree of

Doctor of Philosophy

Ottawa-Carleton Institute for Electrical Engineering
School of Information Technology and Engineering
Faculty of Engineering
University of Ottawa
Ottawa, Canada

September, 1997

ACKNOWLEDGEMENTS

It is a pleasure to acknowledge the patient guidance provided throughout this research by Dr. E. Petriu and Dr. G. Vukovich and the members of the Committee, Dr. J.-F. Rivest and Dr. R.L. Morris. The valuable comments of the examiners, Dr. D. Coll, Dr. S. Das, Dr. D. Ionescu and, in particular, Dr. J. de Lafontaine, were also highly appreciated.

The support of the Canadian Space Agency (CSA) for this research is warmly acknowledged. The following individuals at CSA, listed in alphabetical order, have helped in various ways and capacities to make this research project possible and successful: D.A. Bassett, M. Bedirian, R.G. Brown, D. Cormier, Dr. K.H. Doetsch, M. Doyon, Dr. I. Hu, D.G. Hunter, Dr. S.G. MacLean, M. McKay, Dr. J.C. Piedboef, Dr. A. Poirier, F. Terrillon, C.P. Trudel and Dr. S.K. Yeung. Their contributions, big and small, are all gratefully acknowledged. Special thanks are due to Dr. G. Vukovich (again!) for his support of the laboratory activities carried out at CSA.

For my parents

SUMMARY

The objective of this study is to advance the state-of-the-art in the control of space manipulators. In the microgravity environment of space, large robots like the Space Station Remote Manipulator System are able to manipulate enormous payloads, with masses several orders of magnitude larger than the mass of the manipulator itself. Resulting low-frequency structural oscillations give rise to dynamic stability problem when the robot is controlled by a vision system measuring the payload motion. This problem is not unique to space robotics applications but is generic for the control of structurally flexible systems when the motion is measured at a distance from the actuator controlling the motion.

This study develops analytical criteria for the selection of the number, type and location of suitable sensors for robust control of mechanical systems with flexible bodies. Sensors meeting these criteria are called "hyperstability sensors". A dynamic sensor data fusion approach is developed to integrate additional "performance sensors" such as vision-based sensors, addressing the problem of using non-collocated sensors and actuators in the active control of flexible structures. An extended hyperstability concept is developed to enable robust control of complex systems with conventional or intelligent control systems. The model-free methodology is applicable to the broad class of non-linear and time-variant system governed by Hamilton's Principle which encompasses most mechanical systems.

The new methodology is applied to a flexible link robot and experimentally validated. The tests involve the measurement and control of the end-point motion of the flexible link using a vision system and real-time image processing. The methodology is shown to be effective in the experiment, enabling robust control as expected from the theory, and relatively simple to implement. Simulations complementing the hardware tests extend the scope of the evaluation. A comparison with a Kalman-filter-based control design confirms the superior robustness properties of the proposed approach.

ASPECTS OF VISION-BASED SENSING AND CONTROL FOR SPACE ROBOTS

Table of Contents

CHAPTER 1

INTRODUCTION

Motivation

Robotic systems are playing an important role in the exploration of space. They enable planetary exploration and the construction and servicing of vehicles and platforms in space. Robotic systems increase the productivity of humans in space and reduce hazards to astronauts. As the tasks performed by space robots become more complex, the need for more human-like characteristics emerges. As with humans, the sense of sight is essential to enabling efficient interaction with the environment. More important than the sense of sight per se is the ability to process images in such a way as to enable more efficient, accurate and autonomous control of the robot.

The Mobile Servicing System (MSS) shown in Figure 1.1 is a state-of-the-art robotic system presently being developed by the Canadian Space Agency for the assembly and external maintenance of the International Space Station (ISS). The installation of an airlock on the Space Station shown in Figure 1.2 and the attachment of a truss segment shown in Figure 1.3 are typical assembly operation performed by the Space Station Remote Manipulator System (SSRMS) of the MSS.

This study is motivated by the need for very precise motion control of space robots relative to the task environment during assembly and servicing operations. The microgravity environment of orbiting platforms enables the manipulation of massive payloads by large but lightweight manipulators. The SSRMS, for example, is 17.1 m long and can move payloads up to 116,000 kg, nearly 100 times its own mass. For such systems the motion control problem is aggravated by the effects of structural flexibility of the manipulator. A high payload-to-mass ratio results in very low fundamental frequencies of oscillation, affecting the stability and efficacy of motion control and thus limiting the operational efficiency of the system.

Objectives

The overall objective of this study is to advance the state-of-the-art in precision control of space manipulators. Motivated by the development of a Space Vision System (SVS) by the Canadian Space Agency that is able to measure the position of objects on the Space Station, particular problems of vision-based sensing and automatic control for space robots are addressed in this study. Vision-based sensing of the robot payload motion leads to the non-collocation of sensing and control action on the robot which is known to introduce stability problems and performance limitations when structural oscillations are a factor.

A major goal is the development of new techniques for instrumentation design and sensor fusion enabling the robust and effective control of flexible robots. This goal encompasses both the analytical development and the experimental demonstration of new methodologies, culminating in the hardware demonstration of vision-based real-time automatic control of a robot emulating certain the dynamic characteristics of a space manipulator.

Relevance to Other Applications

Although this study is motivated by problems in space robotics, it is also relevant to terrestrial robotics and many other applications where sensing and control are key issues. The sensing technology using real-time image processing has the potential to be applied in many domains where the position and velocity of objects need to be measured or tracked in real time, e.g. vehicle guidance in warehouses, factories and hospitals etc.

Although today the structural flexibility of robots is of concern primarily in space applications, the speed and performance of terrestrial robots is also limited ultimately by flexibility effects when conventional control systems are used. Hence the sensor fusion and control techniques developed for the solution of the space robotics problem constitutes enabling technology for the future use of fast, lightweight robots in terrestrial applications.

The solutions to the structural control problem have not only applications in robotics, but also in many other domains which require high-performance control

of systems with structurally flexible or compressible elements.

- Computer hardware: Fast and precise position control for read/write heads of hard drives;
- Aircraft: Active vibration suppression in wing structures and reduced bending motions in fuselage structures;
- Road/rail vehicles and aircraft: Active cabin noise reduction;
- Large satellites: Attitude and shape control for large satellites for communications, solar power, and remote sensing applications.

Hence, this study contributes to generic sensing, instrumentation and control technologies with a broad spectrum of potential applications in a number of different domains.

Outline of the Study

This study is organized into the following Chapters:

Chapter 2 defines the objectives of the research and highlights specific unresolved problems in simple examples.

Chapter 3 provides an overview of relevant characteristics of the Space Station Remote Manipulator System (SSRMS) and an introduction to the dynamics of space robots in order to establish the formalism necessary for the description and analysis of the robot sensing and control problems. A simple analytical model of a space robot is used to illustrate some of the dynamic properties of importance to this research. This model is retained and used throughout the study as an illustrative example.

Based on this analytical background, Chapter 4 reviews the state-of-the-art in sensing and control for manipulators with flexible links and discusses the advantages and shortcomings of various known techniques.

A new approach for instrumentation and control design for flexible robots is developed in Chapter 5. The concept of hyperstability is extended by a sensor fusion process which supports the robust integration of non-collocated sensors in

structural control problems and the introduction of purposeful "active" behaviour into a "passive" approach.

Chapter 6 investigates hyperstability sensors for flexible robotic systems and establishes a set of necessary and sufficient conditions for number, type and location of hyperstability sensors.

In Chapter 7, the new concept is applied to a single link flexible robot. The process of instrumentation and sensor fusion design and implementation is illustrated on a simple example. The theory is validated by experiments and the properties of the design are evaluated against conventional alternatives by simulation.

Chapter 8 summarizes the study. The specific contributions made by this research are highlighted in Section 8.2

Six Appendices provide additional detail on mathematical derivations, the Space Vision System, simulation models, and a list of symbols.

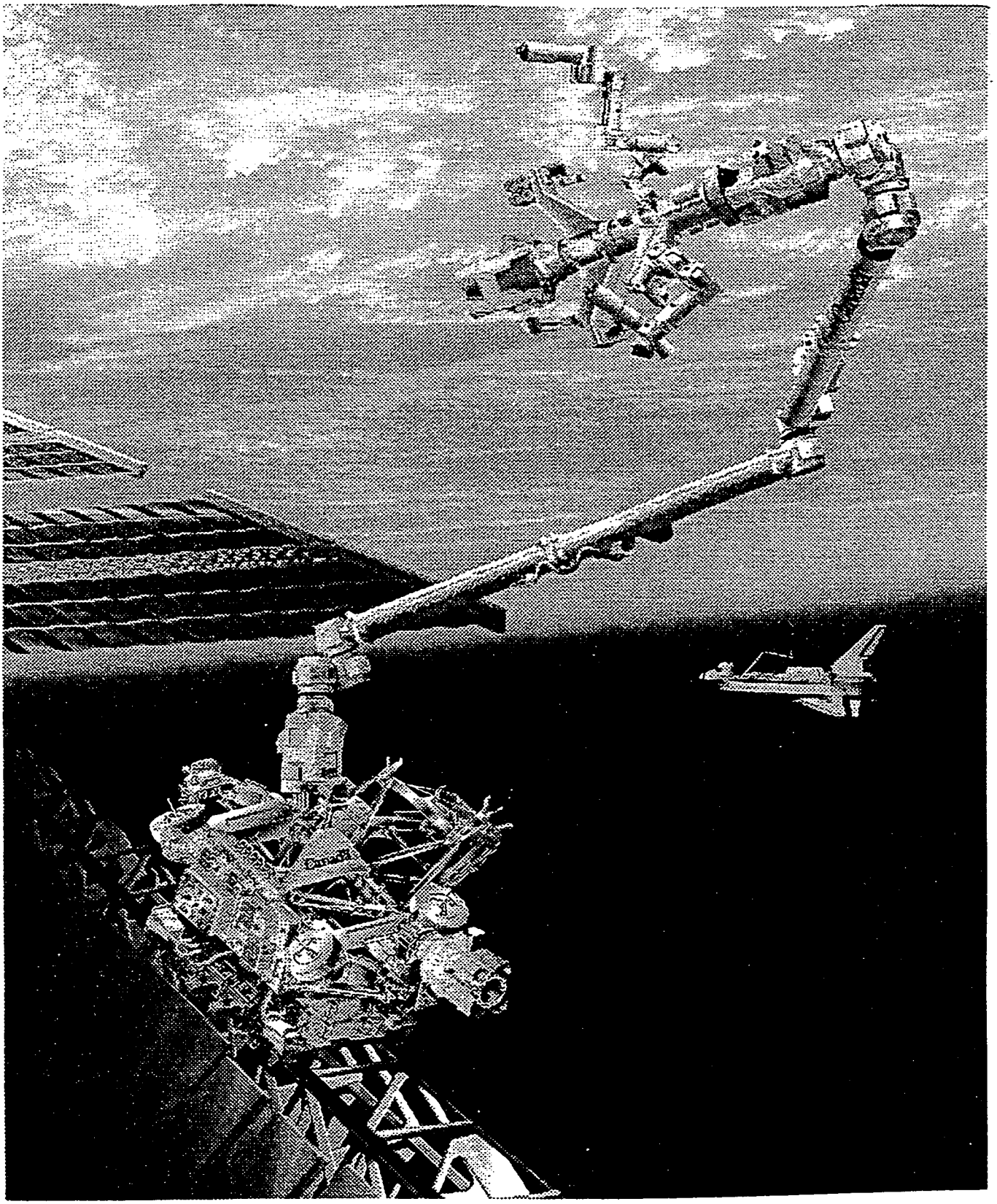

Figure 1.1: Mobile Servicing System with Space Station Remote Manipulator System (SSRMS)

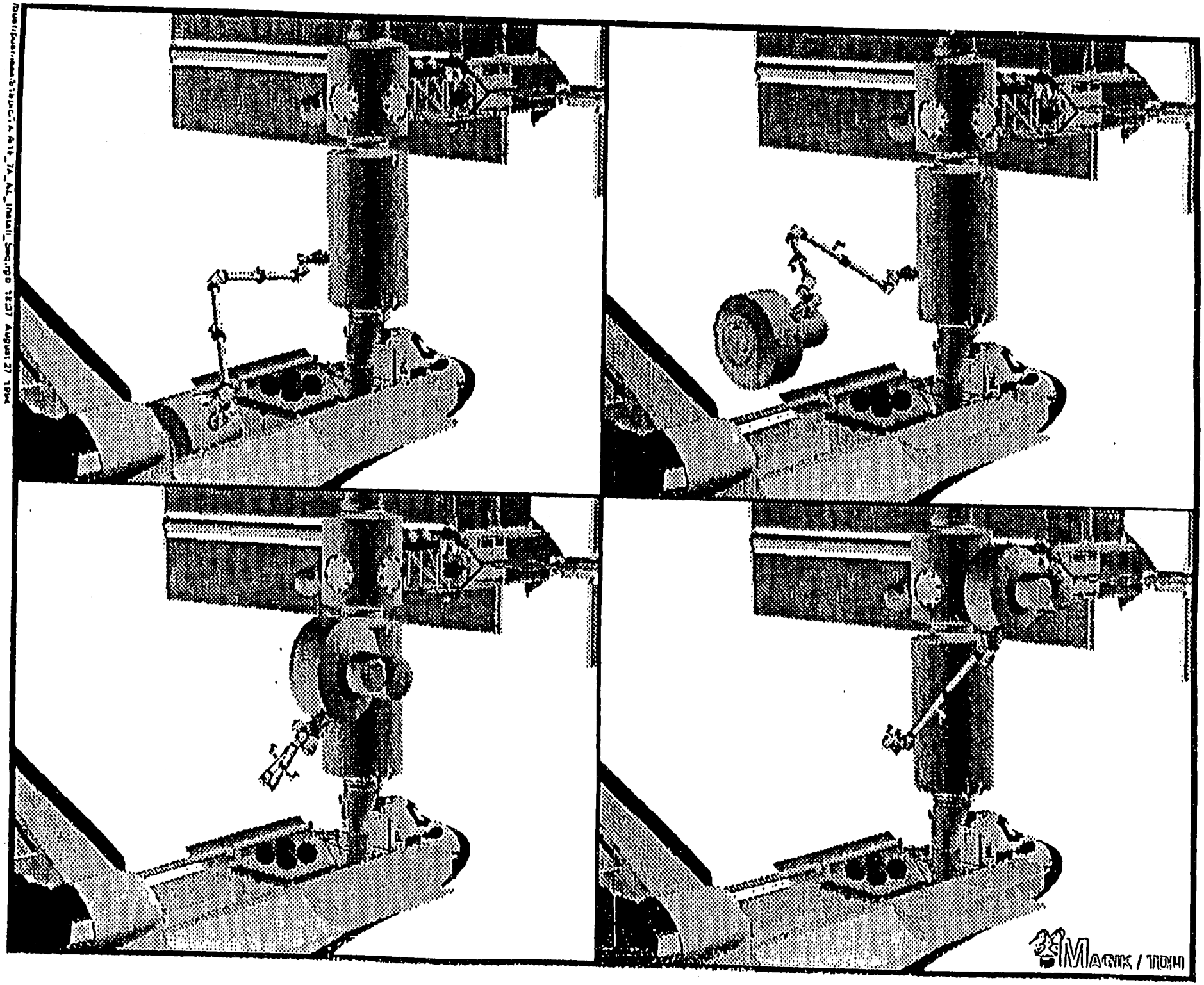

Figure 1.2: Installation of Airlock on the International Space Station by the SSRMS

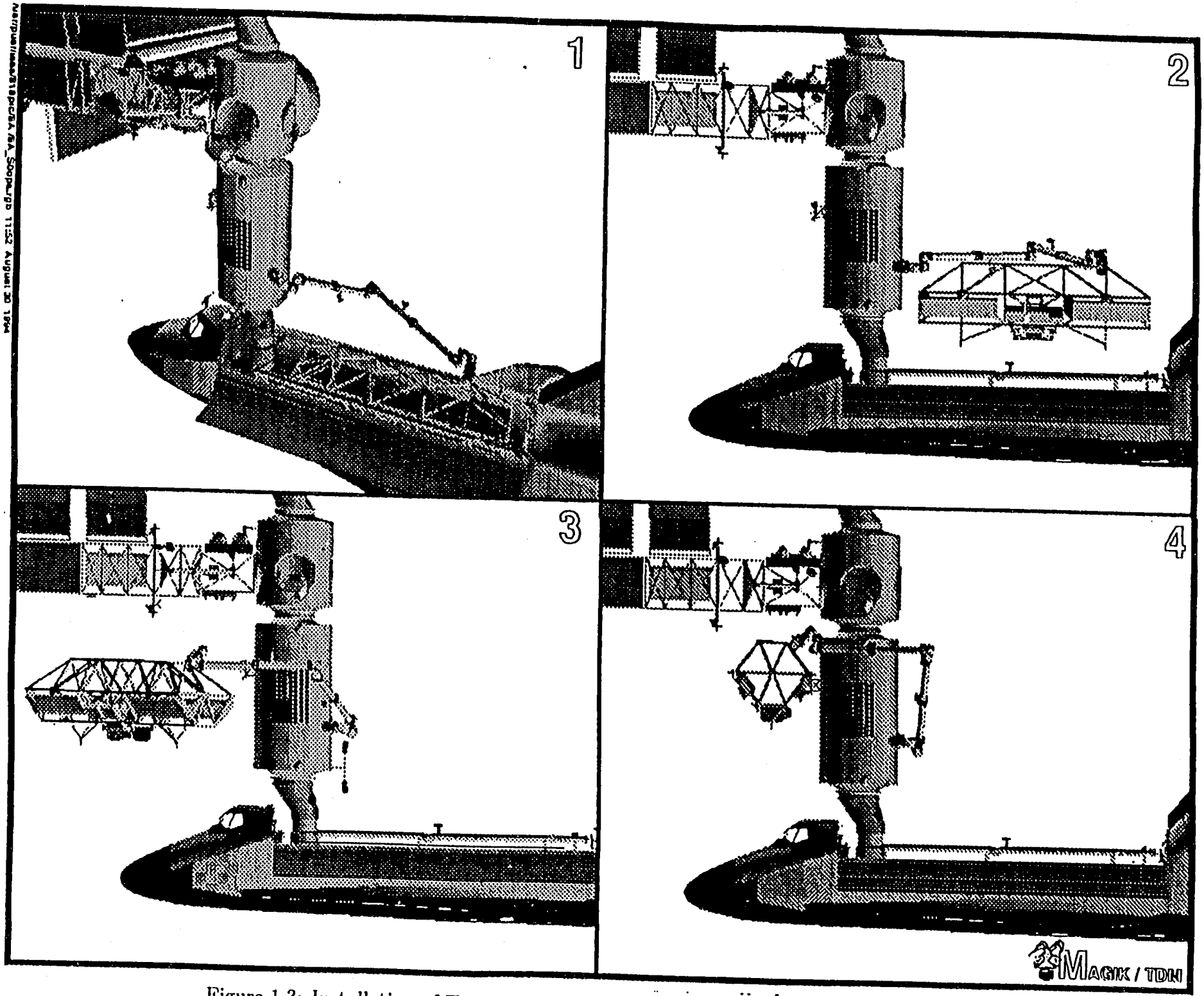

Figure 1.3: Installation of Truss Segment on the International Space Station by the SSRMS

CHAPTER 2

PROBLEM DEFINITION

2.1 Objectives

Requirements

The objective of this study is to advance the state-of-the-art in high-performance vision-based control of space manipulators. The functional requirements supporting this objective are analyzed in Table 2.1.1 based on the generic characteristics of space robotic systems. A particular and important characteristic in this context is the structural flexibility of the lightweight manipulator accentuated by large payload masses, which makes it difficult to control the motion of the payload. The following requirements for sensing, sensor fusion and control are identified in Table 2.1.1:

Sensing

- direct measurement of payload motion relative to objects in task space;
- real-time image processing to measure motion in 6 degrees of freedom;
- high sensing accuracy.

Sensor Fusion and Control

- Performance:
  - precise tracking of commanded trajectory;
  - active damping of structural vibrations.
- Stability robustness with respect to:
  - non-collocated sensors and actuators;
  - flexibility effects;
  - time-variant robot dynamics;
  - non-linear robot dynamics;
  - unknowns in robot dynamics.

Systems Approach

This study touches on all subjects identified above. The focus, though, will be on sensor selection, sensor fusion and control. The associated problems are approached from a systems perspective. Figure 2.1.1 shows a conceptual system block diagram of a generic robotic system and identifies the major functional elements and their interactions. The central element is the robot and payload, which moves in response to the forces and/or torques generated by the robot actuators. The sensors provide measurements of the motion state of the robot/payload and the state of the environment. The sensor fusion/control function provides the intelligent connection between perception and action and ensures that the payload follows some commanded trajectory.

Our focus will be on problems associated with the sensors and the sensor fusion/control function. We will consider these functions not in isolation, but in the context of the characteristics of other elements in the system such as the robot and the actuators. The choice of number, type and location of sensors and actuators, together with the dynamics of the robot, determines the "input-output behaviour" of the robot, which we define on the basis of Figure 2.1.1 to encompass everything between the actuator commands (=input) and the measurements (=output) provided by the sensors.

Key Problems

From a systems perspective, an important factor in vision-based control of space manipulators is that the location of sensors and actuators cannot be chosen arbitrarily. The actuators are located at the joints of the manipulator, and for vision-based control, the measurements made by the vision system refer to the motion of the manipulator payload.

It is well known that a flexible structure with distributed mass and stiffness is difficult to control when it is forced at one point and its response is measured at another point [Spector and Flashner]. The following specific problems arising in this situation are illustrated in Sections 2.2, 2.3 and 2.4 using a simple linear flexible link as an example:

- Non-minimum phase input-output behaviour resulting from non-collocation of sensors and actuators on a flexible structure;
- Dynamic instability resulting from non-collocation of sensors and actuators in flexible structure control systems;
- Dynamic instability due to model truncation in flexible structure control based on state estimation.

Even though these problems are quite fundamental, they are, to some degree, special cases of the wider class of problems caused by the complexity of the robot dynamic behaviour resulting in:

- Uncertainty and limitations of robot dynamic models;
- Time-variance of robot dynamic behaviour;
- Non-linearity of robot dynamic behaviour.

A full discussion of these and related problems is presented in the state-of-the-art review in Chapter 4.

Specific Objectives

Our goal is to investigate and resolve the above problems "from the sensor side" of the system. Whether or not a space robot has an input-output behaviour which enables stable robust control depends critically on the sensors chosen for the system, and how the sensor signals are processed.

In pursuit of this goal this study will:

- Develop a framework for the systematic design of an instrumentation architecture applicable to the space robotics problem;
- Develop an approach for sensor fusion and control of flexible manipulators which supports the integration of a vision system and the use of conventional or intelligent control strategies in a manner which is robust with respect to the uncertainty and complexity of the robot dynamic behaviour;
- Provide an experimental "proof-of-principle" validation for the abstract concepts.

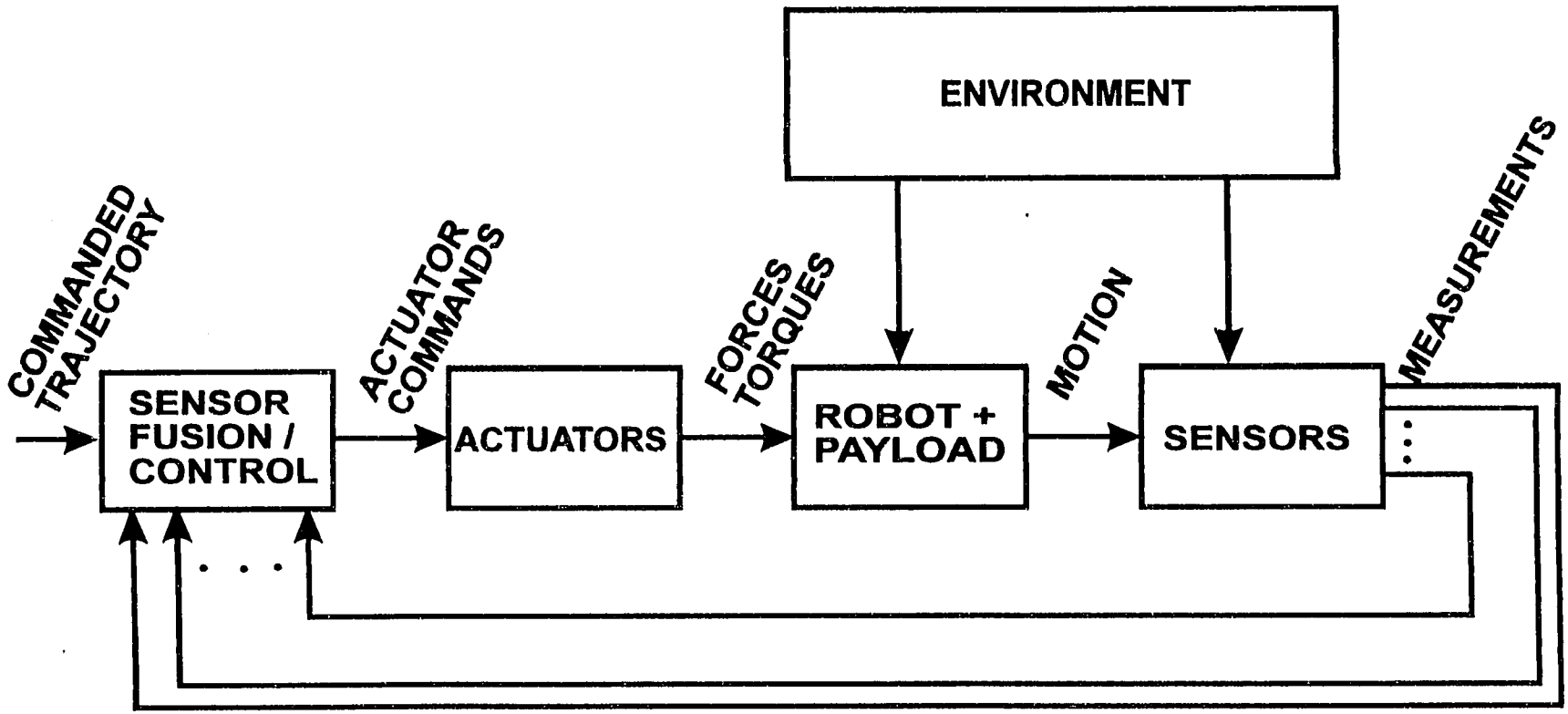

Figure 2.1.1: Functional Elements of Robotic System

Objective >>>	High-performance.....	.....vision-based control.....	...of space manipulators
Implied Characteristics	• fast response • precise positioning	• measurement of motion of manipulator tip/payload relative to objects in workspace • non-collocated sensor/ actuator configuration	• lightweight design • 6-DOF motion • significant elasticity of links and joints • huge payload range • low natural frequencies • time-variant behaviour • non-linear behaviour • dynamic model not verifiable before flight
Implied Requirements	• active control of structural vibrations • high measurement accuracy of payload position • small trajectory tracking errors • high control bandwidth	• real-time image processing to measure 6-DOF motion • robustness of control strategy w.r.t non-collocated sensors/actuators	robustness of control strategy with respect to: • flexibility effects • time-variant behaviour • non-linear behaviour • uncertainty in dynamics models

Table 2.1.1: Objectives and Requirements of the Study

2.2 Effect of Sensor Location on Robot Behaviour

Robot Model

In this and the subsequent Sections, some well known problems arising in the control of flexible structures are illustrated on a relatively simple example of a single flexible link. A complete derivation of the dynamic model used here is provided in Section 3.4 and knowledge of the modelling details and derivation is not required for the present examples. For simplicity, linearity and absence of damping are assumed in the model.

Figure 2.2.1 shows a flexible link of length ℓ with a mass attached to its tip, moving in response to torque inputs $u_T(t)$ applied at the joint located at $x_a = 0$. The motion $v(x,t)$ is defined as a circumferential coordinate dependent on the spatial coordinate along the beam, x and time t. The angular rate $y(t)$ of the link is measured at a sensor location x_s on the link:

$$y(t) = \dot{v}^{(1)}(x_s, t) \tag{2.2.1}$$

Overdots denote temporal derivatives, e.g. $\dot{v} = \frac{dv(t)}{dt}$ and spatial derivatives are denoted by: $v^{(i)} \triangleq \frac{\partial^i v(x)}{\partial x^i}$. We will now look at how changes of the sensor location affect the input-output behaviour of that simple system which can be expressed as a transfer function $G(s) \in \mathbb{C}$ in the frequency domain:

$$G(s) = \frac{Y(s)}{U_T(s)} \tag{2.2.2}$$

after applying a Laplace transformation $\mathcal{L} < \cdot >$ (Laplace operator $s \in \mathbb{C}$):

$$Y(s) = \mathcal{L} < y(t) >$$
$$U_T(s) = \mathcal{L} < u_T(t) >$$

Flexible structures are inherently systems with distributed parameters. The model of the flexible link derived in Section 3.4 is discetized by expanding the motion $v(x,t)$ into mode shape functions $\phi_i(x)$ and modal coordinates $q_i(t)$, including rigid-body modes:

$$v(x,t) = \sum_{i=1}^{n} \phi_i(x) q_i(t) \tag{2.2.3}$$

Assuming only a single angular rate sensor located at position x_s as output, the model (cf.(3.4.43), (3.4.44))reduces to:

$$\ddot{\mathbf{q}} + \mathbf{\Omega q} = \boldsymbol{\phi}^{(1)}(0) u_T \tag{2.2.4}$$

$$y = \boldsymbol{\phi}^{(1)T}(x_s)\dot{\mathbf{q}} \tag{2.2.5}$$

where $\mathbf{q}(t) = [q_1(t), q_2(t), \ldots, q_n(t)]^T$ is a vector of modal coordinates, $\mathbf{\Omega} = \text{diag}\ \{\omega_i^2\}$ is a matrix of modal frequencies, and $\boldsymbol{\phi}^{(1)}(x) = [\phi_1^{(1)}(x), \phi_2^{(1)}(x), \ldots, \phi_n^{(1)}(x)]^T$ is a vector of spatial derivatives of mode shape functions. These quantities will be defined in detail in Chapter 3.

In the frequency domain the relationship (2.2.4) – (2.2.5) between input and output results in the following transfer function $G(s)$:

$$G(s) = \sum_{i=1}^{n} \frac{\phi_i^{(1)}(x_s)\phi_i^{(1)}(0)}{s^2 + \omega_i^2} \tag{2.2.6}$$

Pole-Zero Locations

The input/output behaviour is characterized by the poles and zeros of $G(s)$ in the s-plane. Noting that the common denominator in the sum (2.2.6) is $\prod_{i=1}^{n}(s^2 + \omega_i^2)$, the pole locations s_p are obviously given by ($j = \sqrt{-1}$):

$$s_p = \pm j\omega_i, \quad \forall\, i = 1 \ldots, n.$$

Not surprisingly the poles of the system in the s-plane are on the imaginary axis at values corresponding to the modal frequencies. The effect to note is that the pole location is independent of the choice of the particular input matrix in (2.2.4) and output matrix (2.2.5).

The determination of the zeros of (2.2.6) is not quite as simple. However, it is obvious that the locations of the zeros s_0 are dependent on $\boldsymbol{\phi}(x_s)$, i.e. they are a function of the sensor location x_s. If $G(s_0) = 0$ then $G(-s_0) = 0$, i.e. the zeros appear in pairs, and if there is a zero with $\Re\{s_0\} < 0$ there will also be one with $\Re\{s_0\} > 0$ because $G(s)$ in (2.2.6) is a function of s^2 only. As [Spector and

Flashner] have shown, all zeros lie on the imaginary axis if the sensor is collocated with the actuator, i.e. $x_s = 0$. When x_s moves away from 0, some zeros move off the imaginary axis with positive and negative real parts. When the sensor is at the end of the beam ($x_s = \ell$) all zeros have moved off the imaginary axis, appearing in pairs with equal positive and negative real parts. This effect is shown in our example in Figure 2.2.2 for $n = 4$ and the sensor locations $x_s = 0$, $x_s = \frac{1}{2}\ell$, and $x_s = \ell$. These numerical results corroborate [Spector and Flashner]'s more general analysis.

Characteristics of Non-minimum Phase Systems

The significant effect here is the appearance of zeros with positive real parts indicative for non-minimum phase systems. It is well known that control of a non-minimum phase system is difficult due to the following characteristics:

(1) Linear control will shift the poles towards the zeros. Pole locations in the right-half plane indicate system instability. "Cancellation" of right half zeros by poles is not a robust procedure.

(2) Non-minimum phase systems exhibit a delayed response with a concomitant phase shift in $G(s)$. In a flexible beam, this characteristic is due to the finite propagation speed of elastic deformation waves in the beam.

(3) Modelling inaccuracies can lead to qualitative erroneous control designs by mis-modelling a non-minimum phase system with a minimum phase model.

(4) Most design approaches for adaptive, pole-placement or optimal control systems require that the plant is of minimum phase.

These unfavourable characteristics will have to be addressed by a vision-based control system for space manipulators. Although this example is quite simple it has the generic properties of more complex flexible systems.

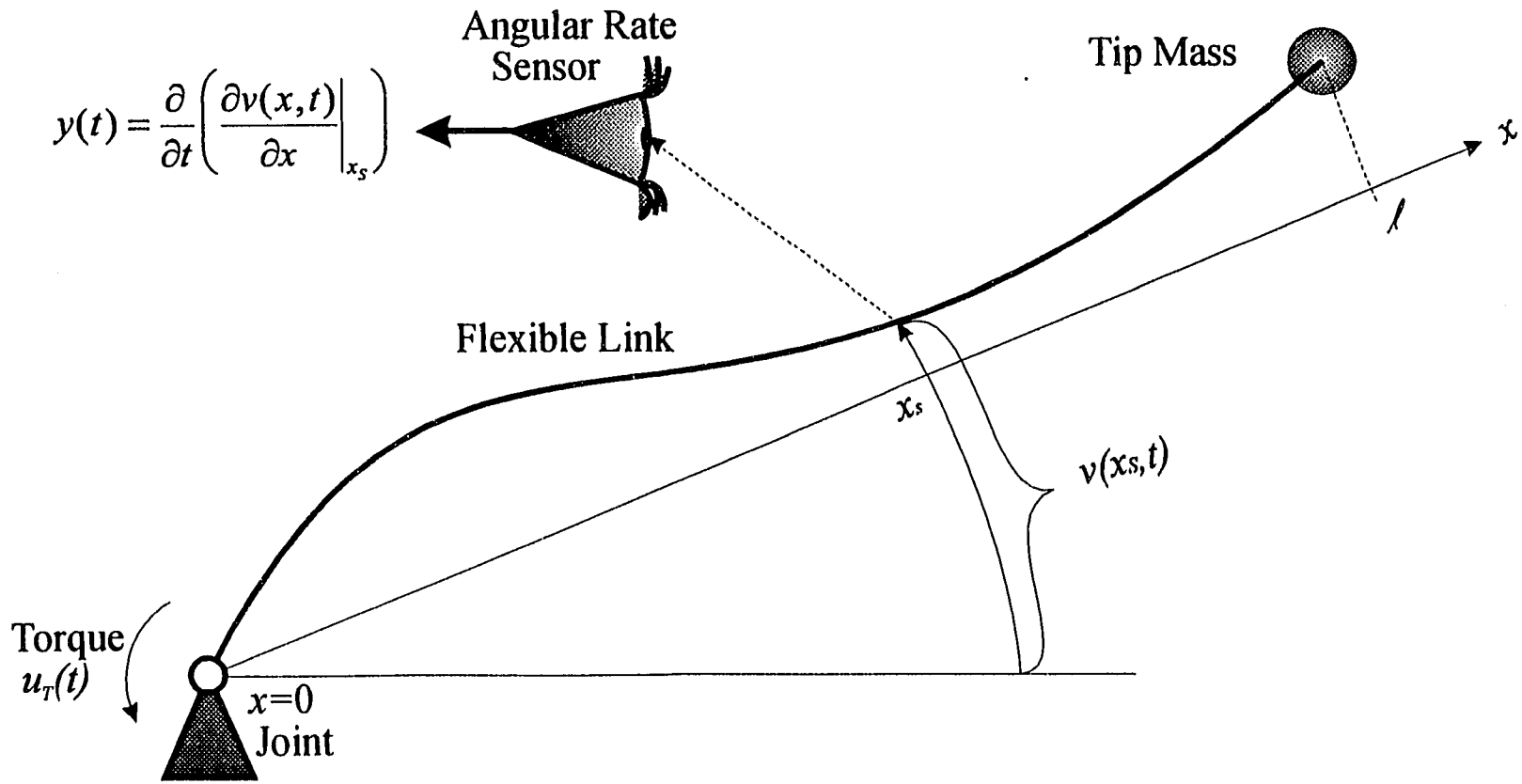

Figure 2.2.1: Flexible Link with Sensor Measuring Motion at $x=x_s$

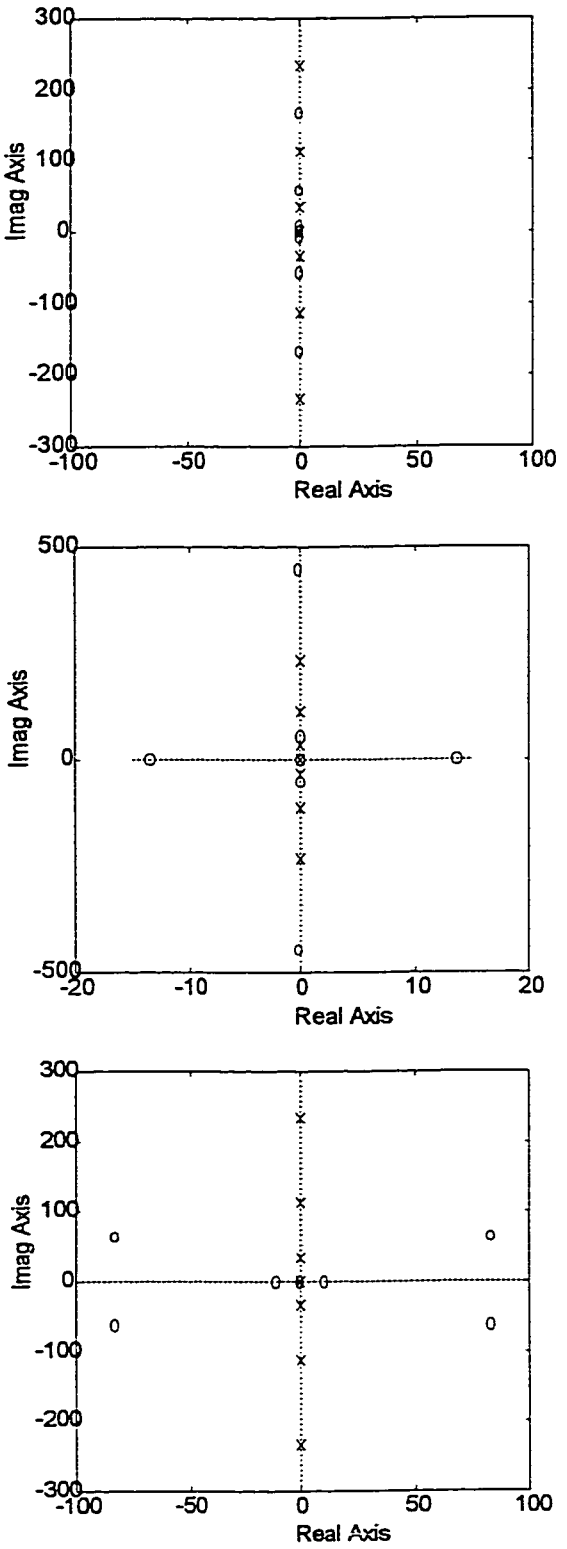

Figure 2.2.2: Poles (X) and Zeros (O) of Flexible Link Transfer Function for Sensor Locations x_S=0 (Top), x_S=$\frac{1}{2}$ (Center) and x_S=1 (Bottom)

2.3 Effect of Sensor Location on Dynamic Stability

Dynamics and Control

We will now investigate the effect of the sensor location on the closed-loop stability of the flexible link controlled by simple output feedback. We use essentially the same flexible link model as before, with the slight generalization of allowing the torque to be applied at a variable location x_a as shown in Figure 2.3.1. The resulting equations of motion are very similar to (2.2.4) and (2.2.5):

$$\ddot{\mathbf{q}} + \mathbf{\Omega q} = \boldsymbol{\phi}^{(1)}(x_a) u_T \tag{2.3.1}$$

$$y = \boldsymbol{\phi}^{(1)T}(x_s)\dot{\mathbf{q}} \tag{2.3.2}$$

These equations describe the transverse flexible motion of a slender beam for all boundary conditions. For greater simplicity of the following analysis we consider only flexible-body modes (i.e. $\omega_i \neq 0$) and make the mild assumption that x_a and x_s are always chosen such that $\phi_i^{(1)}(x_a) \neq 0$ and $\phi_i^{(1)}(x_s) \neq 0 \; \forall i = 1 \ldots n$ to ensure controllability and observability of the system as per the conditions given by [de Lafontaine and Stieber]. Figure 2.3.1 depicts the system with the "direct velocity" feedback control law with a scalar feedback gain constant F:

$$u = -Fy \tag{2.3.3}$$

Stability

If we consider only a single flexible mode i of the closed-loop system (2.3.1)-(2.3.3), its dynamics are governed by

$$\ddot{q}_i + \omega_i^2 q_i = -\phi_i^{(1)}(x_a) F \phi_i^{(1)}(x_s) \dot{q}_i \tag{2.3.4}$$

A stability condition for the single-mode system can be readily established by the Routh-Hurwitz criterion [Hahn]:

$$F\phi_i^{(1)}(x_a)\phi_i^{(1)}(x_s) > 0 \tag{2.3.5}$$

If the function $\phi_i^{(1)}(x)$ is known and x_a and x_s are fixed, this condition can always be fulfilled by choosing the 'right' sign for F. When the sensor is collocated with

the actuator, i.e. $x_s = x_a$, condition (2.3.5) is always met by choosing $F > 0$, independent of the value of $\phi_i^{(1)}(x_a)$. The function $\phi_i^{(1)}(x)$ does not need to be known in this case.

If we consider n modes in the system (2.3.1), (2.3.2), its stability can be determined using the Lyapunov function [Lasalle and Lefschetz]

$$V(t) = \frac{1}{2}\dot{\mathbf{q}}^T\dot{\mathbf{q}} + \frac{1}{2}\mathbf{q}^T\mathbf{\Omega}\mathbf{q} \geq 0. \tag{2.3.6}$$

With the feedback term (2.3.3) the derivative $\dot{V}$ can be expressed as follows:

$$\dot{V} = \dot{\mathbf{q}}^T(\ddot{\mathbf{q}} + \mathbf{\Omega}\mathbf{q}) = -\dot{\mathbf{q}}^T\boldsymbol{\phi}^{(1)}(x_a)F\boldsymbol{\phi}^{(1)T}(x_s)\dot{\mathbf{q}} \tag{2.3.7}$$

Stability of the system requires $\dot{V} < 0 \forall t$ [Lasalle and Lefschetz] which is assured if the following matrix is positive definite [Stieber, Vukovich and Petriu]:

$$F\boldsymbol{\phi}^{(1)}(x_a)\boldsymbol{\phi}^{(1)T}(x_s) > \mathbf{0} \tag{2.3.8}$$

This condition requires that all principal minors of the matrix are positive definite, which is equivalent to meeting condition (2.3.5) simultaneously for all modes $i = 1 \ldots n$, with a single scalar gain factor F:

$$F\phi_i^{(1)}(x_a)\phi_i^{(1)}(x_s) > 0 \quad \forall\, i = 1 \ldots n \tag{2.3.9}$$

Interpretation of Stability Conditions

If sensor and actuator are collocated, i.e. $x_s = x_a$, condition (2.3.9) is obviously met with $F > 0$. It is remarkable that, in this case, the stability of the closed-loop system is guaranteed for any set of system parameters $\mathbf{\Omega}, \boldsymbol{\phi}(x)$ which are a function of the mass and stiffness distribution of the flexible link. We can conclude that the control (2.3.3) is robust with respect to unknowns and variations of the mass and stiffness characteristics of the system. This is indicative of the advantages afforded by sensor/actuator collocation on flexible structures. For $x_s = x_a$ the input-output behaviour of the system (2.3.1), (2.3.2) can be shown to be "hyperstable" (as defined in Section 5.2). As discussed in later Chapters,

a system with this property can be stabilized by "asymptotically hyperstable" feedback such as (2.3.3) in our example.

On the other hand, if $x_s \neq x_a$, the n simultaneous conditions (2.3.9) can only be met in small regions along the beam, which shrink as n increases, and they vanish in the limit $n \rightarrow \infty$. (This is shown mathematically for a similar condition in Appendix A.4). Figure 2.3.2 shows these regions for a flexible beam with pinned-pinned boundary conditions and $n = 3$. The diagram indicates that if the actuation is applied at $x_a = 0$, the sensor location must meet the condition $x_s < \frac{1}{6}\ell$ to maintain stability. Obviously, for vision-based control of space manipulators which implies $x_s = \ell$, this condition is not met. It is interesting to note that for an actuator located at $\frac{1}{6}\ell < x_a < \frac{1}{4}\ell$ two ranges of sensor locations are admissible as indicated by the identical shading of the corresponding squares: $\frac{1}{6}\ell < x_s < \frac{1}{4}\ell$ and $\frac{1}{2}\ell < x_s < \frac{3}{4}\ell$. For a sensor in the first range, condition (2.3.9) requires $F > 0$ while for a sensor in the second range choice $F < 0$ is required.

For a flexible link with pinned-free boundaries the condition (2.3.9) can be evaluated by inspecting the first few mode shape functions of our simple model which are plotted in Table 3.4.1, including the rigid-body mode ($i = 1$). The diagrams show that condition (2.3.9) cannot be met simultaneously by mode 1 and 2 or modes 2 and 3. Hence we can conclude from this simple example that, indeed, robust stabilization can be assured when sensors and actuators are collocated, but falls apart for non-collocated sensors and actuators as required for vision-based control, even when we consider a very simple system model with only a single flexible mode. This example demonstrates one of the fundamental problems to be addressed in this research.

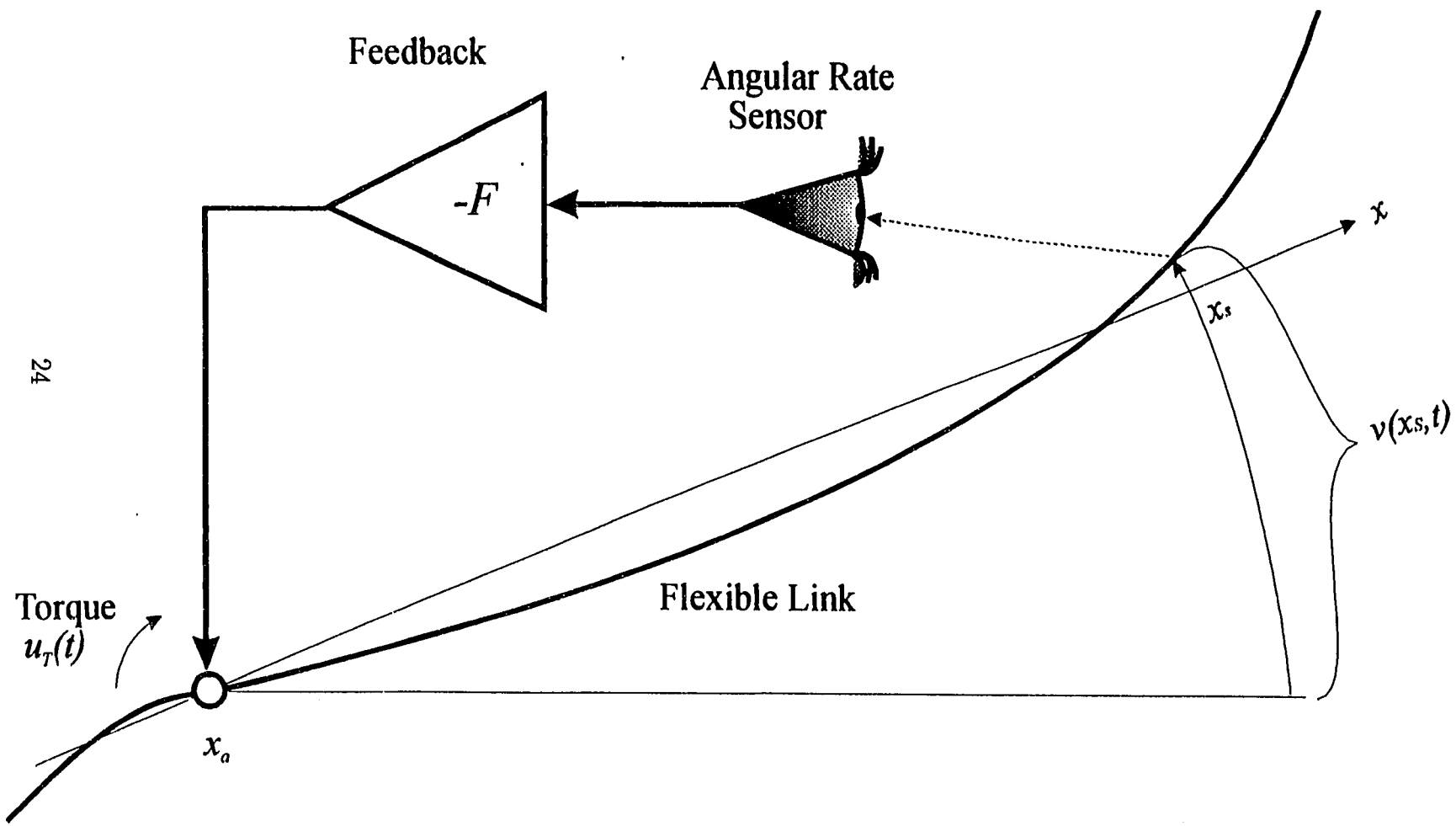

Figure 2.3.1: Flexible Beam with Non-collocated Feedback

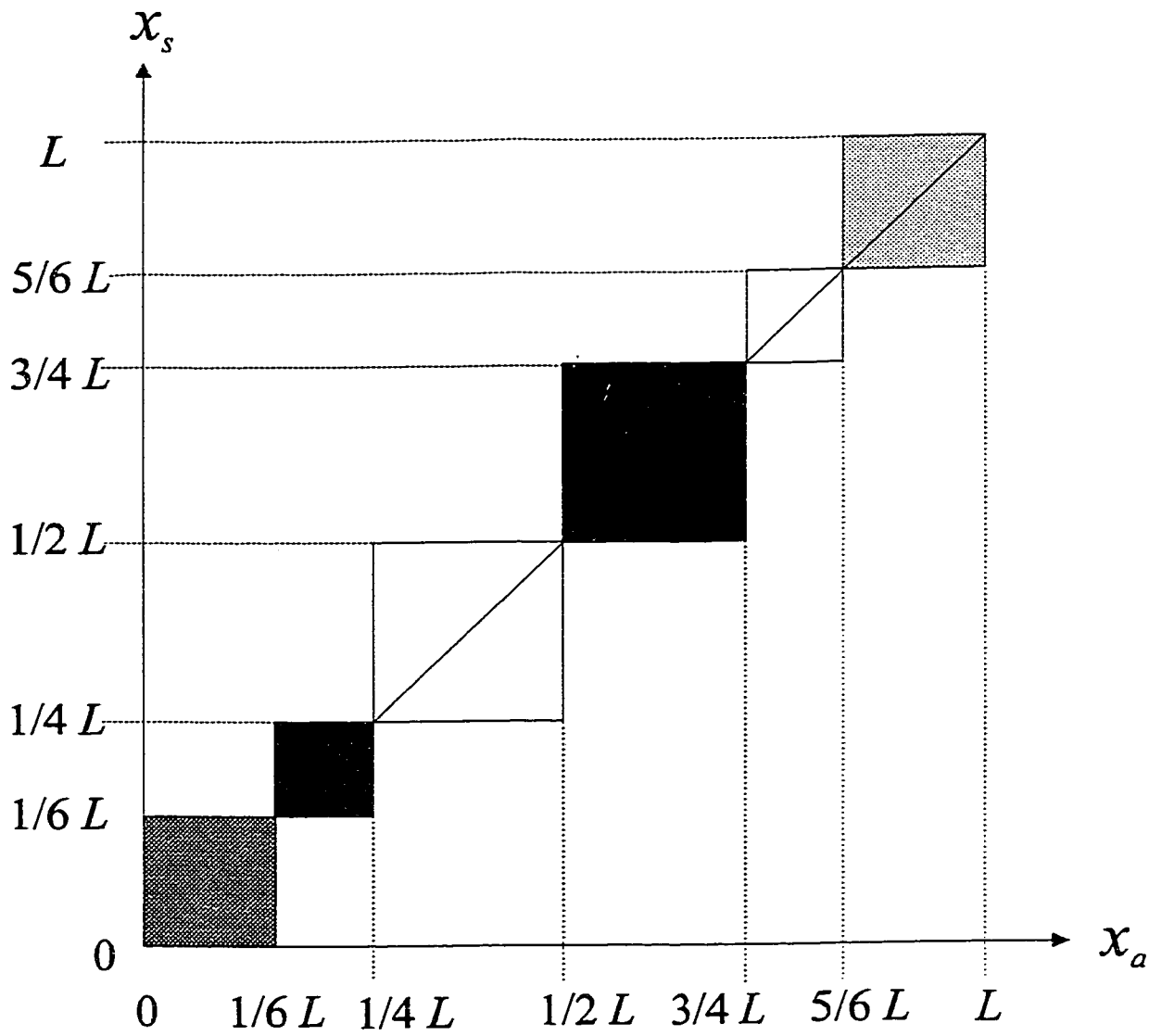

Figure 2.3.2: Admissible Sensor Locations x_S as a Function of Actuator Location x_a on Flexible Beam for 3 Flexible Modes with Pinned-Pinned Boundary Conditions and scalar Feedback of the Form of Eq. (2.3.3)

2.4 Truncation and Spillover

Truncation and Spillover in Model-based Control Systems

The destabilizing effect of sensor non-collocation just highlighted above can, in principle, be overcome by a model-based feedback control system which dynamically estimates the internal state of the flexible link based on the time history of the sensory data. The state estimation is based on a model of the link dynamics including its flexibility effects. However, the very characteristics of systems with significant structural flexibility give rise to a fundamental problem in applying this approach to flexible structures.

While flexible structures are systems with distributed parameters in nature, dynamic models used for state estimation are necessarily based on some form of discretization with a finite and fixed the number of modes, n. The control inputs u_T excite unmodelled residual dynamics in the structure by so-called "control spillover", and the measurements provided by the motion sensors include contributions from unmodelled modes, a phenomenon called "observation spillover". The combination of control and observation spillover can destabilize closed-loop feedback control systems for which the separation principle of control and observation no longer holds due to the model truncation.

Illustration of Truncation and Spillover Effect

The spillover problem can be illustrated by simulation of a flexible link with model-based end-point feedback. To illustrate the effect a model-based feedback control system as shown in Figure 2.4.1 is designed on the basis of the model (2.2.4) –(2.2.5) with the rigid-body mode and one flexible mode ($n = 2$ in (2.2.3) and $x_s = \ell$ in (2.2.5)). The feedback system performs very well when applied to the nominal system model. Figure 2.4.2 shows the tip motion and torque when the system returns to its equilibrium position from an initial tip position of 1 m. When a second unmodelled flexible mode is introduced into the system, tough, it is destabilized by spillover, as evident from the response shown in Figure 2.4.3.

The detailed assumptions, parameters and models used for the simulation are discussed in Section 7.6 and documented in Appendix E. The model-based

control and estimation approach and the destabilizing mechanism of spillover will be discussed in a mathematical framework in Section 4.3. Like the non-collocation problem, the spillover problem is very fundamental to model-based control of flexible structures and has been the subject of intensive research efforts for some time.

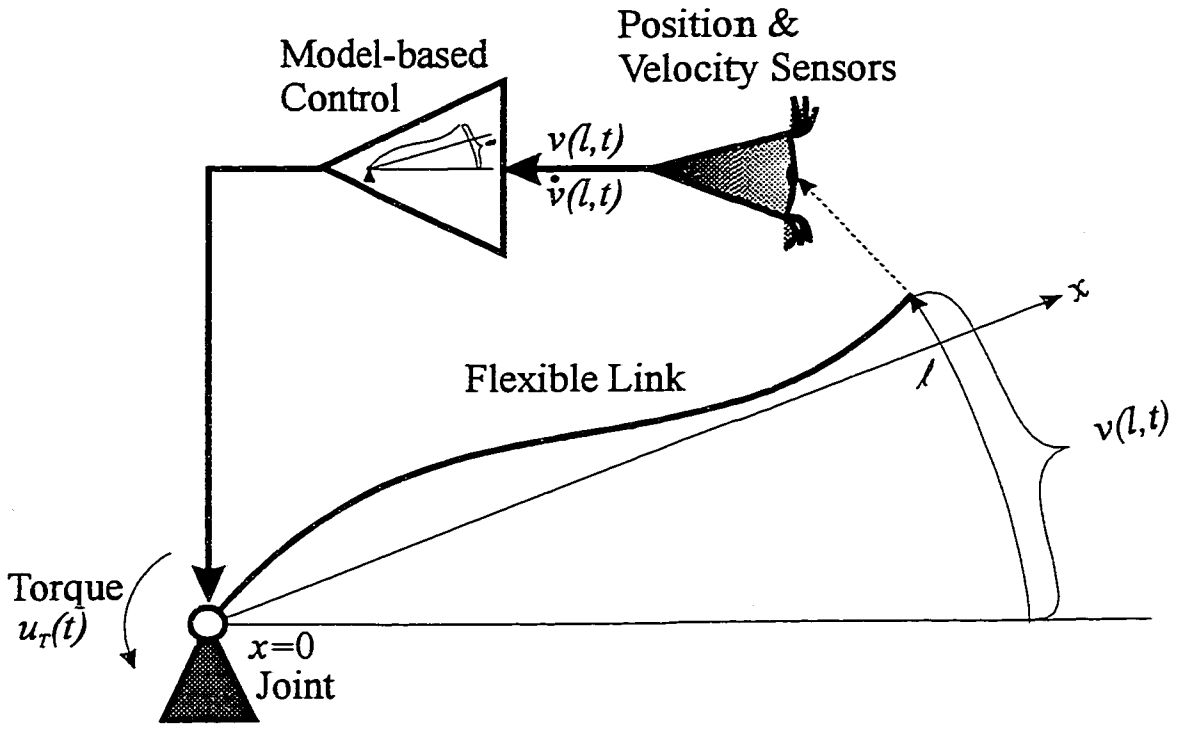

Figure 2.4.1: Flexible Link with Model-Based End-Point Feedback

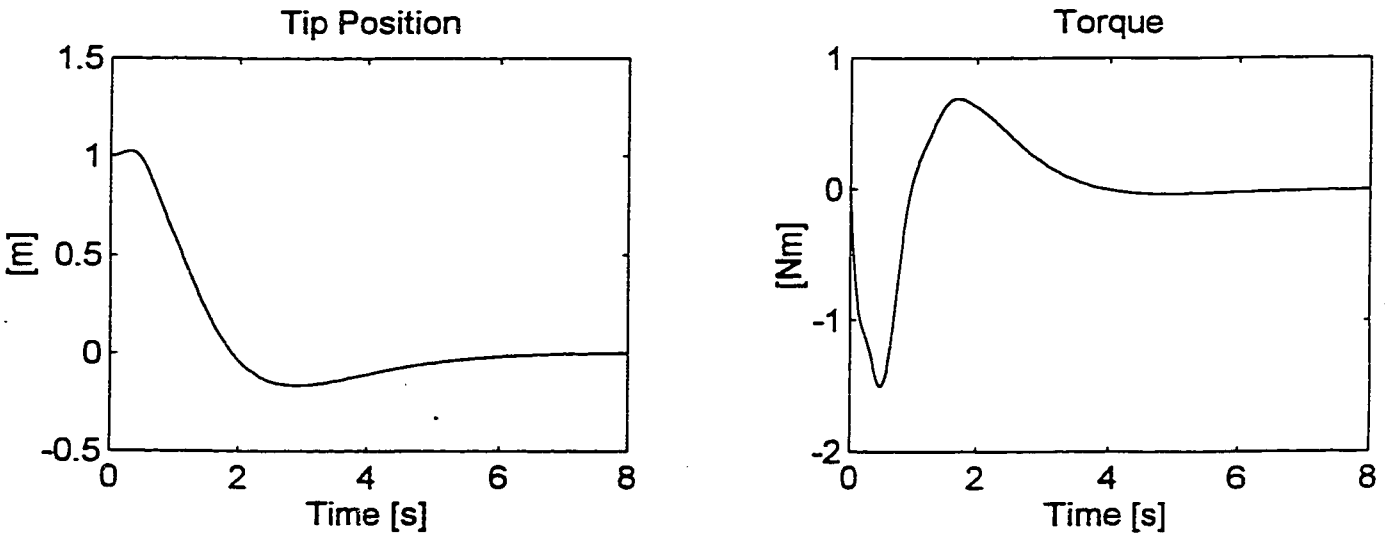

Figure 2.4.2: Stable Response with Nominal Model for Flexible Link

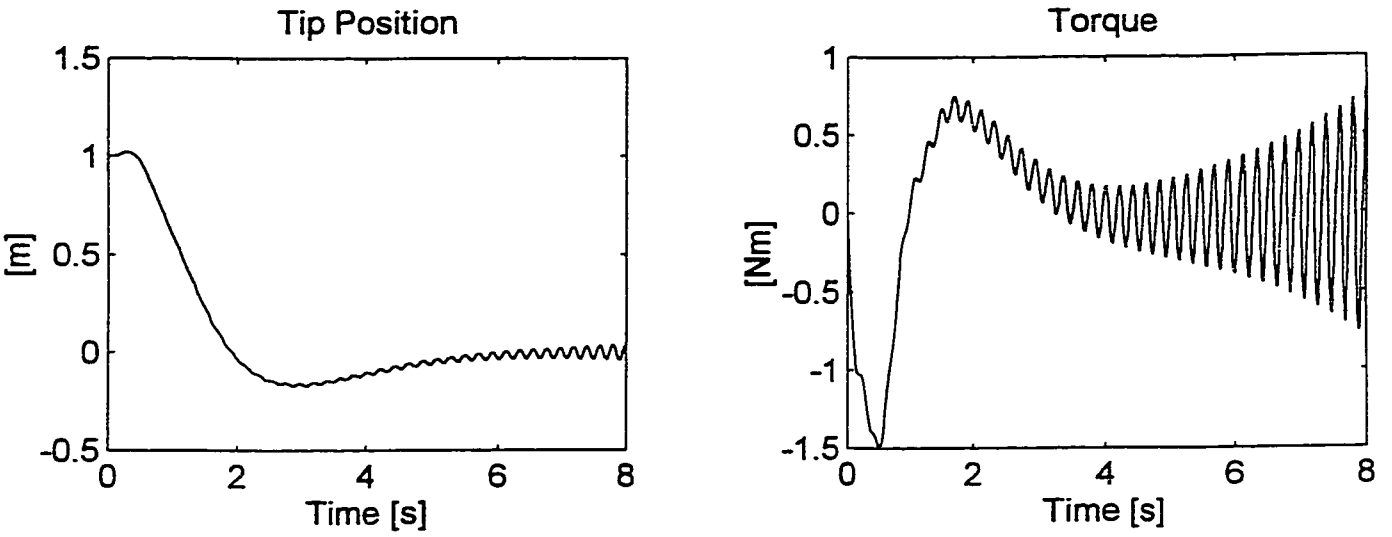

Figure 2.4.3: Instability due to Spillover from Unmodelled Flexible Mode in Link

CHAPTER 3

CHARACTERISTICS OF SPACE ROBOTS

3.1 The Space Station Remote Manipulator System

Mission

The SSRMS shown in Figure 3.1.1 is scheduled for launch to the International Space Station in 1999. It is a major element of the Canadian contribution to this international effort and represents the state-of-the-art in large space robots. Its main mission is the in-orbit assembly of the Space Station. As discussed by [Stieber, Trudel and Hunter], it will also support dexterous robotics operations on the Space Station by positioning the Special Purpose Dexterous Manipulator (SPDM) at its worksite. The success of the SSRMS mission is of critical importance for the entire Space Station.

Design

As shown in Figure 3.1.1, the SSRMS is a 7-joint symmetrical manipulator approximately 17.1 metres in length when fully extended. A symmetrical arrangement of joints and a Latching End-Effector (LEE) at each end allows either end to attach to payloads, or to serve as a base for the SSRMS providing that an appropriate Power Data Grapple Fixture (PDGF) interface is available. Power, data and video may be passed through the SSRMS to operate the SPDM while attached to the SSRMS LEE or to support the keep-alive power, telemetry and command requirements of payloads attached to the LEE. Four video cameras are mounted on the SSRMS, one fixed camera at each end effector, and one with a pan and tilt unit on either side of the elbow joint on the main booms. A light is provided with each of the cameras. Although the majority of SSRMS operations will be performed from the Mobile Base System (MBS), the symmetrical arrangement of joints and LEEs gives the SSRMS a self-relocating capability. PDGFs mounted at strategic locations on the Space Station allow the SSRMS to step from one PDGF to another to access areas which cannot be reached when operating from the MBS. The 7 joints of the SSRMS are arranged in clusters of three joints near each end

of the manipulator to act as a "wrist" and "shoulder" respectively, with an additional joint at the midpoint "elbow" position. Starting from either end, the joint sequence is roll, yaw, pitch, pitch, pitch, yaw, roll. All joints are identical and have a range of travel of +/-270 degrees. Because the number of joints exceeds the 6 degrees-of-freedom in which the manipulator tip is being controlled, the manipulator is kinematically redundant. The kinematic redundancy increases the operational flexibility and is used to avoid kinematically singular configurations.

Operational Characteristics

Operations using the SSRMS involve the handling and positioning of a wide range of payloads with varying shapes and mass properties. The payloads which can be handled by the SSRMS range from zero (i.e., no payload) up to 116,000 kg, which is representative of a fully loaded Shuttle Orbiter. The ability to stop the SSRMS and its attached payload within a known distance when the manipulator is commanded to stop, or when an emergency stop is initiated, is of crucial importance to avoiding damage to the SSRMS or other equipment. The stopping distance/angle requirements of the manipulator tip and payload set the maximum manoeuvring rate requirements for various payload sizes and influence the sizing of joint actuators, drive trains, emergency braking devices, etc. By manoeuvring within the maximum rate, stopping can always be guaranteed within the specified distance (usually 0.3 m) even in the event of failures. Assembly and berthing operations require accurate positioning of payloads within the capture range of berthing mechanisms. The positioning accuracy of the SSRMS based on joint angle measurements is specified as 4.5 cm/0.7 deg at the tip relative to the base of the arm. The resolution of motion capability is better than 1 cm and 0.1 deg. Significant improvement of the positioning capability is therefore possible if good visual cues or information on the payload position are available to the operator. Further improvement of positioning accuracies and the automation of operations could be achieved by automatic vision-based control of the SSRMS based on the methodology developed in this study.

Control

The MSS manipulators are controlled from a Robotics Work Station (RWS) in the pressurized Space Station environment. A capability to control the MSS from a ground-based command source through a radio link is discussed by [Bassett, Wojcik, Zaguli and Stieber]. An important element of the RWS is the Artificial Vision Unit (AVU) which provides the capability of photogrammetric image processing of camera images from any of the MSS or Space Station cameras. The AVU will provide precise measurements of the relative motion of the SSRMS payload with respect to objects in the workspace to the MSS operator in the form of graphical and textual displays. This will enable precision assembly operations on the station in the absence of 'boresight' camera views, as discussed by [MacLean and Pinkney]. The AVU provides a key capability for the implementation of automatic vision-based control of the SSRMS based on this research.

The various control modes and features for the SSRMS are described by [Trudel, Hunter and Stieber]. Motion commands to the manipulators can be resolved-motion commands or joint-by-joint commands. In resolved-motion operation, translational and rotational velocity inputs from an operator or automation software provide commands in a selected Point-of-Resolution (POR) reference frame. The origin of the POR frame is typically chosen to be the arm tip or a point of interest on a payload or tool. Inverse kinematic equations in the arm control software resolve the POR commands into individual joint commands to the joint servos. Although resolved motion operation is the primary means of controlling the manipulators, joint-by-joint operation is an option in both human-in-the-loop and automatic modes. For joint-by-joint operation, commands in the individual joint axes are input directly to the joints. Because of the kinematic redundancy of the 7-joint manipulators, the inverse kinematics equations (3.3.4) in the control laws have a multiplicity of solutions resulting in an unspecified degree of freedom in the arm configuration for a specific tip position and orientation. This problem is handled in the control laws by providing an option to apply an additional constraint to control one of the joints (usually a shoulder joint) to a constant position unless it is required to move in order to avoid a kinematic singularity.

Dynamic Characteristics of the SSRMS

The dynamic behaviour of the SSRMS can be completely described by equations of motion in the form of (3.2.15) discussed in Section 3.2. The derivation of a model based on the Newton-Euler formulation was performed by [Sincarsin and Hughes], [Sincarsin, D'Eleuterio and Hughes], [Hughes and Sincarsin] and [D'Eleuterio.1]. A very detailed dynamics model based on those equations has been implemented by [Spar] in a simulation used for the Space Station program.

The SSRMS has several nonlinear characteristics which are significant for the control system design and the operation of the SSRMS. Friction and stiction effects in the joints are important in various operational scenarios, and ultimately limit the achievable resolution of the tip motion. Backlash in the planetary gear boxes can be more important in space than on the ground due to the absence of a gravity bias and the resulting undetermined joint position within the backlash region. Due to the high gear ratio of 1878 in the SSRMS joints the backlash region on the motor side of the gearbox is significant, even with precision machining of the gears. Due to the large payload size, second-order dynamic effects cannot always be neglected in the analysis of space manipulators like the SSRMS. The damping ratio for oscillations in space manipulators is dependent on payload mass and other factors, and is hard to predict with any accuracy. A damping ratio of 3% has been measured in flight experiments with the Space Shuttle Remote Manipulator System. The SSRMS is expected to display similar damping characteristics.

The overall dynamic characteristics of the SSRMS change significantly with changes in payload and changes of the elbow joint angle which dramatically affects the moment of inertia seen by the shoulder joint. Given the variability of payload size and manipulator configuration, the complex SSRMS dynamics model developed by [Spar] predicts a first natural frequency of the manipulator system in the range from 0.008 Hz to 0.2 Hz. We can conclude from this review of the actual characteristics of a space manipulator that the dynamic characteristics are highly time-variant and that low-frequency oscillations are a significant factor.

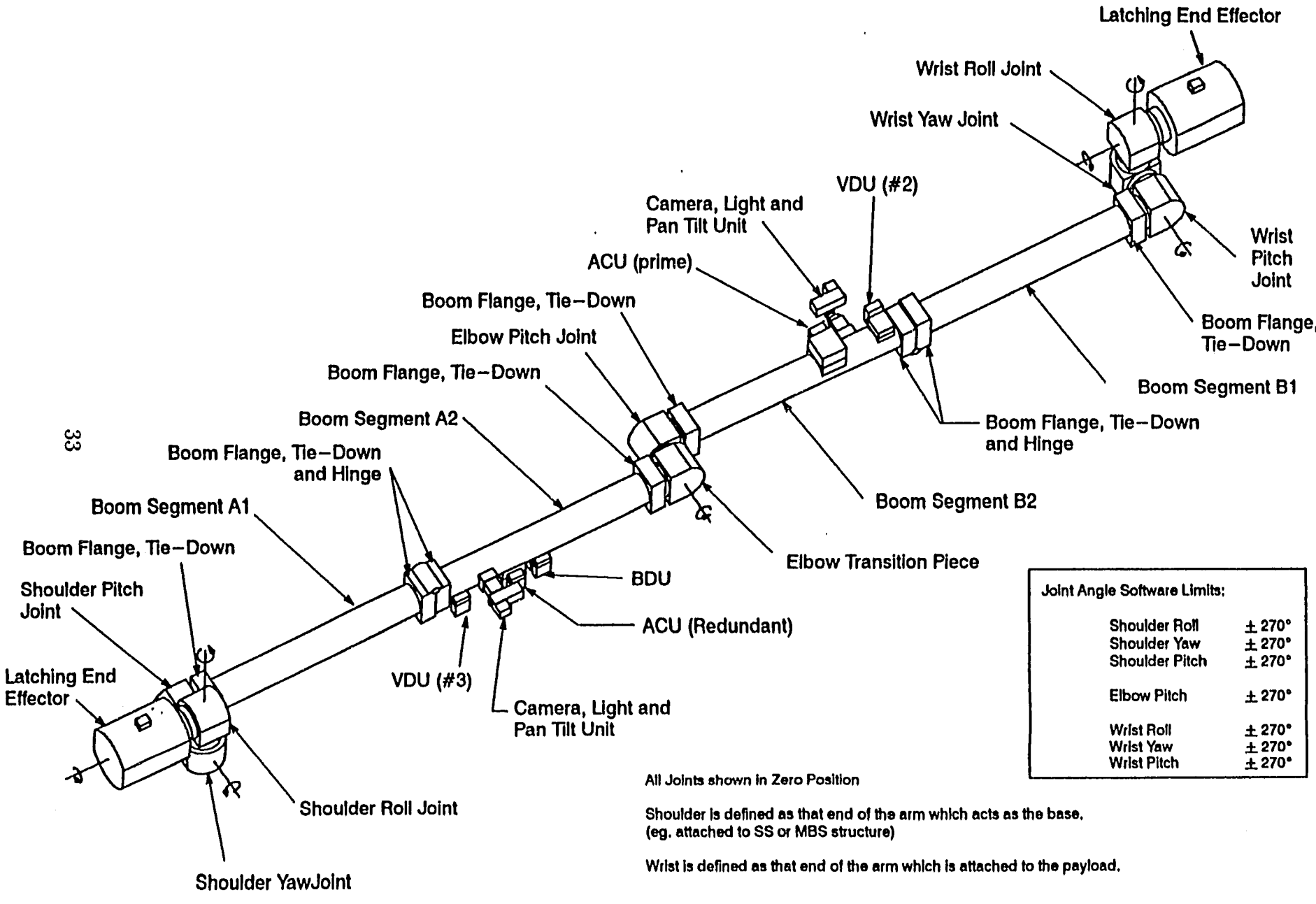

Figure 3.1.1 Space Station Remote Manipulator System (SSRMS)

3.2 Dynamics of Robotic Systems

Motion of Multibody Systems

A necessary first step in a discussion of measurement and control of the motion of a robot is to establish a notation and description for the robot motion in precise terms.

Robotic systems are generally composed of a number of bodies connected to each other and to their environment by various mechanisms which constrain their motion, as shown conceptually in Figure 3.2.1. The number of bodies in motion and the topology of their interconnection may change during the course of a robotic operation. During the assembly operation shown in Figure 1.2 for example, the topology changes from an 'open chain' to a 'closed chain' as the airlock is attached to the Space Station.

It is well-known from classical mechanics that the motions of a multi-body system evolve in a manner consistent with the principles of least action described by [Lanczos], [Meirovitch] and [Goldstein]. Hamilton's extended principle is based on the total kinetic energy in the system, $T(t) \in \mathbb{R}$, and the work done by forces between the bodies of the system and at the boundary of the system, $W(t) \in \mathbb{R}$:

$$\int_{t_1}^{t_2} (\delta T + \delta W) dt = 0 \tag{3.2.1}$$

(The operator δ denotes variation.) This variational principle states that the actual motion of a system renders the value of the integral stationary with respect to all possible neighbouring paths that the systems may be imagined to take between any two instants t_1 and t_2, provided the initial and final configurations of the system are prescribed. The stationary value is actually a minimum. Hamilton's principle does not depend on the coordinates used to describe the motion of the system [Lanczos].

The motion of a multi-body system can be described by a set of generalized coordinates which we denote $q_1, q_2, \ldots, q_n$. A set of generalized coordinates contains the minimum number of coordinates necessary to describe the motion of a

system and can be combined to a vector $\mathbf{q} \in \mathbb{R}^n$:

$$\mathbf{q}(t) = [q_1(t), q_2(t), \ldots, q_n(t)]^T.$$

The generalized coordinates are a function of time. They are not necessarily Cartesian. Their number corresponds to the degrees of freedom of a system, including those associated with the deformation of elastic bodies.

Lagrange's Equation

A system is called *holonomic* if all the constraints on the motion of the bodies introduced e.g. by joints or other interconnections, can be expressed as functions $\mathcal{F}$ only of $\mathbf{q}$ (i.e. not of $\dot{\mathbf{q}}$) of the form $\mathcal{F}(\mathbf{q}, t) = 0$. In the context of space manipulators it is not restrictive to assume that all constraints are holonomic, in which case the generalized coordinates q_i are all independent. Then Lagrange's equation which governs the motion $\mathbf{q}(t)$ of the system can be derived from Hamilton's principle by integration by parts, as shown by [Meirovitch], yielding:

$$\frac{d}{dt}\left(\frac{\partial T}{\partial \dot{\mathbf{q}}}\right) - \frac{\partial T}{\partial \mathbf{q}} = \mathbf{f} \tag{3.2.2}$$

The elegant formulation (3.2.2) is independent of any particular choice of generalized coordinates $\mathbf{q}$, and it does not explicitly contain any of the internal constraint forces in the system.

An alternative to this formulation is the Newton-Euler formulation ('vectorial dynamics') in which the motion of each individual body in the system is modelled. Reviews and surveys of multibody dynamics modelling approaches are provided by [Likins] and [D'Eleuterio.2].

Forces and Torques

In (3.2.2) $\mathbf{f}(t) \in \mathbb{R}^n$ is a vector of forces[1] acting on the system, consisting of conservative forces $\mathbf{f}_c(t)$, dissipative forces $\mathbf{f}_d(t)$ and generalized external forces $\mathbf{f}_e(t)$ which provide the external excitation of the system:

$$\mathbf{f}(t) = \mathbf{f}_c(t) + \mathbf{f}_d(t) + \mathbf{f}_e(t) \tag{3.2.3}$$

[1] The term force is used in a generalized sense throughout this document, implying "force and torque", as appropriate.

The conservative forces are associated with the potential energy $V(\mathbf{q})$, $V \in \mathbb{R}$ contained in the system:

$$\mathbf{f}_c(\mathbf{q}) = -\frac{\partial V(\mathbf{q})}{\partial \mathbf{q}} \tag{3.2.4}$$

The dissipative forces are derived from a dissipation function $R(\dot{\mathbf{q}})$, $R \in \mathbb{R}$:

$$\mathbf{f}_d(\dot{\mathbf{q}}) = -\frac{\partial R(\dot{\mathbf{q}})}{\partial \dot{\mathbf{q}}} \tag{3.2.5}$$

Due to the Second Law of Thermodynamics, the dissipative forces never act as a source of mechanical energy for the system, i.e. the dissipation function always has the property:

$$\dot{\mathbf{q}}^T \frac{\partial R(\dot{\mathbf{q}})}{\partial \dot{\mathbf{q}}} \geq 0 \tag{3.2.6}$$

The external forces are derived from the external work $W_e \in \mathbb{R}$ done on the system:

$$\mathbf{f}_e = \frac{\partial W_e}{\partial \dot{\mathbf{q}}} \tag{3.2.7}$$

The external forces are usually caused by control system actuators and disturbances. The action of l actuators and k sources of disturbances can be described by vector functions $\mathbf{u}(t) = [u_1(t), u_2(t), \ldots u_l(t)]^T$ and $\mathbf{d}(t) = [d_1(t), d_2(t), \ldots d_k(t)]^T$. The actions of actuators and disturbances are mapped into the space of the generalized coordinates $\mathbf{q}$ by projection matrices $\mathbf{B}_u \in \mathbb{R}^{n \times l}$ and $\mathbf{B}_d \in \mathbb{R}^{n \times k}$. These matrices are implicitly defined by the equivalence of equation (3.2.7) and the following 'input equation':

$$\mathbf{f}_e(t) = \mathbf{B}_u \mathbf{u}(t) + \mathbf{B}_d \mathbf{d}(t) \tag{3.2.8}$$

The projection matrices are determined from (3.2.7).

Euler-Lagrange Equation

Equations (3.2.2)–(3.2.7) can be combined into the following form of Lagrange's equations for the system:

$$\frac{d}{dt}\left(\frac{\partial T}{\partial \dot{\mathbf{q}}}\right) + \frac{\partial R}{\partial \dot{\mathbf{q}}} - \frac{\partial (T - V)}{\partial \mathbf{q}} = \frac{\partial W_e}{\partial \dot{\mathbf{q}}} \tag{3.2.9}$$

The difference of the kinetic and potential energies in the system is known as the Lagrangian function $L \in \mathbb{R}$ of the system:

$$L(\mathbf{q}, \dot{\mathbf{q}}) = T(\mathbf{q}, \dot{\mathbf{q}}) - V(\mathbf{q}) \tag{3.2.10}$$

The equation (3.2.9) represents a set of implicit second-order differential equations for the motion $\mathbf{q}(t)$ of a general robotic system in response to external forces. In order to derive an explicit differential equation for a specific system, the kinetic energy T, the potential energy V, the dissipation R and the excitation W_e need to be established as functions of the chosen set of coordinates $\mathbf{q}(t)$ and their derivatives. We will illustrate this derivation in the example presented in Section 3.4.

A general explicit form of (3.2.8) can be established for the common case of natural systems by recognizing that the kinetic energy T in mechanical system can be expressed in the form [Meirovitch]:

$$T(\mathbf{q}, \dot{\mathbf{q}}) = \frac{1}{2}\dot{\mathbf{q}}^T \mathbf{M}(\mathbf{q})\dot{\mathbf{q}} \tag{3.2.11}$$

with a positive-definite mass matrix $\mathbf{M} \in \mathbb{R}^{n \times n}$, $\mathbf{M}(\mathbf{q}) > 0$. Equation (3.2.11) allows us to express the first term in (3.2.9) in the following form where the first term of the right-hand side is familiar from Newton's Second Law:

$$\frac{d}{dt}\left(\frac{\partial T}{\partial \dot{\mathbf{q}}}\right) = \mathbf{M}(\mathbf{q})\ddot{\mathbf{q}} + \frac{d\mathbf{M}(\mathbf{q})}{dt}\dot{\mathbf{q}} \tag{3.2.12}$$

We further define the vector function $\mathbf{c} \in \mathbb{R}^n$ representing dissipative effects, Coriolis and centrifugal forces, as well as forces due to changes in system configuration and mass properties from (3.2.12):

$$\mathbf{c}(\mathbf{q}, \dot{\mathbf{q}}) = \frac{\partial R(\dot{\mathbf{q}})}{\partial \dot{\mathbf{q}}} - \frac{\partial T(\mathbf{q}, \dot{\mathbf{q}})}{\partial \mathbf{q}} + \frac{d\mathbf{M}(\mathbf{q})}{dt}\dot{\mathbf{q}} \tag{3.2.13}$$

The vector function $\mathbf{k} \in \mathbb{R}^n$ represents forces due to the potential energy in the system:

$$\mathbf{k}(\mathbf{q}) = \frac{\partial V(\mathbf{q})}{\partial \mathbf{q}} \tag{3.2.14}$$

with these definitions the Euler-Lagrange equation can now be expressed in the following form often used in the robotics literature such as [Fu, Gonzales and Lee]:

$$\mathbf{M}(\mathbf{q})\ddot{\mathbf{q}} + \mathbf{c}(\mathbf{q}, \dot{\mathbf{q}}) + \mathbf{k}(\mathbf{q}) = \mathbf{B}_u\mathbf{u}(t) + \mathbf{B}_d\mathbf{d}(t) \tag{3.2.15}$$

Equation (3.2.15) can also be expressed in the form of a $2n$ dimensional state-space system where $\mathbf{0}$ are zero-matrices of appropriate dimensions:

$$\frac{d}{dt}\begin{bmatrix}\mathbf{q}\\ \dot{\mathbf{q}}\end{bmatrix} = \begin{bmatrix}\dot{\mathbf{q}}\\ -\mathbf{M}^{-1}(\mathbf{q})\mathbf{k}(\mathbf{q}) - \mathbf{M}^{-1}(\mathbf{q})\mathbf{c}(\mathbf{q}, \dot{\mathbf{q}})\end{bmatrix} + \begin{bmatrix}\mathbf{0} & \mathbf{0}\\ \mathbf{B}_u(\mathbf{q}) & \mathbf{B}_d(\mathbf{q})\end{bmatrix}\begin{bmatrix}\mathbf{u}(t)\\ \mathbf{d}(t)\end{bmatrix} \tag{3.2.16}$$

These equations describe the dynamics of holonomic mechanical systems, including robot manipulators, in full generality including non-linearities and flexibility effects inherent in the system.

Linearization

Sometimes these equations are linearized about an operating point $\mathbf{q}_0$ by defining

$$\mathbf{q}(t) = \mathbf{q}_0 + \boldsymbol{\Delta}\mathbf{q}(t)$$

and appropriate matrices $\mathbf{C}_0 \in \mathbb{R}^{n\times n}$, $\mathbf{K}_0 \in \mathbb{R}^{n\times n}$ following standard technique, resulting in

$$\begin{aligned}&\mathbf{M}(\mathbf{q}_0)\boldsymbol{\Delta}\ddot{\mathbf{q}} + \mathbf{C}_0(\mathbf{q}_0)\boldsymbol{\Delta}\dot{\mathbf{q}} + \mathbf{K}_0(\mathbf{q}_0)\boldsymbol{\Delta}\mathbf{q}\\ &\quad = \mathbf{B}_u(\mathbf{q}_0)\boldsymbol{\Delta}\mathbf{u} + \mathbf{B}_d(\mathbf{q}_0)\boldsymbol{\Delta}\mathbf{d}\end{aligned} \tag{3.2.17}$$

or

$$\begin{aligned}\frac{d}{dt}\begin{bmatrix}\boldsymbol{\Delta}\mathbf{q}\\ \boldsymbol{\Delta}\dot{\mathbf{q}}\end{bmatrix} &= \begin{bmatrix}\mathbf{0} & \mathbf{I}\\ -\mathbf{M}^{-1}(\mathbf{q}_0)\mathbf{K}_0(\mathbf{q}_0) & -\mathbf{M}^{-1}(\mathbf{q}_0)\mathbf{C}_0(\mathbf{q}_0)\end{bmatrix}\begin{bmatrix}\boldsymbol{\Delta}\mathbf{q}\\ \boldsymbol{\Delta}\dot{\mathbf{q}}\end{bmatrix}\\ &\quad + \begin{bmatrix}\mathbf{0} & \mathbf{0}\\ \mathbf{B}_u(\mathbf{q}_0) & \mathbf{B}_d(\mathbf{q}_0)\end{bmatrix}\begin{bmatrix}\boldsymbol{\Delta}\mathbf{u}(t)\\ \boldsymbol{\Delta}\mathbf{d}(t)\end{bmatrix}\end{aligned} \tag{3.2.18}$$

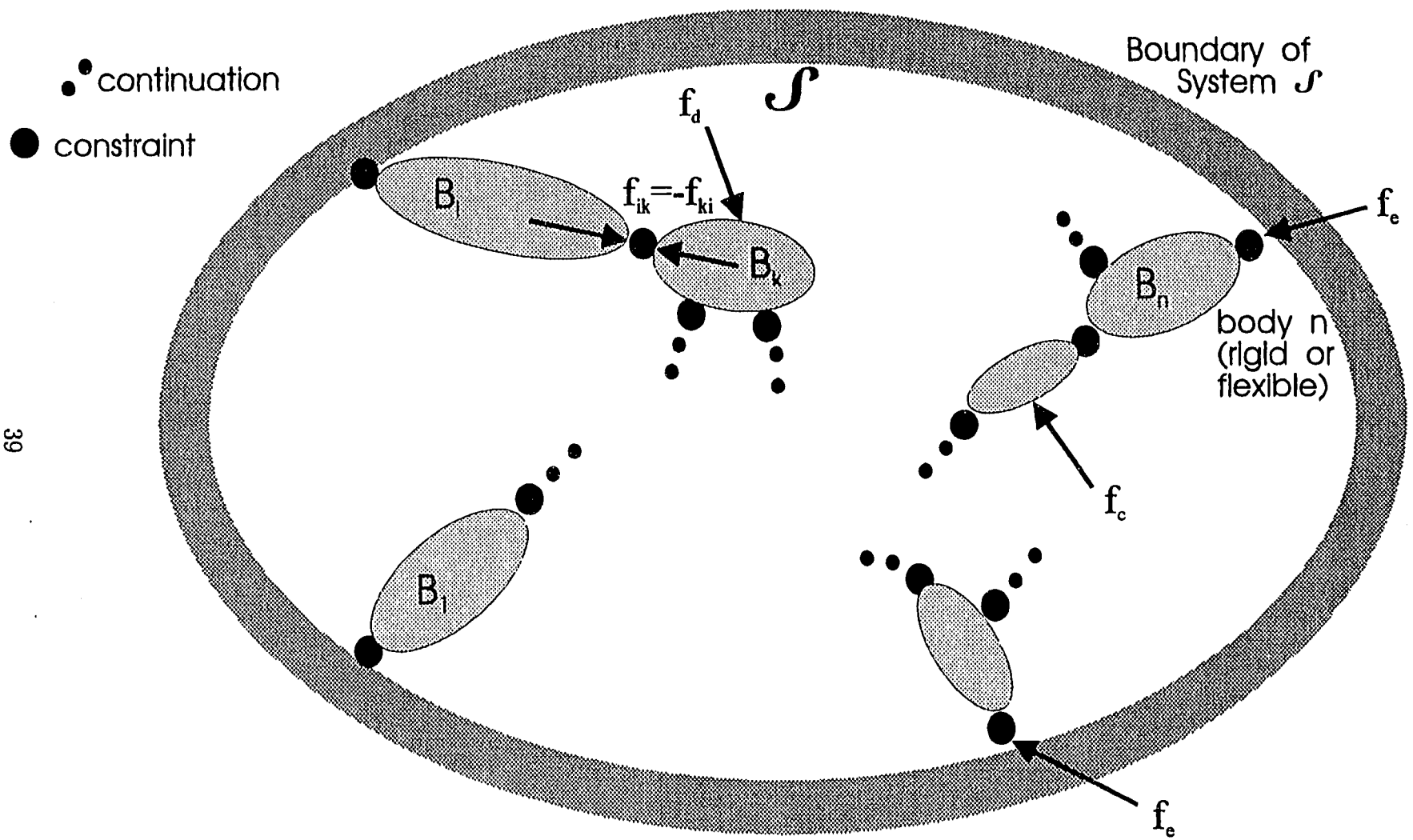

Figure 3.2.1: General Multibody System $\mathcal{S}$

3.3 Kinematics, Sensing and Control

Forward Kinematics

In most robotics applications, the motion ultimately of interest is not the motion of the generalized coordinates $\mathbf{q}(t)$, but the trajectory of a payload or the tip of the manipulator in the task space. This task space trajectory is usually defined in terms of cartesian coordinates $\mathbf{a}(t) \in \mathbb{R}^6$ with 3 translational components and 3 rotational components. The task space trajectory $\mathbf{a}(t)$ is generated by contributions from the various generalized coordinates $\mathbf{q}(t)$:

$$\mathbf{a}(t) = \mathbf{\Gamma}(\mathbf{q}(t)) \tag{3.3.1}$$

For rigid manipulators with joint positions chosen as generalized coordinates, the vector function $\mathbf{\Gamma}(\mathbf{q})$ is known as the forward kinematic relationship of the robot. For most rigid manipulators, $\mathbf{\Gamma}(\mathbf{q})$ can be determined as an explicit function of joint positions and link lengths. The inverse kinematic relationship relating joint positions to the position of a payload in the task space can be found explicitly only in special cases.

At every point $\mathbf{q}$ in the joint space a particular linear relationship exists between the velocities of the joints and the velocity of a payload in the task space:

$$\dot{\mathbf{a}}(t) = \mathbf{J}(\mathbf{q})\dot{\mathbf{q}}(t) \tag{3.3.2}$$

where

$$\mathbf{J}(\mathbf{q}) = \frac{\partial \mathbf{\Gamma}(\mathbf{q})}{\partial \mathbf{q}}$$

is the Jacobian matrix of the robot with appropriate dimensions for $\mathbf{a}$ and $\mathbf{q}$.

Inverse Kinematics

The inverse relationship for the velocities exists for most points in joint space if the number of joints is not less than the dimension of the task space, usually 6. If $\mathbf{a}$ and $\mathbf{q}$ are of the same dimension the matrix $\mathbf{J}$ is square and the inverse kinematic relationship for the velocities is

$$\dot{\mathbf{q}}(t) = \mathbf{J}^{-1}(\mathbf{q})\dot{\mathbf{a}}(t) \tag{3.3.3}$$

Depending on the manipulator design, there usually are a number of singular points in the configuration space for which $\mathbf{J}(\mathbf{q})$ is rank deficient and $\mathbf{J}^{-1}(\mathbf{q})$ does not exist.

For kinematically "redundant" manipulators such as the SSRMS or the human arm, the dimension of $\mathbf{q}$ is higher than that of $\mathbf{a}$ and the inverse kinematic relationship for velocities is

$$\dot{\mathbf{q}}(t) = \mathbf{J}^{\dagger}(\mathbf{q})\dot{\mathbf{a}}(t) + \dot{\mathbf{q}}_N(t) \tag{3.3.4}$$

where $\mathbf{J}^{\dagger}$ is a right inverse of $\mathbf{J}$ and $\dot{\mathbf{q}}_N$ is an arbitrary vector function in the null space of $\mathbf{J}$, representing a combination of joint motions which does not affect the end-point motion.

Sensing

Sensing of the robot motion is a key aspect of the proposed research. Based on the general robot model developed so far we can define a number of different motion sensors. The physical motion resulting from the time history of individual generalized coordinates, e.g. joint angles and joint velocities, as well as motions resulting from sets of generalized coordinates, e.g. structural vibrations, can be described as a projection of the generalized coordinates $\mathbf{q}(t)$ into a space spanned by a vector of measurements $\mathbf{y}_{\mathbf{q}}(t)$:

$$\mathbf{y}_{\mathbf{q}}(t) = \begin{bmatrix} \mathbf{C}_{\mathbf{q}} & \mathbf{0} \\ \mathbf{0} & \mathbf{C}_{\dot{\mathbf{q}}} \end{bmatrix} \begin{bmatrix} \mathbf{q}(t) \\ \dot{\mathbf{q}}(t) \end{bmatrix} \tag{3.3.5}$$

Matrices $\mathbf{C}_{\mathbf{q}}$ and $\mathbf{C}_{\dot{\mathbf{q}}}$ are projection matrices of appropriate dimensions. More general definitions covering sensors such as strain gauges etc. are discussed in Section 6.3.

Sensors like the vision system measure positions and velocities in the task space. Their output vector $\mathbf{y}_{\mathbf{a}}(t)$ can be considered a projection of the task space motion trajectory $\mathbf{a}(t)$.

$$\mathbf{y}_{\mathbf{a}}(t) = \begin{bmatrix} \mathbf{C}_{\mathbf{a}} & \mathbf{0} \\ \mathbf{0} & \mathbf{C}_{\dot{\mathbf{a}}} \end{bmatrix} \begin{bmatrix} \mathbf{a}(t) \\ \dot{\mathbf{a}}(t) \end{bmatrix} \tag{3.3.6}$$

The forward kinematics equations (3.3.1), (3.3.2) establish the link from (3.3.6) to the generalized coordinates.

Control

The control system of the robot has the task to make the robot end effector or payload trajectory $\mathbf{a}(t)$ closely follow a trajectory $\mathbf{w}(t)$ prescribed in the task space relative to other elements in the task space. A criterion often used to define the term "closely follow" is that of a vanishing steady state error:

$$\lim_{t\to\infty}(\mathbf{a}(t)-\mathbf{w}(t_0))=\mathbf{0}\ ;\quad t_0 \text{ finite} \tag{3.3.7}$$

The sensor fusion and control algorithm $\mathcal{C}$ which we will investigate in detail in Chapters 4, 5 and 7 can generally be described as a vector function of the prescribed trajectory and the sensor outputs:

$$\mathbf{u}(t)=\mathcal{C}(\mathbf{w}(t),\mathbf{y_q}(t),\mathbf{y_a}(t)). \tag{3.3.8}$$

When the prescribed trajectory is defined in the task space, the control algorithm usually has to contain some representation of the inverse kinematic equations (3.3.3) or (3.3.4). [Fu, Gonzales and Lee] describes a number of established techniques for the control of manipulators with rigid links.

3.4 Modelling of a Flexible Link Robot

Description

We will now illustrate the use of Hamilton's Principle and the Euler-Lagrange formulation in the derivation of a model for the simple flexible robot arm already familiar from Section 2.2. The system is shown in Figure 3.4.1 and consists of a single rotary joint applying a torque $u_T(t)$ to one end of a flexible link carrying a point mass μ at the other end. In this 2-dimensional model the motion of the link is restricted to a plane. A sensor measures the motion of the beam at position x_s.

This system is chosen as an example because it permits the closed-form analysis of certain important characteristics of flexible-body system. In spite of its simplicity the example has the generic properties of more complex flexible systems and can be considered a very simple model for the flexibility aspects of space manipulator systems. Therefore this system is used as an example throughout this study.

This simple model already has served to illustrate input-output behaviour and stability problems in Chapter 2 and will aid in the understanding of the limitations of state-of-the-art in sensing and control for flexible robots discussed in Chapter 4. In Chapter 7 we will discuss the experimental evaluation of a new sensing and control strategy on a flexible link robot whose dynamics can be approximated by the simple system shown in Figure 3.4.1.

Assumptions

The link of length ℓ is modelled as a beam with uniform mass density ρ and uniform bending stiffness κ along its length. In order to focus on the effects relevant to this study several simplifying assumptions consistent with the Euler-Bernoulli beam theory are made:

(1) The cross-sectional dimensions of the beam are small compared to its length. Under this assumption, the effects of shear deformations and rotary inertia effects associated with flexible beam deformations can be neglected.

(2) Flexible deformations are small compared to the length of the beam.

(3) The angular velocity of all elements of the beam is sufficiently low to be able to neglect certifugal and Coriolis forces.

(4) The neutral axis of the beam does not stretch under deformation and the material has no hysteresis and damping.

(5) Gravity does not affect the motion of the beam, either because the plane of motion is horizontal, or because the system operates in orbit.

These assumptions limit the validity of the model to "slender" beams and low to medium vibrational frequencies. The beam theories of Raleigh and [Timoshenko] address more general cases.

Energy Terms

As shown in Figure 3.4.1, the position of any element of the beam can be described by the radial coordinate x defined along the beam, and a circumferential coordinate v composed of the beam transverse flexible deformation ψ and the rigid body joint angle θ as follows:

$$v(x,t) = \psi(x,t) + x\theta(t) \tag{3.4.1}$$

In order to apply Hamilton's Principle (3.2.1) or the Euler-Lagrange formulation (3.2.9) to the system, we need to determine the kinetic and potential energy in the system, and the external work due to the torque input.

With the Assumptions (1) and (3), the kinetic energy of a mass element dm of the beam is given by

$$T_{dm} = \frac{1}{2}\rho\dot{v}^2(x,t) \tag{3.4.2}$$

The total kinetic energy T of the system hence is:

$$T(t) = \frac{1}{2}\int_0^\ell \rho\dot{v}^2(x,t)dx + \frac{1}{2}\mu\dot{v}^2(\ell,t) \tag{3.4.3}$$

Under the assumptions made above the potential energy V of the system is given by the strain energy in the deformed beam:

$$V(t) = \frac{1}{2}\kappa \int_0^{\ell} \frac{\partial \psi(x,t)}{\partial x^2} dx \tag{3.4.4}$$

Noting from (3.4.1) that $\frac{\partial^2 v}{\partial x^2} = \frac{\partial^2 \psi}{\partial x^2}$, (3.4.4) can also be expressed as:

$$V(t) = \frac{1}{2}\kappa \int_0^{\ell} \frac{\partial^2 v(x,t)}{\partial x^2} dx \tag{3.4.5}$$

The external work W_e generated by the joint torque $u_T(t)$ is a function of the instantaneous angular velocity of the beam at $x = 0$:

$$W_e(t) = -\int_0^t u_T(\tau) \frac{d}{d\tau} \Big(\frac{\partial v(x,\tau)}{\partial x}\Big|_{x=0} \Big) d\tau \tag{3.4.6}$$

Continuum Model

The expressions (3.4.3), (3.4.5) and (3.4.6) established above for T, V and W_e are functions of $v(x,t)$, i.e. of time and space instead of only functions of time, as a result of treating the flexible beam as a continuum with distributed mass and stiffness properties. Hence, the variable $v(x,t)$ in its current form is not suitable as a generalized coordinate required to apply the Euler-Lagrange equation (3.2.9). However, Hamilton's Principle (3.2.1) can be directly applied, recognizing that:

$$W(t) = W_e(t) - V(t) \tag{3.4.7}$$

Substituting (3.4.3), (3.4.5), (3.4.6) and (3.4.7) into (3.2.1), taking the variation, integrating by parts with respect to t and x to eliminate temporal and spatial derivatives of δv, and restricting the solution to virtual displacements that vanish at t_1 and t_2 leads to the following boundary value problem for the motion of the continuum system:

$$\kappa v^{(4)}(x,t) + \rho \ddot{v}(x,t) = 0, \tag{3.4.8}$$

with the boundary conditions:

$$v(0,t) = 0 \quad \text{pinned} \tag{3.4.9}$$

$$\kappa v^{(2)}(0,t) = u_T(t) \quad \text{input torque} \tag{3.4.10}$$

$$v^{(2)}(\ell,t) = 0 \quad \text{bending moment} \tag{3.4.11}$$

$$\kappa v^{(3)}(\ell,t) = \mu\tilde{v}(\ell,t) \quad \text{shear force} \tag{3.4.12}$$

A complete step-by-step derivation of the boundary-value problem for a vibrating beam based on Hamilton's Principle is described by [Meirovitch].

Modal Expansion

A standard approach to the solution of the partial differential equation (3.4.8) is the separation of the solution $v(x,t)$ into functions dependent only on space and time. To that effect we express $v(x,t)$ as a modal expansion:

$$v(x,t) = \sum_{i=1}^{\infty} \phi_i(x) q_i(t) \tag{3.4.13}$$

Here the $\phi_i(x) \in \mathbb{R}$ are a set of orthogonal "mode shape" functions spanning the function space which contains all possible deformations of the beam. They must meet the boundary conditions for $v(x,t)$ at $x = 0$ and $x = \ell$. Other properties of the $\phi_i(x)$ and how they are generated will be discussed later. The $q_i(t)$ are "modal coordinates" describing the time history of excitations of each mode. For the practical reason to keep the number of coordinates finite, the infinite sum (3.4.13) is usually truncated to a finite sum of n modal motions,

$$v(x,t) = \sum_{i=1}^{n} \phi_i(x) q_i(t). \tag{3.4.14}$$

This truncation, which is equivalent to a spatial discretization of the problem, allows us to collect the mode shape functions in a vector

$$\boldsymbol{\phi}(x) = [\phi_1(x), \phi_2(x), \ldots, \phi_n(x)]^T$$

and express $v(x,t)$ as an inner product:

$$v(x,t) = \boldsymbol{\phi}^T(x)\mathbf{q}(t) \tag{3.4.15}$$

Euler-Lagrange Equations

The modal coordinates $\mathbf{q}(t)$ are a suitable choice for generalized coordinates due to the orthogonality of the mode shape functions. Using $\mathbf{q}$ as defined in (3.4.15) as generalized coordinates, we now can apply the Euler-Lagrange equation (3.2.9) to the energy terms (3.4.3), (3.4.5) and (3.4.6).

By substituting (3.4.15) in (3.4.3) and (3.4.5) we find the following Lagrangian function for the flexible link robot:

$$\begin{aligned} L(\mathbf{q},\dot{\mathbf{q}},t) = & \frac{1}{2}\rho\,\dot{\mathbf{q}}^T(t)\int_0^\ell \phi(x)\phi^T(x)dx\,\dot{\mathbf{q}}(t) \\ & + \frac{1}{2}\mu\,\dot{\mathbf{q}}^T(t)\phi(\ell)\phi^T(\ell)\dot{\mathbf{q}}(t) \\ & - \frac{1}{2}\kappa\mathbf{q}^T(t)\int_0^\ell \frac{d^2\phi(x)}{dx^2}\frac{d^2\phi^T(x)}{dx^2}dx\,\mathbf{q}(t) \end{aligned} \tag{3.4.16}$$

The explicit terms for the Euler-Lagrange equation (3.2.9) are given by the following vectors:

$$\frac{d}{dt}\Big(\frac{\partial T}{\partial\dot{\mathbf{q}}}\Big) = \rho\int_0^\ell \phi(x)\phi^T(x)dx\,\ddot{\mathbf{q}}(t) + \mu\phi(\ell)\phi^T(\ell)\ddot{\mathbf{q}}(t) \tag{3.4.17}$$

$$\frac{\partial(T-V)}{\partial\mathbf{q}} = -\kappa\int_0^\ell \frac{d^2\phi(x)}{dx^2}\frac{d^2\phi^T(x)}{dx^2}dx\,\mathbf{q}(t) \tag{3.4.18}$$

$$\frac{\partial W_e}{\partial\dot{\mathbf{q}}} = \frac{d\phi}{dx}\Big|_{x=0} u_T(t) \tag{3.4.19}$$

From the expressions (3.4.17)–(3.4.19) we can easily identify the mass, stiffness and input distribution matrices of a linear second order system:

$$\mathbf{M}\ddot{\mathbf{q}}(t) + \mathbf{K}\mathbf{q}(t) = \mathbf{B}_u u_T(t) \tag{3.4.20}$$

with

$$\mathbf{M} = \rho \int_0^{\ell} \phi(x)\phi^T(x)dx + \mu\phi(\ell)\phi^T(\ell) \tag{3.4.21}$$

$$\mathbf{K} = \kappa \int_0^{\ell} \frac{d^2\phi(x)}{dx^2}\frac{d^2\phi^T(x)}{dx^2}dx \tag{3.4.22}$$

$$\mathbf{B}_u = \frac{d\phi}{dx}\Big|_{x=0} \tag{3.4.23}$$

Mode Shape Functions

Obviously the choice of the mode shape functions $\phi_i(x)$ will have an effect on the properties of the matrices $\mathbf{M}$, $\mathbf{K}$, $\mathbf{B}_u$ and on the convergence of the summation (3.4.14). There are a number of different ways to find suitable mode shape functions, as discussed by [Meirovitch]. Either "natural modes" defined by eigenvalue/eigenfunction problems or "assumed modes" found by various techniques such as the finite element method, cubic splines or Raleigh-Ritz/Galerkin discretization can be used. They have to satisfy the boundary coordinates of the structure and must be orthogonal in order to span the space of all possible spatial functions $v(x,t)$ and generate independent generalized coordinates. The infinite sum (3.4.13) will converge for all the different mode shape functions meeting the above requirements. However, the rate of convergence depends critically on the particular choice of mode shape functions, and the accuracy/validity of the finite approximation (3.4.14) used in practice depends very much on the choice of the mode shapes and the number of modes included in the model. How many modes really "exist" in structures and which ones are important has been a subject of some discussion. Some insight into this question is offered by [Hughes].

Another approach to defining modes used for modelling flexible links is to treat the rigid-body motion separately from the flexible motion. This permits the use of other boundary conditions, such as "clamped-free", for the definition of flexible modes, which can be advantageous in certain respects [Piedboef].

Natural Modes

When so-called natural modes are chosen, the expansion (3.4.13)/(3.4.14) converges uniformly and absolutely in accordance with the Expansion Theorem

discussed by [Meirovitch]. With the use of natural modes the self-adjoint boundary value (3.4.8) problem associated with the Euler-Bernoulli beam can be decomposed into two sets of n ordinary differential equations, one in the space domain and one in the time domain:

$$\kappa\phi_i^{(4)}(x) - \omega_i^2\rho\phi_i(x) = 0, \quad i = 1\ldots n \tag{3.4.24}$$

$$\ddot{q}_i(t) + \omega_i^2 q_i(t) = 0, \quad i = 1\ldots n \tag{3.4.25}$$

The last set of equations governs the temporal evolution of the modal coordinates and has a set of harmonic functions as homogeneous solutions:

$$q_i(t) = \epsilon_i e^{j\omega_i t}, \quad i = 1\ldots n \tag{3.4.26}$$

where the constants ϵ_i ensue from initial conditions and the constants ω_i can be identified as natural frequencies.

The space-domain equations (3.4.24) generate a set of eigenfunctions $\phi_i(x)$ which are the natural mode shape functions. The mode shape functions have the following general form for $\lambda_i \neq 0$:

$$\phi_i(x) = a_i \sin(\lambda_i x) + b_i \cos(\lambda_i x) + c_i \sinh(\lambda_i x) + d_i \cosh(\lambda_i x) \tag{3.4.27}$$

where the eigenvalue λ_i associated with the modal frequency ω_i is defined by

$$\lambda_i^4 = \omega_i^2 \frac{\rho}{\kappa}. \tag{3.4.28}$$

The eigenvalues λ_i and the coefficient a_i, b_i, c_i, d_i are determined from the geometric and natural boundary conditions (3.4.9) – (3.4.12) associated with the homogeneous system which must be satisfied by all mode shape functions $\phi_i(x)$. Homogeneous conditions, i.e. $u_T(t) = 0$ in our case, are assumed for the eigenvalue problem because the time history of the excitation at the boundary is unknown. The "pinned" boundary at $x = 0$ then is represented by the following conditions:

$$\phi_i(x = 0) = 0 \tag{3.4.29}$$

$$\phi_i^{(2)}(x = 0) = 0 \tag{3.4.30}$$

The "free" end at $x = \ell$ with the point mass μ is characterized by the following torque and force balances per (3.4.11), (3.4.12) and (3.4.26). The boundary condition associated with the force balance is dependent on the eigenvalues.

$$\phi_i^{(2)}(x = \ell) = 0 \tag{3.4.31}$$

$$\kappa\phi_i^{(3)}(x = \ell) - \mu\omega_i^2\phi_i(x = \ell) = 0 \tag{3.4.32}$$

It follows immediately from (3.4.29)–(3.4.30) that $b_i = 0$ and $d_i = 0$ and the mode shape functions reduce to:

$$\phi_i(x) = a_i\left(\sin(\lambda_i x) + \frac{\sin(\lambda_i\ell)}{\sinh(\lambda_i\ell)} \cdot \sinh(\lambda_i x)\right) \tag{3.4.33}$$

From the boundary condition (3.4.32) the following condition ensues for the eigenvalues:

$$\lambda_i^2(\cosh(\lambda_i\ell)\sin(\lambda_i\ell) - \cos(\lambda_i\ell)\sin(\lambda_i\ell)) + 2\lambda_i^3\frac{\mu}{\rho}\sin(\lambda_i\ell)\sinh(\lambda_i\ell) = 0 \tag{3.4.34}$$

The solution of the eigenvalue problem (3.4.34) and the computation of the mode shape functions with the symbolic mathematics package "Maple" is demonstrated in Appendix E.1. The solution $\lambda_1^2 = 0$ is associated with the rigid-body mode of the link and is characterized by the special mode shape function

$$\phi_1(x) = \frac{a_1}{\ell}x. \tag{3.4.35}$$

The normal modes ϕ_i satisfy the following orthonormality properties:

$$\int_0^\ell \rho\phi_i(x)\phi_j(x)dx + \mu\phi_i(\ell)\phi_j(\ell) = \delta_{ij} \tag{3.4.36}$$

$$\int_0^\ell \kappa\phi_i^{(2)}(x)\phi_j^{(2)}(x)dx = \omega_i^2\delta_{ij} \tag{3.4.37}$$

where we used the definition of the Kronecker delta

$$\delta_{ij} = \begin{cases} 0 & \forall\, i \neq j \\ 1 & \forall\, i = j. \end{cases} \tag{3.4.38}$$

Based on condition (3.4.36) the normalization factors a_i of the mode shape functions per (3.4.33) are chosen as follows and have the physical unit of $\mathrm{kg}^{-\frac{1}{2}}$:

$$a_i = \left(2\mu \sin(\lambda_i \ell) + \int_0^\ell \rho(\sin(\lambda_i x) + \frac{\sin(\lambda_i \ell)}{\sinh(\lambda_i \ell)} \cdot \sinh(\lambda_i x))^2 dx \right)^{-\frac{1}{2}} \tag{3.4.39}$$

The evaluation of (3.4.39) is demonstrated in Appendix E.1. Condition (3.4.37) can be used to calculate the modal frequencies ω_i and thus perform an independent check of numerical results as shown in Appendix E.1. For the special case of the rigid-body mode the normalization factor is:

$$a_1 = \frac{1}{\sqrt{\rho \frac{\ell}{3} + \mu}} \tag{3.4.40}$$

Matrix Form of Link Model

Due to their orthonormality properties (3.4.36)–(3.4.37) the use of natural modes decouples the set of equations (3.4.20) by diagonalizing the mass and stiffness matrices as already indicated in (3.4.25):

$$\mathbf{M} = \mathbf{I} \tag{3.4.41}$$

$$\mathbf{K} = \mathbf{\Omega} \tag{3.4.42}$$

where $\mathbf{I} = \mathrm{diag}\ \{1\}$ is the $n \times n$ identity matrix and $\mathbf{\Omega} = \mathrm{diag}\ \{\omega_i^2\}$, $i = 1 \ldots n$. Equation (3.4.20) can then be expressed in the first-order form introduced in 3.2.16:

$$\frac{d}{dt} \begin{bmatrix} \mathbf{q} \\ \dot{\mathbf{q}} \end{bmatrix} = \begin{bmatrix} \mathbf{0} & \mathbf{I} \\ -\mathbf{\Omega} & \mathbf{0} \end{bmatrix} \begin{bmatrix} \mathbf{q} \\ \dot{\mathbf{q}} \end{bmatrix} + \begin{bmatrix} \mathbf{0} \\ \boldsymbol{\phi}^{(1)}(0) \end{bmatrix} u_T(t) \tag{3.4.43}$$

The output of various motion sensors for the system are defined by appropriate temporal and spatial derivatives of the beam position $v(x_s, t)$ at a sensor location x_s; $\dot{v}(x_s, t)$ defines the translational velocity of the beam at x_s, $v^{(1)}(x_s, t)$ defines the angle of the beam at x_s, and $\dot{v}^{(1)}(x_s, t)$ the angular velocity. Based on the

expansion (3.4.14) these four measurements are defined by the output equation:

$$\begin{bmatrix} v(x_s,t) \\ \dot{v}(x_s,t) \\ v^{(1)}(x_s,t) \\ \dot{v}^{(1)}(x_s,t) \end{bmatrix} = \begin{bmatrix} \phi^T(x_s) & 0 \\ 0 & \phi^T(x_s) \\ \phi^{(1)T}(x_s) & 0 \\ 0 & \phi^{(1)T}(x_s) \end{bmatrix} \begin{bmatrix} \mathbf{q} \\ \dot{\mathbf{q}} \end{bmatrix} \tag{3.4.44}$$

Other sensors can be defined based on higher-order spatial derivatives as discussed in Section 6.3.

Observations

An interesting and important observation regarding the system defined by (3.4.43) and (3.4.44) is that the mode shape functions ϕ_i define both the system input matrix and the system output matrix. The action of both sensors and actuators are defined by various spatial derivatives of the mode shape functions evaluated at the location of the sensor or actuator. As demonstrated in Section 2.2 the selection and placement of sensors and actuators has fundamental effects on the input/output behaviour of the system. Sensors and actuators are called 'dual' if they are defined by a spatial derivative of the same order evaluated at the same location. In the above link model for instance, an angular rate sensor located at the joint, defined by $\dot{v}^{(1)}(x_s = 0, t)$ is dual to the torque actuator defined as input in (3.4.43). The effects of the selection and placement of sensors and actuators on the controllability and observability of systems like (3.4.43)–(3.4.44) has been investigated by [de Lafontaine and Stieber].

We also observe that with the introduction of the natural modes and their orthogonality properties, the system matrix governing the transient behaviour now only contains the modal frequencies as variables. Although (3.4.43)–(3.4.44) were derived for the simple example illustrated in Figure 3.4.1, these equations exhibit the generic structure typical for undamped linear systems transformed to natural modal coordinates, as shown in Appendix A. Hence, our observations apply to a much wider class of systems than the simple example.

Model Parameters for Laboratory Robot and SSRMS

The model (3.4.43) – (3.4.44) of the flexible link is used in the study (Sections 7.5 & 7.6) for simulation of the experimental robot shown in Figure 7.2.1. This robot has a flexible link consisting of a thin steel beam which can rotate in the horizontal plane. The modal parameters ω_i, $\phi_i(x)$, $\phi_i^{(1)}(x)$ for the first few modes of the flexible link of the laboratory robot, including the rigid-body mode, are presented in Tables 3.4.1 and Table 3.4.2, for the unloaded case and for the case with a 1.2 kg payload respectively. The symbolic and numerical calculations based on (3.4.33) – (3.4.40) are presented in Appendix E.1 for four different payloads. The corresponding matrices for the state-space model (3.4.43) – (3.4.44) are documented in Appendix E.2.

The simple single-link model can also be used as a very crude first-order approximation for the flexibility effects of the SSRMS. The range of fundamental frequencies of the SSRMS is roughly matched by the single link model with the following parameters:

$$\ell = 17.1\text{m}$$
$$\rho = 100 \text{ kg/m}$$
$$\kappa = 1 \cdot 10^6 \text{ Nm}^2$$
$$\mu = 0 \ldots 116,000 \text{ kg}$$

These parameters are based on matching the first cantilever mode frequency [1] for the link of Figure 3.4.1, i.e., assuming that the joint is "locked". Under this assumption the first fundamental frequency ω_1, in rad/s, is

$$\omega_1 = \sqrt{\frac{3\kappa}{\ell^3(\mu + 0.24\ell\rho)}} \tag{3.4.45}$$

[1] The ratio of the first flexible mode frequency for the "pinned-free" case and the "clamped-free" (cantilever) case is 4.39 for a slender uniform beam without tip mass.

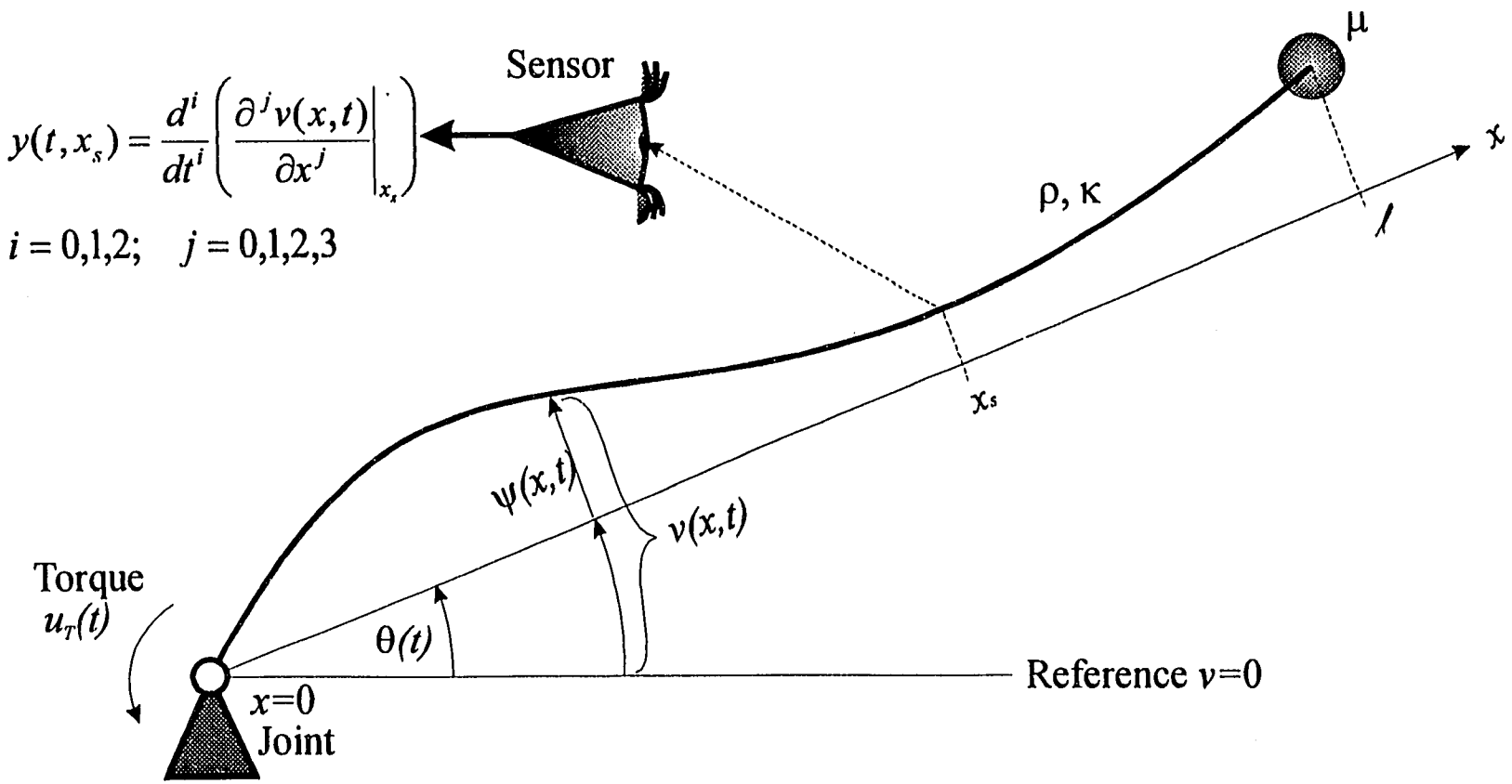

Figure 3.4.1: Flexible Link with Tip Mass and Sensor

Table 3.4.1: Parameters of Laboratory Robot Flexible Link without Payload

1. Physical Parameters

$\mu = 0.14$ kg $\quad \ell = 1.585$ m $\quad \rho = 1.17$ kg m^{-1} $\quad \kappa = 3.5$ Nm^2

2. Modal Parameters

Normal modes for "pinned-free" boundary conditions

Frequency	Shape Function
$\omega_1 = 0$ s^{-1}	$\phi_1(\frac{x}{\ell}) = 1.15\frac{x}{\ell}$ (rigid-body mode)
$\omega_2 = 9.48$ s^{-1}	$\phi_2(\frac{x}{\ell}) = 1.01\cdot[\sin(3.71\frac{x}{\ell}) - 2.63\cdot 10^{-2}\sinh(3.71\frac{x}{\ell})]$
$\omega_3 = 31.3$ s^{-1}	$\phi_3(\frac{x}{\ell}) = 1.02\cdot[\sin(6.74\frac{x}{\ell}) + 1.05\cdot 10^{-3}\sinh(6.74\frac{x}{\ell})]$
$\omega_4 = 66.2$ s^{-1}	$\phi_4(\frac{x}{\ell}) = 1.03\cdot[\sin(9.81\frac{x}{\ell}) - 4.11\cdot 10^{-5}\sinh(9.81\frac{x}{\ell})]$

3. Diagrams of Mode Shape Functions and their Spatial Derivatives

$\phi_i(\frac{x}{\ell}), i = 1\cdots 4$ $\qquad$ $\phi_i^{(1)}(\frac{x}{\ell}), i = 1\cdots 4$

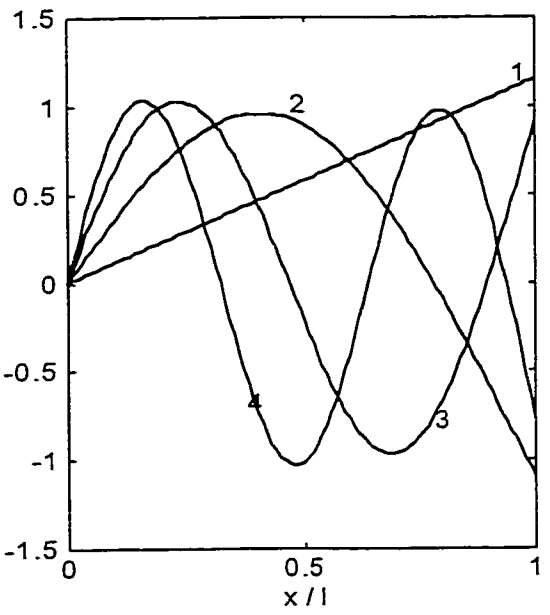

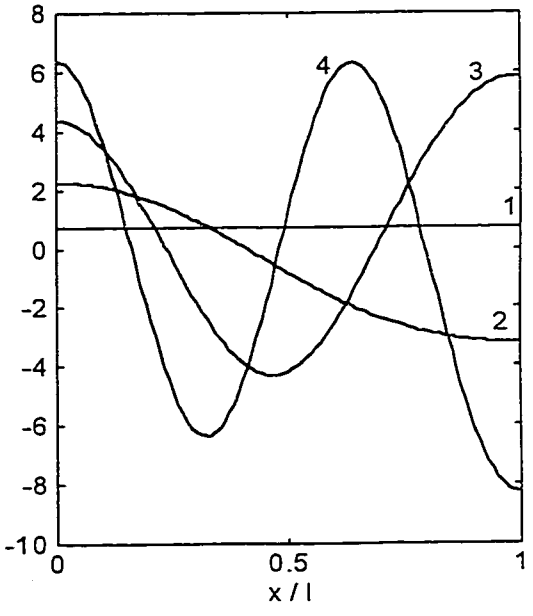

Table 3.4.2: Parameters of Laboratory Robot Flexible Link with Payload

1. Physical Parameters

$\mu = 1.2$ kg $\quad \ell = 1.585$ m $\quad \rho = 1.17$ kg m^{-1} $\quad \kappa = 3.5$ Nm^2

2. Modal Parameters

Normal modes for "pinned-free" boundary conditions

Frequency	Shape Function	
$\omega_1 = 0$ s^{-1}	$\phi_1(\frac{x}{\ell}) = 0.742\frac{x}{\ell}$	(rigid-body mode)
$\omega_2 = 7.62$ s^{-1}	$\phi_2(\frac{x}{\ell}) = 1.02 \cdot [\sin(3.33\frac{x}{\ell}) - 1.33 \cdot 10^{-2} \sinh(3.33\frac{x}{\ell})]$	
$\omega_3 = 28.1$ s^{-1}	$\phi_3(\frac{x}{\ell}) = 1.03 \cdot [\sin(6.39\frac{x}{\ell}) + 3.60 \cdot 10^{-4} \sinh(6.39\frac{x}{\ell})]$	
$\omega_4 = 62.1$s^{-1}	$\phi_4(\frac{x}{\ell}) = 1.04 \cdot [\sin(9.50\frac{x}{\ell}) - 1.12 \cdot 10^{-5} \sinh(9.50\frac{x}{\ell})]$	

3. Diagrams of Mode Shape Functions and their Spatial Derivatives

$\phi_i(\frac{x}{\ell}), i = 1 \cdots 4$

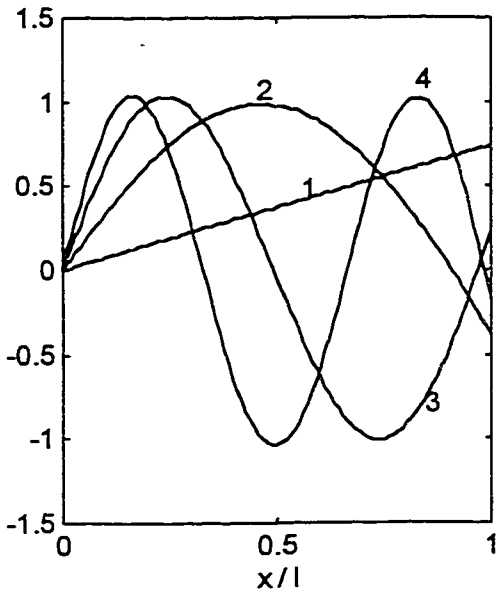

$\phi_i^{(1)}(\frac{x}{\ell}), i = 1 \cdots 4$

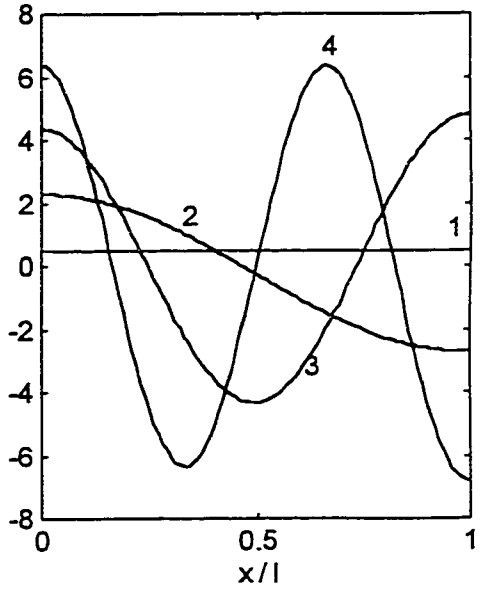

CHAPTER 4
SENSING AND CONTROL FOR FLEXIBLE ROBOTS

4.1 Overview

Active Vibration Control

Various technologies can be employed to improve the payload handling performance of robots with flexible links. The main objective is to reduce the effects of elastic deformations in links and joints on the position of the payload or end effector. The use of stiffer, lighter materials for example will increase the fundamental frequencies of oscillation. Structural damping may be increased by improved materials and passive damping treatments or devices so that the vibrations "die out" quickly. This can be achieved 'passively' by adding surface treatments such as "constrained layer damping" as proposed by [Alberts, Book and Dickerson], or by incorporating damping elements in the structural design as proposed for the SRMS by [Alberts, Xia and Chen]. The advantages offered by these technologies are usually accompanied by cost, weight, complexity and other penalties. The use of the available sensors and actuators for active control is more attractive in that regard, promising significant gains for an insignificant cost by replacing bulky structural material with a small amount of smart silicon to achieve the same functional objective. Motivated by this potential, a number of studies on active vibration control and the control of flexible-link manipulators have been carried out. As the problems of sensor selection, placement and fusion for systems with flexible bodies is closely linked to the control of vibrations in structures, we will review the literature on structural control as well as on the sensing aspects.

Model-based Methods

Most of the studies on flexible robots identify space manipulators as their domain of application and many are motivated by the Shuttle Remote Manipulator System (SRMS), which is a precursor to the SSRMS and has similar dynamic characteristics. Some of the more advanced techniques proposed for flexible manipulators build on results developed for vibration control for large space structures. Most of these developments are "model-based" and assume a known linear

time-invariant dynamic behaviour of structures. Most of the literature on sensor selection and placement is also based on these assumptions and it is usually assumed that sensors and actuators of various kinds can be placed almost arbitrarily on the structure. The books on the subject by [Joshi], [Junkins and Kim] reflect these assumptions.

Model-free Methods

As discussed in Chapters 2 and 3, these assumptions are generally not valid for space manipulators, due to their strongly time-variant behaviour and their non-linearities. Therefore methods which do not rely on the explicit knowledge of an accurate dynamics model offer advantages over model-based methods. In this study these approaches are generally labelled "model-free" although it is important to make the following distinctions within that group:

- 'Truly model-free' methods which do not use a mathematical model of the system in any way, for instance neural network or fuzzy logic methods;
- Methods which assume that the system behaviour is consistent with the basic principles of physics, such as Hamilton's Principle, the Principle of Conservation of Energy, or Newton's Laws, but which do not require explicit knowledge of particular details of the system behaviour. The methodology based on an extension of the hyperstability concept developed in this study falls into this category;
- Methods which assume that the behaviour of the system can be predicted by a model for which however the parameters are not known and might be subject to slow variations. The performance and robustness of these methods are critically dependent on the correct modelling assumptions, for instance the model order. Adaptive control methods fall into this category.

The "model-free" approaches discussed below do usually require the collocation of all sensors and actuators.

4.2 Model-free Methods

Control Methods Which Ignore Flexibility Effects

Ignoring the effects of structural flexibility during the control design process has the advantages of simplifying both control design and implementation, and of not requiring a flexible body dynamics model for the design process. This approach represents the standard practice for industrial robots where control system designs is usually based on kinematics and rigid-body dynamics of the robot. This usually implies the assumption that the tip motion of the robot can be deduced from joint sensors with sufficient accuracy. [Book, Maizza-Neto and Whitney] investigated the application of rigid body control design to flexible manipulation, using a linearized rigid-body model of the form (3.2.17) to derive a feedback gain matrix $\mathbf{F} \in \mathbb{R}^{k \times 2n}$ for a linear state-feedback control law of the form

$$\mathbf{u} = \mathbf{F} \begin{bmatrix} \mathbf{q} \\ \dot{\mathbf{q}} \end{bmatrix}. \tag{4.2.1}$$

In his methods termed 'Independent Joint Control' and 'General Rigid Control' Book uses pole-placement techniques to derive the gain matrix $\mathbf{F}$. In applying these techniques to a 2-link flexible manipulator example, Book found, not surprisingly, that the performance of the technique was limited by the manipulator fundamental frequency.

Many present generation robots for space and terrestrial applications use decentralized control schemes relying on 'tight' joint servo mechanisms, usually with Proportional-Integral-Derivative (PID) control of the joint velocity, to counter dynamic effects, as described by [Fu, Gonzales and Lee]. The velocity commands for the joint servo mechanisms are generated from payload trajectory commands via the inverse kinematics relationships (3.3.9) of robot. This relatively simple method works particularly well for manipulators with rotary joints and a high gear ratio in the joint gear train, because the dynamic coupling between the motion of the various joints reduces with the square of the gear ratio.

When sensors and actuators are collocated, this method is also robust with respect to flexibility effects, as will be shown in more detail later. Due to this

favourable property, this method has been successfully applied to the design of the control systems of the SRMS and the SSRMS as discussed by [Ravindran and Doetsch] and [Stieber, Laurenzio and Fung]. However, the performance achievable with this method is limited by the manipulator fundamental frequency of oscillation, and the desirable robustness properties are lost when non-collocated sensors and actuators are used, as in vision-based control.

Adaptive Control

Various forms of adaptive control have been proposed to deal with the problem of unknown or changing robot dynamic characteristics. The basic idea is to identify unknown system parameters and adapt the control law to slowly changing system characteristics.

The method of Model Reference Adaptive Control (MRAC) described by [Landau] and [Narendra and Annaswamy] is based on the idea to control a system such that its output will track those of an external 'reference model' which is chosen to be a stable linear system. A difficulty in applying MRAC to flexible robot arms is the low number of control inputs compared to that of the state variables. To overcome this problem it is suggested by [Siciliano, Yuan and Book] to apply MRAC to a flexible robot arm system with a nominal controller based on a linear model. The added adaptive control is designed to ensure global stability of the controlled system. For a single-link robot the method has been shown by [Siciliano, Yuan and Book] to be successful. It is not clear, however, how this approach is extended to more complex systems.

Another adaptive control method is self-turning adaptive control (STAC) pioneered by [Astrom and Wittenmark]. In this method the plant is assumed to be linear and its unknown dynamics are usually modelled as an Autoregressive Moving Average (ARMA) model of the form

$$S_1(\mathfrak{z}^{-1})\mathbf{y}(k) = \mathfrak{z}^{-d}S_2(\mathfrak{z}^{-1})\mathbf{u}(k) + \mathbf{e}(k) \tag{4.2.2}$$

where $\mathbf{u}(k)$ is the output, $\mathbf{y}(k)$ is the control input at discrete sampling times k and S_1, S_2 are polynomials in the shift operator $\mathfrak{z}^{-1}$ of the $\mathfrak{z}$-Transformation, and

$\mathbf{e}(k)$ represents modelling errors. The coefficients of S_1 and S_2 are determined by on-line recursive least-squares estimation. Various control schemes such as optimal control discussed in Section 4.3, Equations (4.3.5)–(4.3.14) can be applied to the estimated model. In most robot applications, the parameter estimator must converge more rapidly than the changes in system dynamics. Also, the control law has to be recalculated in real-time, e.g. in the case of optimal control by solution of (4.3.11)–(4.3.14). The application of STAC to a single flexible link robot was investigated by [Nemir, Koivo and Kashyap].

Although adaptive control has been successfully applied to rigid robots with success, at least in a research setting, the application of adaptive control techniques to robots with significant flexibilities and nonlinearities is hampered by the complexity of the behaviour of flexible robot systems and the fact that the order of the system is an unknown, while most adaptive control methods require a priori knowledge of the system order. When non-collocated sensor/actuator configurations are introduced into the problem, like in vision-based control of the payload motion, the theoretical basis for most stability results in adaptive control is eroded due to the non-minimum phase characteristics of the linearized system dynamics. Although recent results by [Suarez and Lozano] address adaptive control for non-minimum phase plants, their method is not applicable to the space robotics problem as it requires a priori knowledge of the system order.

Rule-Based Methods

A rule-based control method for a flexible link robot was proposed by [Moudgal, Passino and Yurkovich]. This method is not based on any explicit dynamics model of the system but on intuitive knowledge of flexible robot control, encoded in fuzzy logic. Good performance of the system was achieved in laboratory tests, providing an attractive alternative to conventional control methods. However, [Moudgal, Passino and Yurkovich] state that there is need for investigations into the theoretical foundation of fuzzy control approaches and rule-based supervisory control approaches (e.g. stability analysis), and for a more systematic methodology for constructing direct and supervisory rule-based controllers.

Passive Control

[Benhabib, Iwens and Jackson] proposed the 'positivity' concept for the robust control of large satellites with flexible appendages. The analysis is based on a linear model of a flexible structure without damping in modal form familiar from our example (3.4.43):

$$\frac{d}{dt}\begin{bmatrix}\mathbf{q}\\ \dot{\mathbf{q}}\end{bmatrix} = \begin{bmatrix}\mathbf{0} & \mathbf{I}\\ -\boldsymbol{\Omega} & \mathbf{0}\end{bmatrix}\begin{bmatrix}\mathbf{q}\\ \dot{\mathbf{q}}\end{bmatrix} + \begin{bmatrix}\mathbf{0}\\ \boldsymbol{\phi}^{(1)}(x_a)\end{bmatrix} u_T. \tag{4.2.3}$$

For simplicity we have assumed that the system only has a single torque actuator located at a position x_a on the structure. A key element of the method is to choose the system output y to be "dual" to the input u_T, in this case by placing an angular velocity sensor at the actuator location x_a as discussed in Section 3.4:

$$y = [\mathbf{0}\ \boldsymbol{\phi}^{(1)T}(x_a)]\begin{bmatrix}\mathbf{q}\\ \dot{\mathbf{q}}\end{bmatrix} \tag{4.2.4}$$

Under this assumption of 'duality' of the system inputs and outputs, the system (4.2.3), (4.2.4) with $\omega_i^2 > 0$ is "positive real" and can be stabilized by any positive real feedback control system as explained by [Desoer and Vidyasagar]. [Junkins and Kim] discuss essentially the same concept under the name 'symmetrical output feedback'. A simple control law suggested by [Balas] is 'direct velocity feedback' already familiar from the example presented in Section 2.3:

$$u_T = -Fy \tag{4.2.5}$$

with $F > 0$. Dynamic stability of the closed loop system (4.2.3)–(4.2.5) was established by Lyapunov's method in Section 2.3.

The strength of this general approach is that the dynamic stability of the closed-loop system is independent of any particular values for the natural frequencies ω_i and any particular function for the mode shapes $\boldsymbol{\phi}$. Since modal frequencies and mode shapes result from a model transformation of the mass and stiffness properties of the system, stability can be guaranteed independently of

any particular mass and stiffness parameters of the system. Hence, the positivity approach promises to overcome the robustness problems identified with other approaches, as accurate knowledge of a dynamic model is not required.

These promising features have motivated a number of researchers to extend this methodology. [McLaren and Slater] investigated the design of positive real state-feedback control systems of the form (4.3.8)–(4.3.9) for application to large space structures. [Kelkar, Joshi and Alberts.1&2], [Joshi, Maghami and Kelkar], [Juang, Wu, Phan and Longman] recently showed that the methodology can be applied also to nonlinear flexible multibody systems.

Even though "positivity" or "passivity" control promises robust control for nonlinear flexible multibody systems, in its present form it cannot be applied to our vision-based control problem because of the underlying assumption of input-output duality per (4.2.3)–(4.2.4), implying sensor/actuator collocation. This assumption central to the approach is not compatible with the direct measurement of a robot payload motion by a vision system and control of the robot with joint motors. This limitation was explored in Section 2.3. A second limitation with regards to the application of 'positive' control to robotics is its lack to provide a purposeful motion control capability apart from damping vibrations.

4.3 Model-based Methods

Feedback Methods

When flexibility effects of robots cannot be ignored in the control design process because of the performance limitations associated with this approach, they can, at least in principle, be accounted for by including them in the dynamic model used for a model-based design. Such a model can generally be represented in the state space form (3.2.16) with an output equation of the form (3.3.5). When such a model contains flexibility effects, the number of states is usually much larger than the number of inputs and outputs, even though the flexibility model will usually be "truncated", i.e. of reduced order when compared to the actual system. Hence, some form of state estimation is usually required in addition to the sensor outputs in order to take flexibility effects into account in a feedback control law. Most proposed approaches use linear control theory for the synthesis of control laws based on a linearized robot dynamics model per (3.2.18). [Junkins and Kim] provide a comprehensive overview of the application of linear control theory to flexible structure control. We introduce the following abbreviations to express the model (3.2.18) more concisely.

$$\mathbf{x}_M = \begin{bmatrix} \mathbf{q} \\ \dot{\mathbf{q}} \end{bmatrix} \tag{4.3.1}$$

$$\mathbf{A}_M = \begin{bmatrix} \mathbf{0} & \mathbf{I} \\ -\mathbf{M}^{-1}(\mathbf{q}_0)\mathbf{K}_0 & -\mathbf{M}^{-1}(\mathbf{q}_0)\mathbf{C}_0 \end{bmatrix} \tag{4.3.2}$$

$$\mathbf{B}_M = \begin{bmatrix} \mathbf{0} \\ \mathbf{B}_u \end{bmatrix} \tag{4.3.3}$$

$$\mathbf{C}_M = \begin{bmatrix} \mathbf{C}_\mathbf{q} & \mathbf{0} \\ \mathbf{0} & \mathbf{C}_{\dot{\mathbf{q}}} \end{bmatrix} \tag{4.3.4}$$

With these abbreviations the model (3.2.18) can be expressed as follows:

$$\dot{\mathbf{x}}_M = \mathbf{A}_M\mathbf{x}_M + \mathbf{B}_M\mathbf{u} + \mathbf{d}_M \tag{4.3.5}$$

$$\mathbf{y} = \mathbf{C}_M\mathbf{x}_M + \mathbf{e}_M \tag{4.3.6}$$

The state disturbances $\mathbf{d}_M(t)$ and measurement errors $\mathbf{e}_M(t)$ are often modelled as stationary Gaussian white noise processes characterized by their expectation $\mathcal{E}(\cdot)$ and covariance matrix cov$(\cdot)$. Assuming uncorrelated zero-mean disturbance processes, these characteristics can be defined by

$$\begin{aligned} \mathcal{E}(\mathbf{d}_M) &= \mathbf{0}, \quad \text{cov}\ (\mathbf{d}_M) = \mathbf{V}_1 > \mathbf{0}, \\ \mathcal{E}(\mathbf{e}_M) &= \mathbf{0}, \quad \text{cov}(\mathbf{e}_M) = \mathbf{V}_2 > \mathbf{0}. \end{aligned} \tag{4.3.7}$$

If the pair $\mathbf{A}_M$, $\mathbf{B}_M$ is controllable and $\mathbf{A}_M$, $\mathbf{C}_M$ observable, this system can be stabilized and controlled by a linear control law of the form [Kwakernaak and Sivan]

$$\mathbf{u} = -\mathbf{F}\hat{\mathbf{x}}_M \tag{4.3.8}$$

where the state estimate $\hat{\mathbf{x}}_M$ is provided by the estimator

$$\dot{\hat{\mathbf{x}}}_M = (\mathbf{A}_M - \mathbf{B}_M\mathbf{F} - \mathbf{K}\mathbf{C}_M)\hat{\mathbf{x}}_M + \mathbf{K}\mathbf{y}. \tag{4.3.9}$$

Linear control theory provides a number of methods for finding a stabilizing state-feedback gain matrix $\mathbf{F}$ and a stabilizing estimation gain matrix $\mathbf{K}$. Most of these methods are variants of pole-placement techniques or optimization techniques. The "optimal control" approach described by [Kwakernaak and Sivan] allows to tailor and optimize the behaviour of the closed-loop system (4.3.5)–(4.3.9) by choosing cost weighting matrices $\mathbf{Q} \geq \mathbf{0}$ and $\mathbf{R} > \mathbf{0}$ in a performance index

$$J = \mathcal{E}\left(\int_0^\infty (\mathbf{x}_M^T\mathbf{Q}\mathbf{x}_M + \mathbf{u}^T\mathbf{R}\mathbf{u})dt\right). \tag{4.3.10}$$

This performance index is minimized by the gain matrices

$$\mathbf{F} = \mathbf{R}^{-1}\mathbf{B}_M\mathbf{P}_1 \tag{4.3.11}$$

$$\mathbf{K} = \mathbf{P}_2\mathbf{C}_M^T\mathbf{V}_2^{-1}. \tag{4.3.12}$$

$\mathbf{P}_1 = \mathbf{P}_1^T > \mathbf{0}$ and $\mathbf{P}_2 = \mathbf{P}_2^T > \mathbf{0}$ are the positive definite solutions of the algebraic Riccati equations [Kwakernaak and Sivan]:

$$\mathbf{A}_M^T\mathbf{P}_1 + \mathbf{P}_1\mathbf{A}_M + \mathbf{Q} - \mathbf{P}_1\mathbf{B}_M\mathbf{R}^{-1}\mathbf{B}_M^T\mathbf{P}_1 = \mathbf{0} \tag{4.3.13}$$

$$\mathbf{A}_M\mathbf{P}_2 + \mathbf{P}_2\mathbf{A}_M^T + \mathbf{V}_1 - \mathbf{P}_2\mathbf{C}_M^T\mathbf{V}_2^{-1}\mathbf{C}_M\mathbf{P}_2 = \mathbf{0} \tag{4.3.14}$$

Although state-feedback control permits the optimization of a multivariable design for a certain performance criterion, the methodology is mainly geared towards linear time-invariant systems of finite order, and is therefore intrinsically not well suited for non-linear and time variant robotic systems with flexible links.

A relatively simple state-feedback control law for a flexible link robot was proposed by [Book, Maizza-Neto and Whitney]. In the approach termed "Flexible Feedback Control" the flexibility model is of such a low order that $\hat{\mathbf{x}}_M$ can be reconstructed directly from $\mathbf{y}$ without the use of a state estimator. The feedback gain matrix $\mathbf{F}$ is determined by pole placement approach. Interestingly, [Book, Maizza-Neto and Whitney] report that the test result indicate that the performance of the "General Rigid Control" method discussed in Section 4.2 was found to be superior to that with "Flexible Feedback Control", due to the sensitivity of the method to the flexibility parameters of the model.

[Cannon and Schmitz] proposed using a reduced-order approximation of the full-order state estimator (4.3.9) in order to overcome implementation problems due to the complexity of the estimator. Experimental results show that, for the robot arm considered, the reduced-order compensation provides good control in the absence of modelling errors. However, changes in the tip mass lead to a rapid degradation of the closed-loop performance.

[Carusone, D'Eleuterio and Buchan] and [Carusone and D'Eleuterio] analyzed and experimentally demonstrated a state-feedback gain scheduling approach, for a 2-link flexible manipulator. To overcome the significant time variance in the dynamics of the manipulator system, the researchers propose to compute a series of fixed feedback gain matrices, $\mathbf{F}$, essentially following the procedure outlined in (4.3.5)–(4.3.14), for a number of operating points throughout the joint space. As the manipulator moves along a trajectory the gain matrix $\mathbf{F}$ is varied continuously by interpolation between the points in the joint space for which $\mathbf{F}$ has been precomputed. The feedback matrices are a function of joint positions only, not their derivatives. Therefore, changing the velocity profile for a trajectory will not require the calculation of additional gain matrices. The approach was demonstrated on a 2-link manipulator with a 2-dimensional joint space. The implementation of this

technique for a manipulator with 6 or 7 degrees of freedom and variable payload would require a very substantial amount of memory.

Feed-Forward Methods

The use of flexibility models has also been proposed in feed-forward control schemes, e.g. by [Goldenberg and Raksha] and [Bayo]. In these methods, the joint actuator torques $\mathbf{u}(t)$ required to move the robot tip along a commanded trajectory are computed from an "inverse dynamics model". In theory this can be achieved by computing $\mathbf{u}(t)$ from (3.2.15) for a given trajectory defined in terms of joint motions. The joint motions for a given trajectory $\mathbf{a}(t)$, $\dot{\mathbf{a}}(t)$ in the work space can be obtained from the inverse kinematic relationships (3.3.1) and (3.3.3). Explicit knowledge of the time-variant quantities $\mathbf{M}(\mathbf{q})$, $\mathbf{c}(\mathbf{q}, \dot{\mathbf{q}})$ and $\mathbf{k}(\mathbf{q})$, as well as $\mathbf{B}_d\mathbf{d}(t)$ if significant, is required for this scheme to work. This is a very challenging prerequisite for this methodology, in particular when flexibility models form part of $\mathbf{M}$, $\mathbf{c}$ and $\mathbf{k}$ and payloads with unknown mass properties are being manipulated. Moreover, when sensors and actuators are not collocated as in the case of vision-based control, the non-minimum phase terms of a linear robot model result in a non-causal inverse model, which indicates that the method breaks down in this case. When the full payload trajectory is not known a priori, e.g. in teleoperation or while tracking a moving object, the inverse dynamics/feed forward approach cannot be applied.

For linear systems an alternative approach referred to as input shaping has been proposed by [Singer and Seering]. In this open-loop method commands are processed by a convolution operation such that their effect on a certain vibration modes is cancelled. For example, an impulse input would be shaped into two impulses with the second delayed by one-half of the period of the vibration frequency to be avoided. In principle this method can also be extended for multiple known model frequencies. [Magee and Book] extended this method to the case of a variable frequency, which had to be measured a priori, and proposed to place the input shaping filter inside the control loop. However, it was observed by [Zuo and Wang] that the delays caused by the filter affect the stability of the closed-loop system.

Limitations of Model-Based Approaches

The efficacy of model-based approaches for the control of robots with flexible links obviously depends on the fidelity of the model used as a basis for the design. In some applications, such as large space manipulators, it is not possible to verify analytical models by test before launch and deployment of the system because of the "1-g" environment on the ground. In applications like SRMS and SSRMS, the use of model-based approaches whose stability and performance depend critically on the accuracy of the underlying model may represent an unacceptable technical risk, even if the approach is 'perfect' in every other respect.

Another factor limiting the successful application of model-based approaches to practical problems are the inherent shortcomings of the model description assumed in (4.3.5) and (4.3.6). Besides the problems of not accounting for non-linear and time-varying effects which we already discussed, and the limited fidelity of dynamics models for higher frequencies, the model can only include a limited number of degrees of freedom associated with flexibility effects in order to keep the complexity of the resulting compensator (4.3.8), (4.3.9) finite and manageable for real-time implementation.

Although methods such as Modal Cost Analysis developed by [Skelton and Hughes], and Balanced Realizations by [Moore] exist to reduce the order of a flexibility model while minimizing the effect of the reduction on its open-loop transient response, closing the loop with a reduced-order compensator gives rise to the "spillover" problem illustrated in Section 2.4 which we will now investigate in more detail.

Spillover Mechanism

To demonstrate the spillover problem caused by modal truncation in the design model, we make the simplifying assumption that the system to be controlled is linear and that a number of flexible modes are modelled perfectly by (4.3.5) – (4.3.6), but that some residual unmodelled flexible modes exist in the real system. These simplifying assumptions do not affect the general conclusion, because the

situation with regard to assuring stability will just deteriorate further when non-linearities and other modelling errors are considered on top of modal truncation.

With these assumptions the real system can be described, in modal form, as an uncoupled combination of the system model (4.3.5) –(4.3.6) and the residual unmodelled dynamics characterized by a state vector $\mathbf{x}_R$ and state-space matrices $\mathbf{A}_R, \mathbf{B}_R, \mathbf{C}_R$. We also neglect the error terms $\mathbf{d}$ and $\mathbf{e}$ which are not of consequence to this discussion and arrive a the following description for the combined system:

$$\begin{bmatrix} \dot{\mathbf{x}}_M \\ \dot{\mathbf{x}}_R \end{bmatrix} = \begin{bmatrix} \mathbf{A}_M & \mathbf{0} \\ \mathbf{0} & \mathbf{A}_R \end{bmatrix} \begin{bmatrix} \mathbf{x}_M \\ \mathbf{x}_R \end{bmatrix} + \begin{bmatrix} \mathbf{B}_M \\ \mathbf{B}_R \end{bmatrix} \mathbf{u}(t) \tag{4.3.15}$$

$$\mathbf{y} = [\mathbf{C}_M \quad \mathbf{C}_R] \begin{bmatrix} \mathbf{x}_M \\ \mathbf{x}_R \end{bmatrix} \tag{4.3.16}$$

A feedback control law (4.3.8) – (4.3.9) is designed for the combined system based on the reduced-order design model (4.3.5) – (4.3.6). The state-space equations for the closed-loop system formed by (4.3.15) – (4.3.16) and (4.3.8) – (4.3.9) has the following form:

$$\begin{bmatrix} \dot{\mathbf{x}}_M \\ \dot{\hat{\mathbf{x}}}_M \\ \dot{\mathbf{x}}_R \end{bmatrix} = \begin{bmatrix} \mathbf{A}_M & -\mathbf{B}_M\mathbf{F} & \mathbf{0} \\ \mathbf{K}\mathbf{C}_M & \mathbf{A}_M - \mathbf{B}_M\mathbf{F} - \mathbf{K}\mathbf{C}_M & \mathbf{K}\mathbf{C}_R \\ \mathbf{0} & \mathbf{B}_R\mathbf{F} & \mathbf{A}_R \end{bmatrix} \begin{bmatrix} \mathbf{x}_M \\ \hat{\mathbf{x}}_M \\ \mathbf{x}_R \end{bmatrix} \tag{4.3.17}$$

The submatrix $\begin{bmatrix} \mathbf{A}_M & -\mathbf{B}_M\mathbf{F} \\ \mathbf{K}\mathbf{C}_M & \mathbf{A}_M - \mathbf{B}_M\mathbf{F} - \mathbf{K}\mathbf{C}_M \end{bmatrix}$ of the system matrix in (4.3.17) is guaranteed to be Hurwitz by the design approach (4.3.10) – (4.3.14) [Kwakernaak and Sivan]. Stability of (4.3.17) however is not ensured due to the coupling with the residual dynamics via the "control spillover" term $-\mathbf{B}_R\mathbf{F}$ and the "observation spillover" term $\mathbf{K}\mathbf{C}_R$. This coupling with the residual dynamics via spillover can lead to instability only if both spillover terms are present (and non-zero).

4.4 Sensor Selection and Placement

Problem Definition

The selection of suitable types and numbers of sensors and the choice of location for the sensors is an important part of the design process for complex controlled systems. Although engineering judgment and trial and error are often used to determine sensor types and locations, several systematic approaches have been proposed for this design problem, in particular in the context of control (position/orientation, shape, vibration) of large flexible space structures which has provided the motivation for most studies.

Sensor Location

An introductory discussion of control/structure interactions with emphasis on the stability implications of sensor and actuator locations is provided by [Gevarter]. [Maghami and Joshi] have advocated optimizing sensor and actuator locations for a criterion linked to the location of transmission zeros in the complex plane. This approach reduces the problem of sensor/actuator positioning to a solution of a non-linear programming optimization. The discrete measurements and control forces are approximated by spatially continuous functions in order to avoid the discontinuity problems when sensors and actuators are reconfigured within the structure. The structure is then divided into several sections, each allocated with a number of sensors and actuators. With the location of the sensors and actuators as design variables, a non-linear programming problem is posed to minimize a performance index. The performance index is chosen such that, when optimized, the transmission zeros of the system are moved farther to the left of the imaginary axis. In example it is shown that the sensors and actuators can be positioned such that the transmission zeros of the system, particularly those close to the imaginary axis, are moved considerably into the left-half plane of the complex frequency domain.

[Chen and Seinfeld] have proposed an optimization approach in which optimal locations for sensors are computed from a finite set of possible locations, using an integer programming technique. [Yang and Lee] have demonstrated the

simultaneous optimization of sensor and actuator locations and feedback gains for a relatively simple vibrating beam problem. Several researchers use metrics based on system observability as a criterion to optimize sensor locations. [Lim, T] proposed to position sensors such as to minimize the spectral condition number of the Hankel matrix of the system, while [Lim, K] advocates using observability and controllability Gramians as an optimization criterion. [Baruh and Choe] used a measure based on the "quality of modal coordinate extraction" as a criterion for sensor placement and proposed "modal filters" to address the problem of modelling errors. [Juang and Rodriguez] used the steady-state solution of the optimal control and estimation problem to study the actuator and sensor locations for space structures.

[Schulz and Heimbold] proposed a method for the integrated design of sensor/actuator positions and feedback gains for control of flexible structures based on maximizing the energy dissipation by the control system. [Barker and Jaquot] determines optimal sensor positions for output feedback control of flexible structures using the reduction of observation spillover as a criterion.

Number of Sensors

[DeLorenzo] proposed a method of successive approximations in which the number of sensors and actuators on a flexible structure is reduced step-by-step by dropping the least effective devices. The effectiveness of a device is assessed by a criterion based on an optimal feedback control approach. [Sepulveda and Schmitt] proposed to locate sensors by a 'brute force' multi-objective constraint optimization approach involving mass and number of sensors in the objective function. [Skelton and Chiu] and [Norris and Skelton] considered a system-order reduction approaches reducing the number of sensors and actuators from a large initial set so as to minimize the effect on a metric of the control performance.

[Wu, Rice and Juang] propose to select reduced-order models for control design and to determine the minimum number of sensors and actuators based on observability and controllability. The observability of continuum systems as a function of sensor type and location was analyzed by [de Lafontaine and Stieber].

When applied to a flexible beam, the conditions require only two types of sensors (e.g. displacement and rotation) located anywhere on the beam (where the motion is not constrained) to ensure observability of all modes (infinite number). Only one sensor is necessary for observability of all modes when it is located at the boundary, e.g. a displacement sensor at a free boundary.

Shortcomings

A shortcoming common to most of the techniques discussed above is that they are based on the assumption that the structure can be modelled as a time-invariant linear system. It is further commonly assumed that an accurate explicit model is known on which the analytical techniques can be based.

The majority of the methods discussed treat the sensor selection and placement problem "open-loop" i.e. they do not consider that the sensors are integral part of a closed-loop system, and that, ultimately, the closed-loop system performance matters. The methods which do consider this important aspect are all based on model-based control and therefore do not necessarily result in sensor configurations suitable for stable robust control.

Most of the methods assume that the sensor positions and the number of sensors can be chosen arbitrarily on a large flexible structure. None considers the constraints on sensor locations inherent in the robotics problem which add considerable challenges over the "spacecraft" problem.

CHAPTER 5

INSTRUMENTATION DESIGN AND SENSOR FUSION CONCEPT

5.1 Overview

In this Section we will develop a theoretical concept for the systematic selection and placement of sensors suitable for the robust control of complex systems, and a sensor data fusion concept for the integration of other sensors necessary to achieve required performance levels.

The theoretical concept is quite general and its application is not limited to the space robotics problem, or mechanical systems in general. Throughout this Section, the development of the concept is carried out for both continuous-time and discrete-time (or sampled-data) systems in parallel.

The proposed concept is based on the theory of hyperstability which is introduced in Section 5.2. On that foundation, the instrumentation design concept is developed in Section 5.3, and the sensor fusion concept in Section 5.4 The overall methodology is summarized in a step-by-step procedural manner in Section 5.5.

5.2 The Concept of Hyperstability

Background

The concept of hyperstability was introduced by [Popov.1] in 1963 as a generalization of absolute stability. As an introduction to this concept we will briefly review the definition of absolute stability which uses the well-known property of global asymptotic stability as defined in [Hahn].

Definition 5.2.1. Absolute Stability: A scalar closed-loop system as shown in Figure 5.2.1 is called absolutely stable in a sector $[0, K]$, *if the system is globally asymptotically stable for all feedback functions* $F(y)$ *lying within the sector* $[0, K]$.

For this definition it is assumed that the function $F(y) \in \mathbb{R}$ is a single-valued function defined for $-\infty < y < \infty$ with the property $F(y = 0) = 0$. As a result of the sector condition on $F(y)$ per Definition 5.2.1, which is also illustrated in Figure 5.2.1, $F(y)$ satisfies the conditions:

$$\begin{aligned} 0 \leq F(y) \leq Ky \quad &\text{if } y \geq 0 \\ 0 \geq F(y) \geq Ky \quad &\text{if } y < 0. \end{aligned} \tag{5.2.1}$$

These two conditions can be combined to:

$$0 \leq F(y)y \leq Ky^2 \tag{5.2.2}$$

After introducing the variable $b = F(y)$ per Figure 5.2.1, (5.2.2) can also be expressed in the form

$$0 \leq by \leq Ky^2 \tag{5.2.3}$$

A first step in generalizing the concept of absolute stability is to consider operations in the feedback path which satisfy (5.2.3) only in the mean. When "averaging" is performed by temporal integration, and the sector condition is extended to the limit $K \to \infty$, the following condition ensues from (5.2.3):

$$\int_{t_0}^{t_1} b(t)y(t)dt \geq 0 \quad \forall\ t_1 > t_0 \tag{5.2.4}$$

This form of integral inequality condition plays a central role in the theory of hyperstability and has been called the Popov Integral Inequality in [Landau].

Definition of Hyperstability

We will now review a definition of hyperstability of a system given by [Popov.2], which is no longer tied to the feedback system structure of the introductory example shown in Figure 5.2.1. Continuous and discrete-time systems are covered at the same time. The equations pertaining to continuous systems are identified by suffix '*c*' in the equation number, and equations for discrete-time systems by suffix '*d*'. The system $\mathcal{S}$ under consideration is assumed to admit a state-space representation. The evolution of its state vector $\mathbf{x}$ then can be described by the following differential equations, or difference equations, respectively:

$$\dot{\mathbf{x}}(t) = \mathbf{g}(\mathbf{x}(t), \mathbf{u}(t), t), \tag{5.2.5c}$$

$$\mathbf{x}(k+1) = \mathbf{g}(\mathbf{x}(k), \mathbf{u}(k), k), \tag{5.2.5d}$$

Here $\mathbf{u}$ denotes the input vector and $\mathbf{g}$ is a vector function. This system description covers non-linear and time variant systems, such as (3.2.16). It is assumed that $\mathbf{x}$ and $\mathbf{u}$ exist $\forall\ t \geq t_0$ or $k \geq k_0$ and, in the continuous case, that $\mathbf{g}$ and $\mathbf{u}(t)$ are piecewise continuous functions $\forall\ t \geq t_0$.

We associate the following functions with the system $\mathcal{S}$:

$$\eta(t_0, t_1) = [\varphi(\mathbf{x}(t), t)]_{t_0}^{t_1} + \int_{t_0}^{t_1} \nu(\mathbf{x}(t), \mathbf{u}(t))dt \tag{5.2.6c}$$

$$\eta(k_0, k_1) = [\varphi(\mathbf{x}_k, k)]_{k_0}^{k_1+1} + \sum_{k=k_0}^{k_1} \nu(\mathbf{x}_k, \mathbf{u}_k) \tag{5.2.6d}$$

It is assumed that the scalar functions φ and ν exist $\forall\ t \geq t_0$ or $k \geq k_0$.

Definition 5.2.2 Hyperstability: The system (5.2.5c/d) with the associated function (5.2.6c/d) is called hyperstable if there exist positive constants[1] $\alpha > 0$, $\beta_0 \geq 0$,

[1] This definition can be further generalized by defining $\alpha, \beta_0, \beta_1, \gamma$ and ξ as elements of a class of functions of generalized norms, as described by [Popov.2], i.e. $\alpha(\mathbf{x})$ instead of $\alpha\|\mathbf{x}\|$. For our purposes this generalization is not necessary and we assume the use of the Euclidean norm throughout.

$\beta_1 > 0$, $\gamma > 0$, $\xi > 0$ *such that the following two properties are satisfied:*

(1) For every interval $[t_0, t_1]$, $(t_1 > t_0)$, *or* $[k_0, k_1]$, $(k_1 > k_0)$ *and for every constant* $\beta_0 \geq 0$ *satisfying*

$$\eta(t_0, t) \leq \beta_0^2 \quad \forall\ t \in [t_0, t_1] \tag{5.2.7c}$$

$$\eta(k_0, k) \leq \beta_0^2 \quad \forall\ k \in [k_0, k_1], \tag{5.2.7d}$$

the following inequality also holds:

$$\alpha\|\mathbf{x}(t)\| \leq \beta_0 + \beta_1\|\mathbf{x}(t_0)\| \ \forall\ t \in [t_0, t_1] \tag{5.2.8c}$$

$$\alpha\|\mathbf{x}(k)\| \leq \beta_0 + \beta_1\|\mathbf{x}(k_0)\| \ \forall\ k \in [k_0, k_1] \tag{5.2.8d}$$

(2) For every interval $[t_0, t_1]$, $(t_1 > t_0)$, *or* $[k_0, k_1]$, $(k_1 > k_0)$ *the following inequality is satisfied* $\forall\ t \in [t_0, t_1]$ *or* $\forall\ k \in [k_0, k_1]$*:*

$$\eta(t_0, t) \geq -(\gamma^2\|\mathbf{x}(t_0)\|)^2 - \xi\|\mathbf{x}(t_0)\| \sup_{t_0 \leq \tau \leq t} \alpha\|\mathbf{x}(\tau)\| \tag{5.2.9c}$$

$$\eta(k_0, k) \geq -\gamma^2\|\mathbf{x}(k_0)\| - \xi\|\mathbf{x}(k_0\| \max_{k_0 \leq i \leq k} \alpha\|\mathbf{x}(i)\| \tag{5.2.9d}$$

It follows immediately from (5.2.8c/d) that hyperstability does not imply asymptotic stability. However, (5.2.8c/d) implies that the norm of the state vector of a hyperstable system is bounded throughout its trajectory by the norm of the initial conditions and a constant. Based on (5.2.8c/d) the following condition for hyperstability can be derived as shown in Appendix C.1:

$$\alpha^2\|\mathbf{x}(t)\|^2 \leq \eta(t_0, t) + \beta_1^2\|\mathbf{x}(t_0)\|^2 \ \forall\ t > t_0 \tag{5.2.10c}$$

$$\alpha^2\|\mathbf{x}(k)\|^2 \leq \eta(k_0, k) + \beta_1^2\|\mathbf{x}(k_0)\|^2 \ \forall\ k > k_0 \tag{5.2.10d}$$

Illustration of the Hyperstability Concept

We will now illustrate the application of the hyperstability concept for the stability analysis in a simple example using a continuous-time linear system described by state-space equations similar to (4.3.5), (4.3.6):

$$\dot{\mathbf{x}}(t) = \mathbf{A}\mathbf{x}(t) + \mathbf{B}\mathbf{u}(t) \tag{5.2.11}$$

We associate the following integral relation, which is similar in form to (4.3.10), with the system:

$$\eta(t_0, t_1) = \int_{t_0}^{t_1} (\mathbf{x}^T \mathbf{Q} \mathbf{x} + \mathbf{u}^T \mathbf{R} \mathbf{u}) dt \tag{5.2.12}$$

with positive definite matrices $\mathbf{Q} > \mathbf{0}$ and $\mathbf{R} > \mathbf{0}$.

If the system and the associated integral satisfy (5.2.7c) we have

$$\int_{t_0}^{t_1} (\mathbf{x}^T \mathbf{Q} \mathbf{x} + \mathbf{u}^T \mathbf{R} \mathbf{u}) dt \leq \beta_0^2 \ \forall \ t_1 > t_0 \tag{5.2.13}$$

Based on these conditions we can draw conclusions about the stability of the system (5.2.11) without direct reference to the properties of matrices $\mathbf{A}, \mathbf{B}$ using the following arguments: It follows from (5.2.12) that $\dot{\eta} \geq 0 \ \forall t_1 > t_0$. Hence (5.2.13) implies

$$\lim_{t \to \infty} (\mathbf{x}^T \mathbf{Q} \mathbf{x} + \mathbf{u}^T \mathbf{R} \mathbf{u}) = 0. \tag{5.2.14}$$

With $\mathbf{Q} > \mathbf{0}$, $\mathbf{R} > \mathbf{0}$ we can further conclude:

$$\begin{aligned} \lim_{t \to \infty} \mathbf{x}(t) &= \mathbf{0} \quad \forall \ \mathbf{x}(t_0) \\ \lim_{t \to \infty} \mathbf{u}(t) &= \mathbf{0} \end{aligned} \tag{5.2.15}$$

Hence (5.2.8c) is also satisfied, as is (5.2.9c) due to $\eta \geq 0 \ \forall \ t \geq t_0$ per (5.2.13). A system with these properties is termed "asymptotically hyperstable" by [Popov.2], and is also globally asymptotically stable in the sense of Lyapunov [Hahn].

Hyperstable Blocks

In order to focus our analysis towards sensors we will now consider systems described by (5.2.5c/d) which are augmented by an output equation of the form

$$\mathbf{y}(t) = \mathbf{h}(\mathbf{x}(t), \mathbf{u}(t), t) \tag{5.2.16c}$$

$$\mathbf{y}(k) = \mathbf{h}(\mathbf{x}(k), \mathbf{u}(k), k). \tag{5.2.16d}$$

The vector function $\mathbf{h}(\cdot)$ describes the function of sensors which map the system states and inputs into an output vector $\mathbf{y}$. The function $\mathbf{h}$ is assumed to be

piecewise continuous in the continuous-time case. Based on the output vector $\mathbf{y}$ we can now define "hyperstable blocks" following [Popov.2] when the system $\mathcal{S}$ can be associated with a special form of the function (5.2.6c/d).

Definition 5.2.3 Hyperstable Block: The system (5.2.5c/d) forms a hyperstable block if it is hyperstable with the associated function

$$\eta(t_0, t_1) = \int_{t_0}^{t_1} \mathbf{u}^T(t)\mathbf{y}(t)dt \tag{5.2.17c}$$

$$\eta(k_0, k_1) = \sum_{k=k_0}^{k_1} \mathbf{u}^T(k)\mathbf{y}(k). \tag{5.2.17d}$$

From the definition of the associated integral/sum based on the inner product of the input and output vectors $\mathbf{u}$ and $\mathbf{y}$, it is obvious that a hyperstable block has to have the same number of inputs and outputs. In the remainder of this Section we will assume that the number of inputs and outputs are identical.

Hyperstable blocks as defined by (5.2.5c/d), (5.2.16c/d) and (5.2.17c/d) have certain properties related to other stability concepts. It follows from (5.2.8c/d) that hyperstable blocks have bounded output, provided that the input remains bounded, in accordance with (5.2.7c/d) and (5.2.9c/d). Hence, a hyperstable block is stable in the bounded-input bounded-output (BIBO) sense. In the special case of an autonomous system with $\mathbf{u} = \mathbf{0}$, $\eta = 0$ follows from (5.2.17c/d), and condition (5.2.7c/d) is satisfied with $\beta_0 = 0$. It then follows from (5.2.8c/d) that the norm of the trajectory $\mathbf{x}$ of the system (5.2.5c/d) is bounded by the initial conditions. Hence, a hyperstable block with $\mathbf{u} = \mathbf{0}$ is always stable in the sense of Lyapunov [Hahn].

Combination of Hyperstable Blocks

A key element of the hyperstability concept is the possibility of determining stability properties of systems composed of a combination of subsystems, based on the hyperstability properties of the individual subsystems. It is fairly easy to recognize that the parallel combination of two hyperstable blocks $\mathcal{S}_1$ and $\mathcal{S}_2$ with

common inputs $\mathbf{u}$ and combined outputs $\mathbf{y} = \mathbf{y}_{\mathcal{S}1} + \mathbf{y}_{\mathcal{S}2}$ as shown in figure 5.2.2, results in a hyperstable overall system with the associated integral/sum

$$\eta(t_0, t_1) = \int_{t_0}^{t_1} \mathbf{u}^T(\mathbf{y}_{\mathcal{S}1} + \mathbf{y}_{\mathcal{S}2})dt = \eta_{\mathcal{S}1}(t_0, t_1) + \eta_{\mathcal{S}2}(t_0, t_1) \tag{5.2.18c}$$

$$\eta(k_0, k_1) = \sum_{k=k_0}^{k_1} \mathbf{u}^T(\mathbf{y}_{\mathcal{S}1} + \mathbf{y}_{\mathcal{S}2}) = \eta_{\mathcal{S}1}(k_0, k_1) + \eta_{\mathcal{S}2}(k_0, k_1). \tag{5.2.18d}$$

It is quite remarkable, though, that also the feedback connection of two hyperstable blocks $\mathcal{S}_1$ and $\mathcal{S}_2$ as shown in Figure 5.2.3, results in a hyperstable overall system. The feedback connection is defined for both continuous and discrete-time by the relations

$$\begin{aligned} \mathbf{u}_{\mathcal{S}1} &= \mathbf{u} - \mathbf{y}_{\mathcal{S}2} \\ \mathbf{u}_{\mathcal{S}2} &= \mathbf{y}_{\mathcal{S}1} \\ \mathbf{y} &= \mathbf{y}_{\mathcal{S}1}. \end{aligned} \tag{5.2.19}$$

In the continuous-time case the integral relationship associated with the overall system is given by:

$$\begin{aligned} \eta(t_0, t_1) &= \int_{t_0}^{t_1} \mathbf{y}^T \mathbf{u} dt \\ &= \int_{t_0}^{t_1} \mathbf{y}_{\mathcal{S}1}^T \mathbf{u} dt \\ &= \int_{t_0}^{t_1} \mathbf{y}_{\mathcal{S}1}^T (\mathbf{u}_{\mathcal{S}1} + \mathbf{y}_{\mathcal{S}2}) dt \\ &= \int_{t_0}^{t_1} (\mathbf{y}_{\mathcal{S}1}^T \mathbf{u}_{\mathcal{S}1} + \mathbf{u}_{\mathcal{S}2}^T \mathbf{y}_{\mathcal{S}2}) dt \\ &= \eta_{\mathcal{S}1}(t_0, t_1) + \eta_{\mathcal{S}2}(t_0, t) \end{aligned} \tag{5.2.20c}$$

Remarkably, this is the same result as for the parallel connection, (5.2.18c) which implies that the overall closed-loop system per Figure 5.2.3 is hyperstable if both

subsystems are hyperstable. The relationship for the discrete-time case can be derived in a similar manner, resulting the same conclusion based on the following expression associated with the closed-loop feedback system which is identical to (5.2.18d):

$$\eta(k_0, k_1) = \eta_{S1}(k_0, k_1) + \eta_{S2}(k_0, k_1) \tag{5.2.20d}$$

Properties

We will now summarize some of the properties of hyperstable systems and blocks. These properties hold equally for continuous and discrete-time systems. The term "hyperstability in the large" (i.t.l.) will be defined in Section 5.3.

Property 1: Any hyperstable system is bounded-input-bounded-output (BIBO) stable.

Property 2: Any hyperstable system with zero input ($\mathbf{u} = \mathbf{0}$) is globally stable in the sense of Lyapunov.

Property 3: Hyperstable blocks have the same number of inputs and outputs.

Property 4: The parallel combination (see Figure 5.2.2) of two blocks which are hyperstable (i.t.l.) forms a block which is hyperstable (i.t.l.).(Modifications in brackets apply jointly.)

Property 5: The feedback combination (see Figure 5.2.3) of a hyperstable block and another block which is hyperstable (i.t.l) forms a hyperstable system.

Property 6: The feedback combination of two blocks which are hyperstable in the large forms a system which is hyperstable in the large.

Property 7: Linear time-invariant finite-order systems are (asymptotically) hyperstable if and only if they have a (strictly) positive real transfer matrix. (Modifications in brackets apply jointly.)

Property 8: Linear time-invariant finite-order hyperstable systems are minimum phase.

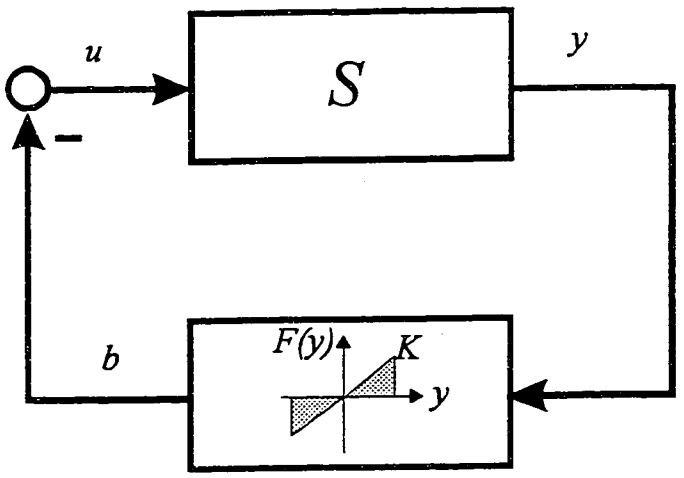

Figure 5.2.1: Feedback System for Definition of Absolute Stability

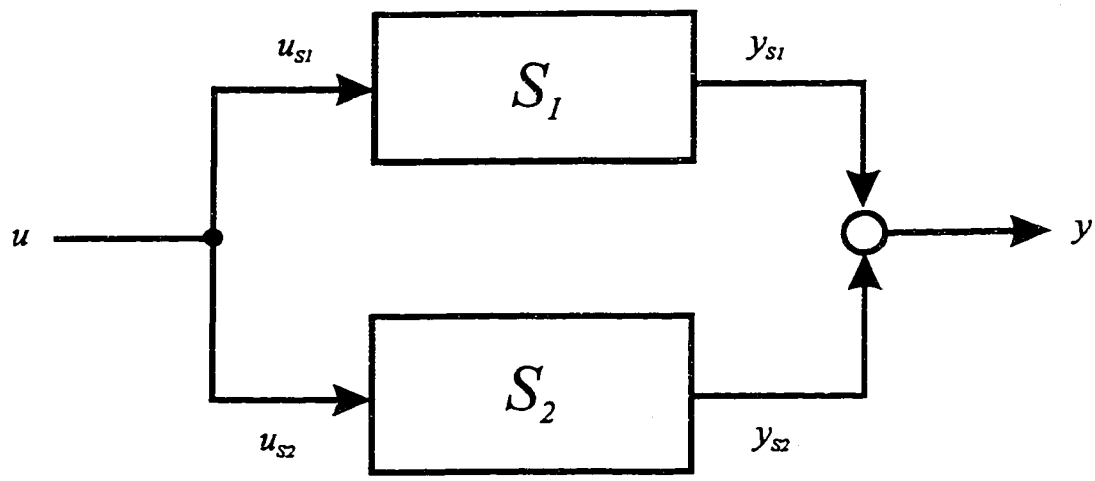

Figure 5.2.2: Parallel Connection of two Systems

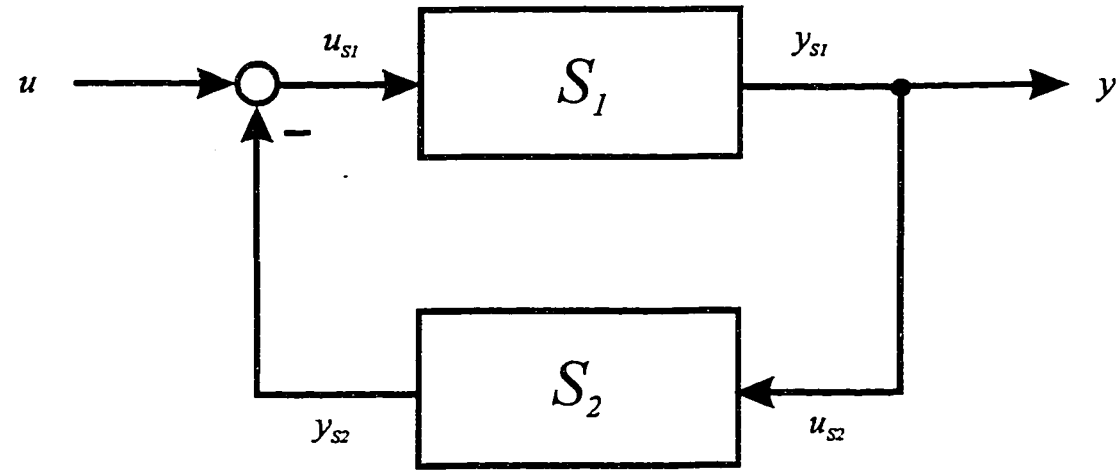

Figure 5.2.3: Feedback Connection of two Systems

5.3 Instrumentation Design Concept

Objective

Our objective is to establish criteria for the selection of sensors for complex systems such that they collectively enable control of the system by relatively simple, model-free control algorithms. We specifically include the possibility of intelligent control, such as rule-based and fuzzy logic control.

The starting point for our considerations is the system of Figure 5.3.1, showing a robotic system with associated sensors and actuators, in a closed loop system configuration with a control function $\mathcal{C}$ and the interconnection $\mathbf{u} = -\mathbf{b}$. The discussion in this Section applies equally to many other systems, and the reference to a robotic system in Figure 5.3.1 is intended as an example relevant to this study, rather than to restrict the generality of our development.

The robotic system and its sensor and actuators can be combined to a system $\mathcal{S}$ as indicated in Figure 5.3.1. Our goal is to find a set of sensors which will make $\mathcal{S}$ "easy to control". The development of the instrumentation design concept proceeds in two stages: First, a preliminary concept is developed under certain assumptions. Then, the concept is generalized and the initial assumptions are relaxed in order to extend the practical applicability of the concept.

Initial Assumptions

We assume, for the moment, that both $\mathcal{C}$ and $\mathcal{S}$ are "square" systems, i.e. that their input and output vectors are of the same dimension: $\mathbf{b} \in \mathbb{R}^l$, $\mathbf{u} \in \mathbb{R}^l$, $\mathbf{y} \in \mathbb{R}^l$. Later, in Section 5.4, this restrictive assumption will be relaxed. We further assume that $\mathcal{C}$ is a hyperstable block admitting a state-space description of the general form

$$\dot{\mathbf{x}}_{\mathcal{C}}(t) = \mathbf{g}_{\mathcal{C}}(\mathbf{x}_{\mathcal{C}}(t), \mathbf{y}(t), t) \tag{5.3.1c}$$

$$\mathbf{b}(t) = \mathbf{h}_{\mathcal{C}}(\mathbf{x}_{\mathcal{C}}(t), \mathbf{y}(t), t) \tag{5.3.2c}$$

$$\mathbf{x}_{\mathcal{C}}(k+1) = \mathbf{g}_{\mathcal{C}}(\mathbf{x}_{\mathcal{C}}(k), \mathbf{y}(k), k) \tag{5.3.1d}$$

$$\mathbf{b}(k) = \mathbf{h}_{\mathcal{C}}(\mathbf{x}_{\mathcal{C}}(k), \mathbf{y}(k), k), \tag{5.3.2d}$$

with an associated integral relation

$$\eta_{\mathcal{C}}(t_0, t_1) = \int_{t_0}^{t_1} \mathbf{b}^T(t)\mathbf{y}(t)dt \tag{5.3.3c}$$

$$\eta_{\mathcal{C}}(k_0, k_1) = \sum_{k=k_0}^{k_1} \mathbf{b}^T(k)\mathbf{y}(k). \tag{5.3.3d}$$

Assuming that $\mathcal{C}$ is a hyperstable block, implies that (5.3.1)–(5.3.3) are subject to the conditions (5.2.7)–(5.2.10) arising from Definition 5.2.2.

These conditions are not very restrictive as $\mathcal{C}$ is not fixed or given but is chosen as part of the overall design process. In fact, it is proposed to make the above conditions the basis of the instrumentation design for $\mathcal{S}$, in the sense that we consider $\mathcal{S}$ "easy to control", if all that is required to stabilize it, in the BIBO sense, is hyperstable feedback $\mathcal{C}$. In other words, we are looking to find a set of sensors for $\mathcal{S}$ such that the system will be stabilized by any hyperstable control function $\mathcal{C}$.

Hyperstable Feedback Systems

Adaptive control algorithms often are hyperstable by design, and constructive methods exist for hyperstability design of various conventional and intelligent control algorithms. We will investigate a general framework for hyperstable sensor fusion and control in Section 5.4.

A number of approaches for the synthesis of hyperstable feedback systems have been published over the past decade. Two very recent papers by [Geromel and Gapski] and [Turan, Safonov and Huang] indicate a continuing interest in this topic by the controls community. Appendix B describes a methodology for the synthesis of hyperstable feedback algorithms which was developed during this study. This method is based on the design approach outlined in Section 4.3 equations (4.3.1) – (4.3.9) and constructs a state estimator with the property of rendering the feedback system hyperstable.

Feedback algorithms not specifically designed for hyperstability can be tested

for this property. The hyperstability analysis of fuzzy logic-based control functions is discussed by [Marin and Titli] and [Bretthauer and Opitz].

Definition of Hyperstability Sensors

Based on the earlier discussion on feedback connection of hyperstable blocks in Section 5.2, we may conclude that sufficient conditions for the sensor selection are given by the conditions for hyperstability of $\mathcal{S}$, because hyperstability of $\mathcal{S}$ in conjunction with a hyperstable block $\mathcal{C}$ per the assumptions would ensure BIBO stability of the closed loop system.

However, hyperstability of $\mathcal{S}$ is an unnecessarily strict condition as it requires that the state-vectors of both blocks $\mathcal{S}$ and $\mathcal{C}$ remain bounded. The condition can be relaxed and, at the same time, extended to a more general class of systems $\mathcal{S}$ by not requiring the boundedness of a state-vector, but only the boundedness of the inputs $\mathbf{u}$ and outputs $\mathbf{y}$ of system $\mathcal{S}$.

For this case, the block $\mathcal{S}$ may be described by an input/output relation

$$\mathbf{y}(t) = \mathcal{S} < \mathbf{u}(t) > \tag{5.3.4c}$$

$$\mathbf{y}(k) = \mathcal{S} < \mathbf{u}(k) > \tag{5.3.4d}$$

where $\mathbf{u}$ and $\mathbf{y}$ are piecewise continuous vector functions defined for $t \geq t_0$ ($k \geq k_0$), and $\mathcal{S} < \cdot >$ is an operator acting on the input $\mathbf{u}$. Reference to a state vector of the system is no longer required.

We will now determine conditions on the block $\mathcal{S}$ which will ensure the hyperstability of the overall system of Figure 5.3.1. According to Definition 5.2.2 and condition (5.2.10c/d) the state vector $\mathbf{x}_C$ is bounded by the following expression:

$$\alpha^2 \|\mathbf{x}_C(t)\|^2 \leq \eta_C(t_0, t) + \beta_1^2 \|\mathbf{x}_C(t_0)\|^2 \leq \beta_0^2 + \beta_1^2 \|\mathbf{x}_C(t_0)\|^2 \ \forall\ t > t_0 \tag{5.3.5c}$$

$$\alpha^2 \|\mathbf{x}_C(k)\|^2 \leq \eta_C(k_0, k) + \beta_1^2 \|\mathbf{x}_C(k_0)\|^2 \leq \beta_0^2 + \beta_1^2 \|\mathbf{x}_C(k_0)\|^2 \forall k > k_0 \tag{5.3.5d}$$

For the bound to exist, η_C must be finite. Based on (5.3.3c/d) and the interconnection $\mathbf{u} = -\mathbf{b}$ per Figure 5.3.1 the following sufficient condition on block $\mathcal{S}$ arises

for the bound to exist, and hence for hyperstability of the closed-loop system:

$$\int_{t_0}^{t_1} \mathbf{u}^T(t)\mathbf{y}(t)dt \geq -\beta_0^2 \ \forall t_1 \geq t_0 \tag{5.3.6c}$$

$$\sum_{k=k_0}^{k_1} \mathbf{u}^T(k)\mathbf{y}(k) \geq -\beta_0^2 \ \forall k_1 \geq k_0 \tag{5.3.6d}$$

where β_0^2 is a finite, non-negative constant.

Based on this condition we can now formally define the concept of "hyperstability sensors" introduced by [Stieber, Vukovich and Petriu] and [Stieber, Petriu and Vukovich.2].

Definition 5.3.1 Hyperstability Sensors: A set of sensors providing a set of measurements $\mathbf{y}$ *of the outputs of a system* $\mathcal{S}$ *described by the input/output relation (5.3.4c/d) and excited by inputs* $\mathbf{u}$ *is called a set of hyperstablility sensors iff the measurements* $\mathbf{y}$ *satisfy condition (5.3.6c/d).*

Condition (5.3.6c/d) is a function of the input-output inner product (IOP) $\mathbf{u}^T\mathbf{y}$ of block $\mathcal{S}$, which in turn is a function of the sensors chosen to generate the output vector $\mathbf{y}$. When $\mathbf{y}$ represents hyperstability sensors, the block $\mathcal{S}$ as defined in (5.3.4c/d) is "hyperstable in the large" as defined by [Popov.2]. This implies that it has a certain quality of "passivity" or "positivity" in the sense that the integral over the IOP has a lower bound. Electrical circuits and mechanical systems can satisfy the condition if there is limited energy stored in them initially ($t = t_0$), provided the "right" outputs are selected. Quantities related to internal energy are often a good choice for β_0^2 in (5.3.6c/d) when dealing with electromechanical systems.

Role of Actuators

A concept similar to the hyperstability sensors can also be established for actuators and applied to the simultaneous selection/design of a sensor/actuator configuration for a system per Figure 5.3.1. This is discussed in [Stieber], [Stieber, Petriu and Vukovich.1] and leads to a "dual" problem in terms of the associated mathematical formulations.

We will not further pursue this possibility and consider the actuators given or fixed by the constraints imposed by the system design process. We will rather aim at achieving the required input/output behaviour for the system purely by judicious selection of the sensors.

Hyperstability Sensors for Linear Systems

The sufficient conditions (5.3.6c/d) are valid for general nonlinear systems, and some insight into the physics of the problem is usually required to use them for the selection of hyperstability sensors as they do not, by themselves, offer much guidance in that regard. In the case, though, in which the system can be meaningfully linearized, e.g. for flexible structures with small elastic deformations, it is possible to find explicit conditions for hyperstability sensors. The linearization of the system $\mathcal{S}$ can be expressed in the form of state-space equations (5.3.7c/d) and (5.3.8c/d) with constant system, input, output, and throughput matrices $\mathbf{A}, \mathbf{B}, \mathbf{C}$ and $\mathbf{D}$. In many cases of practical interest we have $\mathbf{D} = \mathbf{0}$.

$$\dot{\mathbf{x}}_{\mathcal{S}}(t) = \mathbf{A}\mathbf{x}_{\mathcal{S}}(t) + \mathbf{B}\mathbf{u}(t) \tag{5.3.7c}$$

$$\mathbf{y}(t) = \mathbf{C}\mathbf{x}_{\mathcal{S}}(t) + \mathbf{D}\mathbf{u}(t) \tag{5.3.8c}$$

$$\mathbf{x}_{\mathcal{S}}(k+1) = \mathbf{A}\mathbf{x}_{\mathcal{S}}(k) + \mathbf{B}\mathbf{u}(k) \tag{5.3.7d}$$

$$\mathbf{y}(k) = \mathbf{C}\mathbf{x}_{\mathcal{S}}(k) + \mathbf{D}\mathbf{u}(k) \tag{5.3.8d}$$

For the following analysis it is required that the linearized system (5.3.7c/d) and (5.3.8c/d) be time-invariant and completely controllable and observable. A necessary and sufficient condition for hyperstability of the linearized system (5.3.7c/d) and (5.3.8c/d) is the existence of a symmetric positive definite matrix $\mathbf{S} = \mathbf{S}^T > \mathbf{0}$ satisfying the Lyapunov equation and other algebraic relations (5.3.9c/d)–(5.3.11c/d), with matrices $\mathbf{L}$ and $\mathbf{N}$ arbitrary and of appropriate dimensions:

$$\mathbf{S}\mathbf{A} + \mathbf{A}^T\mathbf{S} = -\mathbf{L}\mathbf{L}^T \tag{5.3.9c}$$

$$\mathbf{B}^T\mathbf{S} + \mathbf{N}^T\mathbf{L}^T = \mathbf{C} \tag{5.3.10c}$$

$$\mathbf{D} + \mathbf{D}^T = \mathbf{N}^T\mathbf{N} \tag{5.3.11c}$$

$$\mathbf{A}^T\mathbf{S}\mathbf{A} - \mathbf{S} = -\mathbf{L}\mathbf{L}^T \tag{5.3.9d}$$

$$\mathbf{B}^T\mathbf{S}\mathbf{A} - \mathbf{C} = -\mathbf{N}^T\mathbf{L}^T \tag{5.3.10d}$$

$$\mathbf{B}^T\mathbf{S}\mathbf{B} - (\mathbf{D}^T + \mathbf{D}) = -\mathbf{N}^T\mathbf{N} \tag{5.3.11d}$$

These conditions are known as the Kalman-Yakubovich-Lemma [Popov.2] or the Positive-Real-Lemma [Anderson.2]. A derivation based on Definition 5.2.2 of hyperstability is provided in Appendix C.2.

Explicit conditions for hyperstability sensors as a function of the system characteristics and known constraints are obtained by solving (5.3.9c/d)–(5.3.11c/d) for the "free" parameters of $\mathbf{B}, \mathbf{C}$ and $\mathbf{D}$. This can sometimes be done symbolically as demonstrated in Appendix A, but numerical solutions are often required.

The "linear" conditions (5.3.9c/d) – (5.3.11c/d) and the "nonlinear" conditions (5.3.6c/d) are to some extent complementary. When the system can be linearized, conditions (5.3.9c/d) – (5.3.11c/d) provide explicit necessary conditions for hyperstability sensors and consequently for assuring asymptotic stability of the closed-loop system under feedback $\mathcal{C}$. But even when a linearization exists, the sufficient condition (5.3.6c/d) is still useful to gain physical insight and to provide the comfort of BIBO stability beyond the range of validity of assumptions on linearity and time-invariance.

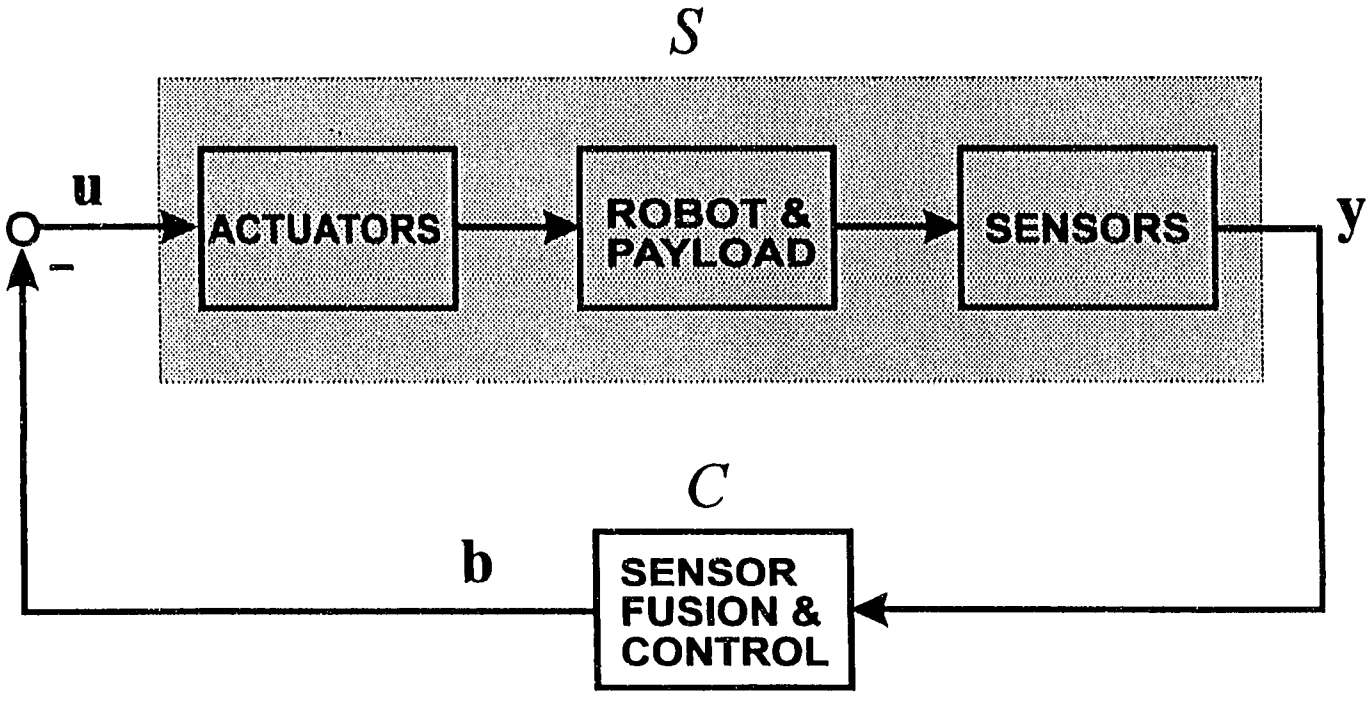

Figure 5.3.1: Partitioning of System for Basic Hyperstability Concept

5.4 Sensor Fusion Concept

Performance Sensors

While hyperstability sensors play a key role in our instrumentation concept, its applicability would be quite limited if *all* sensors were required to be hyperstability sensors per condition (5.3.6c/d). Therefore we now consider the integration of "other" sensors into the system. As these sensors are usually needed to achieve the performance requirements for the closed-loop system, we call them "performance sensors" to distinguish them from the hyperstability sensors. There are no conditions placed on the choice of the performance sensors and they are selected by standard principles of systems engineering. The measurements of the set of $m \geq 0$ performance sensors are combined to a measurement vector

$$\mathbf{z} = [z_1 \dots z_m]^T, \quad \mathbf{z} \in \mathbb{R}^m.$$

This definition also applies to sampled-data measurements. In the continuous-time case, the $z_i(t)$ are piecewise continuous functions defined for $t \geq t_0$. The system $\mathcal{S}$ to be controlled now has an output vector $\sigma \in \mathbb{R}^{l+m}$ defined by:

$$\sigma(t) = \begin{bmatrix} \mathbf{y}(t) \\ \mathbf{z}(t) \end{bmatrix} \tag{5.4.1c}$$

$$\sigma(k) = \begin{bmatrix} \mathbf{y}(k) \\ \mathbf{z}(k) \end{bmatrix} \tag{5.4.1d}$$

Our earlier definition (5.3.4c/d) of the system $\mathcal{S}$ is amended to generate this vector by the general input/output relation

$$\sigma(t) = \mathcal{S} < \mathbf{u}(t) > \tag{5.4.2c}$$

$$\sigma(k) = \mathcal{S} < \mathbf{u}(k) > . \tag{5.4.2d}$$

The system $\mathcal{S}$ is no longer required to be "square" with an equal number of inputs and outputs, but has l inputs and $l+m$ outputs ($l > 0$, $m \geq 0$).

Sensor Fusion Concept

All sensors may be used for feedback control as indicated in the block diagram Figure 5.4.1, which reflects the classification of sensors into performance sensors

and hyperstability sensors. The measurements of the performance sensors are integrated with those of the hyperstability sensors and system input commands $\mathbf{w}$ by a data fusion and control vector function $\mathcal{C} \in \mathbb{R}^l$:

$$\mathbf{u}(t) = \mathcal{C}\{\mathbf{w}(t),\ \mathbf{y}(t),\ \mathbf{z}(t)\} \tag{5.4.3c}$$

$$\mathbf{u}(k) = \mathcal{C}\{\mathbf{w}(k),\ \mathbf{y}(k),\ \mathbf{z}(k)\} \tag{5.4.3d}$$

$\mathcal{C}$ may be composed of algebraic, integral, differential or fuzzy logic operations on $\mathbf{w}, \mathbf{y}, \mathbf{z}$. $\mathcal{C}$ will stabilize any system $\mathcal{S}$ with properties (5.4.2c/d) and (5.3.6c/d) in the BIBO sense, if $\mathcal{C}$ satisfies the following condition for an arbitrary finite constant $\bar{\gamma} \geq 0$:

$$\int_{t_0}^{t_1} \mathbf{y}^T \mathcal{C}\{\mathbf{w}, \mathbf{y}, \mathbf{z}\} dt < \bar{\gamma}\ \forall\ t_1 \geq t_0 \tag{5.4.4c}$$

$$\sum_{k=k_0}^{k_1} \mathbf{y}^T(k) \mathcal{C}\{\mathbf{w}(k), \mathbf{y}(k), \mathbf{z}(k)\} < \bar{\gamma}\ \forall\ k_1 \geq k_0 \tag{5.4.4d}$$

To demonstrate convergence we consider the continuous-time system of Figure 5.4.2. In this modified system it is assumed for the command input that $\mathbf{w} = \mathbf{0}$, and the effect of the command input $\mathbf{w}$ on $\mathbf{u}$ per (5.4.3 c/d) is replaced by a test signal $\mathbf{w}^* \in \mathbb{R}^l$ defined by:

$$\mathbf{w}^* = \mathbf{u} - \mathbf{u}^* \tag{5.4.5}$$

where we used the definition $\mathbf{u}^* = \mathcal{C}\{\mathbf{w} = \mathbf{0}, \mathbf{y}, \mathbf{z}\}$.

Closed-loop stability of the system per Figgure 5.4.2 can be determined based on the response of $\mathbf{y}$ to the test signal $\mathbf{w}^*$. The following bounds on the IOP integral can be established from the above assumptions:

$$\begin{aligned} \int_{t_0}^{t_1} \mathbf{y}^T \mathbf{w}^* dt = & \underbrace{\int_{t_0}^{t_1} \mathbf{y}^T \mathbf{u}\, dt}_{\geq -\beta_0^2 \text{ per (5.3.6c)}} - \underbrace{\int_{t_0}^{t_1} \mathbf{y}^T \mathbf{u}^* dt}_{< \bar{\gamma} \text{ per (5.4.4)}} \\ & \geq -\underbrace{(\beta_0^2 + \bar{\gamma})}_{>0} \quad \forall \quad t_1 > t_0 \end{aligned} \tag{5.4.6}$$

With this result hyperstability and hence BIBO stability of the system with inputs $\mathbf{w}^*$ and outputs $\mathbf{y}$ can be inferred from condition (5.3.6c). Convergence for the discrete-time case can be demonstrated in an analogous manner.

Although the very general but implicit condition (5.4.4c/d) guarantees stability of the system of Figure 5.4.1, it is not constructive in the sense that it does not offer much guidance for the development of an actual sensor fusion algorithm. We will therefore now investigate three explicit algorithms which satisfy condition (5.4.4c/d). Other suitable algorithms exist.

Sensor Fusion Algorithm 1

A class of stable operators $\mathcal{C}$ can be defined as follows:

$$\mathcal{C}\{\mathbf{w},\mathbf{y},\mathbf{z}\} = \begin{cases} \mathcal{C}_B\{\mathbf{w},\mathbf{y},\mathbf{z}\} & \text{if } \Lambda \\ \mathcal{C}_F\{\mathbf{w}\} & \text{if not } \Lambda \end{cases} \tag{5.4.7}$$

with the fusion logic $\Lambda \in$ (true, false):

$$\Lambda = [\mathbf{y}^T \mathcal{C}_B\{\mathbf{w},\mathbf{y},\mathbf{z}\} < 0]. \tag{5.4.8}$$

This definition can be applied both to continuous-time and discrete-time systems. Figure 5.4.3 represents (5.4.7) and (5.4.8) in a conceptual block diagram. The functions $\mathcal{C}_B$ and $\mathcal{C}_F$ can be considered feedback and feedforward control algorithms, respectively, in conventional control systems terminology. It is required that the feedforward term $\mathcal{C}_F$ is stable in the BIBO sense in order not to introduce dynamic stability problems into the system. Under this assumption, the dynamic stability of the system of Figure 5.4.1 can be assessed on the basis of the modified system per Figure 5.4.4 by considering the response of $\mathbf{y}$ to inputs $\mathbf{w}^*$.

For the stability analysis the following real-valued function ζ can be defined based on the binary logic variable Λ:

$$\zeta = \begin{cases} 1 & \text{if } \Lambda \\ 0 & \text{if not } \Lambda \end{cases}$$

For continuous-time systems BIBO stability can be established as follows based on condition (5.3.6c) and the above definition.

$$\begin{aligned}\int_{t_0}^{t_1} \mathbf{y}^T \mathbf{w}^* dt &= \int_{t_0}^{t_1} \mathbf{y}^T \mathbf{u}\, dt - \int_{t_0}^{t_1} \mathbf{y}^T \mathbf{u}^* dt \\ &= \int_{t_0}^{t_1} \mathbf{y}^T \mathbf{u}\, dt - \int_{t_0}^{t_1} \mathbf{y}^T \mathcal{C}\{\mathbf{w},\mathbf{y},\mathbf{z}\} dt \\ &= \underbrace{\int_{t_0}^{t_1} \mathbf{y}^T \mathbf{u}\, dt}_{\geq -\beta_0^2} - \underbrace{\int_{t_0}^{t_1} \zeta \mathbf{y}^T \mathcal{C}_B\{\mathbf{w},\mathbf{y},\mathbf{z}\} dt}_{\leq 0 \text{ per(5.4.8)}} \\ \therefore \quad &\geq -\beta_0^2 \quad \forall\, t_1 \geq t_0\end{aligned} \tag{5.4.9}$$

The demonstration of convergence for discrete-time systems parallels (5.4.9).

With the mild restriction of BIBO stability of $\mathcal{C}_F$, the functions $\mathcal{C}_B$ and $\mathcal{C}_F$ can be chosen freely, e.g. based on conventional control engineering principles, as stability is guaranteed by the fusion logic (5.4.8). Of course, the performance of the closed-loop system will depend on the design of $\mathcal{C}_B$ and $\mathcal{C}_F$.

Sensor Fusion Algorithm 2

Another class of stable operators $\mathcal{C} = [\mathcal{C}_1 \ldots \mathcal{C}_i \ldots \mathcal{C}_l]^T$ can be defined on an element-by element basis ($\forall i = 1 \ldots l$) as follows:

$$\mathcal{C}_i = \begin{cases} \mathcal{C}_{Bi}\{\mathbf{w},\mathbf{y},\mathbf{z}\} & \text{if } \Lambda_i \\ \mathcal{C}_{Fi}\{\mathbf{w}\} & \text{if not } \Lambda_i \end{cases} \tag{5.4.10}$$

with the associated fusion logic $\Lambda_i \in$ (true, false):

$$\Lambda_i = [y_i \mathcal{C}_{Bi}\{\mathbf{w},\mathbf{y},\mathbf{z}\} < 0] \tag{5.4.11}$$

The above definition again covers both the continuous and the discrete-time case. As before, it is assumed that all functions $\mathcal{C}_{Fi}$ are BIBO stable. With this assumption and the definition

$$\zeta_i = \begin{cases} 1 & \text{if } \Lambda_i \\ 0 & \text{if not } \Lambda_i \end{cases}$$

closed-loop stability can be demonstrated for continuous-time systems in a similar manner as before, based on the system block diagram 5.4.4:

$$\begin{aligned}
\int_{t_0}^{t_1} \mathbf{y}^T \mathbf{w}^* dt &= \int_{t_0}^{t_1} \mathbf{y}^T \mathbf{u} dt - \int_{t_0}^{t_1} \mathbf{y}^T \mathbf{u}^* dt \\
&= \int_{t_0}^{t_1} \mathbf{y}^T \mathbf{u} dt - \int_{t_0}^{t_1} \Big(\sum_{i=1}^{l} y_i \mathcal{C}_{Bi} \Big) dt \\
&= \int_{t_0}^{t_1} \mathbf{y}^T \mathbf{u} dt - \sum_{i=1}^{l} \int_{t_0}^{t_1} y_i \mathcal{C}_{Bi} dt \\
&= \underbrace{\int_{t_0}^{t_1} \mathbf{y}^T \mathbf{u} dt}_{\geq -\beta_0^2} - \sum_{i=1}^{l} \underbrace{\int_{t_0}^{t_1} \varsigma_i y_i \mathcal{C}_{Bi} dt}_{\leq 0 \text{ per(5.4.11)}} \\
&\geq -\beta_0^2 \quad \forall t_1 \geq t_0
\end{aligned} \tag{5.4.12}$$

The demonstration of convergence for discrete-time systems parallels (5.4.12).

Sensor Errors

The measurement process performed by the hyperstability sensors can be described by a mapping of physical quantities $\mathbf{y}$ per (5.3.6c/d) and (5.4.1c/d), (5.4.2c/d) onto a vector of measurements $\bar{\mathbf{y}} = [\bar{y}_1 \dots \bar{y}_i \dots \bar{y}_l]^T$ of the same dimension, l, as $\mathbf{y}$:

$$\bar{\mathbf{y}} = \mathbf{m}(\mathbf{y}) \tag{5.4.13}$$

where $\mathbf{m} = [m_1 \dots m_i \dots m_l]^T$ is a vector function characterizing the measurement process for the set of l sensors.

If the absolute measurement errors are bounded per Figure 5.4.5, the individual measurement processes m_i can be characterized by mapping functions

$$\bar{y}_i = m_i(y_i, \varepsilon_i) \tag{5.4.14}$$

where the mapping function $m_i(y_i, \varepsilon_i)$ is defined as follows:

$$\left.\begin{array}{ll} \bar{y}_i > \varepsilon_i & \forall\ y_i > 2\varepsilon_i \\ \bar{y}_i \geq y_i - \varepsilon_i & \forall\ 0 \leq y_i \geq 2\varepsilon_i \\ \bar{y}_i \leq y_i + \varepsilon_i & \forall\ 0 \leq y_i \leq -2\varepsilon_i \\ \bar{y}_i < -\varepsilon_i & \forall\ y_i \leq -2\varepsilon_i \end{array}\right\} \quad \forall\ i = 1 \ldots l \tag{5.4.15}$$

Here $\varepsilon_i \geq 0$ is a constant describing bounds on the measurement error for hyperstability sensor i in a region around the origin of the $\bar{y}_i - y_i$-plane, as shown in Figure 5.4.5. The actual characteristic $\bar{y}_i(y_i)$ of the sensor does not need to be known and may lie in any area of the $\bar{y}_i - y_i$-plane permitted by (5.4.15), as depicted in Figure 5.4.5. Areas which are not permissible are shaded in the Figure.

Sensor Fusion Algorithm 3

Figure 5.4.6 shows the extended hyperstability concept incorporating the measurement errors. We will now extend 'Algorithm 2' to include the measurement process (5.4.14).

As shown in Appendix C.3, the condition

$$\bar{y}_i \mathcal{C}_{Bi}\{\mathbf{w}, \mathbf{y}, \mathbf{z}\} + \varepsilon_i |\mathcal{C}_{Bi}\{\mathbf{w}, \mathbf{y}, \mathbf{z}\}| < 0 \tag{5.4.16}$$

with $\bar{y}_i$ per (5.4.15) always implies

$$y_i \mathcal{C}_{Bi}\{\mathbf{w}, \mathbf{y}, \mathbf{z}\} < 0. \tag{5.4.17}$$

It follows then from (5.4.12) that the sensor fusion and control operator (5.4.10) is also stable with the following fusion logic $\bar{\Lambda}_i \in$ (true, false) based on the hyperstability measurement $\bar{y}_i$ with error characteristics per (5.4.15):

$$\bar{\Lambda}_i = [\bar{y}_i \mathcal{C}_{Bi}\{\mathbf{w}, \mathbf{y}, \mathbf{z}\} + \varepsilon_i |\mathcal{C}_{Bi}\{\mathbf{w}, \mathbf{y}, \mathbf{z}\}| < 0] \tag{5.4.18}$$

As condition (5.4.17) does not necessarily imply (5.4.16), the logic (5.4.18) is different from (5.4.11), although it still guarantees stability.

We further may replace $\mathbf{y}$ by $\bar{\mathbf{y}}$ in (5.4.10) and (5.4.18) without jeopardizing stability. We can now restate (5.4.10) and (5.4.18) based on hyperstability sensors subject to measurement errors, $\bar{\mathbf{y}}$, as our third sensor fusion algorithm:

$$\mathcal{C}_i = \begin{cases} \mathcal{C}_{Bi}\{\mathbf{w}, \bar{\mathbf{y}}, \mathbf{z}\} & \text{if } \bar{\Lambda}_i \\ \mathcal{C}_{Fi}\{\mathbf{w}\} & \text{if not } \bar{\Lambda}_i \end{cases} \quad \forall\ i = 1 \ldots l \tag{5.4.19}$$

with $\bar{\Lambda}_i \in$ (true, false):

$$\bar{\Lambda}_i = [\bar{y}_i \mathcal{C}_{Bi}\{\mathbf{w}, \bar{\mathbf{y}}, \mathbf{z}\} + \varepsilon_i |\mathcal{C}_{Bi}\{\mathbf{w}, \bar{\mathbf{y}}, \mathbf{z}\}| < 0] \quad \forall\, i = 1 \ldots l \tag{5.4.20}$$

Key Features of the Extended Hyperstability Concept

The introduction of the sensor fusion process into the hyperstability framework breaks the symmetry between inputs and outputs required in [Popov.2]'s hyperstability concept as applied to robotic systems per Figure 5.3.1, and thus gives rise to a new concept captured in Figure 5.4.6 which we call "extended hyperstability". While its key feature is the capability to integrate performance sensors into the hyperstability concept, without restriction on the number, type and locations of the sensors, it also introduces other new features which we will highlight now.

As discussed, the sensor fusion process can tolerate static errors in the hyperstability sensors, per Figure 5.4.5. This may appear to be a detail, but it is actually an important advance considering that, without sensor fusion, the hyperstability concept is limited to sensors which meet a 'sector condition' in terms of accuracy, according to [Joshi]. This sector condition is in essence a special case of the condition depicted in Figure 5.4.5 for error parameter $\varepsilon_i = 0$. The significance of allowing non-zero errors is that, to the knowledge of this author, no sensors exist which meet the sector condition as it requires infinite sensor precision around the zero-point. Hence the standard hyperstability concept is not on a practical footing in terms of its requirements on the sensors. In Section 6.2 we will further extend the allowable error characteristics of hyperstability sensors to also include dynamic errors such as low-pass characteristics.

Another important consequence of introducing the performance sensors is that the hyperstability sensors are no longer the sole source of measurements required to achieve the performance objectives of the closed-loop control system. Although a dual collocated hyperstability sensor is still required for each actuator to feed the fusion logic, the sensor accuracy requirements can be relaxed and the implementation cost reduced. The hyperstability sensors only need to provide the

"correct sign", with tolerances, i.e. their resolution could be reduced to 1 bit in the limit.

A further subtle yet profound effect of introducing the sensor fusion concept is the ability to introduce 'active' behaviour into the hyperstability concept which is also known as a 'passive' concept (yin) and hence not well suited as a framework for endowing a robot with a 'purposeful' behaviour. The fusion process allows the injection of energy (yang) into the system when necessary, via the command input. As known from Chinese philosophy, only the proper interaction of yin and yang can result in the purposeful behaviour required for robotic systems.

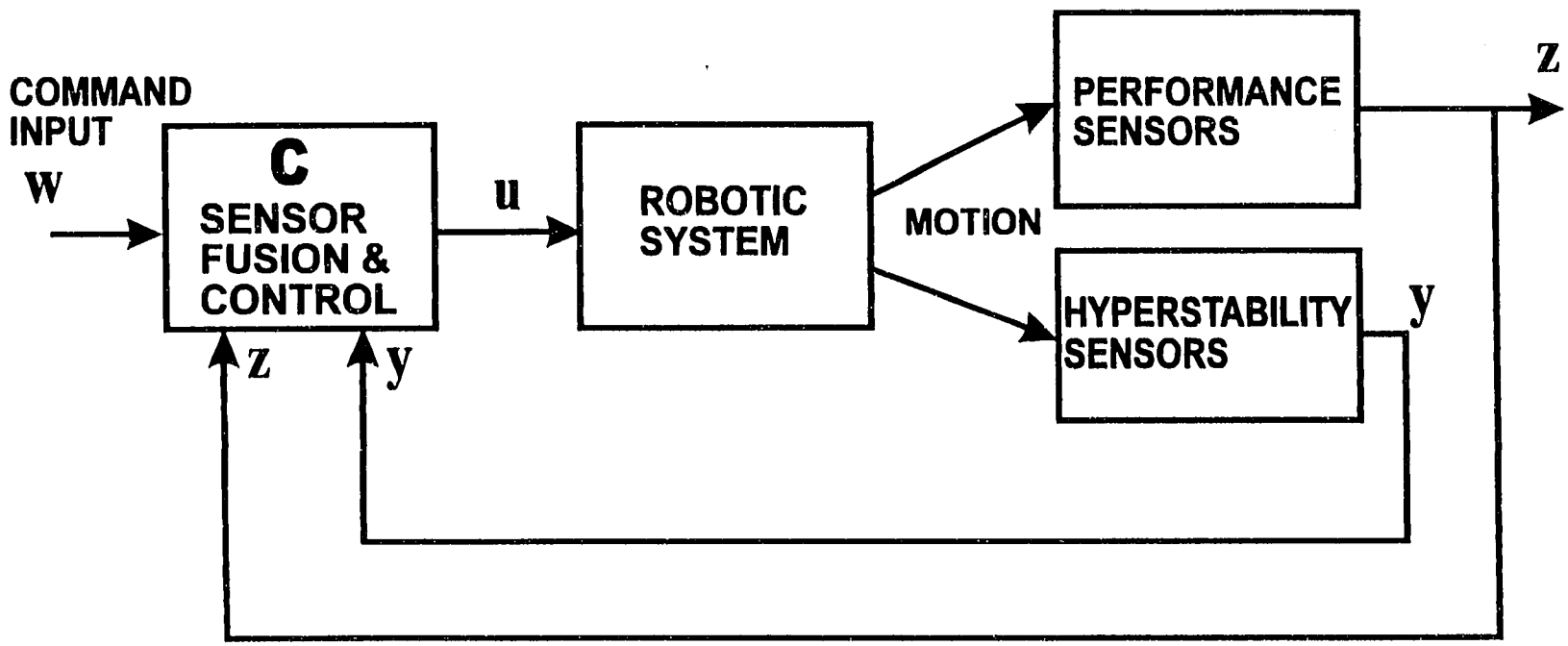

Figure 5.4.1: Extended Hyperstability Concept for Sensor Fusion and Control

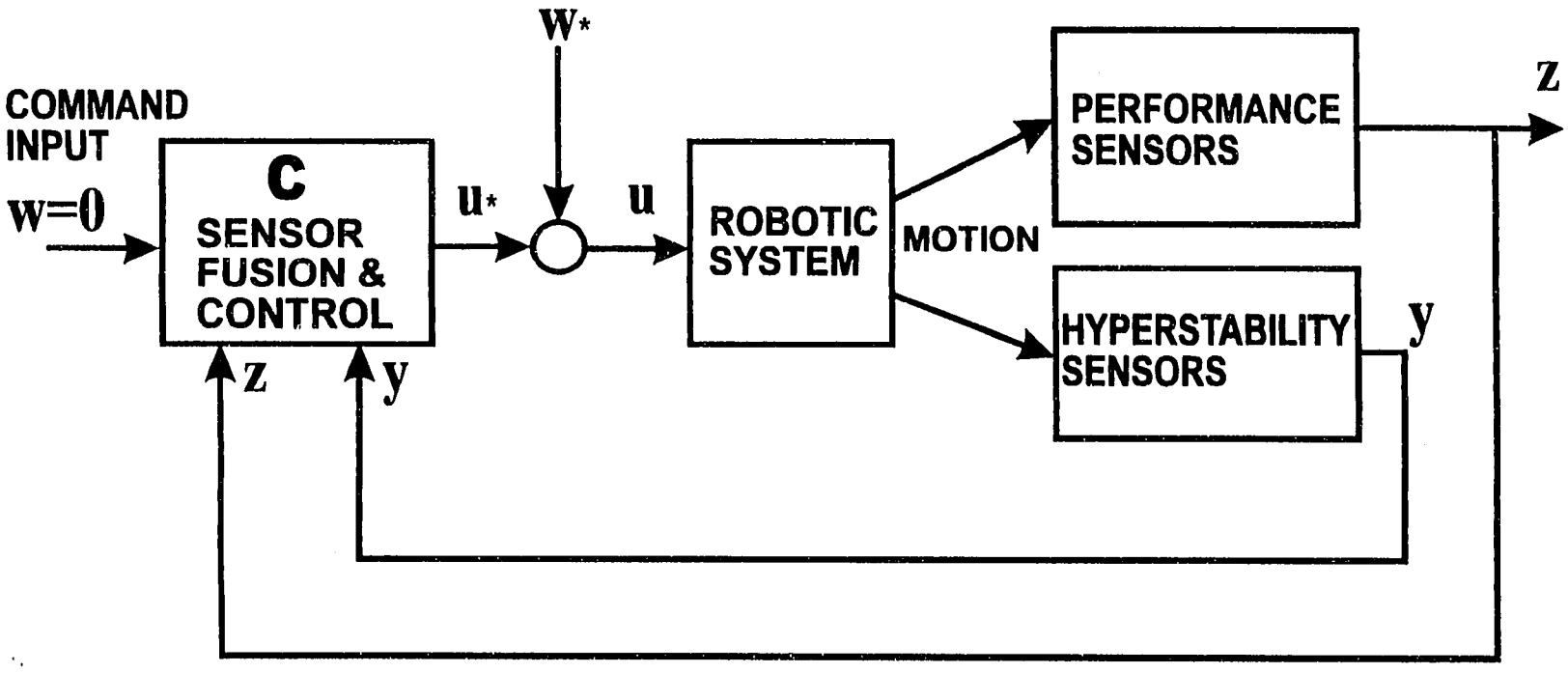

Figure 5.4.2: Modified System for Stability Analysis of Algorithm (5.4.3) - (5.4.4)

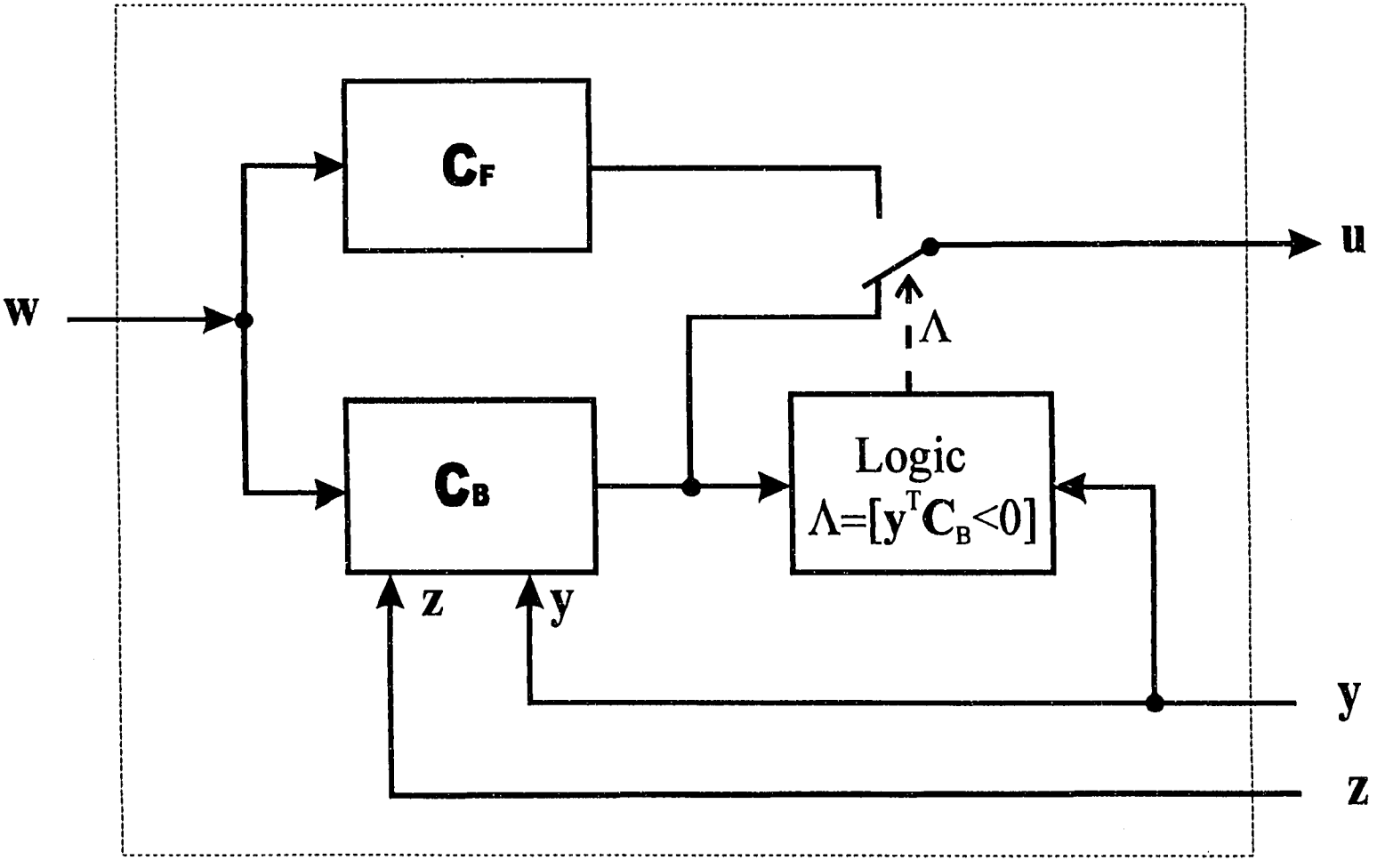

Figure 5.4.3: Conceptual Block Diagram for "Algorithm 1"

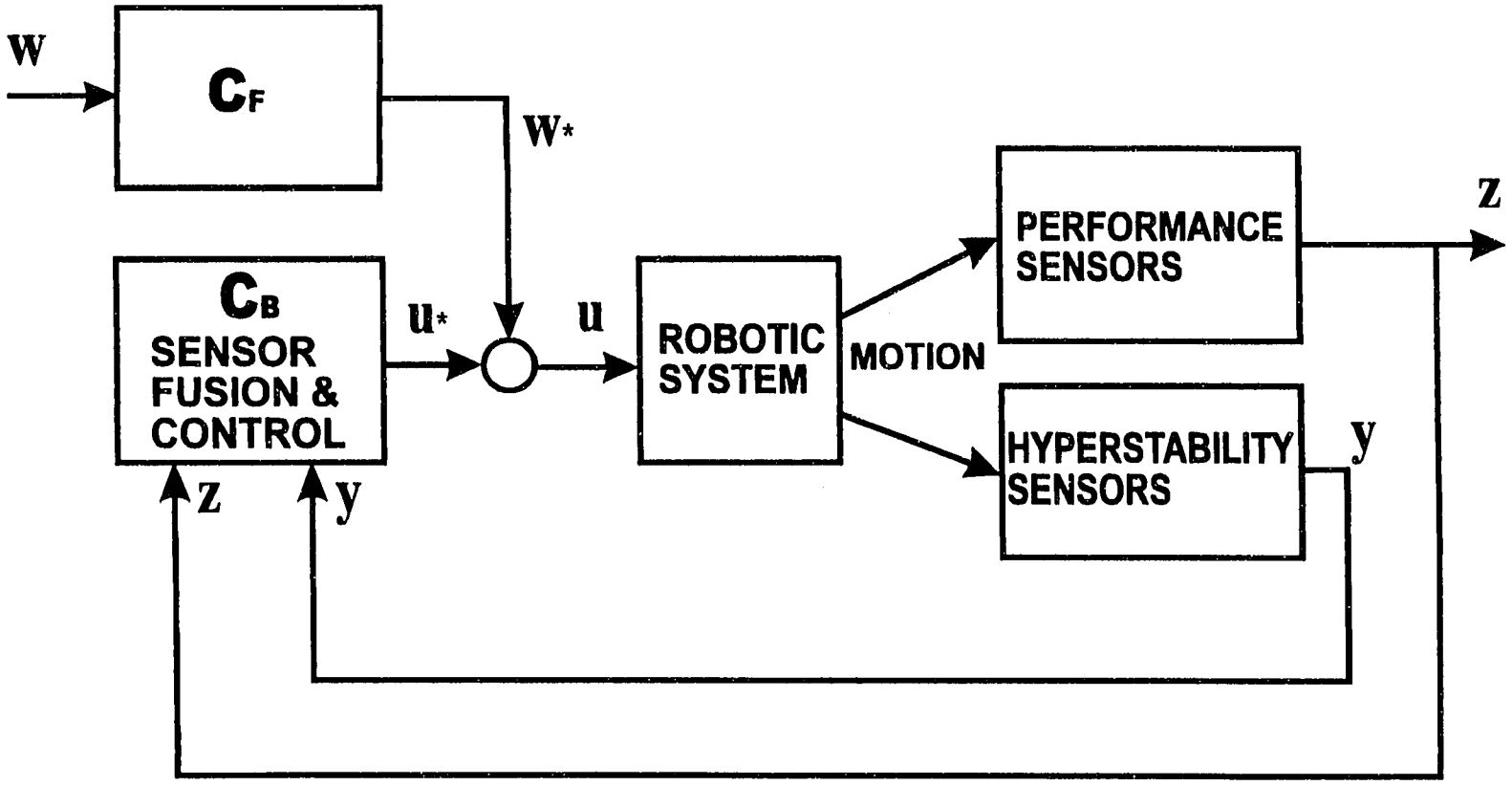

Figure 5.4.4: Modified System for Proof of Stability of "Algorithm 1"

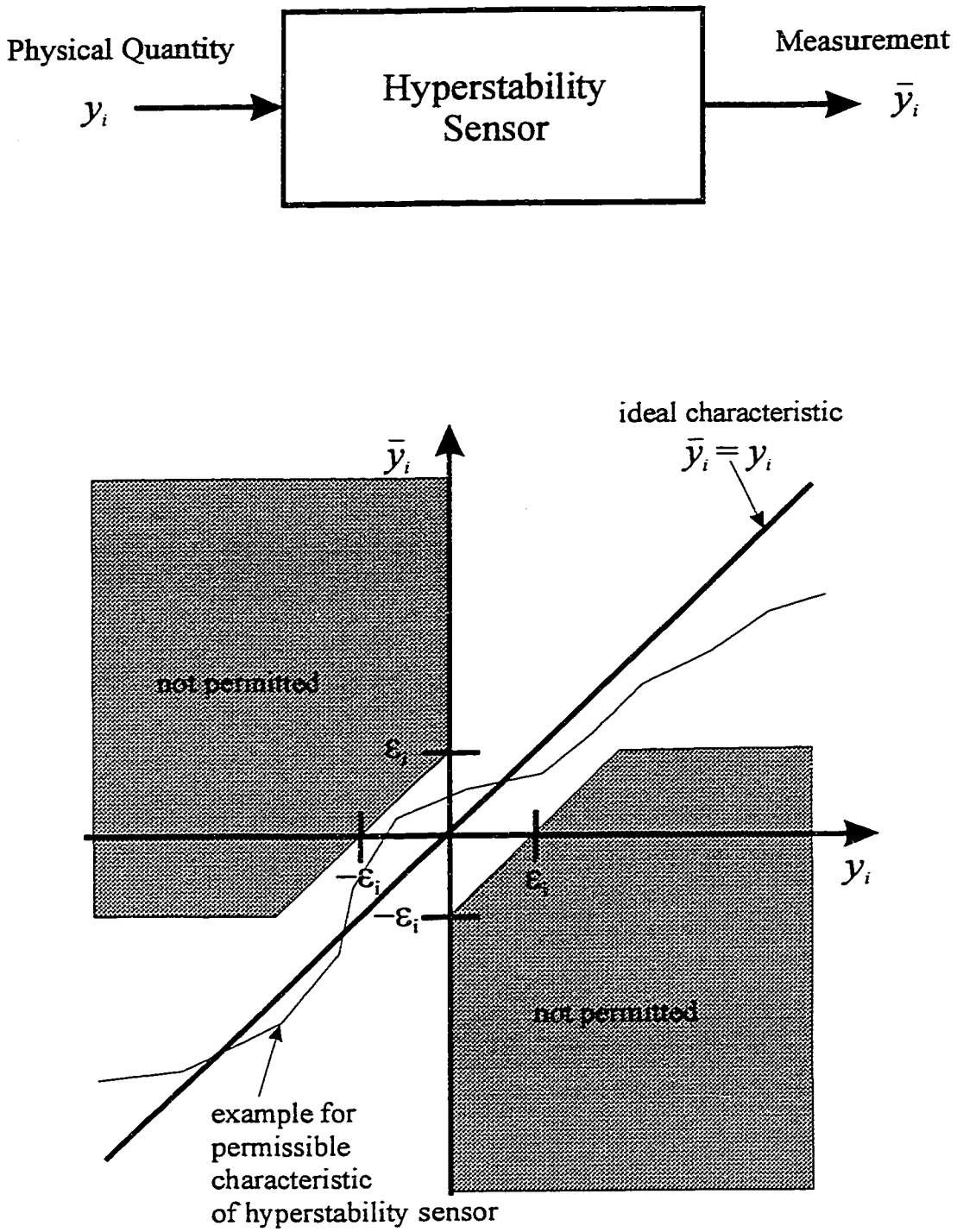

Figure 5.4.5: Permissible Measurement Errors of Hyperstability Sensors

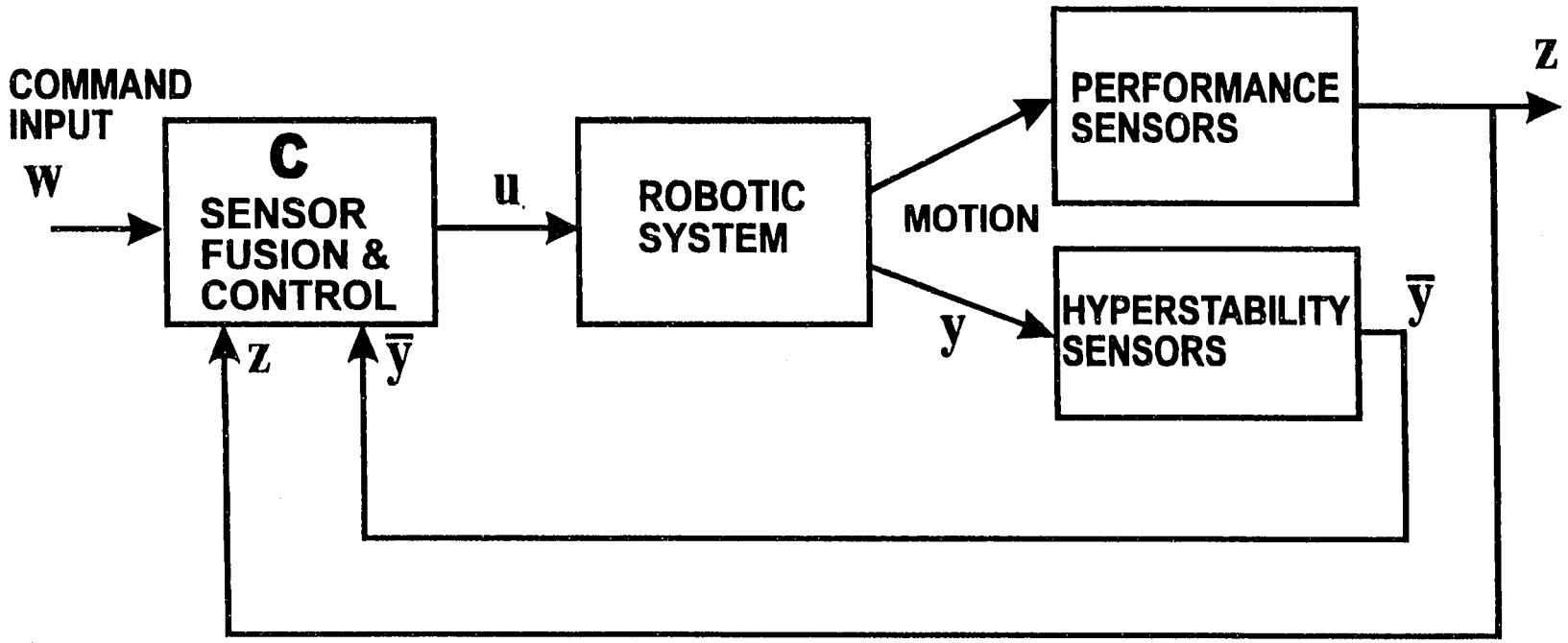

Figure 5.4.6: Concept for Sensor Fusion and Control with Measurement Errors

5.5 Design Procedure

Objective

This Section outlines how the various concepts developed above are applied to a general instrumentation and control design problem in a systematic step-by-step procedure. Based on the system architecture developed in Section 5.4 the following steps are required in the design process as summarized in Figure 5.5.1:

- Determine the set of hyperstability sensors;
- Determine the set of performance sensors;
- Design sensor fusion and control algorithm.

We will now describe each step of the process.

Step 1: Determine the Complement of Hyperstability Sensors

For each actuator or input of the system, u_i, one "matching" hyperstability sensor y_i is required. The match must result in a "meaningful" IOP $\mathbf{u}^T\mathbf{y}$ with a bounded integral as required by condition (5.3.6c/d). How this process is performed depends somewhat on the application domain and will be discussed at length in Chapter 6 for the the specific domain of mechanical systems with nonlinear and flexible elements. When the system can be meaningfully linearized, conditions (5.3.9c/d)–(5.3.11c/d) provide explicit requirements for hyperstability sensors. These conditions can be solved for free parameters, such as sensor location, in sets of candidate sensors. Once the hyperstability sensors have been determined and measurement errors are a significant factor, the error parameter $\varepsilon_i \geq 0$ is estimated for each hyperstability sensor, in accordance with the mapping function (5.4.15).

An important advantage of this methodology over standard passivity or hyperstability approaches discussed in Section 4.2 is that the hyperstability sensors are required to feed the fusion logic, but may not be needed in the feedback control loop. In this case hyperstability sensors with very low resolution may suffice.

Step 2: Determine the Complement of Performance Sensors

The performance sensors are selected such as to achieve closed-loop system performance requirements. Standard instrumentation and control engineering methodology is used for the selection/design process. The overall methodology proposed in this research does not impose any restrictions with regard to the number, type, location or other characteristics of the performance sensors.

Step 3: Design of Sensor Fusion and Control Algorithms

An algorithm $\mathcal{C}$ for sensor fusion and control is suitable within the context of this approach, if and only if it satisfies condition (5.4.4c/d). We identified 3 explicit algorithms, (5.4.7) – (5.4.8), (5.4.10) – (5.4.11) and (5.4.19) – (5.4.20) which meet the criteria and may all be used. These three algorithms use two types of control functions: a feedforward control function $\mathcal{C}_F$ and a feedback control function $\mathcal{C}_B$. With some mild restrictions such as the BIBO stability of $\mathcal{C}_F$, essentially "arbitrary" algorithms may be chosen. Although closed-loop stability is not compromised by a "poor choice", the proper functioning and performance of the system is dependent on using suitable control algorithms. The feedforward control function is required in many applications to inject energy into the system and to drive it towards the commanded state.

Various types of algorithms based on different design philosophies may be used. In conjunction with intelligent control, e.g. fuzzy logic, the proposed methodology offers the very significant advantage of guaranteed closed-loop stability in the BIBO sense. In conjunction with simple conventional techniques, the proposed approach supports the application of single-input single-output (SISO) techniques, such as PID control, in multi-input multi-output (MIMO) problem settings. In conjunction with more complex model-based techniques, the proposed method assures stability robustness in the event of a model mismatch due to model truncation, uncertainties, or time variance in the system behaviour. Once the control functions are chosen, the sensor fusion algorithm is fully determined by (5.4.8), (5.4.11) or (5.4.20), ensuring closed-loop stability of the system.

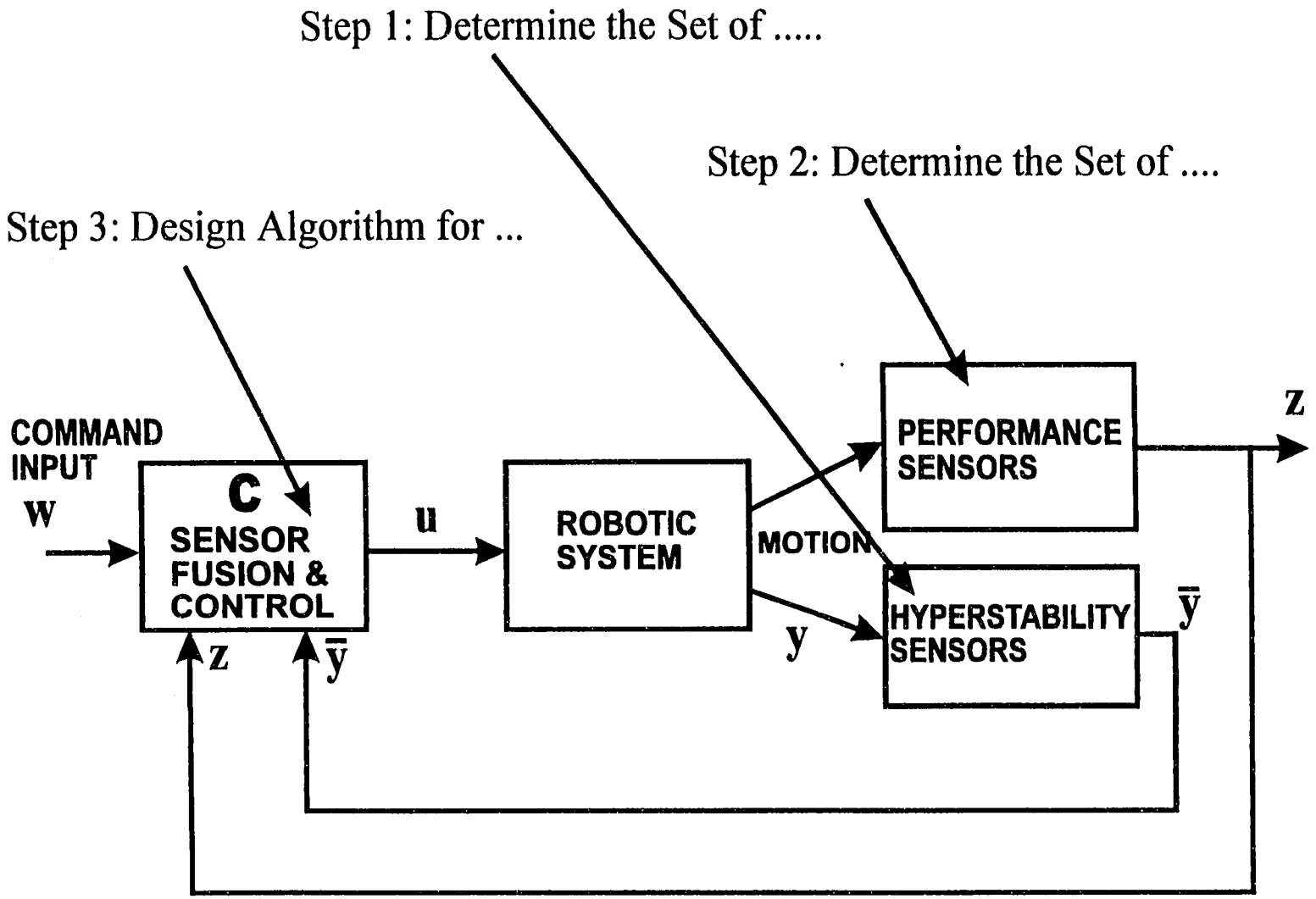

Figure 5.5.1: 3-Step Process for Design of Instrumentation Architecture and Sensor Fusion Algorithm

CHAPTER 6
HYPERSTABILITY SENSORS FOR FLEXIBLE ROBOTS

6.1 Overview

The instrumentation design and sensor fusion concept developed in Chapter 5 is completely general and may, in principle, be applied to "any" system. A critical step of the 3-step design procedure outlined in Section 5.5 is the identification and implementation of suitable hyperstability sensors. The usefulness of the abstract concept of hyperstability sensors per Definition 5.3.1 depends on the application domain. In this Chapter we will focus on the application to robotic systems with flexible links and other flexible structures. Our objective is to establish the most general conditions, both necessary and sufficient, for hyperstability sensors for robotic systems and provide a physical interpretation of those conditions.

In Section 6.2 we will establish sufficient conditions for the hyperstability sensors for general non-linear mechanical systems. Necessary conditions, though, are difficult to establish directly for the general case. Therefore, to complement the general sufficient conditions, we look at necessary conditions for hyperstability sensors on linear flexible structures in Section 6.3 and perform a comparison and synthesis of the results for the linear and non-linear case. In Section 6.4 the conditions are reviewed in the context of the design of a real robot, exemplified by the SSRMS, to determine the impact of including hyperstability sensors into a robot design.

6.2 Hyperstability Sensors for General Robotic Systems

Link between Hyperstability and Robot Dynamics

As discussed in Section 3.2, the dynamics of robot manipulators can be described, in their most general form, by the Euler-Lagrange equation (3.2.15) which is re-stated below:

$$\mathbf{M}(\mathbf{q})\ddot{\mathbf{q}} + \mathbf{c}(\mathbf{q}, \dot{\mathbf{q}}) + \mathbf{k}(\mathbf{q}) = \mathbf{B}_u\mathbf{u}(t) + \mathbf{B}_d\mathbf{d}(t). \tag{6.2.1}$$

This equation derived in Section 3.2 describes the dynamics of holonomic mechanical systems which may have non-linearities and flexibility effects, and are excited by l control inputs $\mathbf{u}(t)$ and k disturbances $\mathbf{d}(t)$.

A link between the robot dynamics (6.2.1) and the definition of hyperstability sensors can be established by considering that the actuators do work on the system per (3.2.1) and (3.2.7), and that the power $P_A \in \mathbb{R}$ transferred to the system (6.2.1) by the actuators $\mathbf{u}(t)$ at any time is given by

$$P_A(t) = \dot{\mathbf{q}}^T(t)\mathbf{B}_u\mathbf{u}(t). \tag{6.2.2}$$

$P_A > 0$ indicates energy flowing into the robotic system.

Similarly, the instantaneous power transferred by external disturbances is

$$P_D(t) = \dot{\mathbf{q}}^T(t)\mathbf{B}_d\mathbf{d}(t). \tag{6.2.3}$$

For typical space manipulators such as the SSRMS, the level of environmental disturbance forces is negligible in comparison to the torques provided by joint motors sized for the inertial loads resulting from the accelerating and decelerations during manipulation tasks. This holds also true for most other robotic applications. For applications in a gravity environment, the gravitational forces are not considered disturbances in (6.2.1), but are included in the term $\mathbf{k}(\mathbf{q})$ describing conservative forces per (3.2.4) and (3.2.14). Hence we assume in the following that the lasting net effect of disturbances on the internal energy of the system is bounded, since

they are usually relatively small and tend to "average out". This assumption can be expressed mathematically by

$$\left| \int_{t_0}^{t_1} P_D(t)dt \right| \leq E_D \ \forall \ t_1 \geq t_0 \tag{6.2.4}$$

where $E_D \geq 0$ is finite.

As a consequence of the principle of conservation of energy implied in (3.2.1) and the Second Law of Thermodynamics expressed in condition (3.2.6) the following inequality holds for the system (6.2.1) with the assumption (6.2.4):

$$\int_{t_0}^{t_1} P_A(t)dt \geq -E(t_0) - E_D \ \forall \ t_1 \geq t_0 \tag{6.2.5}$$

Here $E(t_0)$ denotes the total energy stored in the system at t_0 which can be expressed as the sum of the kinetic and potential energy:

$$E(t_0) = T(t = t_0) + V(t = t_0) \geq 0 \tag{6.2.6}$$

$E(t_0)$ is non-negative and finite.

Expanded with (6.2.2), (6.2.5) can be written as

$$\int_{t_0}^{t_1} \mathbf{u}^T(t)\mathbf{B}_u^T\dot{\mathbf{q}}(t)dt \geq -E(t_0) - E_D \ \forall \ t_1 \geq t_0 \tag{6.2.7}$$

This expression formally matches the general condition for hyperstability sensors (5.3.6c) when we introduce the following formal equalities:

$$\beta_0^2 = E(t_0) + E_D \tag{6.2.8}$$

and

$$\mathbf{y}(t) = \mathbf{B}_u^T\dot{\mathbf{q}}(t). \tag{6.2.9}$$

β_0^2 is a constant which may be chosen arbitrarily in (5.3.6c), with the only restriction that it be finite and non-negative (≥ 0). Hence, the choice implied by (6.2.8)

is unconditionally 'valid' in the sense that no contradictions arise. Other choices for β_0^2 are possible. Equation (6.2.9) can be compared to (3.3.5) and represents a sufficient condition for hyperstability sensors for the general system (6.2.1) in the following sense: if sensors are chosen such that they produce measurements $\mathbf{y}$ in accordance with (6.2.9), they are hyperstability sensors per Definition 5.3.1. Condition (6.2.9) provides a general mathematical definition for duality of sensors with respect to actuators.

Sensor Location

$\mathbf{B}_u$ in (6.2.9) is the input matrix of system (6.2.1) which projects the actuator inputs onto the space defined by the generalized coordinates as discussed in conjunction with (3.2.7) and (3.2.8). In our linear modelling example of Section 3.4, $\mathbf{B}_u$ was composed of a set of mode shape functions ϕ and their spatial derivatives, evaluated at the actuator locations (see (3.4.6), (3.4.19) and (3.4.23)). The mode shape functions ϕ in turn are related to the mass and stiffness distribution per (3.4.21) and (3.4.22), and the number of modes is equal to the number of modal coordinates $\mathbf{q}$. Even though "modes" are not defined for the general non-linear system (6.2.1), we can expect in analogy to the linear case that $\mathbf{B}_u$ generally is a function of the mass and stiffness distribution, the choice of generalized coordinates, and the actuator location. However, it is not necessary that $\mathbf{B}_u$ is known explicitly in order to select a complement of sensors in accordance with (6.2.9). Since $\mathbf{B}_u$ is defined by the complement of actuators, it is sufficient to collocate suitable sensors with the actuators as further explored below, in order to find a set of hyperstability sensors.

This procedure establishes a set of hyperstability sensors without requiring explicit system modelling information. If we take a robot driven by electrical motors in the joints as an example, tachometers mounted on the shaft of each joint motor would fulfill the location requirement for hyperstability sensors. No modelling or mathematical analysis for the particular case is required to reach that conclusion.

In conjunction with the sensor fusion and control concept discussed in Sec-

tion 5.4, these hyperstability sensors enable the robust control of any mechanical system of the rather general form (6.2.1), regardless of system order, mass and stiffness distribution, including time-variance of these parameters, which is quite remarkable.

Sensor Types

We will now discuss the implications of the sufficient conditions (6.2.8) and (6.2.9) on the choice of sensor types for hyperstability sensors. The "output equation" (6.2.9) implies that the sensor signals $\mathbf{y}$ are a mapping $\dot{\mathbf{q}} \mapsto \mathbf{y}$ of the generalized *velocities* $\frac{d\mathbf{q}}{dt}$ only, and do not include functions dependent on displacement $\mathbf{q}$ or accelerations $\frac{d^2\mathbf{q}}{dt^2}$.

Translational and angular velocities are typical functions of the generalized velocities, but there are also other possibilities as we will see in Section 6.3. The choice (6.2.8) implies the following *sufficient* condition for hyperstability sensors:

$$\mathbf{u}^T(t)\mathbf{y}(t) = P_A(t) \tag{6.2.10}$$

This condition indicates that it is sufficient to choose hyperstability sensors $\mathbf{y}$ such that their inner product with the system inputs provides a measure of the instantaneous power P_A transferred to the system by the actuators. Equation (6.2.10) can be broken down into components by defining the power transferred by each actuator u_i:

$$P_{Ai}(t) = \sum_{j=1}^{n} \dot{q}_j(t)(\mathbf{B}_u)_{ij}u_i(t) \quad \forall\, i = 1 \ldots l \tag{6.2.11}$$

where $(\mathbf{B}_u)_{ij}$ denotes element i, j of matrix $\mathbf{B}_u$. With this definition (6.2.10) can be written as

$$\sum_{i=1}^{l} u_i(t)y_i(t) = \sum_{i=1}^{l} P_{Ai}(t) \tag{6.2.12}$$

A sufficient condition for $\mathbf{y}$ to satisfy (6.2.12) is obviously

$$u_i(t)y_i(t) = P_{Ai}(t) \quad \forall\, i = 1 \ldots l. \tag{6.2.13}$$

This condition implies that it is sufficient for the selection of hyperstability sensors to match one sensor with each actuator such that the instantaneous power P_A transferred by that actuator can be determined from the associated hyperstability sensor.

The example of a tachometer on a motor shaft discussed above in the context of sensor location also meets the sufficient condition (6.2.13) for sensor type.

Dynamic Sensor Errors

The sufficient condition (6.2.13) can be further generalized and relaxed by incorporating a first-order lag term, with a finite time constant $\tau_i > 0$, which can be thought of as enveloping the dynamics of the hyperstability sensor and actuator:

$$u_i(t)y_i(t) = \hat{P}_{Ai}(t) \quad \forall\, i = 1 \ldots l \tag{6.2.14}$$

$$\tau_i \dot{\hat{P}}_{Ai}(t) + \hat{P}_{Ai}(t) = P_{Ai}(t) \quad \forall\, i = 1 \ldots l \tag{6.2.15}$$

It can be demonstrated as follows that sensors y_i as defined by (6.2.14) and (6.2.15) are acceptable hyperstability sensors:

$$\int_{t_0}^{t_1} \mathbf{u}^T \mathbf{y} dt = \int_{t_0}^{t_1} \sum_{i=1}^{l} \hat{P}_{Ai} dt \qquad \text{per (6.2.14)}$$

$$= \int_{t_0}^{t_1} \sum_{i=1}^{l} P_{Ai} dt - \int_{t_0}^{t_1} \sum_{i=1}^{l} \tau_i \dot{\hat{P}}_{Ai} dt \qquad \text{per (6.2.15)}$$

$$= \int_{t_0}^{t_1} P_A dt - \sum_{i=1}^{l} \tau_i \int_{t_0}^{t_1} \dot{\hat{P}}_{Ai} dt \qquad \text{per (6.2.11)}$$

$$\geq -E(t_0) - E_D - \underbrace{\sum_{i=1}^{l} \underbrace{\tau_i (\hat{P}_{Ai}(t_1) - \hat{P}_{Ai}(t_0))}_{\text{finite}}}_{\text{finite}} \qquad \text{per (6.2.5)}$$

$$\geq -\beta_0^2 \quad \forall t_0 > t_1$$

The last equation appears to be contradicting (6.2.8). However the choice $\beta_0^2 = E(t_0) + E_D$ for the constant β_0^2 was made somewhat arbitrarily to formally match

(6.2.7) with (5.3.6c). It is quite acceptable to amend this choice to cover the situation of dynamic sensor errors by defining

$$\beta_0^2 \geq E(t_0) + E_D + \Delta E \tag{6.2.16}$$

where ΔE is an arbitrary finite constant. The particular choice of β_0^2 per (6.2.8) is a special case of (6.2.16)for $\Delta E = 0$.

Properties of Hyperstability Sensors for Non-Linear Mechanical Systems

We will now summarize the properties of hyperstability sensors for the general mechanical system (6.2.1). The following sufficient conditions for hyperstability sensors $\mathbf{y}$ were developed in this Section:

(6.2.9) : $\mathbf{y}(t) = \mathbf{B}_u^T \dot{\mathbf{q}}(t)$

(6.2.10) : $\mathbf{y}^T(t)\mathbf{u}(t) = P_A(t)$

(6.2.13) : $y_i(t)u_i(t) = P_{Ai}(t) \quad \forall\, i = 1 \ldots l$

(6.2.14) : $y_i(t)u_i(t) = \hat{P}_{Ai}(t) \quad \forall\, i = 1 \ldots l$ with $\hat{P}_{Ai}$ per (6.2.15)

While conditions (6.2.9), (6.2.10) and (6.2.13) have been known, (6.2.14) appears to be a 'new' development. All four conditions are sufficient conditions and a set of sensors $\mathbf{y}$ satisfying any one of the conditions is a set of hyperstability sensors per Definition 5.3.1. The above conditions, together with the more general conditions of Chapter 5, imply the following characteristics for hyperstability sensors of systems governed by the Euler-Lagrange equation (6.2.1) such as flexible space robots:

- Number of hyperstability sensors:
  - One hyperstability sensor is required for each actuator.
- Location of hyperstability sensors:
  - Collocation of hyperstability sensors with their associated actuator satisfies the sufficient condition.
  - No explicit system modelling information is required when sensors are collocated with actuators.

- Type of hyperstability sensors:
  - Hyperstability sensors measure quantities derived from the general velocities $\dot{\mathbf{q}}$.
  - Hyperstability sensors must be matched to the type of the associated actuator such that the product of actuation input and measurement output provides an approximate measure of the power transformed by the actuator.
  - Examples: An angular rate sensor is a matching sensor for a torque actuator, a translational velocity sensor matches a force actuator. (This set of examples is not exhaustive; other suitable pairs exist.)
- Errors of hyperstability sensors
  - Significant measurement errors characterized by (5.4.15) and (6.2.14)/(6.2.15) are permissible for hyperstability sensors in the sensor fusion and control concept per Figure (5.4.1) applied to general robotic systems.

6.3 Hyperstability Sensors for Linear Flexible Robots

Outline

Having established sufficient conditions for hyperstability sensors of general non-linear systems we will now examine linear flexible structures and establish necessary and sufficient conditions for hyperstability sensors, based on (5.3.9c)–(5.3.11c). The detailed analysis required to apply these conditions is presented in Appendix A. In this Section we will summarize the modelling assumptions and the results obtained with them. The model used emphasizes the structural flexibility aspects which are important to the space robotics application.

Linear Model

Based on a continuum modelling approach, a dynamic model for a one-dimensional vibrating structure excited by a spatial/temporal forcing function $f(x,t)$ is developed in Appendix A. The model is linear and neglects structural damping and gyroscopic effect. Similar to the model developed in Section 3.4, and in analogy to (3.4.14), the spatial/temporal displacement $v(x,t)$ is expanded into:

$$v(x,t) = \sum_{i=1}^{n} \phi_i(x) q_i(t) \tag{6.3.1}$$

As in Section 3.4, x is the spatial co-ordinate, ϕ_i are mode shapes and the q_i are modal coordinates associated with the individual modes of vibration, and n is the number of vibration modes included in the model. The modal coordinates are governed by the following set of decoupled harmonic equations familiar from (3.4.25) or (3.4.20) with (3.4.41) and (3.4.42):

$$\ddot{q}_i(t) + \omega_i^2 q_i(t) = f_i(t), \quad i = 1, 2, \ldots, n \tag{6.3.2}$$

where the ω_i are the modal frequencies. The modal excitations $f_i(t)$ are the components of the spatial/temporal forcing function $f(x,t)$ along the basis functions $\phi_i(t)$:

$$f_i(t) = \int_{\mathcal{D}} \phi_i^T(x) f(x,t) dx. \tag{6.3.3}$$

Sensors

Different type of sensors are defined by forming temporal and spatial derivatives of the displacement, at certain positions. The order of the stiffness operator in the model is denoted[1] p ($p = 2$ for string equation, $p = 4$ for beam). As discussed in Appendix A the first p spatial derivatives (0^{th} to $(p-1)^{\text{st}}$) are significant. Here we will consider the possibility of having 'point'[2] sensors for all significant spatial derivatives of the displacement. Further, we will consider sensors for the first three time derivatives (0^{th} to 2^{nd}) because there are devices for the direct measurement of displacement, rate and acceleration. After these considerations we arrive at $3p$ possible sensor types derived from the displacement, v, as shown in Table 6.3.1.

	$\frac{\partial^j}{\partial t^j}$	$j=0$	$j=1$	$j=2$
$\frac{\partial^i}{\partial x^i}$	Interpretation	Displacement	Rate	Acceleration
$i=0$	Translation	v	$\dot{v}$	$\ddot{v}$
$i=1$	Rotation	$v^{(1)}$	$\dot{v}^{(1)}$	$\ddot{v}^{(1)}$
$i=2$	Strain	$v^{(2)}$	$\dot{v}^{(2)}$	$\ddot{v}^{(2)}$
$i=3$	Shear	$v^{(3)}$	$\dot{v}^{(3)}$	$\ddot{v}^{(3)}$
$\vdots$		$\vdots$	$\vdots$	$\vdots$
$i=p-1$	?	$v^{(p-1)}$	$\dot{v}^{(p-1)}$	$\ddot{v}^{(p-1)}$

Table 6.3.1: $3p$ types of Sensors Based on Displacement $v(x,t)$.

We consider sensors at l locations, x_{sk}, and define a sensor displacement vector, $\mathbf{v}_s(t)$, with lp elements describing the displacement with all its p significant spatial derivatives, at all l sensor locations:

$$\begin{aligned}\mathbf{v}_s(t) = \Big[& v(x_{s1},t)\; v(x_{s2},t) \ldots v(x_{sl},t) \ldots \\ & \Big(\frac{\partial v(t)}{\partial x}\Big)_{x_{s1}} \Big(\frac{\partial v(t)}{\partial x}\Big)_{x_{s2}} \cdots \Big(\frac{\partial v(t)}{\partial x}\Big)_{x_{sl}} \cdots \\ & \Big(\frac{\partial^{p-1} v(t)}{\partial x^{p-1}}\Big)_{x_{s1}} \Big(\frac{\partial^{p-1} v(t)}{\partial x^{p-1}}\Big)_{x_{s2}} \cdots \Big(\frac{\partial^{p-1} v(t)}{\partial x^{p-1}}\Big)_{x_{sl}} \Big]^T . \end{aligned} \tag{6.3.4}$$

[1] This order is always even, and usually denoted by $2p$ in the literature [Meirovitch]. Here we digress from the standard notation for brevity and clarity of the equations.

[2] a point sensors measures a quantity at one point in space as opposed to averaging it over a region.

We allow for the possibility that any one of the sensors measures either displacement, rate, or acceleration, by defining the system output vector, $\mathbf{y} \in \mathbb{R}^{lp}$, as follows:

$$\mathbf{y}(t) = \mathbf{C}_1 v_s(t) + \mathbf{C}_2 \dot{v}_s(t) + \mathbf{C}_3 \ddot{v}_s(t) \tag{6.3.5}$$

where $\mathbf{C}_1, \mathbf{C}_2$ and $\mathbf{C}_3$ are matrices with l^2p^2 constant coefficients which can be used to select displacement, rate or acceleration output from any of the lp sensors.

Actuators

A basic requirement for hyperstable blocks per Definition 5.2.3 is to have an equal number of system inputs and outputs. Thus we have to define lp inputs in order to match the outputs defined above.

As discussed in Appendix A, we assume a force distribution generated by p 'types' of point actuators, that can each excite one of the first p spatial derivatives of a vibrating structure at any one of l points x_{ak}. This yields the following modal excitations:

$$f_i(t) = \sum_{k=1}^{l} \sum_{j=0}^{p-1} \phi_i^{(j)}(x_{ak}) f^{(j)}(x_{ak}, t) \tag{6.3.6}$$

where $f^{(j)}$ is a 'j^{th}-order force' term as discussed in Appendix A. $f^{(0)}(x_{ak}, t)$ corresponds to a point force at $x = x_{ak}$, and $f^{(1)}(x_{ak}, t)$ corresponds to a point torque acting at $x = x_{ak}$. There is no immediately obvious interpretation for the higher-order force terms or 'higher-order actuators'. Introducing temporal derivatives in $f^{(j)}$ to generate additional types of actuators, in analogy to the definition of rate and acceleration sensors, is not justified because this appears to lack any physical meaning.

Condition on Types of Hyperstability Sensors

The application of the 'positive real lemma' (5.3.9c)–(5.3.11c) to the linear structural model with sensors and actuators defined above results in necessary and sufficient conditions for hyperstability sensors, which are derived step-by-step in Appendix A. The following condition is obtained for the coefficients of the output equation (6.3.5) and constitutes a necessary condition for the types of sensors

required:

$$\mathbf{C}_1 = \mathbf{C}_3 = \mathbf{0}. \tag{6.3.7}$$

This condition can be interpreted as follows:

- No displacement ($v^{(j)}$) or acceleration $\left(\frac{\partial^2 v^{(j)}}{\partial t^2}\right)$ measurements are allowed as hyperstability sensors.
- Rate $\left(\frac{\partial v^{(j)}}{\partial t}\right)$ sensors are required, and all spatial derivatives are allowed ($j = 0, 1 \ldots p-1$).

Condition on the Placement of Hyperstability Sensors

As shown in Appendix A, the following necessary and sufficient condition for the location of hyperstability sensors ensues from the Kalman-Yakubovich lemma:

$$\text{sign } \phi_i^{(j)}(x_{sk}) = \text{ sign } \phi_i^{(j)}(x_{ak}) \; \forall \; i = 1 \ldots n, \; k = 1 \ldots l, \; j = 0 \ldots p-1. \tag{6.3.8}$$

It is interesting to note that condition (2.3.9) encountered in Section 2.3 during the stability analysis of a flexible beam with non-collocated feedback has some similarity with (6.3.8), as discussed in more detail in Appendix A.4. The above condition has the following interpretation:

- It is sufficient to collocate hyperstability sensors with corresponding [1] actuators ($x_{sk} = x_{ak} \; \forall \; k$)
- It is necessary to place hyperstability sensors and corresponding[1] actuators at such locations where each one of the mode shapes (or, if higher-order devices are used, the corresponding derivatives) has the same sign.
- For structures with an 'infinite number' of vibration modes, the last condition is, in general, only fulfilled by collocation of sensors and actuators. (This condition can be relaxed for devices located on rigid substructures.)

Although the interpretation of these conditions is similar to that of the known sufficient conditions and points again towards collocated dual sensors, the author is not aware that *necessary* conditions for hyperstability sensors have been previously established.

[1] "Corresponding" sensors and actuators are defined as having the same indices for location, and acting on the same spatial derivative

Necessary vs. Sufficient Conditions

We will now compare the necessary conditions for hyperstability sensors for the linear model with the sufficient conditions for general non-linear systems. At first, the conditions (6.3.7)–(6.3.8) and (6.2.9)–(6.2.10) and (6.2.13)–(6.2.14) appear to be of different nature. However there exist certain relationships between the IOP and the energy contained in linear structures. When the necessary conditions on the types and placement of hyperstability sensors are satisfied, the simplified linear system has an IOP of the following form, as derived in Appendix A.4:

$$\mathbf{u}^T(t)\mathbf{y}(t) = \sum_{i=1}^{n} s_i f_i(t)\dot{q}_i(t); \quad s_i > 0, \tag{6.3.9}$$

where the s_i's are positive but otherwise arbitrary factors without any associated physical units. On the other hand, the change of energy contained in the system is given by:

$$\dot{E}(t) = \sum_{i=1}^{n} f_i(t)\dot{q}_i(t). \tag{6.3.10}$$

Based on the similarity of their right-hand sides we can draw the following conclusions from a comparison of the above equations:

- It is a necessary condition for hyperstability sensors of the linear system that the IOP represents physical power (work).
- It is a necessary condition for hyperstability sensors of the linear system that the IOP qualitatively reflects the power exchanged with each mode of the system; i.e. if the power $f_i\dot{q}_i$ exchanged with any one mode i grows above all bounds, it must show in $\mathbf{u}^T\mathbf{y}$ with the correct sign.

If $s_i = 1 \; \forall \; i \; 1, 2, \ldots, n$ we can obviously equate the left-hand sides of (6.3.9) and (6.3.10), and obtain the following expression which is identical to condition (6.2.10) for the general non-linear system:

$$\mathbf{u}^T\mathbf{y} = \dot{E}. \tag{6.3.11}$$

(Here $P_A = \dot{E}$ because all inputs to the linear simplified structure were assumed to be control inputs.) It is shown in Appendix A.4 that the special case $s_i = 1$

$\forall\ i$ is synonymous with the collocation of sensors and actuators ($x_{sk} = x_{ak}\ \forall\ k$). This in turn was shown to be a sufficient condition for hyperstability of the linear system, becoming a necessary condition when $n \to \infty$ (cf. (6.3.8)).

Hence, we can conclude that the sufficient conditions found in Section 6.2 for hyperstability sensors of general mechanical systems are actually quite sharply focused as they are identical with the necessary condition for hyperstability sensors for a simplified linear structure with an infinite number of vibration modes. Further, the necessary conditions for linear structures were shown to have an interpretation closely related to the sufficient condition for the general system. This is remarkable because the systems considered in Section 6.2 are so much more general than the simplified, one-dimensional linear structure.

We can further conclude from (6.3.11) that the 'higher-order' sensors and actuators which were defined for the linear analysis are also admissible for the general system. Conversely, sensors and actuators with distributed action are admissible for linear hyperstable structures as long as the devices fulfill any of the sufficient conditions for the general case. An interesting example for 'higher-order distributed-action' devices involving the second derivative, $v^{(2)}$, are piezoelectric films which can sense and generate strain in a structure. Piezoelectric devices for vibration damping in flexible structures were investigated by [Bailey and Hubbard].

6.4 Application to SSRMS

Objective

The hard requirement imposed on the system design by the proposed method as summarized in Section 5.5, is the need for suitable hyperstability sensors. After identifying their properties in Sections 6.2 – 6.3 it is in order to perform a reality check and determine to what extent the requirement for hyperstability sensors can be met in an actual robotic system. The SSRMS is used as a reference system for this assessment.

SSRMS Joint Instrumentation

In the case of the SSRMS which is discussed in some detail in Section 3.1, the actuators for the motion of the manipulators are the motors in each of the 7 manipulator joints. Each joint provides a precisely controlled joint rate in response to a rate command from a central computer. To control the joint rates, each joint has a servomechanism which uses measurements of the motor speed and the joint rate. These measurements are provided by high-accuracy resolvers and associated resolver-to-digital-converters (RDC) which convert the raw resolver signals to angular position and rate measurements. The motor resolvers are mounted directly on the motor shafts. These devices meet all the criteria (number, location, type) established above for hyperstability sensors. This favourable situation where a full complement of suitable hyperstability sensors is already designed into a system is not uncommon and, indeed, typical for cases where the actuators form part of servomechanisms.

Conclusion

For robotic systems one can indeed expect that, in most cases, suitable hyperstability sensors are already incorporated into the design to enable precise control of the joints, and that the requirement for hyperstability sensors arising from the proposed method has little negative impact on the robot design, if any. Therefore, the proposed concept is on a realistic footing for its practical implementation.

CHAPTER 7

APPLICATION TO VISION-BASED CONTROL OF FLEXIBLE ROBOT

7.1 Overview

In this Chapter we will focus again on vision-based control of flexible robots, the original problem motivating this study. We will apply the instrumentation and sensor fusion design concept developed in Chapter 5 and the conditions for hyperstability sensors developed in Chapter 6 to a concrete design example and validate the proposed methodology by experiment and simulations.

The main objective of the experimental work is to provide a proof-of-principle demonstration for the concept and to evaluate its robustness and performance characteristics in a setting representative of robotic assembly tasks in space such as the Space Station assembly tasks shown in Figures 1.2 and 1.3.

A robotic reference task and the experimental facility are discussed in Section 7.2. The application of the 3-step procedure for instrumentation design and sensor fusion to the experimental robotic system and the implementation of the sensor fusion and control algorithms are described in Section 7.3.

Experimental results validating the concept are presented in Section 7.4. Performance and robustness properties of the concept are further explored by simulations in Section 7.5, and compared to those of a model-based control system, based on a Kalman filter, in Section 7.6.

7.2 Experimental Apparatus

Robotic Reference Task

As part of this research project the apparatus shown in Figure 7.2.1 was developed for the experimental validation of the methodology. Its design is inspired by space robotics assembly tasks like those shown in Figures 1.1 and 1.2. The use of a Space Vision System (SVS) for the measurement of payload position is described by [MacLean and Pinkney]. A prototype system was tested on the Space Shuttle as an operator aid for manual SRMS operations (i.e. not for automatic control) in preparation of the use of an operational system during the assembly of the Space Station. A critical aspect during robotic assembly operations in space is the precise positioning of the manipulator payload within the capture envelope of the latching mechanisms used to connect the elements.

A related laboratory experiment is the precise positioning of payloads relative to objects in the workspace. To capture those aspects of assembly operations in space which are most relevant to this research, the laboratory experiment must display the dynamic and vibration characteristics typical of space manipulators. Another objective is to use sensors and sensor data processing representative of those used in space. Hence the experimental apparatus developed for this study includes a flexible link and the SVS as a measurement system for payload motion.

A simple test sufficient for a proof-of-principle demonstration can be accomplished by the planar motion of the flexible link with varying payloads as shown conceptually in Figure 7.2.2. This set-up is in principle similar to the example discussed in Section 3.4. The vision system is used to measure the motion $v(\ell, t)$ of a payload mounted at the tip of a flexible beam as it is positioned at, or tracking, a reference position $w(t)$. With a single link / single joint configuration and small elastic deformations $\psi \ll \ell$, the motion $v(\ell, t)$ is obviously constrained to a circle around the joint, and the reference position $w(t)$ must also lie on this circle to be meaningful. Therefore both v and w are scalar circumferential coordinates as indicated in Figure 7.2.2. In the experiment the reference position w can be either externally specified as an absolute position, or it can be determined "on line" by

the SVS using a visual reference target in the workspace.

Although the planar single-link configuration is simple, it is not trivial because of the non-collocated arrangement of sensors and actuators on the flexible beam. It permits the assessment of the performance achieved by the proposed methodology in terms of speed and accuracy of payload manipulation. To be meaningful, the tests must be set up such that flexible motions in the beam are sufficiently excited. A sudden change of the reference position, typically achieved by a step function, leads to a strong excitement of the flexible motions. Variation of the payload mass allows to validate the robustness of the proposed methodology against changes and unknowns in the flexible system dynamics - a key feature of the proposed model-free method.

Overview of Experimental Apparatus

Figure 7.2.3 provides an overview of the experimental apparatus. The central element is a robot with three revolute joints and a flexible link. In analogy to an assembly task in space, the tip motion of the flexible link is measured relative to a reference in the workspace by a vision system. Visual targets are mounted at the tip of the robot arm and at the reference point. These targets are imaged by a video camera and the image is processed in real-time by the SVS processor to determine the position of the targets in the workspace. The design and operational characteristics of the SVS and the targets used are discussed in more detail in Appendix D. The SVS processor communicates via a serial link with the control computer. This 486 PC running DOS hosts the sensor fusion and control algorithm. Even though the SVS internally processes images at the video frame rate of 30 Hz, the interface to the control computer provides only a sampling rate of 6 Hz due to limitations of the SVS software. Besides the measurements from the vision system the control computer receives analog inputs from various sensors on the robot which are processed at a sampling rate of 50 Hz. The computer controls the robot by providing analog input signals to a set of servo-power-amplifiers (SPA) driving the robot joint motors.

Robot Joint Characteristics

The three joints of the robot are of almost identical design. A joint and its various major components are shown in Figure 7.2.4. The actuators are DC servo motors with harmonic drives providing a 120:1 speed reduction. At the output side, the joints are capable of providing a maximum continuous torque of about 50 Nm and a maximum velocity of about 3 rad/s. Static friction of bearings and gearing is in the order of 4 Nm at the joint output. Each joint is instrumented with an encoder and a tachometer on the output side.

The planar motion of the proof-of-principle test case only requires motion of joint 3 while joints 1 and 2 can remain stationary. Joint 3 is configured as a torque servomechanism to reduce the effects of joint friction. Two strain gauges mounted at the root of the flexible beam are configured as a half-bridge to measure the torque applied at the root of the flexible beam by the joint. A torque control loop based on the strain gauge measurements is closed via the control computer at a sampling rate of 50 Hz, cancelling the effects of friction. The SPA driving the motor is configured in "torque mode", i.e. producing a motor current proportional to the SPA input voltage.

Flexible Link

The flexible link of the robot consists of a thin steel beam with a length of 1.585 m. Other dimensions and characteristics are listed in Tables 3.4.1 and 3.4.2. The visual target assembly which is further described in Appendix D, has a mass of 0.14 kg. Various weights up to a total of 1.2 kg can be attached to the tip of the beam to simulate payloads. With the maximum payload the static load in the beam approaches the buckling limit. When the fully loaded beam is moved vigorously, slow non-linear flexible motions in the buckling regime can be observed. Although difficult to model analytically, these motions are a welcome addition to the repertoire of "complex" behaviour of the system.

Modelling Assumptions

The modelling example presented in Section 3.4 provides an analytical description of the key characteristics of the experimental set-up and is used as a

model for the design of the sensor fusion and control algorithm in Section 7.3 and for simulations in Section 7.5 and 7.6. Since we are advocating a robust "model-free" methodology we are not too concerned about the obvious limitations of this model arising from the "usual" simplifying assumptions with regard to: one-dimensionality, linearity, slender beam, no friction or damping, modal truncation and ideal actuator characteristics.

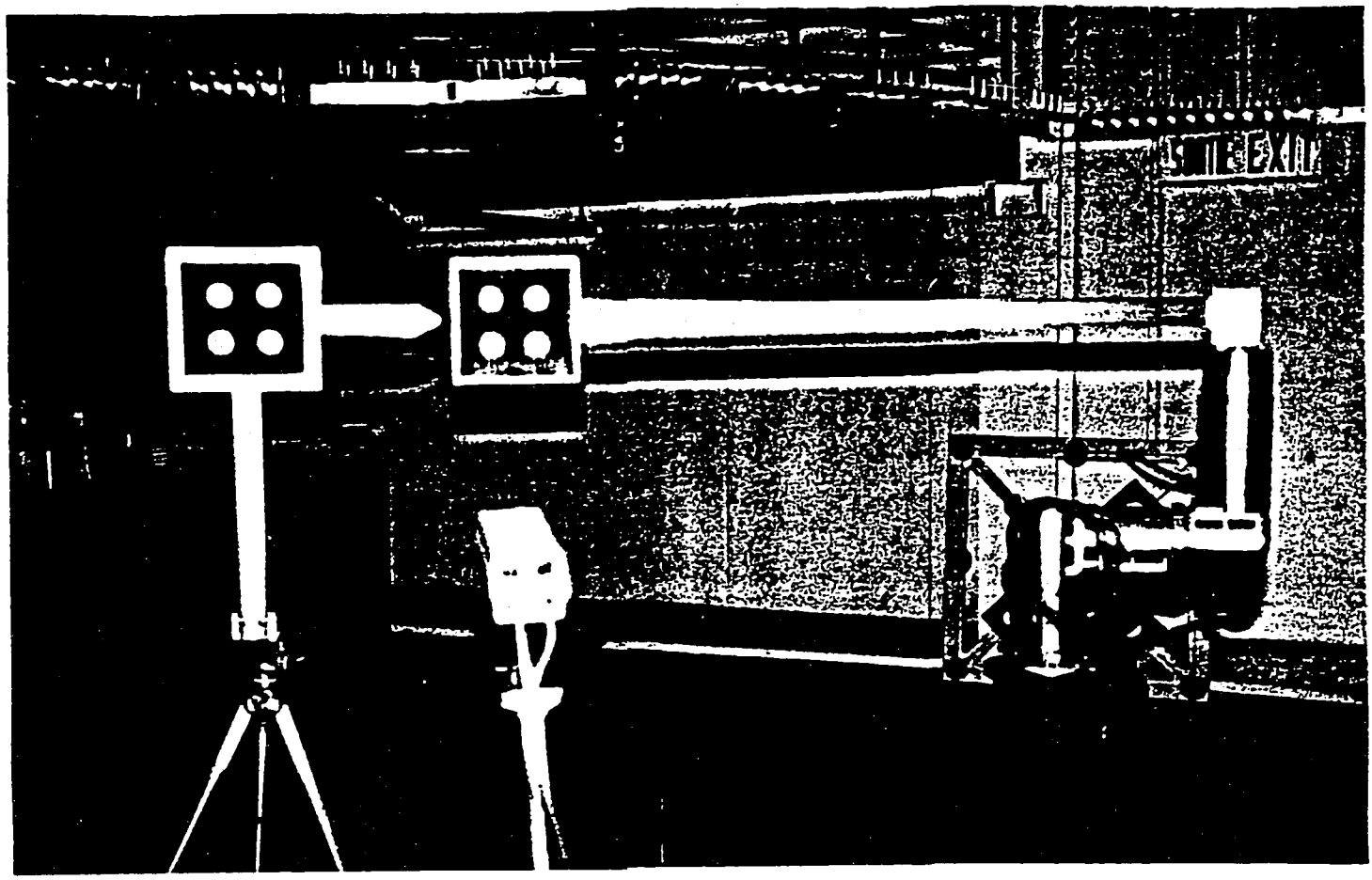

Figure 7.2.1: Laboratory Robot with Visual Targets and Camera

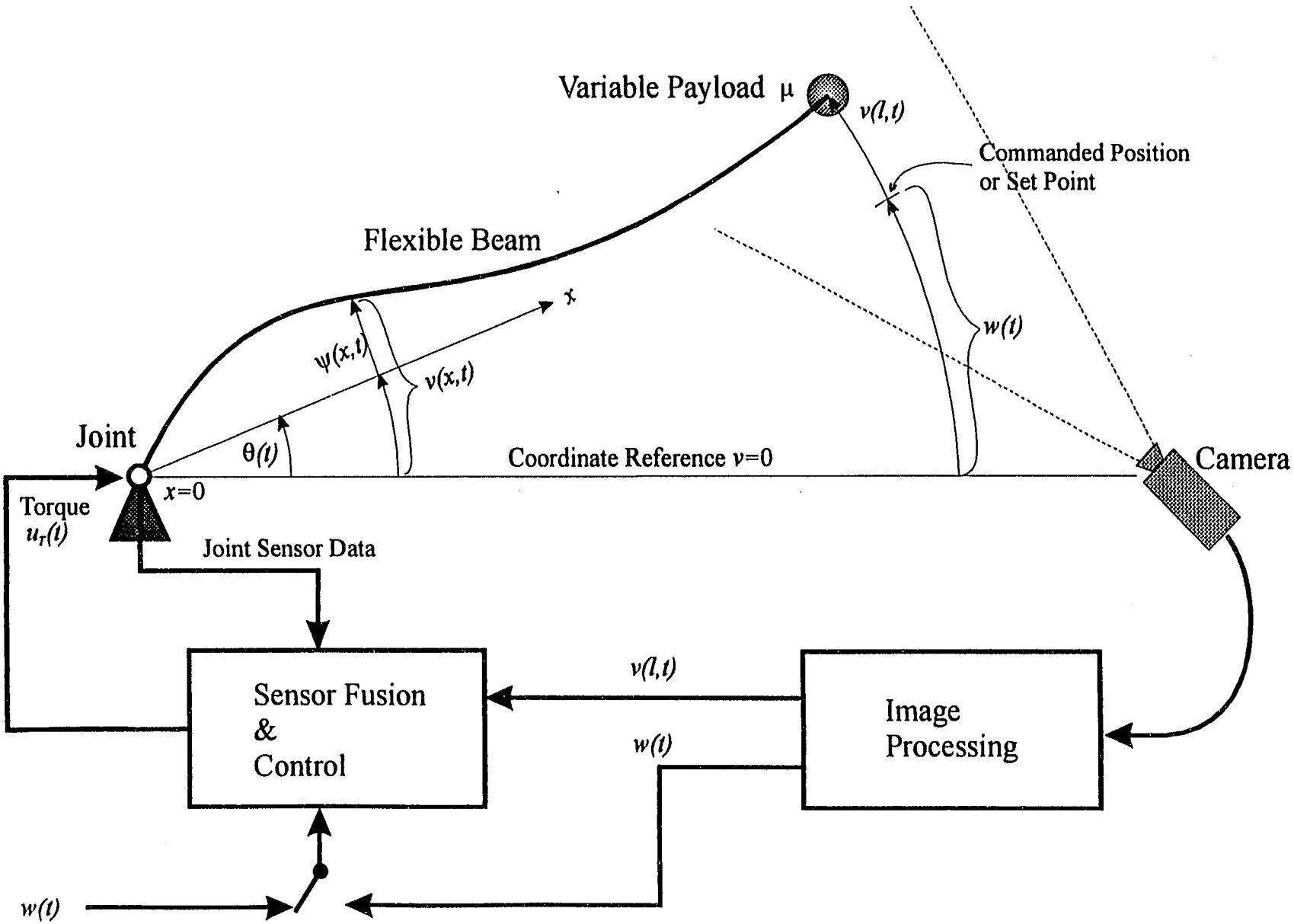

Figure 7.2.2: Proof-of-Principle Test Configuration

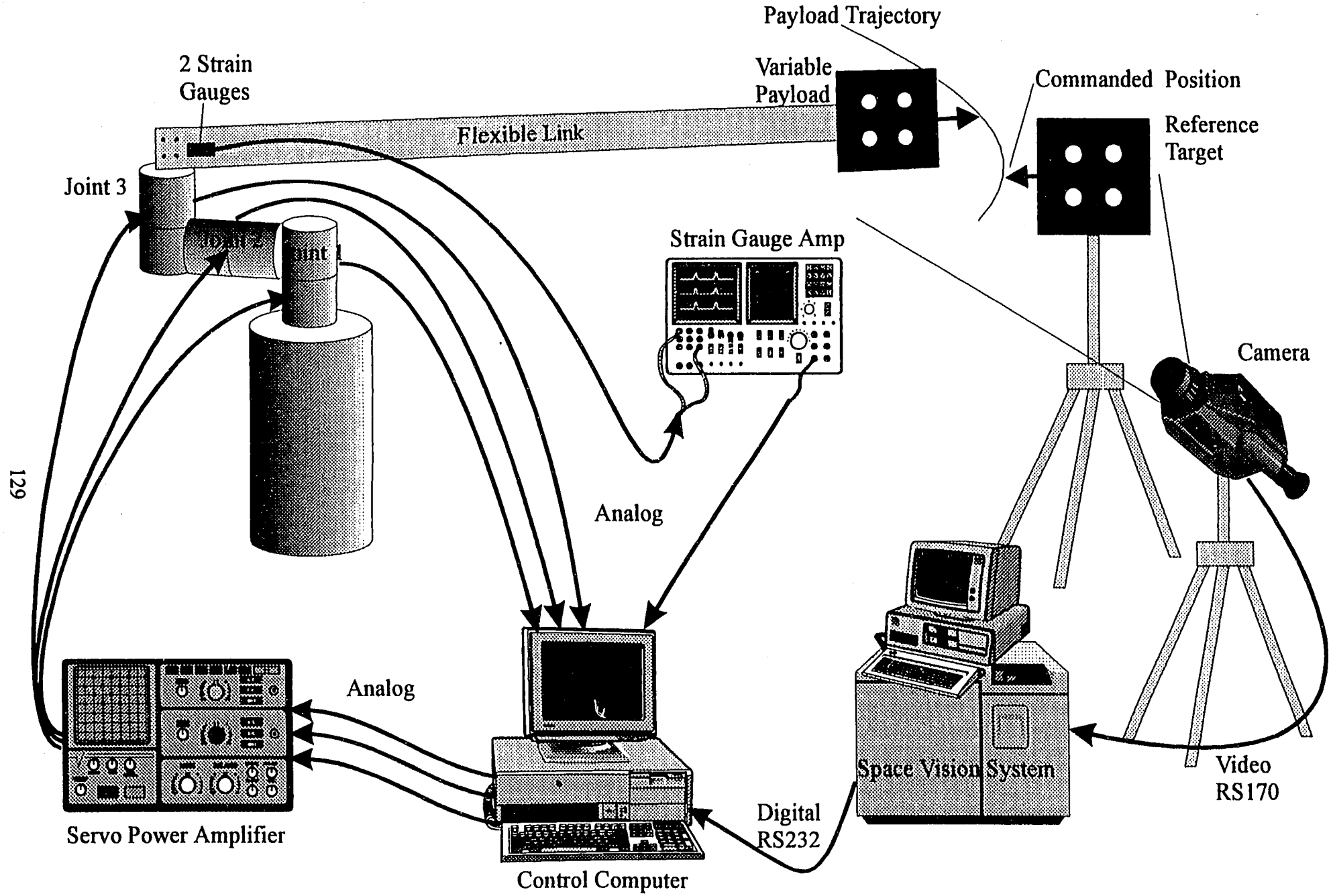

Figure 7.2.3: Experimental Apparatus

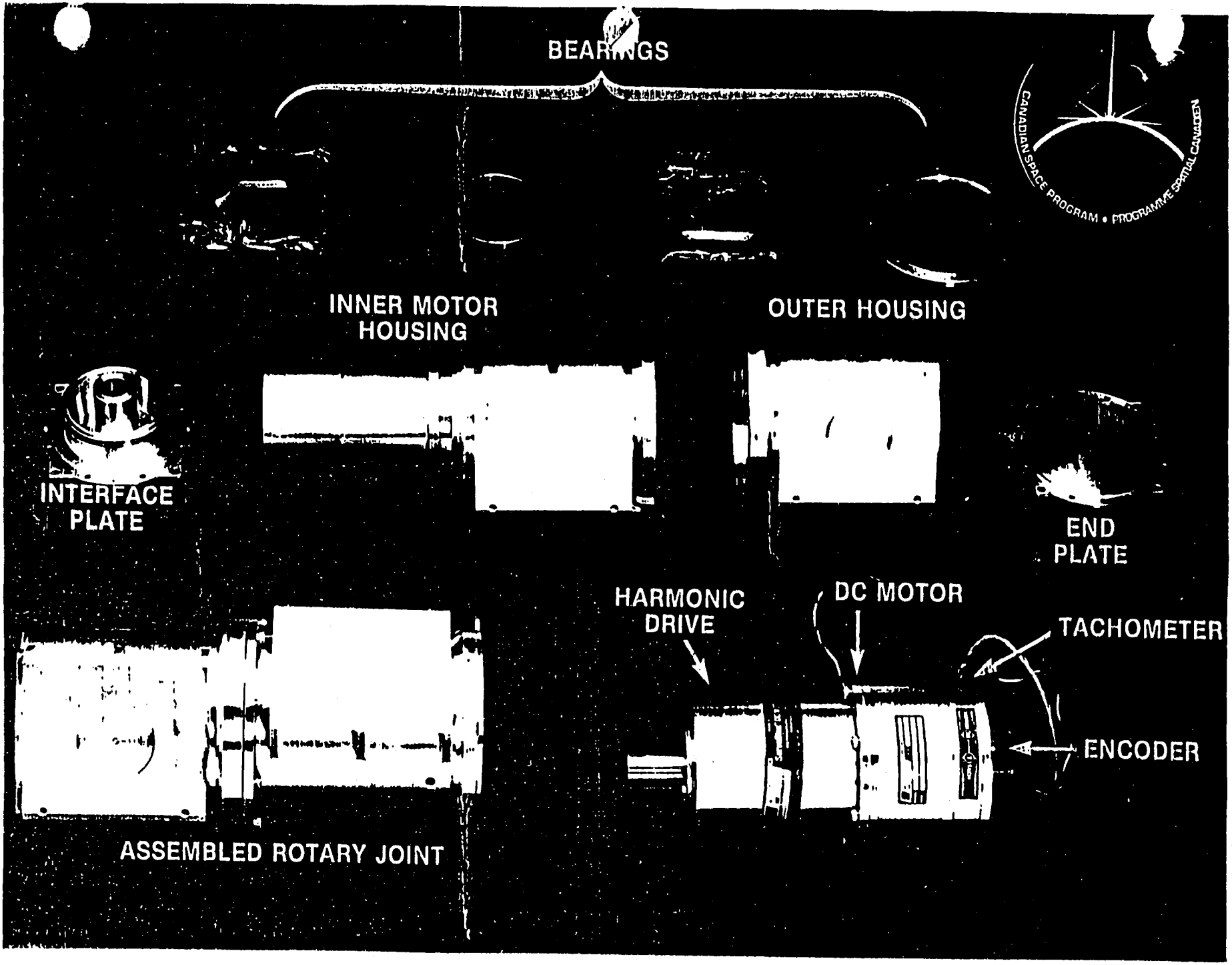

Figure 7.2.4: Components of Robot Joint

7.3 Instrumentation Design and Sensor Fusion Algorithm

Design Procedure

In this Section we will demonstrate how the 3-step design procedure outlined in Section 5.5 is applied to be flexible link robot of the experimental set-up. The simple robot configuration results in a fairly simple scalar design problem suitable for a clear demonstration of the principle. The three steps of the design process are:

1) Determine the complement of hyperstability sensors;
2) Determine the complement of performance sensors;
3) Design of sensor fusion and control algorithms.

We will also discuss the digital implementation of the sensor fusion and control algorithm.

Hyperstability Sensor

Sections 6.2 and 6.3 prepared us for Step 1 by identifying necessary and sufficient conditions for hyperstability sensors on flexible mechanical systems. According to the conditions developed in 5.3 and 6.2, only a single hyperstability sensor is required and allowed because the system only has one actuator. Since an explicit system model is given in Section 3.4 we can apply the sufficient condition (6.2.9) to determine the hyperstability sensor based on (3.4.23):

$$\begin{aligned} y(t) &= \mathbf{B}_u^T \dot{\mathbf{q}}(t) \\ &= \frac{d\phi}{dx}\Big|_{x=0} \dot{\mathbf{q}}(t) \\ &= \dot{v}^{(1)}(x=0,t) \end{aligned} \tag{7.3.1}$$

This equation defines a tachometer located at the joint ($x = 0$) already familiar from earlier examples such as (2.2.1). This choice for the hyperstability sensor is not only sufficient but also necessary, according to conditions (6.3.7) and (6.3.8) for linear systems.

While (7.3.1) defines the physical quantity measured by the hyperstability sensor, its output in the presence of measurement errors, $\bar{y}$, is characterized by a scalar mapping function m defined per (5.4.14) and (5.4.15) with the error parameter ε:

$$\bar{y}(t) = m(y(t), \varepsilon) \tag{7.3.2}$$

When measurement errors are not considered, the sensor output can simply be defined by

$$\bar{y}(t) = y(t). \tag{7.3.3}$$

Performance Sensor

For the simple system shown in Figure 7.2.2, Step 2 of the procedure described in Section 5.5 is straightforward. The vision system measuring the motion of the payload is not a hyperstability sensor as it violates the necessary conditions (6.3.7) and (6.3.8), i.e. because it is not associated with an actuator, and because it measures position and not a rate variable. The measurement of the vision system is required to achieve the performance objective of tracking a variable set point $w(t)$ by the arm tip or payload position $v(\ell, t)$. Hence we designate the vision system as the performance sensor:

$$z(t) = v(\ell, t) \tag{7.3.4}$$

With these simple definitions, the physical system shown in Figures 7.2.2 can be readily mapped into the extended hyperstability concept of Figure 5.4.6, as shown in Figure 7.3.1.

Reference Input

The reference position $w(t)$ can either be measured by the SVS, as indicated in Figure 7.3.1, or it can be entered as an absolute position at the keyboard of the Control Computer during the test. Although physically combined, the function of measuring the reference position by the SVS is logically independent of the measurement of the payload position. The connection between the SVS and w shown in Figure 7.3.1 does not constitute a feedback loop.

Sensor Fusion and Control Algorithm

For sensor fusion and control we may apply any of the algorithms identified in Section 5.4. In the case of our simple scalar example, 'Algorithm 1' and 'Algorithm 2' are identical, and 'Algorithm 3' is essentially identical to 'Algorithm 2' under the assumption that the hyperstability sensor has no measurement errors.

We will apply 'Algorithm 3' per (5.4.19), (5.4.20) to the example problem. It is restated below in a scalar version ($l = 1$) sufficient for our scalar example:

$$\mathcal{C} = \begin{cases} \mathcal{C}_B\{w, \bar{y}, z\} & \text{if } \bar{\Lambda} \\ \mathcal{C}_F\{w\} & \text{if not } \bar{\Lambda} \end{cases} \tag{7.3.5}$$

with $\bar{\Lambda} \in$ (true, false):

$$\bar{\Lambda} = [\bar{y}\ \mathcal{C}_B\{w, \bar{y}, z\} + \varepsilon|\mathcal{C}_B\{w, \bar{y}, z\}| < 0]. \tag{7.3.6}$$

The control functions $\mathcal{C}_B\{w, \bar{y}, z\}$ and $\mathcal{C}_F\{w\}$ of (5.4.19) which are scalar functions of scalar inputs in our example, can be freely chosen, e.g. based on conventional control principles. We will use fairly simple control functions to illustrate the principle and demonstrate that it is not required to use particularly sophisticated functions, although they might improve the performance. A simple, conventional feedback control approach is PID control which we now apply, somewhat naively, to the end point tracking problem, ignoring the destabilizing effect of the link flexibility. In the Laplace domain the PID control law (with band-limited differentiator) is defined as follows (s is the Laplace operator, F_P, F_D, F_I, F_V are gain constants):

$$\mathcal{C}_B\{W(s), Z(s)\} = \left(F_P + \frac{F_I}{s} + \frac{F_D s}{1 + F_V s}\right)(W(s) - Z(s)) \tag{7.3.7}$$

For feed-forward control of robots, several methods to determine torque profiles from trajectory commands have been proposed in the robotics literature, such as [Fu, Gonzales and Lee]. As one of our objectives is to demonstrate that our method does not rely on accurate system models we will use a simple lead filter as

feed-forward, which incorporates only very rudimentary knowledge of the system, such as "which way" to move the joint, but not "how far" or "how fast". For the simple single-joint case, the lead feed-forward control term, with gain and time constants F_1, F_2, is defined in the frequency domain as follows:

$$C_F\{W(s)\} = \frac{F_1 s}{1 + F_2 s}(W(s) - z(t=0)). \tag{7.3.8}$$

While feedforward is an optional feature in most control systems, it is an essential part in this concept since it is the vehicle for injecting energy into the system, a necessary condition for making it do anything useful. With this choice of control functions the design of the sensor fusion and control algorithm is fully defined. The following set of parameters for the above algorithms were established by hardware experimentation:

$$\begin{aligned} F_P &= 3.4 \text{ Nm}^{-1} \\ F_I &= 0 \text{ Nm}^{-1}\text{s}^{-1} \\ F_D &= 1.5 \text{ Nsm}^{-1} \\ F_V &= 0 \text{ s} \\ F_1 &= 0.475 \text{ Nsm}^{-1} \\ F_2 &= 0.25 \text{ s} \end{aligned}$$

Digital Implementation of Algorithm

For implementation on the control computer the algorithms (7.3.7) – (7.3.8) must be discretized for the sampling interval ΔT. For the discrete-time approximation of the integral term of the PID control law (7.3.7) we use Tustin's approximation $\frac{1}{s} \approx \frac{\Delta T}{2}\frac{z+1}{z-1}$, corresponding to the trapeze rule for integration, and for the conversion of the differential term the approximation $s \approx \frac{z-1}{\Delta T z}$, corresponding to the differential operator in the Euler integration scheme. This results in:

$$C_B\{W(\mathfrak{z}), Z(\mathfrak{z})\} = \frac{\vartheta_0 + \vartheta_1 \mathfrak{z}^{-1} + \vartheta_2 \mathfrak{z}^{-2}}{(1 - \mathfrak{z}^{-1})(1 + \chi_1 \mathfrak{z}^{-1})}(W(\mathfrak{z}) - Z(\mathfrak{z})) \tag{7.3.9}$$

with

$$\begin{aligned}
\vartheta_0 &= \frac{1}{1+F_V/\Delta T}(F_P + \frac{\Delta T + F_V}{2}F_I + \frac{F_D + F_V F_P}{\Delta T}) \\
\vartheta_1 &= \frac{1}{1+F_V/\Delta T}(-F_P + \frac{\Delta T}{2}F_I - 2\frac{F_D + F_V F_P}{\Delta T}) \\
\vartheta_2 &= \frac{1}{1+F_V/\Delta T}(\frac{F_D + F_V F_P}{\Delta T} - \frac{1}{2}F_V F_I) \\
\chi_1 &= -\frac{F_V}{\Delta T + F_V}
\end{aligned} \tag{7.3.10}$$

The lead term in (7.3.10) is approximated using $s \approx \frac{z-1}{\Delta T z}$ resulting in:

$$C_F\{W(\mathfrak{z})\} = \frac{F_1}{\Delta T}\frac{1-\mathfrak{z}^{-1}}{(1+F_1/\Delta T) - F_2/\Delta T \mathfrak{z}^{-1}}W(\mathfrak{z}) \tag{7.3.11}$$

The resulting overall discrete-time algorithm is obtained by inverse z-Transform from (7.3.9) and (7.3.11):

$$e(k) = w(k) - z(k) \tag{7.3.12}$$

$$C_B(k) = \vartheta_0 e(k) + \vartheta_1 e(k-1) + \vartheta_2 e(k-2) + (1-\chi_1)C_B(k-1) + \chi_1 C_B(k-2) \tag{7.3.13}$$

$$C_F(k) = \frac{F_2}{F_2 + \Delta T}\, C_F(k-1) + \frac{F_1}{F_2 + \Delta T}(w(k) - w(k-1)) \tag{7.3.14}$$

$$\bar{\Lambda}(k) = [\bar{y}(k)C_B(k) + \varepsilon|C_B(k)| < 0] \tag{7.3.15}$$

$$u_T(k) = \begin{cases} C_B(k) & \text{if } \bar{\Lambda}(k) \\ C_F(k) & \text{if not } \bar{\Lambda}(k) \end{cases} \tag{7.3.16}$$

This algorithm was programmed in C++, in slightly modified form to account for the various sampling rates in the system, and implemented as part of a quasi-real-time program running under DOS on the control computer.

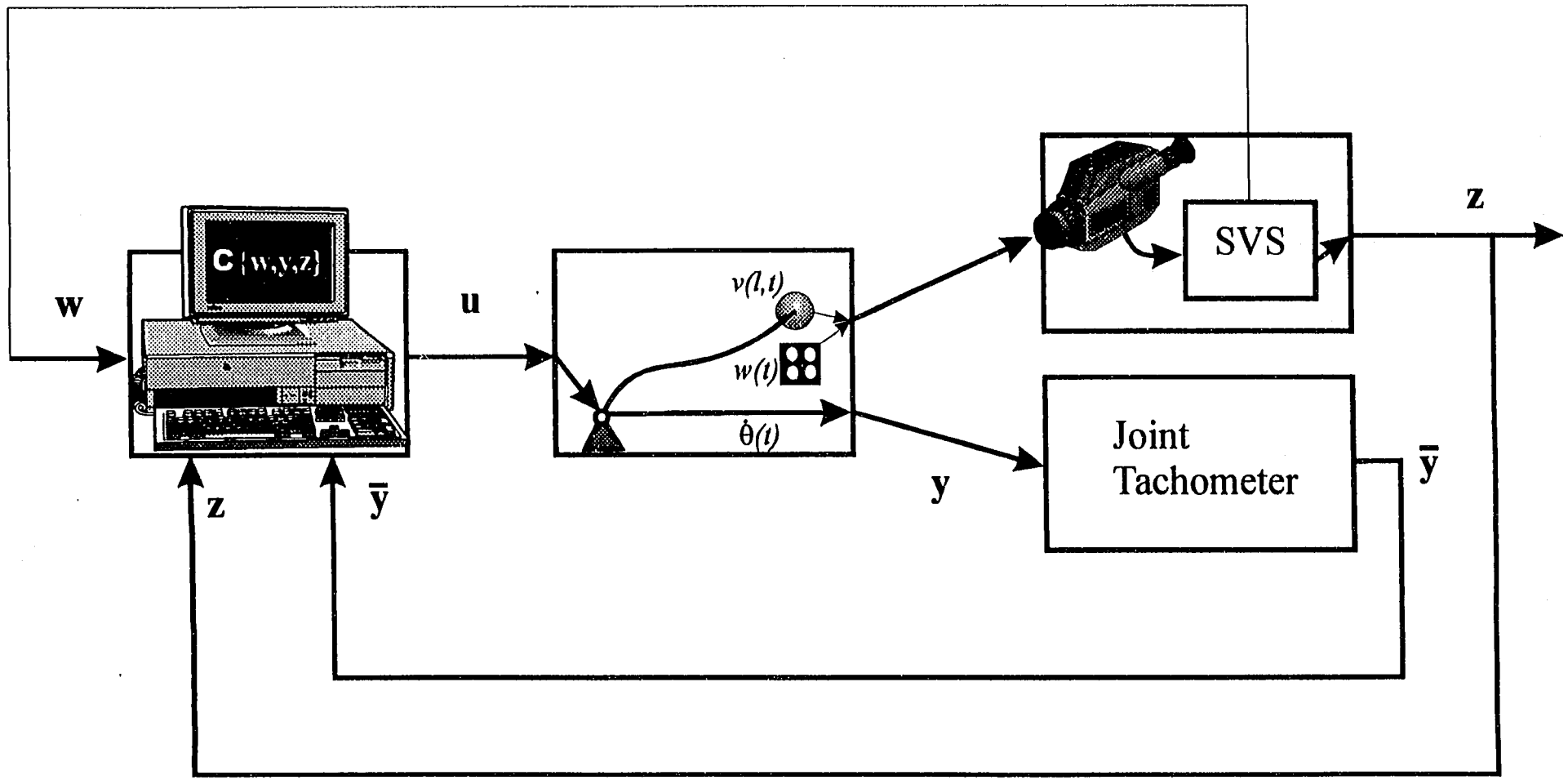

Figure 7.3.1: Mapping of Physical Configuration to Extended Hyperstability Concept

7.4 Experimental Validation

Overview

A number of tests were performed with the experimental apparatus. The most relevant tests in terms of the overall objectives are responses to step changes in the setpoint which tend to strongly excite flexible motions in the link and thus allow to study the effects of link flexibility. The results for two test cases, with and without payload, are discussed in detail below.

Additional tests were performed to investigate other aspects of the sensor fusion and control algorithm (7.3.5) – (7.3.8). For example, the stabilizing effect of the sensor fusion logic was examined by setting the fusion logic variable to '$\bar{\Lambda}$ = true' for one test, and thus running the PID feedback control law (7.3.7) on its own. Violent dynamic instability was observed during this particular test, confirming that PID control with the chosen parameters is unstable on a flexible link with non-collocated sensor/actuator configuration, and, more importantly, that the fusion logic (7.3.6) guarantees the stability of the closed-loop system even if the feedback function C_B on its own induces closed-loop instability.

Performance

Figure 7.4.1 shows the experimental results obtained for a test with only the visual target (0.14 kg) attached to the tip of the link and the step motion command:

$$w(t) = \begin{cases} -0.739 & \text{m for } t \leq 0 \\ -1.310 & \text{m for } t > 0 \end{cases}$$

This command requires a tip motion of 0.571 m. The diagram shows the time history of the tip position $z(t)$, the commanded torque $u_T(t)$, the joint angle $\theta(t)$ and the joint rate $\bar{y}(t)$. The response of the tip position as measured by the SVS indicates a smooth transient converging to the new set-point within about 5 s. The motion of the joint angle measured by the encoder is not used in the sensor fusion and control algorithm. It is interesting to note that the joint angle completes about 30% of its overall travel before the tip of the flexible link even begins to move, roughly at $t = 0.6$ s, indicating significant bending in the flexible

link, equivalent to a tip deflection of about 0.12 m. The joint motion exhibits "pauses" when the feedback is active and the fusion logic variable $\bar{\Lambda}$ = true which is indicated by switching in the torque command. During those periods the joint actually creeps slowly and strain energy is removed from the flexible link, leaving only relative small residual vibrations at the completion of the joint motion. This "pausing" is also evident from the joint rate measured by the tachometer which is the hyperstability sensor in this system and actually controls this behaviour.

This experimental result confirms the stability of the closed loop system with vision-based end-point control of the flexible link as expected from the theoretical development. The result also indicates good dynamic performance, with small overshoot and almost no residual vibration, in conjunction with a fairly simple control strategy and implementation.

Robustness to Changes in System Dynamics

The next test is intended to validate the robustness properties of the proposed approach. The test is performed with the maximum payload mass of 1.2 kg which significantly changes the dynamic characteristics of the flexible link. The same sensor fusion and control algorithm as before is used with identical parameters. The motion command is slightly different from before and produces a total payload motion of 0.737 m:

$$w(t) = \begin{cases} -0.651 & \text{m for } t \leq 0 \\ -1.388 & \text{m for } t > 0 \end{cases}$$

The test results for the same variables $z(t), u_T(t)\theta(t), \bar{y}(t)$ as before are shown in Figure 7.4.2. The convergence of the tip position is somewhat slower than in the unloaded case, as expected, and a little more oscillatory. As before, the strain energy is removed from the flexible beam by the sensor fusion and control algorithm at opportune moments during the motion as indicated by "pausing" or "creeping" of the joint motion.

The experimental results validate the expected robustness of the approach to major unknown changes in the dynamic characteristics of the flexible beam introduced here by the addition of the payload at the tip of the beam.

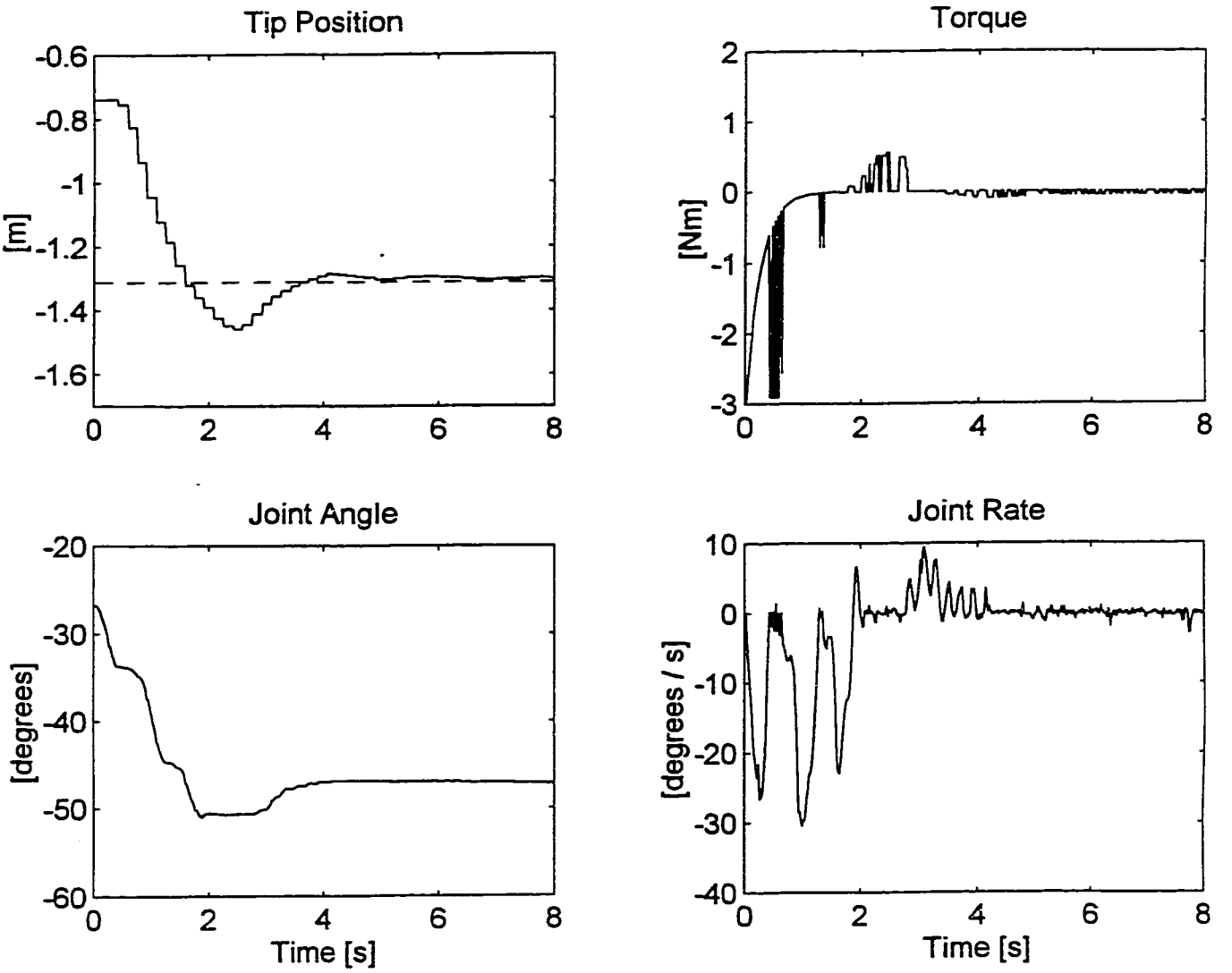

Figure 7.4.1: Test Results for Unloaded Arm

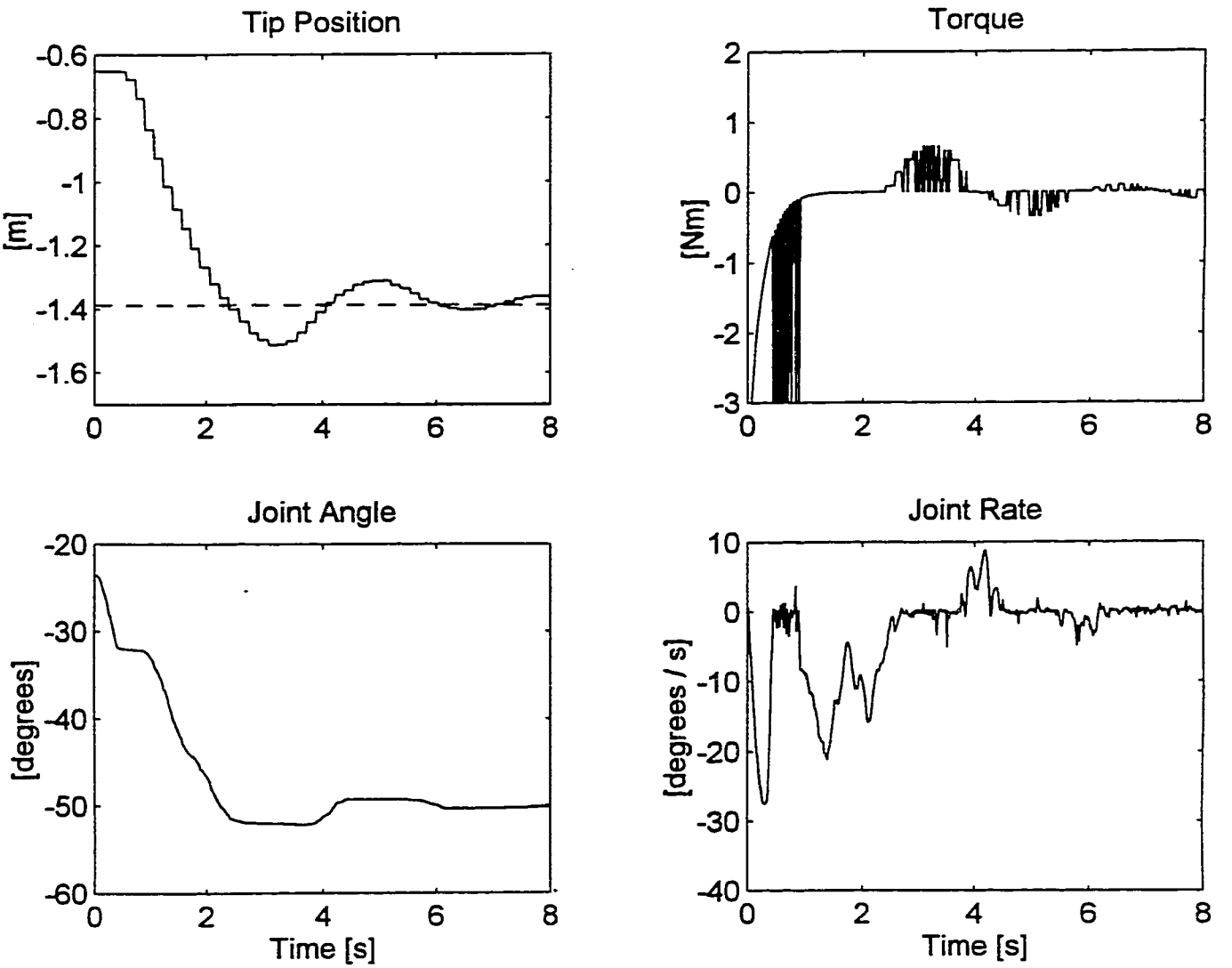

Figure 7.4.2: Test Results with 1.2 kg Payload

7.5 Evaluation by Simulation

Pupose of Simulations

While hardware tests are essential for a credible validation and assessment of the sensor fusion and control concept, numerical simulations are a useful and efficient tool to further explore the concept. Simulations allow to evaluate the concept for a larger range of payloads and investigate effects like "varying the number of modes in the system" which can not be easily done in a physical system.

The objective in constructing a simulation model is to find a simple model which 'adequately' represent the behaviour of the real system. What is 'adequate' depends on the time frame or frequency range considered in the response and is somewhat of a judgment call. In our case however, the availability of experimental data allows the validation of simulations and thus considerably raises the level of confidence in and relevance of simulation results.

Model Description

The model used for the simulations is shown in Figure 7.5.1. The flexible link is modelled by the linear state-space equation (3.4.43). The payload mass is varied from 0.14 kg (mass of the visual targets) to 120 kg, and up to three flexible modes are included in the model in addition to the rigid-body mode, i.e. $n = 2 \ldots 4$. The modal parameters for the various models are listed in Tables 3.4.1 and 3.4.2. and Appendix E.1. The state-space matrices of the model with various payloads and flexible modes used in the simulations are listed in Appendix E.2.

The torque servomechanism providing the actuation for the system is assumed to be "perfect", i.e. having a unity transfer function, over the range of torque levels and frequencies considered in this evaluation.

The sensors measuring joint angular rate and payload position are assumed to be ideal and are represented by equations (7.3.1) and (7.3.4) in conjunction with (3.4.15). The 50 Hz sampling process is approximated by a continuous-time representation in the simulation while the relatively slow data interface between the SVS and the Control Computer is modelled as a 6 Hz sample-and-hold process.

The sensor fusion and control algorithm is implemented in the simulation largely in the continuous-time form given by (7.3.5) – (7.3.8), as the effects of sampling at 50 Hz are not significant for the responses analyzed. An exception is the differentiation in the PD algorithm which is implemented in discrete time consistent with the sampling rate of the SVS interface. The implementation of the sensor fusion and control algorithm (7.3.5) – (7.3.8) in the simulation is further simplified by the following parameter selection consistent with parameters used in the experiment: $F_I = 0, F_V = 0$ and $\varepsilon = 0$.

The setpoint is generated in the simulation by a combination of function generators. Consistent with the reference task described in Section 7.4, a simple step function is used to generate the setpoint function for the simulation runs discussed below.

Validation of Simulation

The simulation model of Figure 7.5.1 is validated by comparing simulations of the experiments against experimental results. Complete agreement between simulation and experiment is not expected due to the many simplifying assumptions and abstractions used in the construction of the model, as well as uncertainties in some of the model parameters. However, a "valid" simulation is expected to exhibit, and predict, the characteristic behaviour of the real system. The validation of complex dynamic simulations is a somewhat subjective process.

Figure 7.5.2 shows the response of the simulation of the unloaded robot with two flexible modes (see Appendix E.2.2 for detailed model information) under the initial conditions and external stimuli of the experiment shown in Figure 7.4.1. The time histories of the tip position, the joint angle, joint rate and the commanded torque of the simulated response are very similar to those measured during the experiment. The simulation reproduces the characteristic step-wise motion of the joint which pauses at an angle of about $-33°, -45°$ and $-51°$. Differences can be seen in the initial response $0 \leq t \leq 0.5$s. In the simulation the joint rate shows sudden acceleration and a double peak instead of the rounded single peak apparent in the experimental results, and the tip position shows an initial transient in the

positive direction. These effects are mainly due to modelling the flexibility effects by a limited number of "pinned-free" modes. The low number of modes leads to the "inverse" initial response characteristic of non-minimum phase systems, while the real system has a delayed response due to the finite speed of wave propagation in the flexible link. The choice of modes based on pinned-free boundary conditions initially presents less moment of inertia to the joint than modes chosen on clamped-free boundary conditions which are therefore advocated for the purpose of simulation by some researchers such as [Piedboef]. Another factor affecting the initial response is the assumption of an "ideal" torque servo, while the real torque servo has a limited bandwidth and limited acceleration capabilities. In spite of these simplifications the model shows good overall agreement with the experimental data for the unloaded case. The real system performs somewhat "better" that the simulation, most likely due to residual friction in the joint, unmodelled damping effects, and unmodelled low-pass characteristics of the torque servo.

Figure 7.5.3 shows the results of simulating the loaded test case for which the experimental results are shown in Figure 7.4.2. The flexible link model used in this case is described in Appendix E.2.4. As in the experiment, the parameters of the sensor fusion and control algorithm are the same as for the unloaded case. The simulation reproduces the characteristic behaviour of the experiment, with the joint angle "pausing" during its motion at approximately $-32°$ and $-53°$. The simulation exhibits the same initial response as in the unloaded case, i.e. a very rapid acceleration of the joint. A discussion of this initial transient was presented above for the unloaded case. While the simulation closely matches the experimental results until about $t = 2$s, the simulation lags a little behind the experiment for the rest of the response, and displays less damping than the experimental results. The slower response is likely due to a parameter mismatch, while the reduced damping can be attributed to simplified modelling assumptions which ignore residual friction in the joint and other damping effects. Overall the relatively simple simulation model is quite representative of the behaviour of the experimental system.

Effects of Model Order

We will now briefly investigate what effects a variation of the model order has on the model fidelity. The simulation of the unloaded experiment is used as a reference. Two flexible modes were included in the model per Appendix E.2.2 used in the reference simulation shown in Figure 7.5.2. Figure 7.5.4 shows the result of including only a single flexible mode in the model of the flexible link per Appendix E.2.1. Although the overall response is still representative of the experimental results, it misses the "detail", in particular in the joint motion, which makes the response 7.5.2 look "realistic" when compared to the experimental results of Figure 7.4.1.

The response of the simulation with three flexible modes in the link model per Appendix E.2.3 is shown in Figure 7.5.5. A comparison with the experimental data indicates that the addition of the third flexible mode does not improve the model, in the sense that the response obtained is not closer to the experimental results. It is suspected that the modal frequency of the third mode is beyond the frequency range over which the simplified model is valid. For higher frequencies the model validity is affected by the assumptions of an ideal torque servomechanism, no damping, and the 'slender beam' assumption.

The comparison of simulations with different numbers of flexible modes and the experimental data confirms that the inclusion of two flexible modes is a good choice for the type of response analyzed.

Evaluation of Robustness and Performance

The comparison of responses with one, two and three flexible modes per Figures 7.5.2, 7.5.3 and 7.5.4, respectively, also corroborates the claim of robustness of the sensor fusion and control concept to variations in the system dynamics. The performance as indicated by the transient of the tip position is virtually identical in all three cases.

The simulation allows to investigate the robustness and performance of the sensor fusion and control concept for a range of robot payloads beyond the capability of the hardware experiment where the payload mass is limited to about

1.2 kg due to buckling of the flexible beam under gravitational forces. In the simple planar simulation model the payload mass can be increased several orders of magnitude without regard to gravitational effects, just like in a robotic system operating in Earth Orbit.

To investigate the effect of increased payloads, the behaviour of the experimental system is simulated for payloads of 12 kg and 120 kg (model parameters per Appendix E.2.5 and E.2.6) using the simulation of Figure 7.5.1 and the "loaded" test case familiar from Figure 7.4.2. The simulation results are presented in Figures 7.5.6 and 7.5.7, respectively. As expected from the theoretical properties of the sensor fusion and control concept, the system remains stable in both cases. The response obviously slows down as the payload mass increases, and the damping of the tip motion reduces somewhat. Nevertheless the original algorithm which was not tuned in any way for the larger payloads, produces a fairly consistent behaviour even though the payload mass is varied over four orders of magnitude.

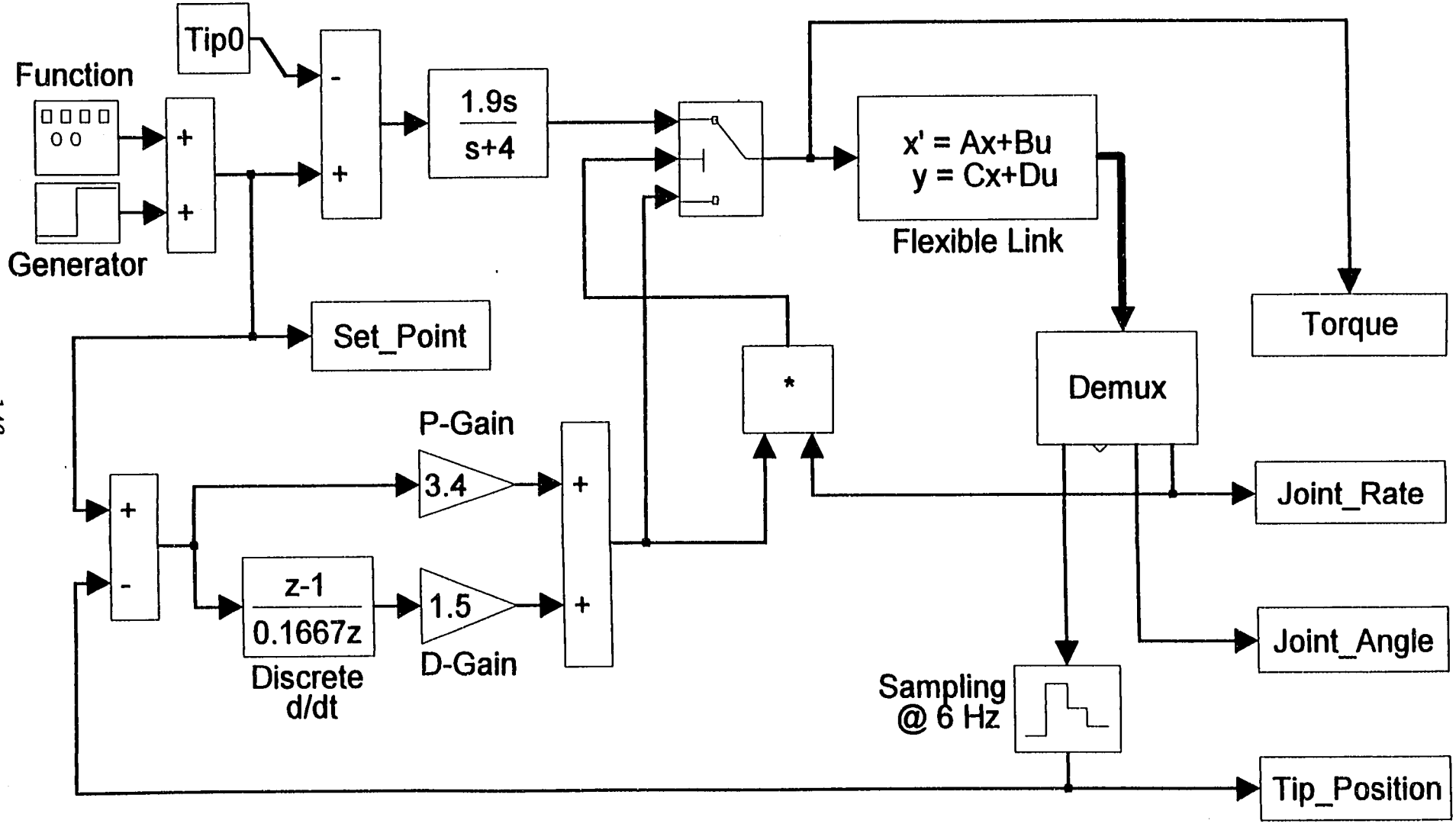

Figure 7.5.1: Simulation of Flexible Link Experiment

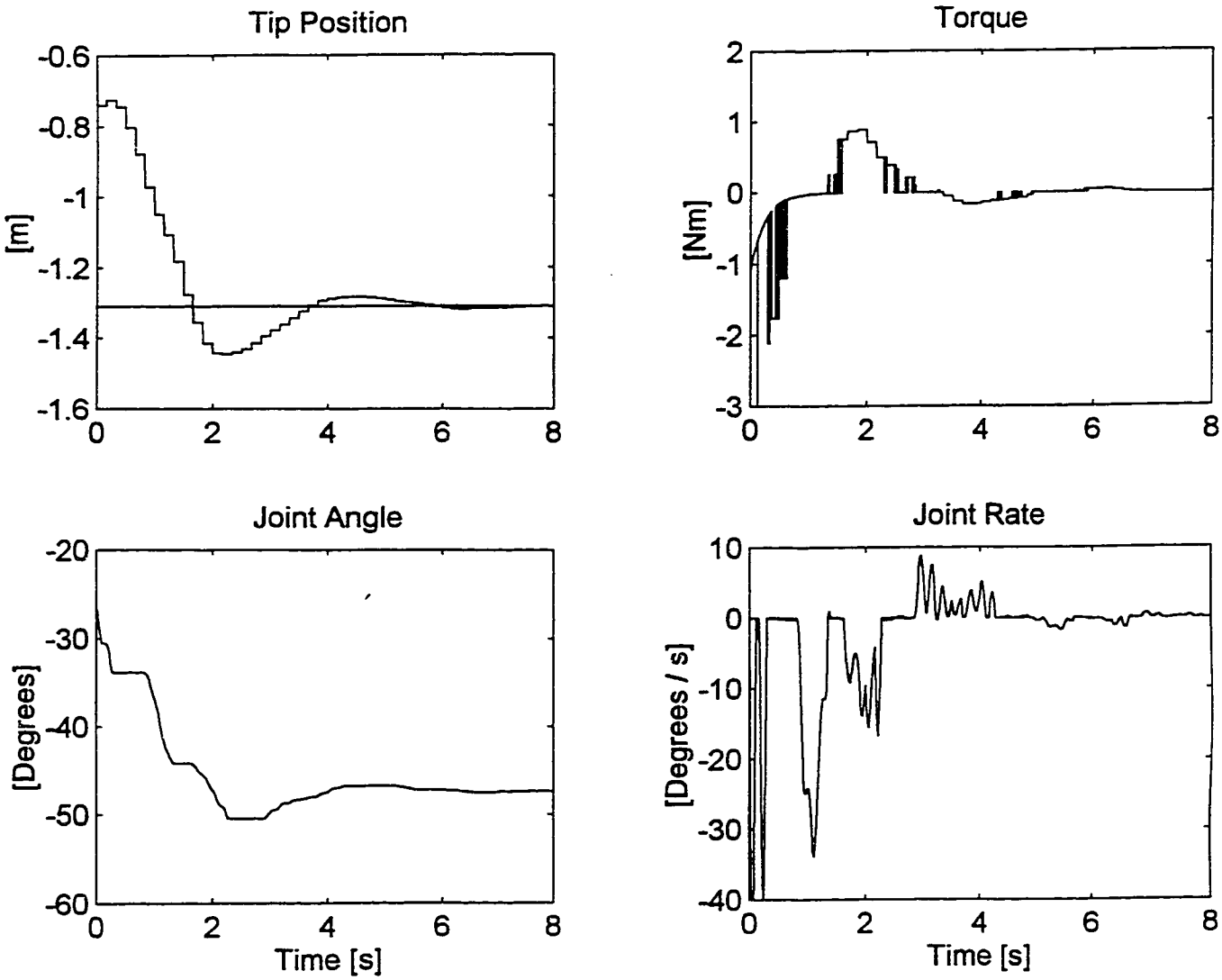

Figure 7.5.2: Simulation Result for 0.14 kg Payload. Parameters per E.2.2

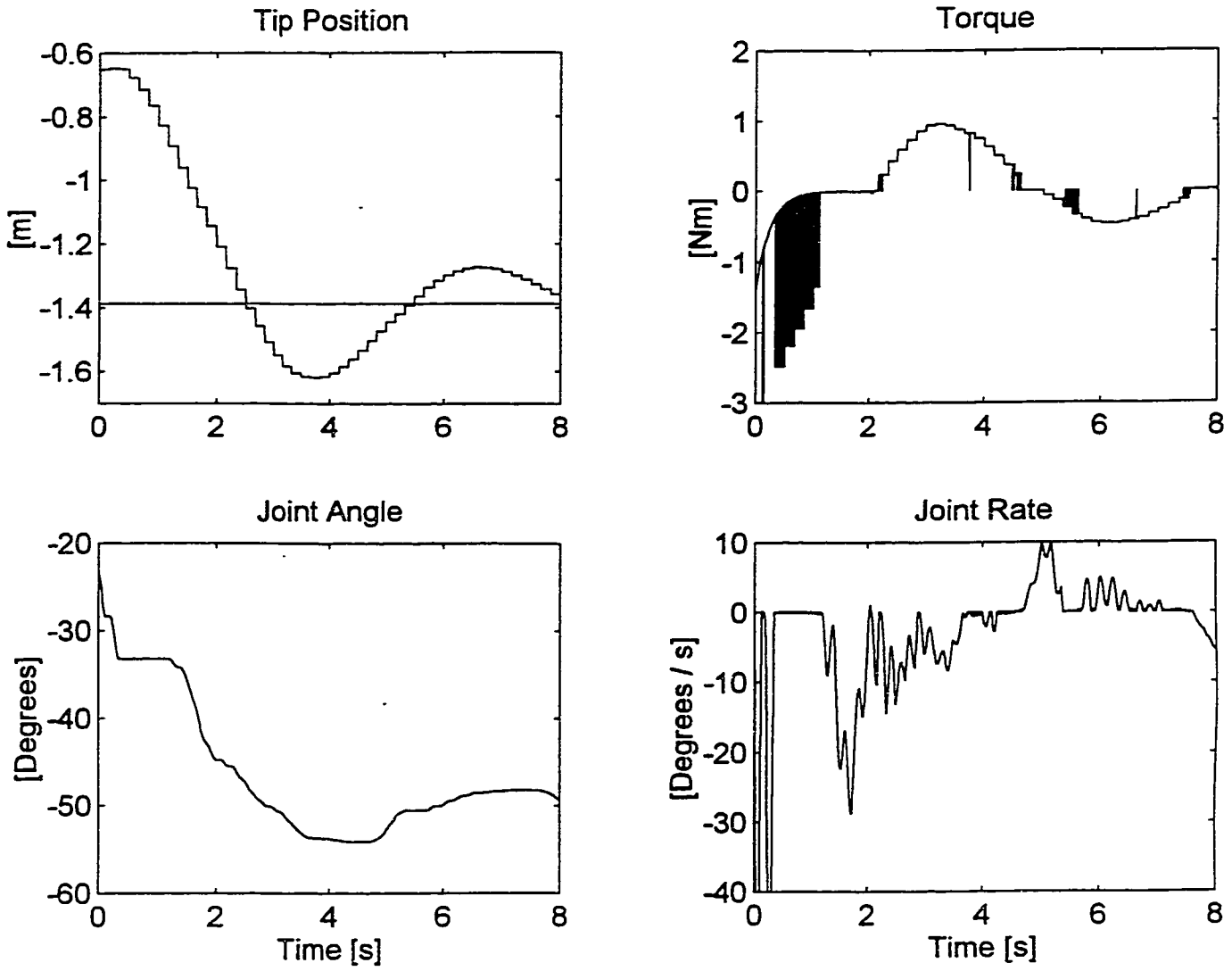

Figure 7.5.3: Simulation Result for 1.2 kg Payload. Parameters per E.2.4

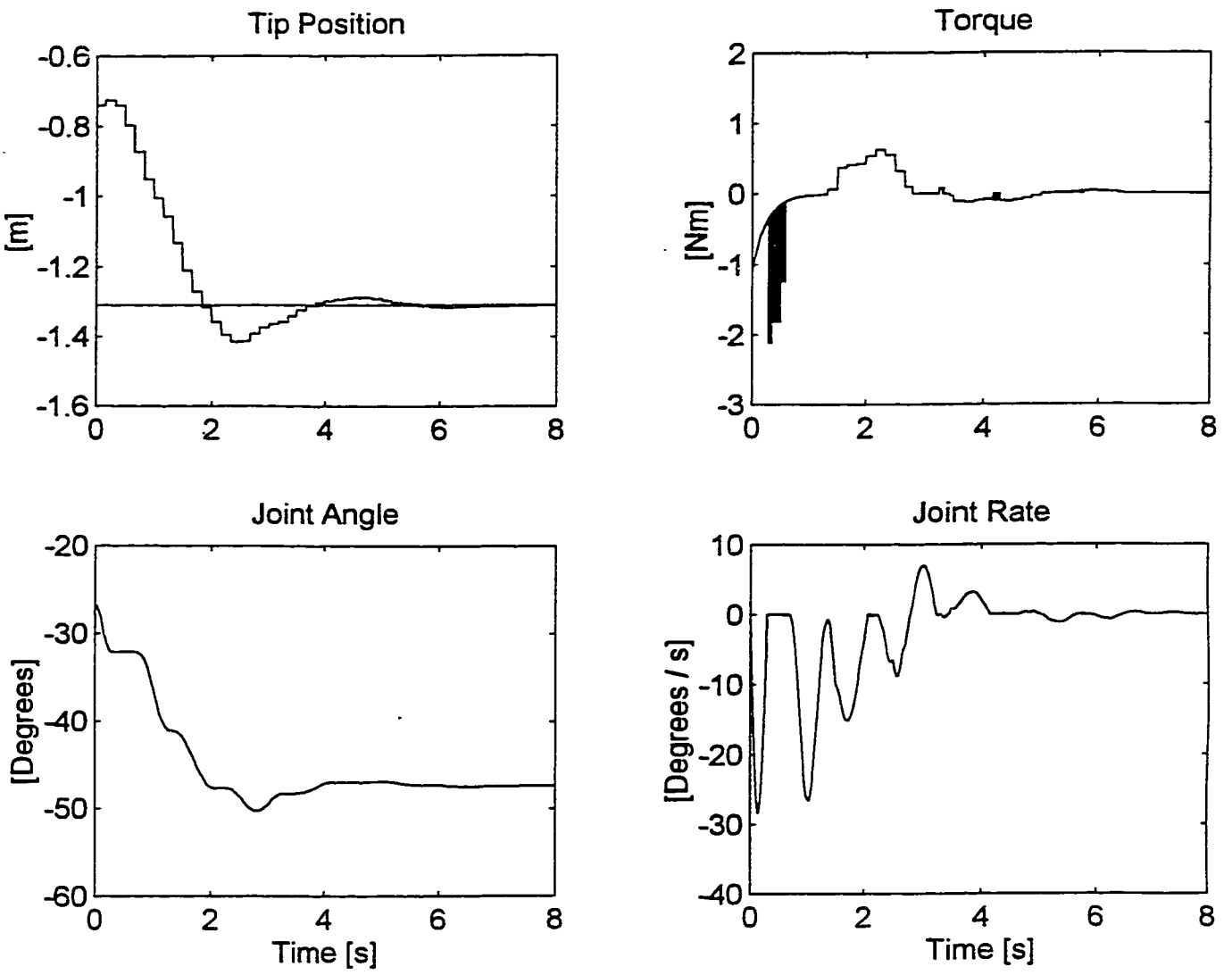

Figure 7.5.4: Simulation Result for 0.14 kg Payload with one Flexible Mode. Parameters per E.2.1

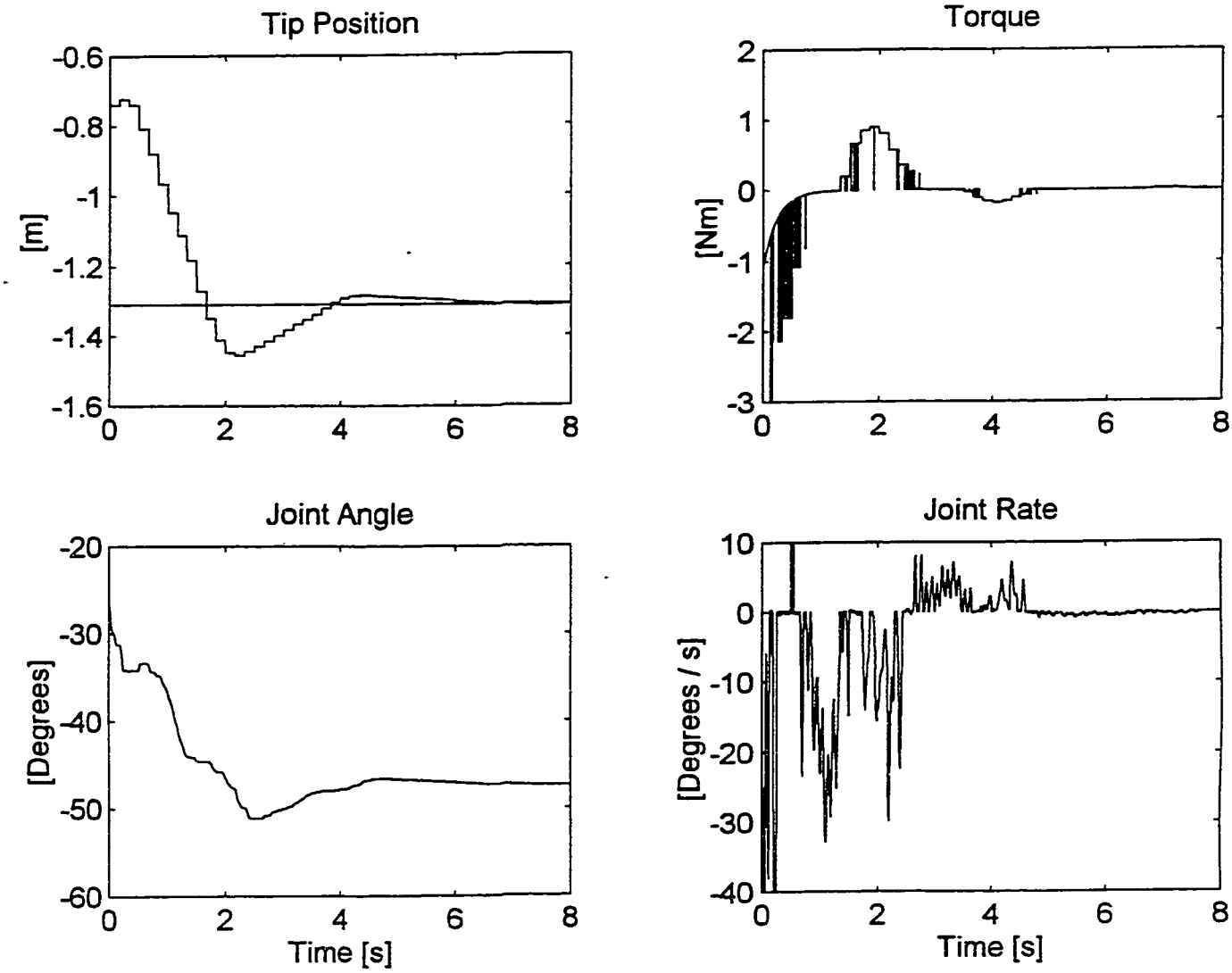

Figure 7.5.5: Simulation Result for 0.14 kg Payload with three Flexible Modes. Parameters per E.2.3

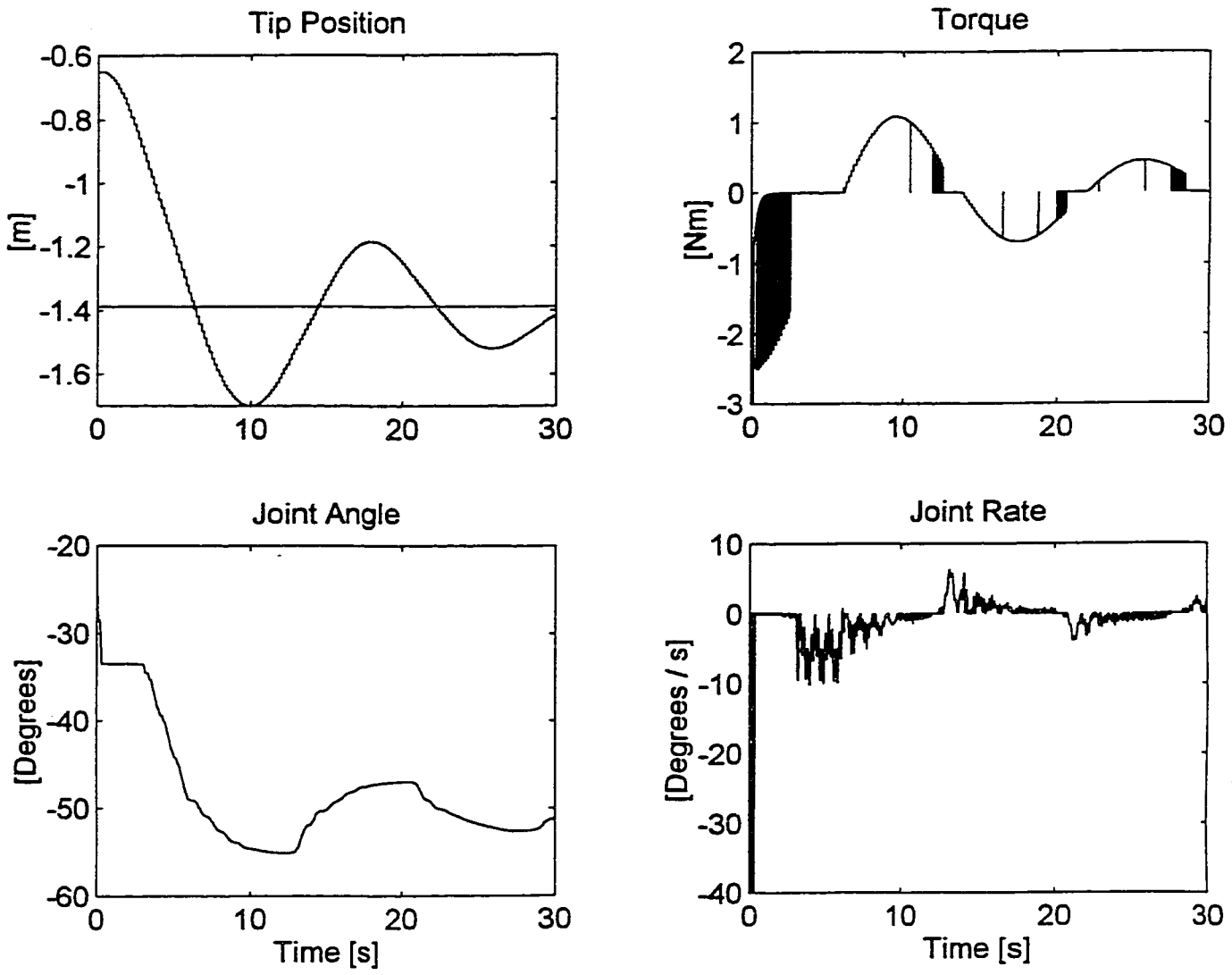

Figure 7.5.6: Simulation Result for 12 kg Payload. Parameters per E.2.5

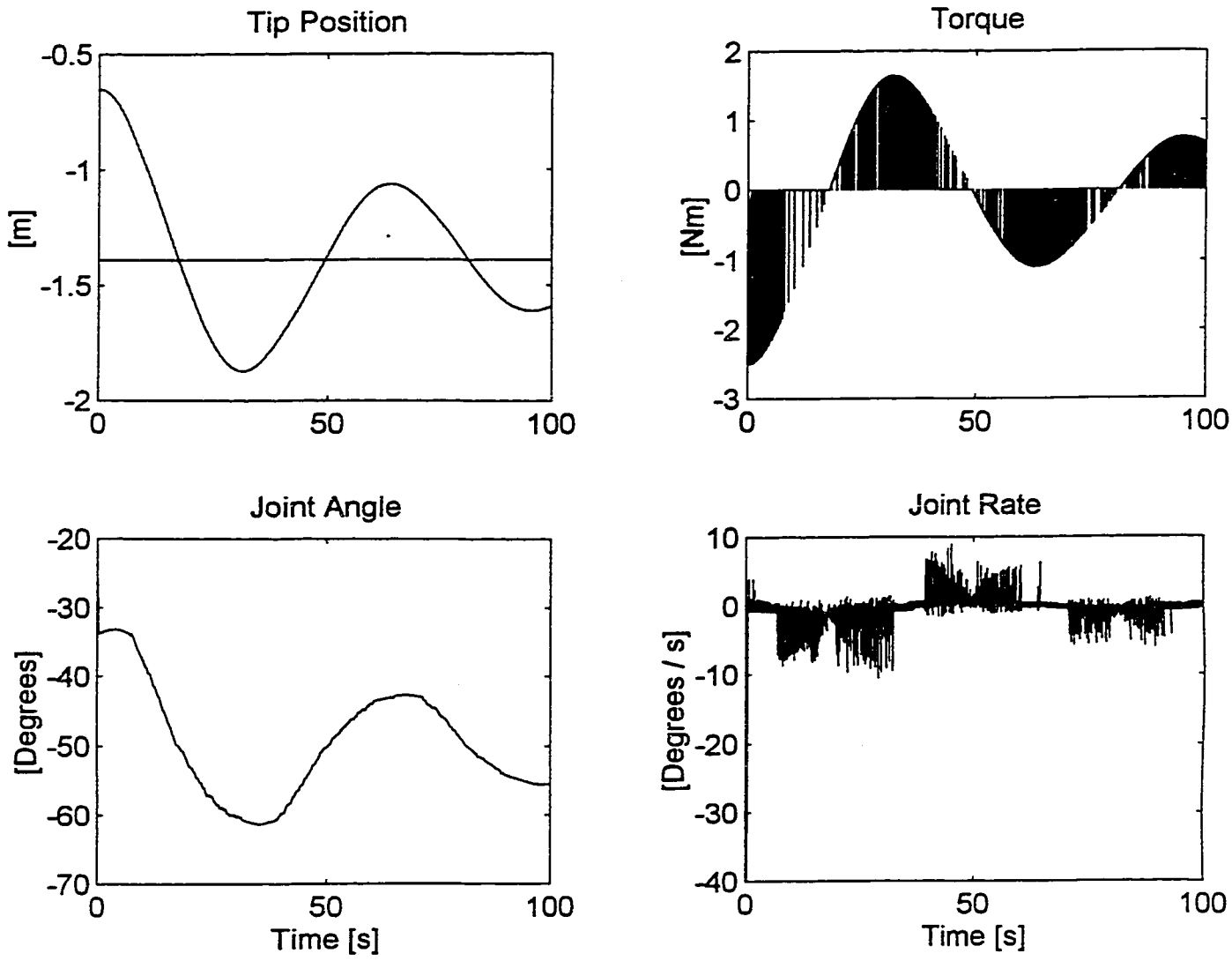

Figure 7.5.7: Simulation Result for 120 kg Payload. Parameters per E.2.6

7.6 Comparison to Model-Based Sensor-Fusion and Control

Objectives

As part of evaluating the instrumentation design and sensor fusion concept it is of interest to compare its performance and robustness to alternate methodologies such as model-based approaches. The generic differences between the various approaches were discussed in various places throughout the study. We will now look how they manifest themselves in the particular test case of the flexible link.

Model-based Design

The design of a model-based control system using a Kalman-Bucy filter for state estimation and sensor fusion is described in Section 4.3 by equations (4.3.1) – (4.3.14). We will now apply this design methodology to the flexible link. A model of the link in the state-space form (4.3.5) necessary for the design process is given by (3.3.43). The robot tip position and velocity are assumed as available system outputs, described by the following output matrix for equation (4.3.6):

$$\mathbf{C}_M = \begin{bmatrix} \phi^T(\ell) & \mathbf{0} \\ \mathbf{0} & \phi^T(\ell) \end{bmatrix} \tag{7.6.1}$$

A first design is based on a model with one flexible mode. The design parameters $\mathbf{V}_1, \mathbf{V}_2, \mathbf{Q}$ and $\mathbf{R}$ are chosen such that the nominal response of the closed-loop system is comparable, in terms of the fundamental time constants, to the response obtained with the algorithm developed in Section 7.3. The full model description, the design parameters and the resulting gain matrices are listed in Appendix E.3.1.

Simulation

The nominal response of the system obtained by simulation per Figure 7.6.1 is shown in Figure 7.6.2. Since the simulated system is completely linear, the transient behaviour is independent of particular initial conditions or excitation levels. Therefore the test case chosen is simply a transient from an initial tip position of 1 m to the state of rest at 0 m and does not match the initial and final conditions of the hardware tests. The transient behaviour per Figure 7.6.2

is comparable to the experimental results of Figure 7.4.1 and simulation results of Figure 7.5.2 in terms of the overall convergence. The smooth and well damped response is a typical characteristic of of the "optimal control" design approach used. The nominal response is based on using the same flexible link model for the design process and the evaluation of the design, i.e. in this case a model with one flexible mode per Appendix E.2.1.

Evaluation of Robustness

Figure 7.6.3 shows the simulated response of the system when a second flexible mode is added to the simulation of the flexible link, per Appendix E.2.2. This change obviously renders the system dynamically unstable due to "spillover" as discussed in Sections 2.4 and 4.3, indicating a lack of robustness to unmodelled system dynamics.

If the modal parameters of the second flexible mode are known and included in the design model, an updated design per Appendix E.3.2 will stabilize the system with two flexible modes as shown in Figure 7.6.4. However, if a third flexible mode is added to the flexible link model in the simulation (per Appendix E.2.3) instability results again due to truncation and spillover as indicated by the response shown in Figure 7.6.5. We conclude that the truncation/spillover problem is quite serious not only in theory but even in a very simple application.

Another system parameter which varies and may be unknown is the robot payload. Figure 7.6.6 shows the response when the payload is increased to 120 kg. Although the response is not dynamically unstable, the performance is clearly much worse than the performance for the proposed sensor fusion and control concept indicated in Figure 7.5.7 due to virtually undamped persistent vibrations in the joint motion and a very slow convergence of the tip motion with large overshoots.

Comparison

The comparison of the model-based system with the model-free hyperstability-based instrumentation and sensor fusion concept illustrates and corroborates the

superior robustness for the latter with respect to uncertainties and changes in system behaviour vis-a-vis a standard 'optimal control' design. (Extensions to the optimal control design methodology presented in Section 4.3, aiming at improving its robustness characteristics, have been proposed.)

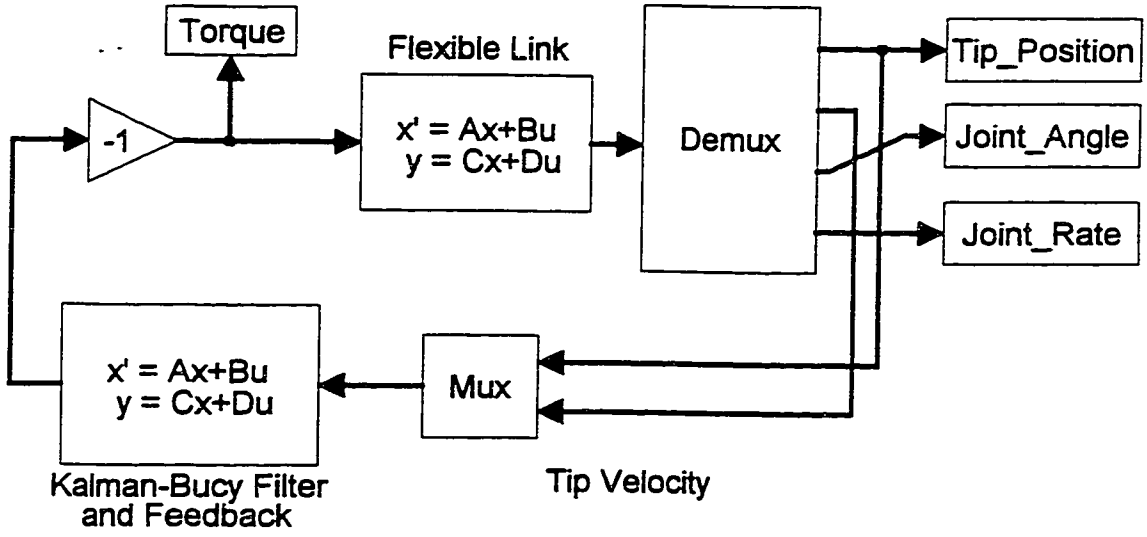

Figure 7.6.1: Simulation of Flexible Link with Model-based Sensor Fusion and Control

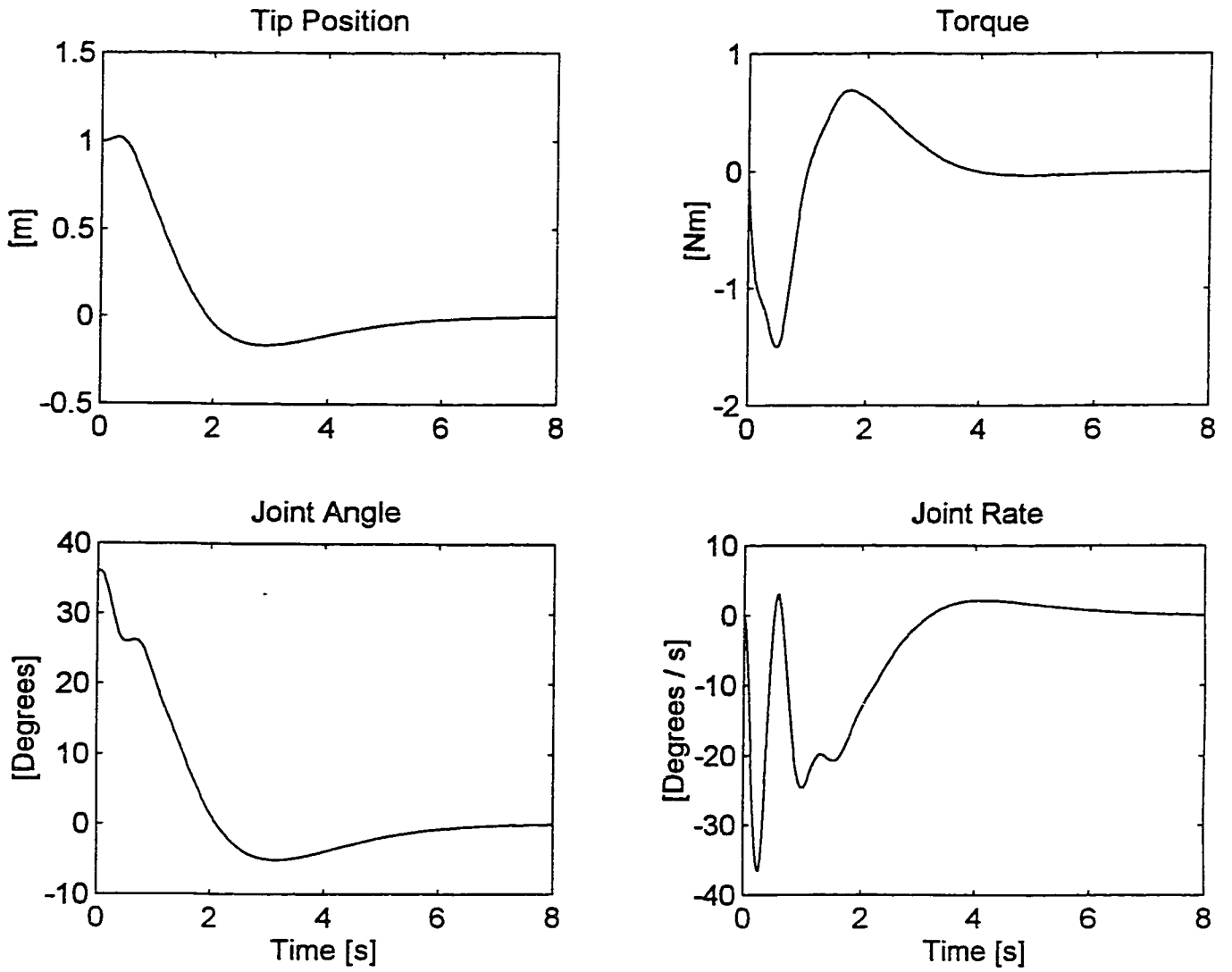

Figure 7.6.2: Nominal Response of Model-based System with 0.14 kg Payload and one Flexible Mode. Parameters per E.2.1, E.3.1

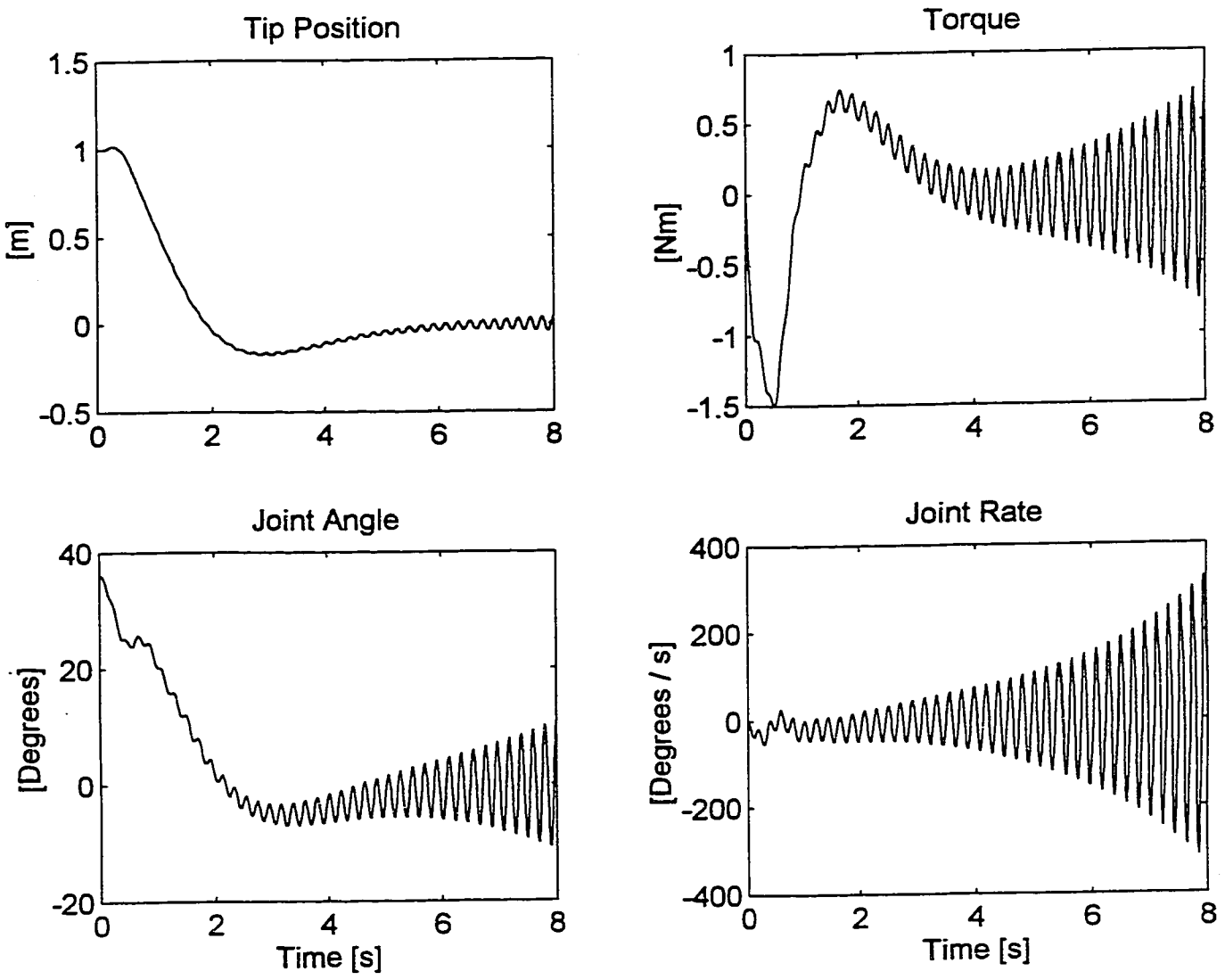

Figure 7.6.3: Instability of Model-based System with 0.14 kg Payload and two Flexible Modes caused by "Spillover". Parameters per E.2.2, E.3.1

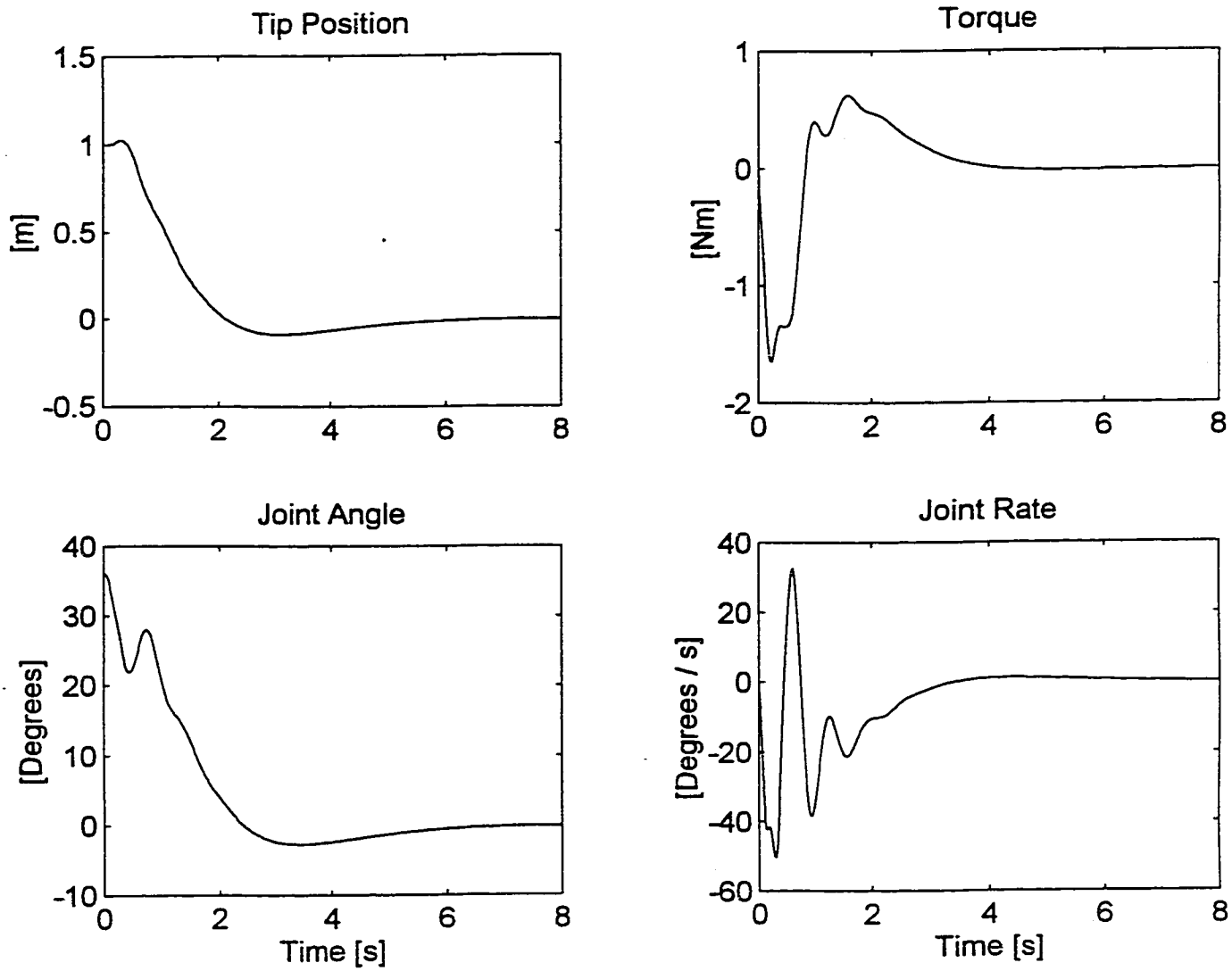

Figure 7.6.4: Nominal Response of Model-based System with 0.14 kg Payload and two Flexible Mode. Parameters per E.2.2, E.3.2

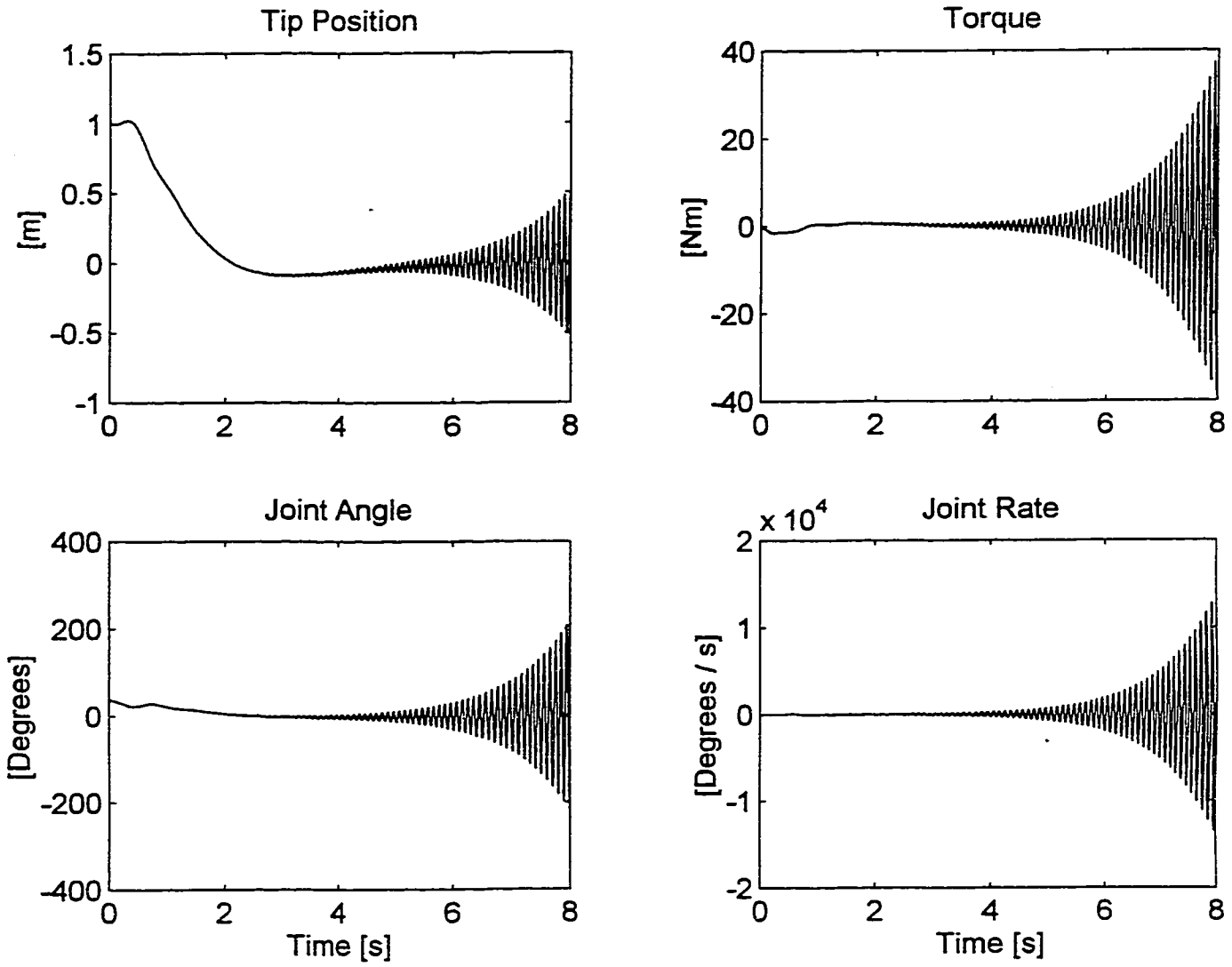

Figure 7.6.5: Instability of Model-based System with 0.14 kg Payload and three Flexible Modes caused by "Spillover". Parameters per E.2.3, E.3.2

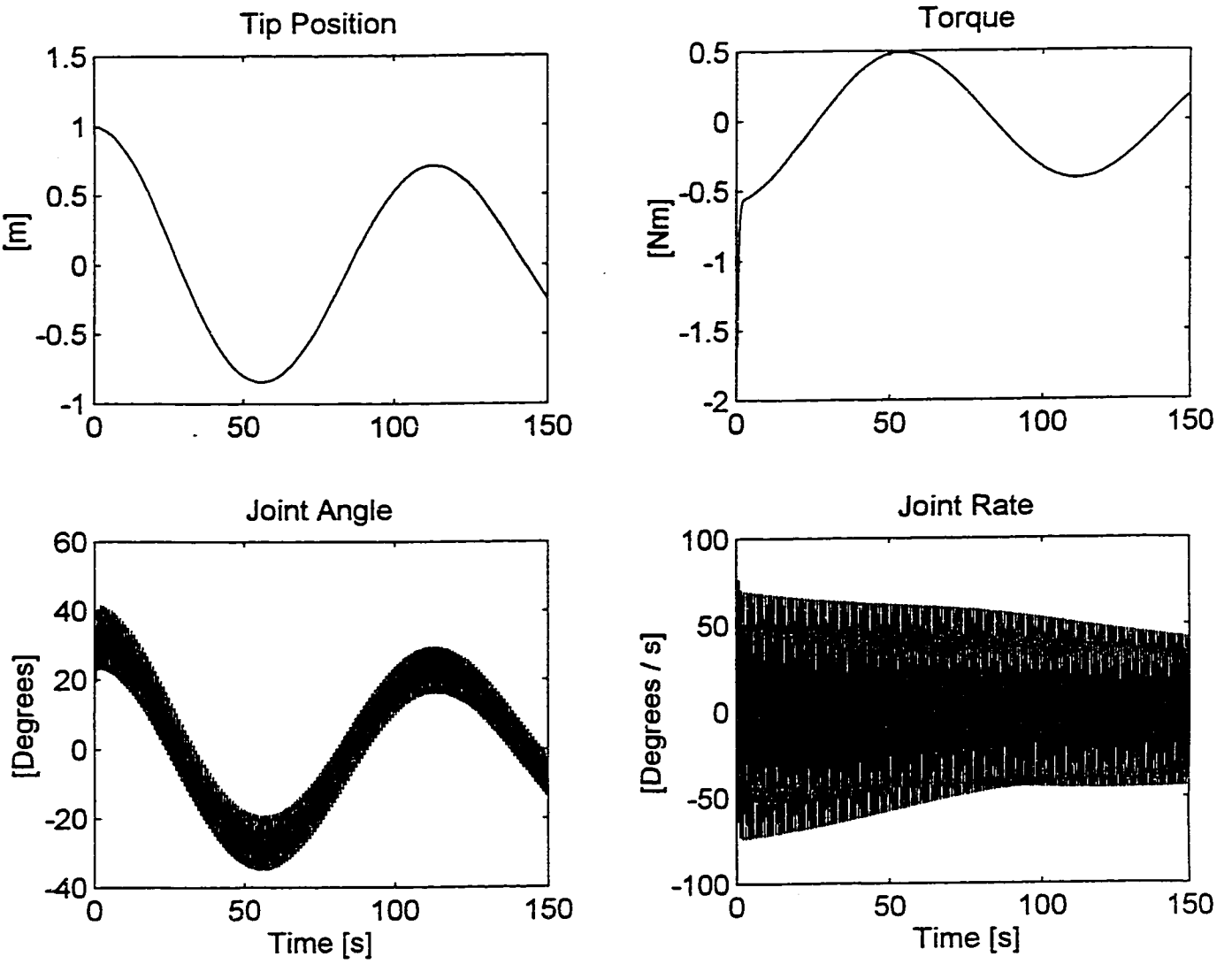

Figure 7.6.6: Marginally Stable Response of Model-based System with 120 kg Payload and one Flexible Mode. Parameters per E.2.6, E.3.1

CHAPTER 8

CONCLUSIONS

8.1 Summary

Problem

In the microgravity environment of space, large robots like the Space Station Remote Manipulator System are able to manipulate enormous payloads, with masses several orders of magnitude larger than the mass of the manipulator itself. Resulting low-frequency structural oscillations give rise to dynamic stability problem when the robot is controlled by a vision system measuring the payload motion. This problem is not unique to space robotics applications but is generic for the control of structurally flexible systems when the motion is measured at a distance from the actuator controlling the motion.

Approach

This study develops analytical criteria for the selection of the number, type and location of suitable sensors for robust control of mechanical systems with flexible bodies. Sensors meeting these criteria are called "hyperstability sensors". A dynamic sensor data fusion approach is developed to integrate additional "performance sensors" such as vision-based sensors, addressing the problem of using non-collocated sensors and actuators in the active control of flexible structures. An extended hyperstability concept is developed to enable robust control of complex systems with conventional or intelligent control systems. The model-free methodology is applicable to the broad class of non-linear and time-variant system governed by Hamilton's Principle which encompasses most mechanical systems.

Validation

The very general methodology is applied to a flexible link robot and experimentally validated. The benchmark tests involve the measurement and control of the end-point motion of the flexible link using a vision system and real-time image processing. The methodology is shown to be effective in the experiment, enabling robust control as expected from the theory, and relatively simple to implement.

Simulations complementing the hardware tests extend the scope of the evaluation. A comparison with a Kalman-filter-based control design demonstrates the superior robustness properties of the proposed approach.

8.2 Contributions

This study makes several contributions in the area of instrumentation, sensing, sensor fusion and control applicable to robotic systems with flexible links, such as large space robots. These contributions are summarized below:

Systematic Design of Instrumentation Architecture

A systematic procedure for the design of the instrumentation architecture for control of complex systems is developed. For this purpose the known concept of hyperstability is extended by the introduction of a sensor fusion process. This new "extended hyperstability" concept overcomes the limitations imposed by the previously required symmetry between sensors and actuators. The sensor fusion process dynamically combines measurements from "hyperstability sensors" and "performance sensors" such that robust stable control of complex systems can be assured, even in the presence of significant errors of various types in the measurement of the hyperstability sensors [Stieber, Petriu and Vukovich.1], [Stieber, Petriu and Vukovich.2]. This new theoretical development was carried out both for continuous-time and sampled-data systems.

Hyperstability Sensors for Mechanical Systems

A set of analytical conditions for hyperstability sensors for complex mechanical systems with time-variant, non-linear and flexible-body dynamic effects is developed. Although the resulting conditions largely reflect previously known requirements for sensor/actuator duality and collocation on flexible structures, the state-of-the art was advanced in the following areas:

- *Necessary* conditions were developed and correlated with known sufficient conditions;

- Sufficient conditions were *generalized* to allow the use of realistic sensors with static and dynamic errors.

Application of New Methodology to Vision-based Control of Flexible Robot

The application of the proposed new methodology and design procedure is demonstrated for vision-based control of a flexible robot. The experimental implementation and test demonstrates the feasibility of using the new methodology in practical applications [Stieber, Petriu and Vukovich.2]. The experimental results also validate the stability and robustness properties of the approach expected from theoretical considerations.

Solution of Robust Stabilization Problem for Flexible Structures with partially non-collocated Sensors and Actuators

It was shown analytically and verified experimentally that the new sensor fusion and control problem overcomes long standing problems associated with robust control of flexible structures with partially non-collocated sensors and actuators [Stieber, Vukovich and Petriu]. While most of the prior analysis of this problem reported in the literature was performed for linear time-invariant flexible body systems, the new methodology represents a solution also for non-linear and time-variant flexible body systems, and it does not require accurate models of the system dynamics. While sensor/actuator duality and collocation is still required for a subset of the sensors, they are no longer required to be in the "main control loop" and can be implemented by crude and cheap devices, providing, in the limit, only binary output. A comparison with a conventional model-based approach using a Kalman filter for the control of a flexible link confirms the superior robustness properties of the new methodology in this particular applications example.

Demonstration of Closed-loop Control of Flexible Robot Arm using the Space Vision System

A contribution of particular interest to the present and future development of robotic flight systems by the Canadian Space Agency is the proof-of-principle hardware demonstration of the use of the Space Vision System for automatic control of a very flexible manipulator with variable payloads [Stieber, McKay, Vukovich and Petriu].

8.3 Future Work

Theoretical Work

This study opens the door to a number of areas which merit further investigation. On the theoretical side, several topics appear promising:

- Based on the fact that passive electrical circuits are governed by an equivalent to Hamilton's Principle, electrical actuators such as DC motors could be included into the definition of complex systems. Hence the theory developed in this study could be extended to cover a wide class of electromechanical systems, with electrical as well as mechanical inputs and outputs. This would strengthen the theory for applications to other robotics problems.

- The development of alternative sensor fusion algorithms, e.g. based on fuzzy logic, might lead to a "smoother" behaviour of the sensor fusion logic.

- Investigating the concept of "degree of stability" for the sensor fusion and control algorithm could make the performance of the system more predictable and aid in the definition or selection of suitable fusion algorithms.

- Investigating / integrating the sensor fusion and control concept together with other types of control algorithms such as intelligent control or more elaborate conventional methods may lead to improved performance and stability robustness in control applications.

Experimental Work

The following possibilities to improve the experimental development and validation of the new concepts merit consideration:

- The testbed as described in this study could be improved considerably by the use of higher-speed computer hardware and other hardware/software upgrades.

- The capabilities of the existing testbed could be greatly extended by a suspension system which would support the use of larger payloads, additional joints and links, and 3-D translational motions.
- The experimental investigation of using "higher-order" devices covered by the theory developed in this study, such as sensors for strain and shear force in a flexible link, as part of the sensor complement for sensor fusion and control in robotics would appear to be a novel and promising endeavour.
- Ultimately, development tests of the new concept for vision-based control should be carried out in orbit, either on the Space Shuttle or on the Space Station.

APPENDICES

APPENDIX A

CONDITIONS FOR HYPERSTABILITY OF LINEAR FLEXIBLE STRUCTURES

A.1 Introduction

In this appendix, we will derive a necessary and sufficient conditions for the hyperstability of linear flexible structures. The modelling of the flexible structure, discussed in Section A.2, proceeds from a continuum modelling approach following [Meirovitch]. An important step is the definition of a set of potentially applicable sensors and actuators in Section A.3. The conditions on type and location of sensors and actuators are found by applying the positive real lemma to the system model, in Section A.4. The solution of the related Lyapunov equation is presented in Section A.5. The hyperstability conditions are summarized in Section A.6.

A.2 Model of Flexible Structures

Assumptions

An elastic body contained in a spatial domain $\mathcal{D}$ spanned by the position.vector $\mathbf{r}$ is modelled by assuming a continuous distribution of its mass and stiffness properties over $\mathcal{D}$. A static force distribution $\mathbf{f}_{\mathcal{D}}(\mathbf{r})$ on the body will induce deformations $\mathbf{v}(\mathbf{r})$ that we assume small. Stress in linearly related to strain through the linear, positive semi-definite, self-adjoint stiffness operator $\mathcal{K}$:

$$\mathcal{K}\mathbf{v}(\mathbf{r}) = \mathbf{f}(\mathbf{r}) \qquad \text{(A.2.1.)}$$

$\mathcal{K}$ contains differentials with respect to $\mathbf{r}$ up to order p[1]. For example, a vibrating string has $p = 2$ while $p = 4$ for a slender flexible beam. Over the boundary of $\mathcal{D}$, these deformations are constrained by conditions of the form

$$\mathcal{B}_j\mathbf{v} = \mathbf{0}, \quad j = 1, 2, \ldots, \frac{p}{2} \qquad \text{(A.2.2)}$$

[1] This order is always even, and usually denoted by $2p$ in the literature [Meirovitch]. In this appendix we digress from the standard notation in order to make the equations more readable.

where the $\mathcal{B}_j$ are also linear differential operators of order through $p-1$. Structural damping and gyroscopic effects are neglected. Further simplifying assumptions will be introduced in Section A.3.

Equations of Motion

When a dynamic force distribution $\mathbf{f}_{\mathcal{D}}(\mathbf{r},t)$ is applied on the flexible body, the dynamics of its vibrations are governed by the following equations [Meirovitch]:

$$\mathcal{M}\ddot{\mathbf{v}}(\mathbf{r},t)+\mathcal{K}\mathbf{v}(\mathbf{r},t)=\mathbf{f}_{\mathcal{D}}(\mathbf{r},t), \tag{A.2.3}$$

$$\mathcal{B}_j\mathbf{v}(\mathbf{r},t)=\mathbf{0}, \quad j=1,2,\ldots,\frac{p}{2}. \tag{A.2.4}$$

The mass operator $\mathcal{M}$ is a linear, positive-definite, self-adjoint operator of order less than p.

Solution for Homogeneous System

Under homogeneous condition, the force distribution $\mathbf{f}_{\mathcal{D}}(\mathbf{r},t)$ in equation (A.2.3) is set to zero. The spatial and temporal coordinates can be separated by substitution of the harmonic solution $\mathbf{v}(\mathbf{r},t)=\boldsymbol{\phi}(\mathbf{r})e^{j\omega t}$ into the boundary-value problem (A.2.4) and the following eigenvalue problem results:

$$(\omega^2\mathcal{M}-\mathcal{K})\boldsymbol{\phi}(\mathbf{r})=\mathbf{0}. \tag{A.2.5}$$

This last differential equation, of order p, together with the boundary conditions, define the infinite-dimensional set of mode shapes $\boldsymbol{\phi}_i(\mathbf{r})$ that characterize the vibrations at frequencies ω_i. From the self-adjoint property of operators $\mathcal{M}$ and $\mathcal{K}$, the following orthonormality conditions can be derived:

$$\int_{\mathcal{D}}\boldsymbol{\phi}_i^T\mathcal{M}\boldsymbol{\phi}_k d\mathbf{r}=\delta_{i,k} \tag{A.2.6}$$

$$\int_{\mathcal{D}}\boldsymbol{\phi}_i^T\mathcal{K}\boldsymbol{\phi}_k d\mathbf{r}=\omega_i\omega_k\delta_{i,k},$$

where $\delta_{i,k}$ is the Kronecker delta. These conditions allow the expansion of the forced response into an infinite series of uncoupled modes.

Solution for Forced System

When an external force distribution $\mathbf{f}_{\mathcal{D}}(\mathbf{r},t)$ is exerted on the body, equations (A.2.3)–(A.2.4) apply. From their linearity, the expansion theorem tells us that the response of the system can be represented as a linear combination of admissible functions that form a complete basis in the domain of the operators. The natural modes $\phi_i(\mathbf{r})$ can be used in this expansion:

$$\mathbf{v}(\mathbf{r},t) = \sum_{i=1}^{\infty} \phi_i(\mathbf{r}) q_i(t) \tag{A.2.7}$$

where the modal coordinates $q_i(t)$ represent the time-varying condition of mode i to the total response. After substitution of solution (A.2.7) into equation (A.2.3), the orthonormality conditions of equations (A.2.6) are invoked to arrive at a set of uncoupled equations:

$$\ddot{q}_i(t) + \omega_i^2 q_i(t) = f_i(t), \quad i = 1, 2, \ldots \tag{A.2.8}$$

the modal excitations $f_i(t)$ are the components of the forcing function along the basis function $\phi_i(\mathbf{r})$:

$$f_i(t) = \int_{\mathcal{D}} \phi_i^T(\mathbf{r}) \mathbf{f}_{\mathcal{D}}(\mathbf{r},t) d\mathbf{r}. \tag{A.2.9}$$

By defining the infinite-dimensional matrices

$$\begin{aligned} \mathbf{q}(t) &= [q_1(t) q_2(t) \ldots]^T, \\ \mathbf{\Omega} &= \text{ diag}\{\omega_1^2, \omega_2^2, \ldots\}, \\ \mathbf{f}(t) &= [f_1(t) f_2(t) \ldots]^T, \end{aligned}$$

the harmonic equations (A.2.8) can be condensed into the familiar form:

$$\ddot{\mathbf{q}}(t) + \mathbf{\Omega}\mathbf{q}(t) = \mathbf{f}(t). \tag{A.2.10}$$

The physical coordinates that describe the vibrations can be recovered from the modal coordinates through the matrix equivalent of (A.2.7):

$$\mathbf{v}(\mathbf{r},t) = \boldsymbol{\phi}^T(\mathbf{r}) \mathbf{q}(t) \tag{A.2.11}$$

where the infinite-dimensional ($\infty \times 6$) matrix of mode shapes $\boldsymbol{\phi}(\mathbf{r})$ is defined as

$$\boldsymbol{\phi}(\mathbf{r}) \triangleq [\boldsymbol{\phi}_1(\mathbf{r})\ \boldsymbol{\phi}_2(\mathbf{r})\ldots]^T. \tag{A.2.12}$$

Although we are starting from a continuum model with a theoretically infinite number of modes, we will later consider models in which the summation (A.2.7) is carried out only over a finite number of modes, n.

A.3 Sensors and Actuators

Sensor Types

In order to keep the mathematics more tractable we will consider a one-dimensional structure from now on. The vibrations $v(x,t)$ are assumed to occur in an orthogonal direction to the spatial coordinate x. The domain $\mathcal{D}$ of x is $0 \leq x \leq \ell$. In the one-dimensional case the expansion of the displacement, $v(x,t)$, yields in analogy to (A.2.7) and (A.2.11):

$$v(x,t) = \sum_{i=1}^{\infty} \phi_i(x) q_i(t) = \boldsymbol{\phi}^T(x)\mathbf{q}(t) \tag{A.3.1}$$

Here $\boldsymbol{\phi}(x) = [\phi_1(x)\ \phi_2(x)\ldots]^T$ is now of dimension $\infty \times 1$. $\mathbf{q}$ is still governed by (A.2.10).

Different type of sensors are defined by forming temporal and spatial derivatives of the displacement, v, at certain positions. It is shown by [de Lafontaine and Stieber] that the first p spatial derivatives (0^{th} to $(p-1)^{\text{st}}$) are significant for the observability of the system, even though higher-order derivatives are lacking an immediately obvious physical interpretation. Here we will consider the possibility of having 'point'[1] sensors for all significant spatial derivatives of the displacement. Only two temporal derivatives of the displacement are significant, because (A.2.10) is of second order. However, we will consider sensors for the first three time derivatives (0^{th} to 2^{nd}) because there are devices for the direct measurement of displacement, rate and acceleration. Hence we have $3p$ possible sensor types derived from $v(x,t)$ as shown in Table A.3.1.

	$\frac{\partial^j}{\partial t^j}$	$j=0$	$j=1$	$j=2$
$\frac{\partial^i}{\partial x^i}$	Interpretation	Displacement	Rate	Acceleration
$i=0$	Translation	v	$\dot{v}$	$\ddot{v}$
$i=1$	Rotation	$v^{(1)}$	$\dot{v}^{(1)}$	$\ddot{v}^{(1)}$
$\vdots$		$\vdots$	$\vdots$	$\vdots$
$i=p-1$	?	$v^{(p-1)}$	$\dot{v}^{(p-1)}$	$\ddot{v}^{(p-1)}$

Table A.3.1: $3p$ types of Sensors Based on Displacement $v(x,t)$.

[1] A point sensors measures a quantity at one point in space as opposed to averaging it over a region.

Output Equations

We consider sensors at l locations, x_{sk}, which can be combined to the vector of sensor locations, $\mathbf{x}_s$:

$$\mathbf{x}_s = [x_{s1} x_{s2} \dots x_{sl}]^T. \tag{A.3.2}$$

We can now define a sensor displacement vector, $\mathbf{v}_s(t)$, which has lp elements describing the displacement with all its p significant spatial derivatives, at all l sensor locations:

$$\begin{aligned}\mathbf{v}_s(t) = \Big[& v(x_{s1},t) \quad v(x_{s2},t) \quad \dots \quad v(x_{sl},t) \\ & \Big(\frac{\partial v(t)}{\partial x}\Big)_{x_{s1}} \quad \Big(\frac{\partial v(t)}{\partial x}\Big)_{x_{s2}} \quad \dots \quad \Big(\frac{\partial v(t)}{\partial x}\Big)_{x_{sl}} \\ & \dots \\ & \Big(\frac{\partial^{p-1} v(t)}{\partial x^{p-1}}\Big)_{x_{s1}} \quad \Big(\frac{\partial^{p-1} v(t)}{\partial x^{p-1}}\Big)_{x_{s2}} \quad \dots \quad \Big(\frac{\partial^{p-1} v(t)}{\partial x^{p-1}}\Big)_{x_{sl}} \Big]^T. \end{aligned} \tag{A.3.3}$$

The sensor displacement vector can be represented in the form of (A.3.1) by:

$$\mathbf{v}_s = \mathbf{B}^T(\mathbf{x}_s)\mathbf{q}(t). \tag{A.3.4}$$

Here we have used the definition

$$\begin{aligned}\mathbf{B}(\mathbf{x}_s) = \Big[& \phi(x_{s1}) \quad \phi(x_{s2}) \quad \dots \quad \phi(x_{sl}) \\ & \Big(\frac{d\phi}{dx}\Big)_{x_{s1}} \quad \Big(\frac{d\phi}{dx}\Big)_{x_{s2}} \quad \dots \quad \Big(\frac{d\phi}{dx}\Big)_{x_{sl}} \\ & \dots \\ & \Big(\frac{d^{p-1}\phi}{dx_{p-1}}\Big)_{x_{s1}} \quad \Big(\frac{d^{p-1}\phi}{dx_{p-1}}\Big)_{x_{s2}} \quad \dots \quad \Big(\frac{d^{p-1}\phi}{dx_{p-1}}\Big)_{x_{sl}} \Big] \end{aligned} \tag{A.3.5}$$

and extended the definition (A.2.12) as follows:

$$\Big(\frac{d^j\phi}{dx^j}\Big)_{x_{sk}} \triangleq \Big[\Big(\frac{d^j\phi_1}{dx^j}\Big)_{x_{sk}} \quad \Big(\frac{d^j\phi_2}{dx^j}\Big)_{x_{sk}} \quad \dots\Big]^T, j = 0, 1, \dots, p-1. \tag{A.3.6}$$

We allows for the possibility that any one of the sensors measures either displacement, rate, or acceleration, by defining the system output vector, $\mathbf{y} \in \mathbb{R}^{lp}$ as follows:

$$\mathbf{y}(t) = \mathbf{C}_1\mathbf{v}_s(t) + \mathbf{C}_2\dot{\mathbf{v}}_s(t) + \mathbf{C}_3\ddot{\mathbf{v}}_s(t) \tag{A.3.7}$$

where $\mathbf{C}_1$, $\mathbf{C}_2$ and $\mathbf{C}_3$ are matrices with l^2p^2 constant coefficients which can be used to select displacement, rate or acceleration outputs from any of the lp sensors. We already noticed earlier that there are only two independent time derivatives in the system, and recalling (A.2.10) and (A.2.16) we can represent $\ddot{\mathbf{v}}_s$ by:

$$\ddot{\mathbf{v}}_s(t) = \mathbf{B}^T(\mathbf{x}_s)[\mathbf{f}(t) - \mathbf{\Omega}\mathbf{q}(t)]. \tag{A.3.8}$$

Thus, the output equation expressed in terms of modal coordinates, $\mathbf{q}, \dot{\mathbf{q}}$ and system inputs, $\mathbf{f}$, takes the form

$$\mathbf{y}(t) = [\mathbf{C}_1\mathbf{B}^T - \mathbf{C}_3\mathbf{B}^T\mathbf{\Omega}]\mathbf{q}(t) + \mathbf{C}_2\mathbf{B}^T\dot{\mathbf{q}}(t) + \mathbf{C}_3\mathbf{B}^T\mathbf{f}(t). \tag{A.3.9}$$

Actuators

A basic requirement for a hyperstable block is to have an equal number of system inputs and outputs. Thus we have to define lp inputs in order to match the outputs defined above.

The modal excitation generated by a forcing function vector $\mathbf{f}_{\mathcal{D}}(\mathbf{r}, t)$ which is spatially distributed over the domain of the structure, is given by (A.2.9). In the one-dimensional case with a force distribution $f_{\mathcal{D}}(x, t)$ we have

$$f_i(t) = \int_{\mathcal{D}} \phi_i(x) f_{\mathcal{D}}(x, t) dx. \tag{A.3.10}$$

We assume that the actuators are 'point' devices located at l locations, x_{ak}, which are combined to an actuator location vector, $\mathbf{x}_a$:

$$\mathbf{x}_a = [x_{a1}\ x_{a2}\ \ldots\ x_{al}]^T. \tag{A.3.11}$$

The types of 'reasonable' actuators seems to be more restricted than the types of sensors. Only forces and torques immediately come to mind. However, it has been shown by [de Lafontaine and Stieber] that the force distributions, $f_{\mathcal{D}}(x, t)$, which can not be readily interpreted as 'point forces' and 'point torques' are significant for the controllability of the system. We therefore assume a force

distribution generated by p 'types' of point actuators, that can each excite one of the first p spatial derivatives of a vibrating structure at any one of l points:

$$f_{\mathcal{D}}(x,t) = \sum_{k=1}^{l} \sum_{j=0}^{p-1} f^{(j)}(t)\delta(x - x_{ak}) \tag{A.3.12}$$

where δ is the Dirac delta function, and $f^{(j)}$ is a 'j^{th}-order force' term.

Given the force distribution (A.3.12) the modal excitations follow from (A.3.10):

$$f_i(t) = \sum_{k=1}^{l} \sum_{j=0}^{p-1} \phi_i^{(j)}(x_{ak}) f_{\mathcal{D}}^{(j)}(x_{ak}, t) \tag{A.3.13}$$

The modal forcing vector, $\mathbf{f}(t)$, thus can be represented in the form

$$\mathbf{f}(t) = \mathbf{B}(\mathbf{x}_a)\mathbf{u}(t) \tag{A.3.14}$$

after recalling (A.3.5), and defining the system input vector

$$\mathbf{u}(t) = [f^{(0)}(x_{a1}) \dots f^{(0)}(x_{al}) \dots f^{1}(x_{a1}) \dots f^{(p-1)}(x_{al}) \dots]^T. \tag{A.3.15}$$

Obviously $f^{(0)}(x_{ak}, t)$ corresponds to a point force at $x = x_{ak}$, and $f^{(1)}(x_{ak}, t)$ corresponds to a point torque acting at $x = x_{ak}$, i.e. the first l elements of $\mathbf{u}$ are forces and the second l elements of $\mathbf{u}$ are torques. There is no immediately obvious interpretation for the higher-order force terms or 'higher-order actuators'. Introducing time derivatives to generate additional types of actuators, in analogy to the rate and acceleration sensors, is not justified because this appears to lack any physical meaning.

State-Space System Model

We will now present a summary of the flexible structure model developed above in first-order state-space form, which can be easily derived from the modal form (A.2.10) and the input/output equations (A.3.14) and (A.3.9), respectively:

$$\dot{\mathbf{z}} = \mathbf{A}\mathbf{z} + \mathbf{B}_s\mathbf{u} \tag{A.3.16}$$

$$\mathbf{y} = \mathbf{C}\mathbf{z} + \mathbf{D}\mathbf{u} \tag{A.3.17}$$

with state vector

$$\mathbf{z} = \begin{bmatrix} \mathbf{q} \\ \dot{\mathbf{q}} \end{bmatrix} \tag{A.3.18}$$

system matrix

$$\mathbf{A} = \begin{bmatrix} \mathbf{0} & \mathbf{I} \\ -\mathbf{\Omega} & \mathbf{0} \end{bmatrix} \tag{A.3.19}$$

input matrix

$$\mathbf{B}_s = \begin{bmatrix} \mathbf{0} \\ \mathbf{B}(\mathbf{x}_a) \end{bmatrix} \tag{A.3.20}$$

output matrix

$$\mathbf{C} = \left[\mathbf{C}_1\mathbf{B}^T(\mathbf{x}_s) - \mathbf{C}_2\mathbf{B}^T(\mathbf{x}_s)\mathbf{\Omega}^2\mathbf{C}_2\mathbf{B}^T(\mathbf{x}_s)\right] \tag{A.3.21}$$

throughput matrix

$$\mathbf{D} = \mathbf{C}_3\mathbf{B}^T(\mathbf{x}_s)\mathbf{B}(\mathbf{x}_a). \tag{A.3.22}$$

The system has *lp* inputs and *lp* outputs, and matrices, $\mathbf{B}_s, \mathbf{C}$ and $\mathbf{D}$ have appropriate dimensions.

In the subsequent analysis we will consider an approximation of the above infinite-dimensional system by a system with an arbitrarily high but finite number of modes, n. The state vector $\mathbf{z}$, then has $2n$ elements, and matrices $\mathbf{A}, \mathbf{B}_s$ and $\mathbf{C}$, have corresponding dimensions.

We will further require complete controllability and observability of the system. This can[3] be guaranteed by our choice of sensors and actuators as shown by [de Lafontaine and Stieber] under the additional assumption that the system has no rigid body modes:

$$\mathbf{\Omega} > \mathbf{0} \tag{A.3.23}$$

[3] i.e. as long as the choice of the matrices $\mathbf{C}_1, \mathbf{C}_2, \mathbf{C}_3$ is not pathologic, such as $\mathbf{C}_1 = \mathbf{C}_2 = \mathbf{C}_3 = \mathbf{0}$

A.4 Hyperstability Conditions

Positive Real Lemma

Hyperstability, or 'positivity', of linear systems can be determined from the 'Kalman-Yakubovich Lemma' derived in Appendix C.2:

Lemma A.4.1 (Hyperstability) *A linear time- invariant multivariable (LTIM) system as described by* (A.3.16) *and* (A.3.17), *which is completely controllable and observable, is hyperstable if and only if there exist a symmetric positive definite matrix* $\mathbf{S}$, $(\mathbf{S} = \mathbf{S}^T > \mathbf{0})$, *and matrices* $\mathbf{L}$ *and* $\mathbf{N}$ *such that:*

$$\mathbf{SA} + \mathbf{A}^T\mathbf{S} = -\mathbf{L}\mathbf{L}^T, \tag{A.4.1}$$

$$\mathbf{B}_s^T\mathbf{S} + \mathbf{N}^T\mathbf{L}^T = \mathbf{C}, \tag{A.4.2}$$

$$\mathbf{D} + \mathbf{D}^T = \mathbf{N}^T\mathbf{N}. \tag{A.4.3}$$

Lemma A.4.2 (Asymptotic Hyperstability) *A LTIM system is asymptotically hyperstable if and only if the system is hyperstable according to Lemma* A.4.1 *and the matrix* $\mathbf{L}\mathbf{L}^T$ *is positive definite* $(\mathbf{L}\mathbf{L}^T > \mathbf{0})$.

The above lemmas provide necessary and sufficient conditions for (asymptotic) hyperstability. As proved in Section A.5, a system (A.3.16) (A.3.17) with a system matrix of the form of (A.3.19) can fulfill condition (A.4.1) only with a diagonal $\mathbf{S}$ matrix, and $\mathbf{L} = \mathbf{0}$. Consequently the system can not be asymptotically hyperstable. Further, after inserting (A.3.20), (A.3.21) into (A.4.2), this condition can be separated into the following two equations:

$$\mathbf{0} = \mathbf{C}_1\mathbf{B}^T(\mathbf{x}_s) - \mathbf{C}_3\mathbf{B}^T(\mathbf{x}_s)\boldsymbol{\Omega}^2 \tag{A.4.4}$$

$$\mathbf{B}^T(\mathbf{x}_a)\mathrm{diag}\{s_i\} = \mathbf{C}_2\mathbf{B}^T(\mathbf{x}_s); \quad s_i > 0 \;\forall\; i = 1 \ldots n \tag{A.4.5}$$

Equation (A.4.5) constitutes conditions for the relative positioning of sensors and actuators and will be analyzed later. Equation (A.4.4) represents conditions for the types of sensors allowed in a hyperstable flexible structure. As shown below we have $\mathbf{C}_3 = \mathbf{0}$, which conveniently takes care of condition (A.4.3), with $\mathbf{D} = 0$ (see (A.3.22)) and $\mathbf{N} = \mathbf{0}$.

Conditions for Sensor Types

We will now investigate the solutions $\mathbf{C}_1$ and $\mathbf{C}_3$ for (A.4.4). By inspection of the output equation (A.3.8) we see that condition (A.4.4) implies that there can be no 'net' displacement feedback in a hyperstable structure, i.e. the contributions of displacement sensors and accelerating sensors are not independent, and must exactly cancel each other. We will see shortly that, in general, condition (A.3.21) implies that one cannot have displacement or acceleration sensors as outputs of a hyperstable structure.

The matrix equation (A.4.4) is equivalent to nlp linear equations of the following form (n = number of modes lp = number of sensors):

$$\sum_{k=1}^{lp}(\mathbf{B})_{jk}[(\mathbf{C}_1)_{ik} - \omega_j^2(\mathbf{C}_3)_{ik}] = 0 \;\forall\; i = 1, 2, \ldots lp;\; j = 1, 2 \ldots n, \tag{A.4.6}$$

where $(\cdot)_{ik}$ denotes the element i, k of the matrix in brackets. We have, in general, to assume that all ω_j^2 are different. The maximum multiplicity of eigenvalues of (A.2.5) is p. Therefore the only matrices $\mathbf{C}_1$ and $\mathbf{C}_3$ which are independent of $\mathbf{B}$ and $\mathbf{\Omega}$ and fulfill condition (A.4.6) are:

$$\mathbf{C}_1 = \mathbf{0}, \tag{A.4.7}$$

$$\mathbf{C}_3 = \mathbf{0}. \tag{A.4.8}$$

In fact these are the only solutions to (A.4.6) for $n > 2lp$, i.e if the number of modes exceeds twice the number of sensors, because (A.4.6) represents lnp linear equations with $2lp$ free parameters in $\mathbf{C}_1$ and $\mathbf{C}_3$.

The characteristics of solutions other than (A.4.7), (A.4.8) for $n \leq 2lp$ are not further investigated because these solutions would be functions of $\mathbf{B}(\mathbf{x}_s)$ and $\mathbf{\Omega}$ which is not desirable in the context of robust control, and in general, we have many more modes than sensors. It has been shown by [de Lafontaine and Stieber] that at most p sensors are necessary to render the system (A.3.16)–(A.3.22) completely observable.

Conditions for Sensor/Actuator Placement

With $\mathbf{C}_1 = \mathbf{C}_3 = \mathbf{0}$ the output equation (A.3.7) degenerates to:

$$\mathbf{y}(t) = \mathbf{C}_2 \dot{\mathbf{v}}_s(t). \tag{A.4.9}$$

There is no need to keep the coefficient matrix $\mathbf{C}_2$ completely general since $\mathbf{C}_1, \mathbf{C}_2$ and $\mathbf{C}_3$ were introduced mainly to select/deselect certain contributions to the output. We therefore may choose

$$\mathbf{C}_2 = \mathbf{I}, \tag{A.4.10}$$

and obtain the following simplified output equation from (A.4.9) and (A.3.4), which reflects the necessary conditions on the sensor types:

$$\mathbf{y}(t) = \mathbf{B}^T(\mathbf{x}_s)\dot{\mathbf{q}}(t). \tag{A.4.11}$$

With (A.4.10) condition (A.4.5) simplifies to:

$$\mathbf{B}^T(\mathbf{x}_a)\mathrm{diag}\{s_i\} = \mathbf{B}^T(\mathbf{x}_s). \tag{A.4.12}$$

This matrix equation is equivalent to *nlp* scalar equations. Using definition (A.3.5) and $s_i > 0 \ \forall \ i = 1 \ldots n$ we obtain the following condition which is equivalent to (A.4.12):

$$\mathrm{sign}\phi_i^{(j)}(x_{sk}) = \mathrm{sign}\phi_i^{(j)}(x_{ak}) \ \forall \ i = 1 \ldots n, \ k = 1 \ldots l, \ j = 0 \ldots p-1. \tag{A.4.13}$$

Condition (A.4.13) can roughly be interpreted as follows: Corresponding sensors and actuators (i.e. those with the same position index k and acting on the same derivative j) must be placed at locations, x_{sk} and x_{ak} respectively, at which each one of the n corresponding mode shape derivatives $\phi_i^{(j)}$ has the same sign.

Figure A.4.1 shows an example for the above conditions as applied to a beam model. The top graph displays the first 3 mode shapes of a pinned-pinned slender beam of length l which are [Blevins]:

$$\phi_i(x) = a_i \sin \frac{i\pi x}{\ell}, \tag{A.4.14}$$

and the admissible position range, x_s, of (0^{th}-order) displacement sensors for an arbitrarily selected force actuator location, x_a. The second graph shows the first spatial derivatives of the first 3 mode shapes,

$$\phi_i^{(1)}(x) = \frac{a_i i\pi}{\ell} \cos \frac{i\pi x}{\ell}, \tag{A.4.15}$$

and the admissible range, x_s, for a 'slope' (first order displacement) sensor, given a torque actuator at x_a. Figure A.4.2 presents the results for this example in a more general form and identifies the admissible location of a 'slope' sensor for any given location of a torque actuator on the beam. The sensor has to be located in "the same square" as the actuator. It is interesting to note that the same pattern is also produced by the stability condition (2.3.9), as shown in Figure 2.3.2. (The Figures have a slightly different interpretation, though, as indicated by the different shading of the squares.)

The permitted range x_s of sensor locations shrinks as the number of modes goes up. It is proved below that the admissible range collapses to the actuator location if the number of modes tends toward infinity. Condition (A.4.13) is always fulfilled for $x_{sk} = x_{ak}\ \forall\ k = 1, 2, \ldots l$, and, in general, this is the only solution for systems with an infinite number of vibration modes.

This can be shown for the above example as follows. The equality

$$\phi_i^{(1)}(x_{0k}) = 0 \tag{A.4.16}$$

defines the i zeros of $\phi_i^{(1)}(x)$, denoted x_{0k}, $k = 1 \ldots i$, which can also be expressed as a function of the mode number i:

$$x_{0k}(i) = \frac{2k-1}{2i}\ell \quad i = 1 \ldots n, \quad k = 1 \ldots i \tag{A.4.17}$$

We assume a single torque actuator at a location x_a on the beam which is not a zero for modes i or $i+1$: $0 \le x_a \le \ell$, $\quad x_a \neq x_{0k}(i)$, $\quad x_a \neq x_{0k}(i+1)$. For any given mode i, the number k_- of the zero just 'left' of the actuator location (i.e. $x_{0k_-} < x_a$) is an integer function of i and x_a:

$$k_-(x_a, i) = \lfloor (\frac{x_a}{\ell} i + \frac{1}{2}) \rfloor \tag{A.4.18}$$

The number k_+ of the closest zero 'right' of the actuator location is simply:

$$k_+(x_a, i) = k_-(x_a, i) + 1 \tag{A.4.19}$$

For any given actuator location x_a condition (A.4.13) can be satisfied for 2 modes i and $i+1$ if the location of a corresponding sensor x_s is constrained by the zeros of $\phi_i^{(1)}$ and $\phi_{i+1}^{(1)}$ as follows:

$$x_{0k_-}(i+1) < x_s < x_{0k_+}(i) \tag{A.4.20}$$

The range of permitted sensor locations can be expressed as a function of the mode number i:

$$x_{0k_+}(i) - x_{0k_-}(i+1) = \frac{2\lfloor(\frac{x_a}{\ell}i + \frac{1}{2})\rfloor + 1}{2i}\ell - \frac{2\lfloor(\frac{x_a}{\ell}(i+1) + \frac{1}{2})\rfloor - 1}{2(i+1)}\ell \tag{A.4.21}$$

Based on the following property of the "floor" function:

$$\lfloor x \rfloor \leq x \leq \lfloor (x+1) \rfloor \tag{A.4.22}$$

the range of the sensor position is bounded by:

$$x_{0k_+}(i) - x_{0k_-}(i+1) \leq \frac{\ell}{i}. \tag{A.4.23}$$

As the mode number i increases, the range shrinks to a point as claimed above:

$$\lim_{i\to\infty}(x_{0k_+}(i) - x_{0k_-}(i+1)) \leq \lim_{i\to\infty}\frac{\ell}{i} = 0 \tag{A.4.24}$$

Interpretation Based on Energy Considerations

For an interpretation of the conditions on the types and placement of sensors required for hyperstable structures, we will now analyze the relationships between the energy of the structural system, and its input/output inner product (IOP). The total energy, E, of the system (A.2.10) is given by the sum of its elastic potential energy and its kinetic energy:

$$E(t) = \frac{1}{2}\mathbf{q}^T(t)\mathbf{\Omega}\mathbf{q}(t) + \frac{1}{2}\dot{\mathbf{q}}^T(t)\dot{\mathbf{q}}(t). \tag{A.4.25}$$

The change of energy is obtained by differentiating (A.4.25):

$$\dot{E}(t) = (\ddot{\mathbf{q}} + \mathbf{\Omega q})^T \dot{\mathbf{q}}. \tag{A.4.26}$$

Recalling (A.2.10) we can also express (A.4.26) by:

$$\dot{E}(t) = \mathbf{f}^T(t)\dot{\mathbf{q}}(t) = \sum_{i=1}^{n} f_i \dot{q}_i \tag{A.4.27}$$

Combining the input equation (A.3.14), the output equation (A.4.11), and the necessary condition (A.4.12) for sensor placement, we obtain the following expression for the system IOP:

$$\mathbf{u}^T(t)\mathbf{y}(t) = \mathbf{f}^T\mathbf{S}\dot{\mathbf{q}}(t) = \sum_{i=1}^{n} f_i s_i \dot{q}_i; \quad s_i > 0 \tag{A.4.28}$$

By comparing (A.4.27) and (A.4.28) and recalling that $\mathbf{S}$ is a diagonal matrix of positive factors without physical dimensions, we can draw the following conclusions:

- It is a necessary condition for hyperstability of the system that the IOP has the physical dimension of power (work), e.g. Nms^{-1}. Besides 'standard' sensors and actuators also the higher-order sensors and actuators are admissible.
- It is a necessary condition for hyperstability of the system that the IOP qualitatively reflects the power exchanged with each mode of the system; i.e. if the power $f_i\dot{q}_i$ exchanged with any one mode i grows above all bounds, it must show in $\mathbf{u}^T\mathbf{y}$ with the correct sign.

When we introduce into (A.4.28) the sufficient condition for hyperstability $\mathbf{x}_a = \mathbf{x}_s$ from which follows $\mathbf{S} = \mathbf{I}$, we obtain:

$$\mathbf{u}^T\mathbf{y} = \dot{E}. \tag{A.4.29}$$

This means that it is sufficient for hyperstability of the system (A.2.10) that the IOP is identical with the power exchanged with the system. Condition (A.4.25) is obviously identical with the sufficient condition (6.2.10) for hyperstability.

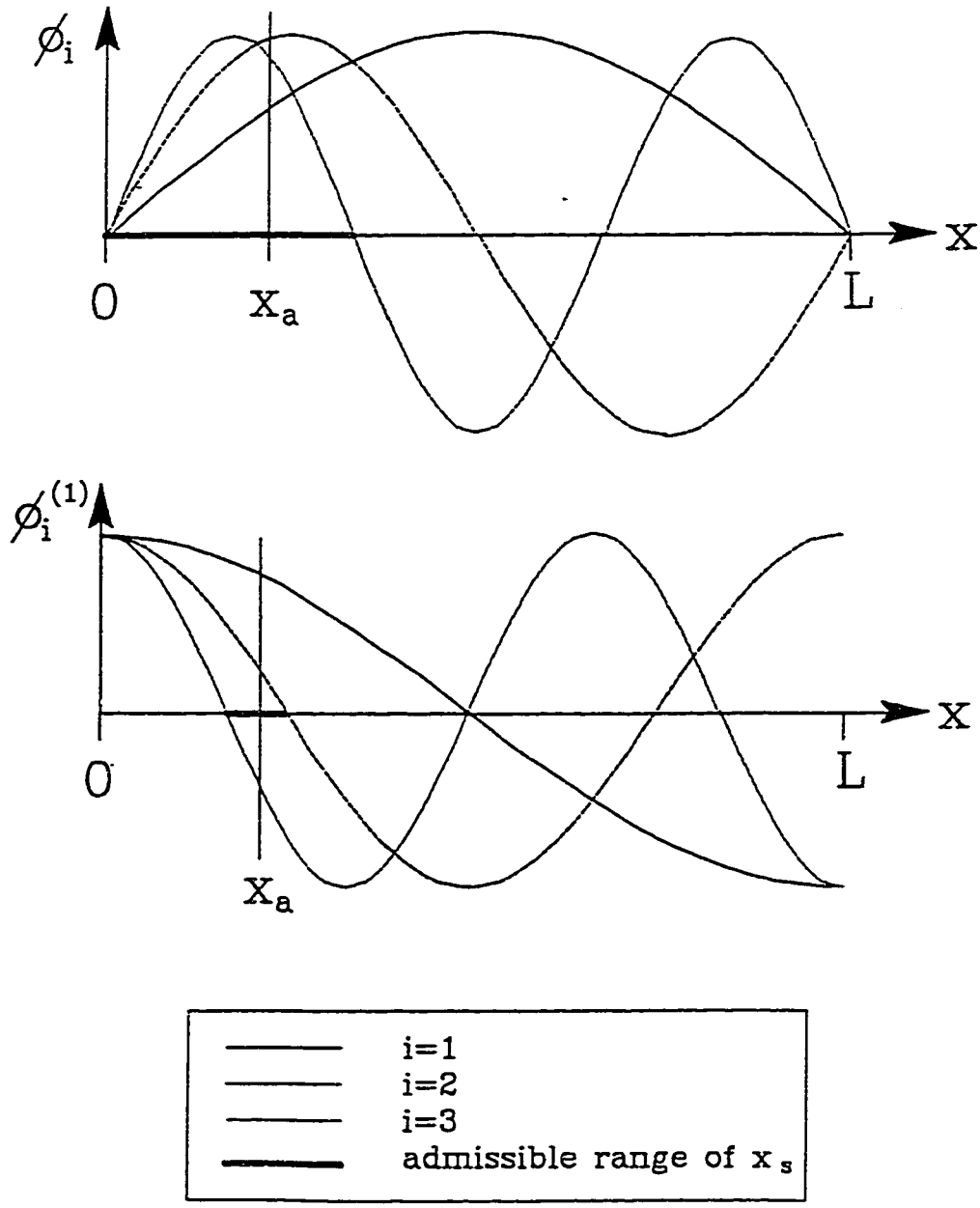

Figure A.4.1: Admissible Sensor Position on Pinned-Pinned Beam

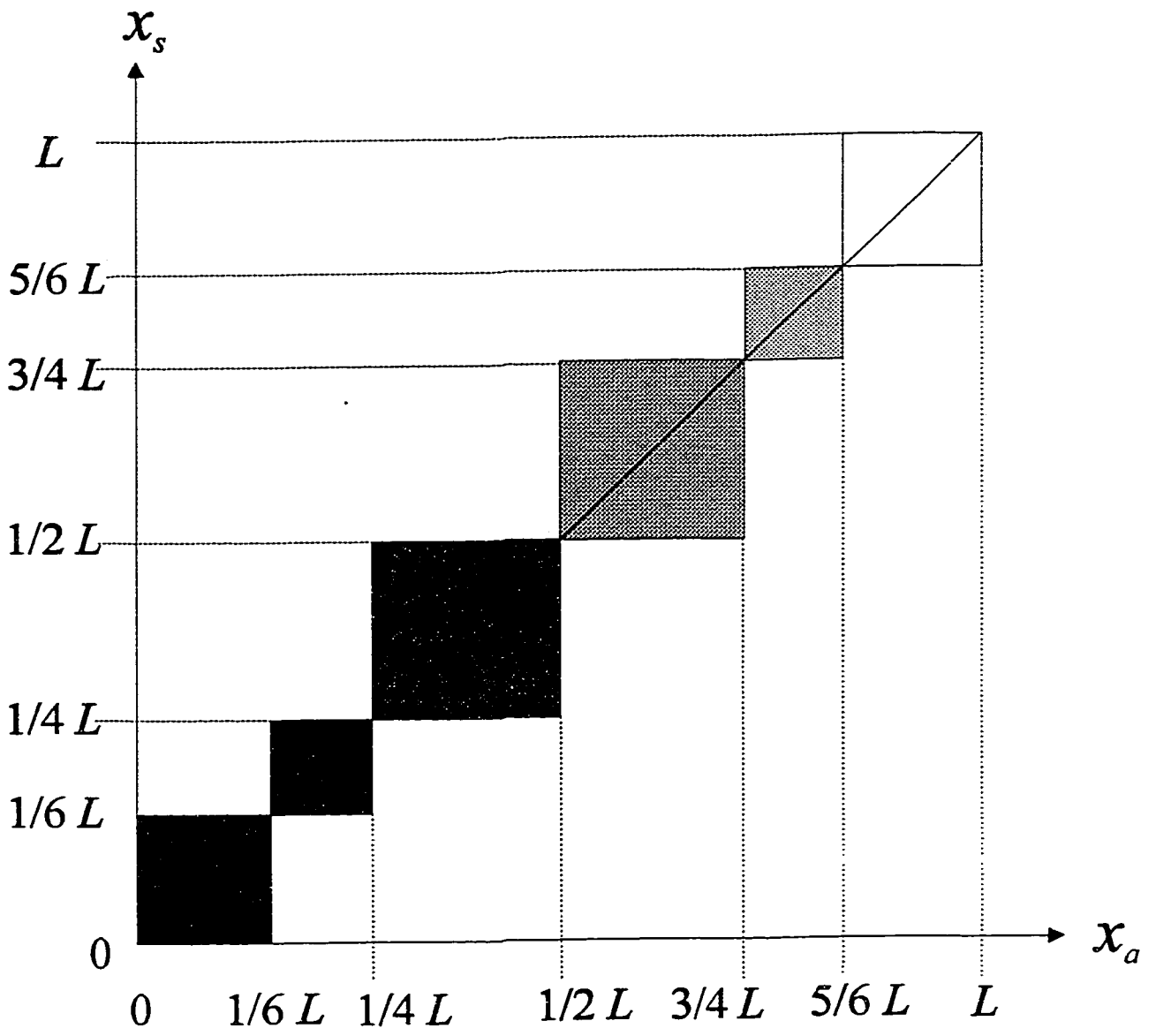

Figure A.4.2: Admissible Sensor Location x_S as a Function of Actuator Location x_a on Flexible Beam (Pinned-Pinned Boundary Conditions) per Condition (A.4.13) for first Derivative (j=1) and 3 Flexible Modes (n=3).

A.5 Solution of Lyapunov Equation

In Section A.4 we have used the fact that the only positive definite solution $\mathbf{S}$ of the Lyapunov equation (A.4.1)

$$\mathbf{SA} + \mathbf{A}^T\mathbf{S} = -\mathbf{L}\mathbf{L}^T$$

is diagonal and that the matrix $\mathbf{L} = \mathbf{0}$ if the matrix $\mathbf{A}$ has the form of (A.3.19). We now will sketch out a proof for this claim:

We first define

$$\mathbf{P} = \mathbf{L}\mathbf{L}^T. \tag{A.5.1}$$

$\mathbf{P}$ obviously has the properties $\mathbf{P} \geq \mathbf{0}$, $\mathbf{P} = \mathbf{P}^T$.

Matrices $\mathbf{S}$ and $\mathbf{P}$ are partitioned into four square submatrices each:

$$\mathbf{S} = \begin{bmatrix} \mathbf{S}_{11} & \mathbf{S}_{12} \\ \mathbf{S}_{21} & \mathbf{S}_{22} \end{bmatrix}, \tag{A.5.2}$$

$$\mathbf{P} = \begin{bmatrix} \mathbf{P}_{11} & \mathbf{P}_{12} \\ \mathbf{P}_{21} & \mathbf{P}_{22} \end{bmatrix}, \tag{A.5.3}$$

It follows from the condition $\mathbf{S} > 0$ and $\mathbf{S} = \mathbf{S}^T$ in Lemma A.4.1 and from (A.5.2) that:

$$\mathbf{S}_{11} = \mathbf{S}_{11}^T > \mathbf{0}, \tag{A.5.4}$$

$$\mathbf{S}_{22} = \mathbf{S}_{22}^T > \mathbf{0}, \tag{A.5.5}$$

$$\mathbf{S}_{12} = \mathbf{S}_{21}^T, \tag{A.5.6}$$

$$\mathbf{S}_{11} = \mathbf{S}_{11}^T > \mathbf{0}, \tag{A.5.7}$$

Similarly, we obtain from (A.5.1) and (A.5.3):

$$\mathbf{P}_{11} = \mathbf{P}_{11}^T > \mathbf{0}, \tag{A.5.8}$$

$$\mathbf{P}_{22} = \mathbf{P}_{22}^T > \mathbf{0}, \tag{A.5.9}$$

$$\mathbf{P}_{12} = \mathbf{P}_{21}^T. \tag{A.5.10}$$

With the definition (A.5.2) and (A.5.3), substitution $\mathbf{a}$ in (A.4.1) by (A.3.19) results in the following set of equations:

$$\mathbf{S}_{12}\boldsymbol{\Omega} + \boldsymbol{\Omega}\mathbf{S}_{12}^T = \mathbf{P}_{11}, \tag{A.5.11}$$

$$\mathbf{S}_{22}\boldsymbol{\Omega} - \mathbf{S}_{11}^T = \mathbf{P}_{12}, \tag{A.5.12}$$

$$-\mathbf{S}_{21} - \mathbf{S}_{21}^T = \mathbf{P}_{22}. \tag{A.5.13}$$

It follows from (A.5.12) and (A.5.9) that

$$\mathbf{S}_{21} \leq \mathbf{0}, \tag{A.5.14}$$

and, together with (A.5.6), that

$$\mathbf{S}_{12} \leq \mathbf{0}. \tag{A.5.15}$$

(A.5.11) has to hold for any diagonal positive definite matrix $\boldsymbol{\Omega}$. By assuming temporarily $\boldsymbol{\Omega} = \mathbf{I}$ it is easy to see from (A.5.8), (A.5.11), (A.5.14) and (A.5.15) that we must have:

$$\mathbf{S}_{12} = \mathbf{S}_{21} = \mathbf{0}, \tag{A.5.16}$$

and

$$\mathbf{P}_{11} = \mathbf{P}_{22} = \mathbf{0}. \tag{A.5.17}$$

in order to avoid a contradiction between equations (A.5.8) and (A.5.11), (A.5.14), and (A.5.15) (or between (A.5.11) and (A.5.13)). It follows from (A.5.17) and (A.5.1) that:

$$\mathbf{P} = \mathbf{0}, \tag{A.5.18}$$

and

$$\mathbf{L} = \mathbf{0}. \tag{A.5.19}$$

We know from Lemma (A.4.2) and equation (A.5.19) that our system is not asymptotically hyperstable. It is hyperstable if we can show that the matrix $\mathbf{S} > \mathbf{0}$ exists, which we will do now.

With (A.5.18), equation (A.5.12) reduces to:

$$\mathbf{S}_{11} = \mathbf{S}_{22}\boldsymbol{\Omega}. \tag{A.5.20}$$

With (A.5.20), (A.5.5) and noting that $\boldsymbol{\Omega}$ is diagonal, we also find:

$$\mathbf{S}_{11} = \mathbf{S}_{11}^T = (\boldsymbol{\Omega})^T\mathbf{S}_{22}^T = \boldsymbol{\Omega}\mathbf{S}_{22}, \tag{A.5.21}$$

and hence

$$\mathbf{S}_{22}\boldsymbol{\Omega} = \boldsymbol{\Omega}\mathbf{S}_{22}. \tag{A.5.22}$$

Because $\mathbf{S}_{22}$ commutes in (A.5.22) while, in general, all ω_i^2 are different, we can infer that $\mathbf{S}_{22}$ must be a diagonal matrix. Because of (A.5.20) $\mathbf{S}_{11}$ must be diagonal, too. One of the (sub-) matrices $\mathbf{S}_{11}, \mathbf{S}_{22}$ can be picked (diagonal, positive definite) and the other matrix will be determined by (A.5.20).

We choose to pick

$$\mathbf{S}_{11} = \text{diag}\{s_i\}; \quad s_i > 0 \quad i = 1 \ldots n \tag{A.5.23}$$

and with (A.5.20) we obtain

$$\mathbf{S}_{22} = \text{diag}\{s_i\omega_i^2\}. \tag{A.5.24}$$

By establishing the results (A.5.19), (A.5.23) and (A.5.24) we provided that $\mathbf{L} = \mathbf{0}$ and S diagonal, as was claimed in Section A.4.

A.6 Summary of Results

We have developed a model for flexible structures based on a continuum modelling approach and standard assumptions such as linearity, no damping, etc. Almost all 'reasonable' point sensors and actuators are considered as potential candidates in the input/output equations. By application of the positive real lemma we found necessary and sufficient conditions for hyperstability of this system.

The conditions (A.4.7), (A.4.8) for the types of sensors required can be interpreted as follows:

- No displacement or acceleration measurements are allowed as outputs of a hyperstable structural (sub)system.
- Rate $\left(\frac{\partial v^{(j)}}{\partial t}\right)$ sensors are required, and all spatial derivatives are allowed $(j = 0, 1 \ldots p-1)$.

The condition for the location of sensors and actuators is given by (A.4.13), and has the following interpretations:

- It is sufficient to collocate corresponding [1] sensors and actuators ($x_{sk} = x_{ak}\ \forall k$)
- It is necessary to place corresponding sensors and actuators at such locations where each of the mode shapes (or if higher-order devices are used, the corresponding derivatives) has the same sign.
- For structures with an 'infinite number' of vibration modes, the last condition can, in general, only be fulfilled by collocation of sensors and actuators. (This conditions can be relaxed for devices located on rigid substructures.)

[1] "Corresponding" sensors and actuators are defined as having the same indices for location, and acting on the same spatial derivative

Appendix B

A Synthesis Method for Hyperstable Control Systems

Assumptions

We will consider the design of hyperstable feedback compensators for multivariable linear systems. We assume a time-invariant system model with a state-space realization with matrices $\mathbf{A}$, $\mathbf{B}$, $\mathbf{C}$ of appropriate dimensions:

$$\dot{\mathbf{x}} = \mathbf{A}\mathbf{x} + \mathbf{B}\mathbf{u}. \tag{B.1}$$

$$\mathbf{y} = \mathbf{C}\mathbf{x}. \tag{B.2}$$

It assumed that the system (B.1), (B.2) has an equal number of inputs and outputs and that it is completely controllable and observable [Kwakernaak and Sivan]:

$$\{\mathbf{A}, \mathbf{B}\} \text{ controllable}, \quad \{\mathbf{A}, \mathbf{C}\} \text{ observable}. \tag{B.3}$$

Although not a necessary condition or assumption, hyperstability of the system (B.1), (B.2) is a sufficient condition for the stability of the closed-loop system resulting from the synthesis procedure outlined below. If the system (B.1), (B.2) is not hyperstable, additional conditions or tests have to be applied to ensure closed-loop system stability.

The output-feedback compensator considered has the structure of a state-feedback controller (gain matrix $\mathbf{F}$) driven by a full-order state-estimator (gain matrix $\mathbf{K}$). This compensator has the following state-space realization [Kwakernaak and Sivan]:

$$\dot{\hat{\mathbf{x}}} = (\mathbf{A} + \mathbf{B}\mathbf{F} + \mathbf{K}\mathbf{C})\hat{\mathbf{x}} + \mathbf{K}\mathbf{v}, \tag{B.4}$$

$$\mathbf{w} = \mathbf{F}\hat{\mathbf{x}}, \tag{B.5}$$

and the feedback connection with the plant (model) (B.1), (B.2) is:

$$\mathbf{v} = \mathbf{y} \tag{B.6}$$

$$\mathbf{u} = -\mathbf{w}. \tag{B.7}$$

After introducing the estimation error

$$\mathbf{e} = \mathbf{x} - \hat{\mathbf{x}}, \tag{B.8}$$

the closed-loop system can be represented in the form

$$\begin{bmatrix} \dot{\mathbf{x}} \\ \dot{\mathbf{e}} \end{bmatrix} = \begin{bmatrix} \mathbf{A}+\mathbf{BF} & -\mathbf{BF} \\ \mathbf{0} & \mathbf{A}+\mathbf{KC} \end{bmatrix} \begin{bmatrix} \mathbf{x} \\ \mathbf{e} \end{bmatrix} \tag{B.9}$$

Synthesis Procedure

Assumption (B.3) guarantees that gain matrices $\mathbf{F}$ and $\mathbf{K}$ exist such that $(\mathbf{A}+\mathbf{BF})$ and $(\mathbf{A}+\mathbf{KC})$ are Hurwitz, i.e $\Re[\lambda(\cdot)] < 0$ for all eigenvalues λ of matrix $(\cdot)$. Finding suitable matrices $\mathbf{F}$ and $\mathbf{K}$ is the output feedback synthesis problem which we will address here.

A stabilizing state-feedback gain matrix, $\mathbf{F}$ can be determined by solving the pole-placement or the linear-optimal regulator problem [Kwakernaak and Sivan]. This is in fact the first step of the control synthesis procedure outlined below:

Step 1: Determine suitable stabilizing state-feedback matrix $\mathbf{F}$, e.g. by pole-placement or linear-quadratic-optimal procedure.

Step 2: Choose a positive definite matrix $\mathbf{T} > \mathbf{0}$ as design parameter such that:

$$\mathbf{U} = \mathbf{T} + \mathbf{C}^T\mathbf{F} + \mathbf{F}^T\mathbf{C} > 0. \tag{B.10}$$

The choice of $\mathbf{T}$ determines the location of the observer poles. Qualitatively, choosing a 'small' $\mathbf{T}$ will result in a 'fast' observer. $\mathbf{T} = \gamma\mathbf{I}$, with a scalar $\gamma > 0$ and $\mathbf{I}$ = identify, has been found to be a suitable choice in most instances.

Step 3: Determine matrix $\mathbf{S} > \mathbf{0}$ from Lyapunov equation (B.11):

$$\mathbf{S}(\mathbf{A}+\mathbf{BF}) + (\mathbf{A}+\mathbf{BF})^T\mathbf{S} = -\mathbf{U}. \tag{B.11}$$

Step 4: Compute observer gain matrix $\mathbf{K}$ from:

$$\mathbf{K} = \mathbf{S}^{-1}\mathbf{F}^T. \tag{B.12}$$

The feedback compensator system (B.4), (B.5) with $\mathbf{F}, \mathbf{K}$ from Step 1 and Step 4 will be asymptotically hyperstable, which implies that it will be asymptotically stable. A sufficient condition for the closed-loop system (B.9) to be asymptotically stable is that the plant (model) is hyperstable. If the closed-loop system is asymptotically stable the observer gain matrix $\mathbf{K}$ determined in Step 4 is a stabilizing gain matrix, because the eigenvalues of the system matrix of (B.9) are identical to the eigenvalues of $(\mathbf{A}+\mathbf{BF})$ and $(\mathbf{A}+\mathbf{KC})$.

Derivation of Synthesis Procedure

We will now show that the feedback compensator (B.4), (B.5) designed with the above procedure is indeed hyperstable, and that a unique positive definite solution $\mathbf{S}$ of the Lyapunov equation (B.11) always exists.

We can conclude from the Kalman-Yakubovich Lemma that the linear time-invariant system (B.4), (B.5) is hyperstable (and that its transfer function matrix is strictly positive real), if there exist a symmetric positive definite matrix $\mathbf{S}$ and a symmetric positive-definite matrix $\mathbf{T}$ such that

$$\mathbf{S}(\mathbf{A}+\mathbf{BF}+\mathbf{KC})+(\mathbf{A}+\mathbf{BF}+\mathbf{KC})^T\mathbf{S}=-\mathbf{T}, \tag{B.13}$$

$$\mathbf{K}^T\mathbf{S}=\mathbf{F}. \tag{B.14}$$

While the design of controllers and observers can usually be performed independently (separation principle [Kwakernaak and Sivan]), in this case the gain matrices $\mathbf{F}$ and $\mathbf{K}$ are directly related by (B.14). This equation is used in synthesis Step 4.

We will now show that matrices $\mathbf{S}=\mathbf{S}^T>\mathbf{0}$ and $\mathbf{T}=\mathbf{T}^T>\mathbf{0}$ consistent with (B.13), (B.14) co-exist with any stabilizing gain matrix $\mathbf{F}$.

Choose any $\mathbf{S}=\mathbf{S}^T>\mathbf{0}$. Then $\mathbf{S}^{-1}=(\mathbf{S}^{-1})^T>\mathbf{0}\ \exists$

It follows from (B.14) that

$$\mathbf{KC}=\mathbf{S}^{-1}\mathbf{F}^T \tag{B.15}$$

(B.13) yields with (B.15):

$$(\mathbf{C}^T\mathbf{F}+\mathbf{F}^T\mathbf{C})+\mathbf{S}(\mathbf{A}+\mathbf{BF})+(\mathbf{A}+\mathbf{BF})^T\mathbf{S}=-\mathbf{T} \tag{B.16}$$

With the definition

$$\mathbf{U} = \mathbf{T} + \mathbf{C}^T\mathbf{F} + \mathbf{F}^T\mathbf{C} \tag{B.17}$$

(B.16) can be written as a Lyapunov equation

$$\mathbf{S}(\mathbf{A}+\mathbf{BF}) + (\mathbf{A}+\mathbf{BF})^T\mathbf{S} = -\mathbf{U}. \tag{B.18}$$

The Lyapunov criterion (Theorem 2.6-1 of [Kailath] states that: "$(\mathbf{A}+\mathbf{BF})$ is Hurwitz if and only if for any given positive-definite symmetric matrix $\mathbf{U}$ there exists a positive-definite symmetric matrix $\mathbf{S}$ that satisfies (B.18)."

Thus, for every Hurwitz matrix $(\mathbf{A}+\mathbf{BF})$ there exists a matrix $\mathbf{S} = \mathbf{S}^T > \mathbf{0}$ that satisfied (B.18) for any $\mathbf{U} = \mathbf{U}^T > \mathbf{0}$. It remains to be shown that there also exists a matrix $\mathbf{T} = \mathbf{T}^T > \mathbf{0}$ such that $\mathbf{U} = \mathbf{U}^T > \mathbf{0}$. This can be done as follows:

It follows from (B.17) that

$$\mathbf{U} = \mathbf{T} + \underbrace{(\mathbf{C}+\mathbf{F})^T(\mathbf{C}+\mathbf{F})}_{\geq \mathbf{0}} - \underbrace{\mathbf{C}^T\mathbf{C}}_{\geq \mathbf{0}} - \underbrace{\mathbf{F}^T\mathbf{F}}_{\geq \mathbf{0}} \tag{B.19}$$

It follows from (B.19) that if we choose

$$\mathbf{F} = \mathbf{\Gamma} + \mathbf{C}^T\mathbf{C} + \mathbf{F}^T\mathbf{F}, \text{ with matrix } \mathbf{\Gamma} > \mathbf{0}, \tag{B.20}$$

then $\mathbf{U} > \mathbf{0}$ and $\mathbf{T} > \mathbf{0}$. q.e.d.

This particular choice of $\mathbf{T}$ was used here to show that this matrix always exists. For an actual design, however, (B.20) has been found to be conservative, usually resulting in very slow observers. Therefore, the choice of $\mathbf{T}$ for design purposes should be based on (B.17), with the added requirement $\mathbf{U} > \mathbf{0}$, $\mathbf{T} > \mathbf{0}$, as indicated in the outline of the synthesis procedure.

Special Case: LQG Balancing

[Opdenacker and Jonckheere] investigate LQG control systems in a 'LQG-balanced' state-space setting where by definition the solutions to the algebraic control and observation Riccati equations are equal and diagonal. It is shown by [Opdenacker and Jonckheere] that LQG controllers for passive, symmetric LQG-balanced plants are hyperstable. This appears to be a special case of the problem discussed above when $\mathbf{S} = \mathbf{I}$.

APPENDIX C PROOFS AND DERIVATIONS

Table of Contents

C.1 Proof of Statement (5.2.10c)

Taking the square of both sides of (5.2.8c) yields:

$$\alpha^2\|\mathbf{x}(t)\|^2 \leq \beta_0^2 + 2\beta_0\beta_1\|\mathbf{x}(t_0)\| + \beta_1^2\|\mathbf{x}(t_0)\|^2 \tag{C.1.1}$$

Because $\beta_0\beta_1\|\mathbf{x}(t_0)\| \geq 0$ per assumptions made in Definition 5.2.2, (C.1.1) will always be satisfied if

$$\alpha^2\|\mathbf{x}(t)\|^2 \leq \beta_0^2 + \beta_1^2\|\mathbf{x}(t_0)\|^2. \tag{C.1.2}$$

With (5.2.7c) we find

$$\alpha^2\|\mathbf{x}(t)\|^2 \leq \eta(t_0,t) + \beta_1^2\|\mathbf{x}(t_0)\|^2 \quad \forall\, t > t_0, \quad \text{q.e.d.} \tag{C.1.3}$$

The proof for the discrete-time case is analogous.

C.2 Derivation of the Kalman-Yakubovich Lemma

We consider a linear time-invariant system governed by the continuous-time state-space equations

$$\dot{\mathbf{x}}(t) = \mathbf{A}\mathbf{x}(t) + \mathbf{B}\mathbf{u}(t) \tag{C.2.1}$$

$$\mathbf{y}(t) = \mathbf{C}\mathbf{x}(t) + \mathbf{D}\mathbf{u}(t) \tag{C.2.2}$$

and the associated integral function:

$$\eta(t_0, t_1) = \int_{t_0}^{t_1} \mathbf{u}^T(t)\mathbf{y}(t)dt. \tag{C.2.3}$$

It is assumed that conditions (5.2.7c) and (5.2.9c) of Definition 5.2.2 are met. We will derive conditions on the system matrices $\mathbf{A}, \mathbf{B}, \mathbf{C}, \mathbf{D}$ required to meet also condition (5.2.8c) which is restated here in simplified form ($\alpha = 1$):

$$\|\mathbf{x}(t)\| \leq \beta_0 + \beta_1\|\mathbf{x}(t_0)\| \;\forall\; t \in [t_0, t_1], \quad \beta_0 > 0,\ \beta_1 > 0. \tag{C.2.4}$$

As shown in an example in equations (5.2.12) – (5.2.15), conclusions about the evolution of $\mathbf{x}(t)$ can be drawn from (C.2.3) if the integrand is a positive semidefinite function of $\mathbf{x}$ and $\mathbf{u}$. (C.2.3) becomes a function of $\mathbf{x}$ and $\mathbf{u}$ only if we substitute (C.2.2) into (C.2.3), resulting in:

$$\eta(t_0, t_1) = \frac{1}{2}\int_{t_0}^{t_1} \mathbf{u}^T(\mathbf{D} + \mathbf{D}^T)\mathbf{u} + \mathbf{u}^T\mathbf{C}\mathbf{x} + \mathbf{x}^T\mathbf{C}^T\mathbf{u})dt. \tag{C.2.5}$$

With the introduction of the following abbreviations

$$\mathbf{z}^T = [\dot{\mathbf{x}}^T \quad \mathbf{u}^T \quad \mathbf{x}^T] \tag{C.2.6}$$

$$\mathbf{F} = [\mathbf{I} \quad -\mathbf{B} \quad -\mathbf{A}] \tag{C.2.7}$$

$$\mathbf{M} = \begin{bmatrix} \mathbf{0} & \mathbf{0} & \mathbf{0} \\ \mathbf{0} & \mathbf{D} + \mathbf{D}^T & \mathbf{C} \\ \mathbf{0} & \mathbf{C}^T & \mathbf{0} \end{bmatrix} \tag{C.2.8}$$

(C.2.1) and (C.2.5) can be expressed in the form:

$$\mathbf{F}\,\mathbf{z} = \mathbf{0} \tag{C.2.9}$$

$$\eta(t_0, t_1) = \int_{t_0}^{t_1} \mathbf{z}^T(t)\mathbf{M}\mathbf{z}(t)dt. \tag{C.2.10}$$

With (C.2.9) we can formally expand the integrand of (C.2.10) as follows without affecting the value of the integral η:

$$\mathbf{z}^T\mathbf{M}\mathbf{z} = \mathbf{z}^T\mathbf{M}\mathbf{z} + \mathbf{z}^T\mathbf{T}^T\mathbf{F}\mathbf{z} + \mathbf{z}^T\mathbf{F}^T\mathbf{T}\mathbf{z} = \mathbf{z}^T\mathbf{M}^*\mathbf{z} \tag{C.2.11}$$

where $\mathbf{T}$ is a transformation matrix of a system invariant transformation defining the matrix:

$$\mathbf{M}^* = \mathbf{M} + \mathbf{F}^T\mathbf{T} + \mathbf{T}^T\mathbf{F} \tag{C.2.12}$$

Based on (C.2.11), (C.2.10) can be expressed as follows:

$$\eta(t_0, t_1) = \frac{1}{2}\int_{t_0}^{t_1} \mathbf{z}^T(t)\mathbf{M}^*\mathbf{z}(t)dt. \tag{C.2.13}$$

A hyperstable system should admit a positive semi-definite matrix $\mathbf{M}^* \geq \mathbf{0}$ which can be defined as follows:

$$\mathbf{M}^* = \begin{bmatrix} \mathbf{0} & \mathbf{0} & \mathbf{S} \\ \mathbf{0} & \mathbf{N}^T\mathbf{N} & \mathbf{N}^T\mathbf{L}^T \\ \mathbf{S} & \mathbf{L}\mathbf{N} & \mathbf{L}\mathbf{L}^T \end{bmatrix} \quad \text{with} \quad \mathbf{S} = \mathbf{S}^T \geq \mathbf{0} \tag{C.2.14}$$

When $\mathbf{T}$ is also partitioned into three submatrices, $\mathbf{T} = [\,\mathbf{T}_1 \quad \mathbf{T}_2 \quad \mathbf{T}_3\,]$, equation (C.2.12) can be expressed as:

$$\begin{bmatrix} \mathbf{0} & \mathbf{0} & \mathbf{S} \\ \mathbf{0} & \mathbf{N}^T\mathbf{N} & \mathbf{N}^T\mathbf{L}^T \\ \mathbf{S} & \mathbf{L}\mathbf{N} & \mathbf{L}\mathbf{L}^T \end{bmatrix} = \begin{bmatrix} \mathbf{T}_1 + \mathbf{T}_1^T & \mathbf{T}_2 - \mathbf{T}_1^T\mathbf{B} & \mathbf{T}_3 - \mathbf{T}_1^T\mathbf{A} \\ \mathbf{T}_2^T - \mathbf{B}^T\mathbf{T}_1 & \mathbf{D} + \mathbf{D}^T - \mathbf{T}_2^T\mathbf{B} - \mathbf{B}^T\mathbf{T}_2 & \mathbf{C} - \mathbf{T}_2^T\mathbf{A} - \mathbf{B}^T\mathbf{T}_3 \\ \mathbf{T}_3^T - \mathbf{A}^T\mathbf{T}_1 & \mathbf{C}^T - \mathbf{T}_3^T\mathbf{B} - \mathbf{A}^T\mathbf{T}_2 & -\mathbf{T}_3^T\mathbf{A} - \mathbf{A}^T\mathbf{T}_3 \end{bmatrix} \tag{C.2.15}$$

(C.2.15) yields the following submatrices of the transformation matrix $\mathbf{T}$:

$$\begin{aligned} \mathbf{T}_1 &= \mathbf{0} \\ \mathbf{T}_2 &= \mathbf{0} \\ \mathbf{T}_3 &= \mathbf{S} \end{aligned} \tag{C.2.16}$$

With (C.2.16) the relations of the Kalman-Yakubovich Lemma ensue directly from (C.2.15):

$$\mathbf{SA} + \mathbf{A}^T\mathbf{S} = -\mathbf{L}\mathbf{L}^T \tag{C.2.17}$$

$$\mathbf{B}^T\mathbf{S} + \mathbf{N}^T\mathbf{L}^T = \mathbf{C} \tag{C.2.18}$$

$$\mathbf{D} + \mathbf{D}^T = \mathbf{N}^T\mathbf{N} \tag{C.2.19}$$

(C.2.17) – (C.2.19) represent necessary and sufficient conditions for the hyperstability of the system (C.2.1) – (C.2.2). The matrices $\mathbf{L}$ and $\mathbf{N}$ can be choosen arbitrarily, and a positive semi-definite matrix $\mathbf{S} \geq \mathbf{0}$ per (C.2.14) must exist to satisfy the conditions. (C.2.17) is a Lyapunov equation which will always have a positive definite solution $\mathbf{S} > \mathbf{0}$ if the matrix $\mathbf{A}$ is Hurwitzian. Hence, in the case of linear time-invariant systems hyperstability implies also stability in the sense of Lyapunov.

Based on (C.2.12) – (C.2.14), the integral function (C.2.3) can now be expressed as follows, which allows the derivation of additional stability results.

$$\eta(t_0, t_1) = \frac{1}{2}\mathbf{x}^T\mathbf{S}\mathbf{x} + \frac{1}{2}\int_{t_0}^{t_1} \|\mathbf{N}\mathbf{u} + \mathbf{L}^T\mathbf{x}\|^2 dt. \tag{C.2.20}$$

C.3 Proof for (5.4.17)

Given is the logic condition (5.4.16) restated below:

$$\bar{y}_i \mathcal{C}_{Bi}\{\mathbf{w},\mathbf{y},\mathbf{z}\} + \varepsilon_i |\mathcal{C}_{Bi}\{\mathbf{w},\mathbf{y},\mathbf{z}\}| < 0 \tag{C.3.1}$$

This condition is true only in the following two cases:

Case 1: $\mathcal{C}_{Bi} < 0, \quad \text{and} \quad \bar{y}_i > \varepsilon_i$

Case 2: $\mathcal{C}_{Bi} > 0, \quad \text{and} \quad \bar{y}_i < -\varepsilon_i$

The value of the logic condition (5.4.17) restated here

$$y_i \mathcal{C}_{Bi}\{\mathbf{w},\mathbf{y},\mathbf{z}\} < 0 \tag{C.3.2}$$

can be readily determined for these two cases by considering the inverse of the mapping function (5.4.15) restated below:

$$\begin{array}{ll} \bar{y}_i > \varepsilon_i & \forall\ y_i > 2\varepsilon_i \\ \bar{y}_i \geq y_i - \varepsilon_i & \forall\ 0 \leq y_i \geq 2\varepsilon_i \\ \bar{y}_i \leq y_i + \varepsilon_i & \forall\ 0 \leq y_i \leq -2\varepsilon_i \\ \bar{y}_i < -\varepsilon_i & \forall\ y_i \leq -2\varepsilon_i \end{array} \tag{C.3.3}$$

By evaluating (C.3.2) for these cases we find:

Case 1: $\bar{y}_i > \varepsilon_i \Rightarrow y_i > 2\varepsilon_i \geq 0 \Rightarrow y_i \mathcal{C}_{Bi} < 0$

Case 2: $\bar{y}_i < -\varepsilon_i \Rightarrow y_i \leq -2\varepsilon_i \leq 0 \Rightarrow y_i \mathcal{C}_{Bi} < 0$

Hence the logic condition (C.3.1) always implies the logic condition (C.3.2), q.e.d. The inverse is generally not true.

APPENDIX D
VISION SYSTEM

Space Vision System

The vision system used in the laboratory is functionally equivalent to the Space Vision System (SVS) successfully tested by [MacLean and Pinkney] on the Space Shuttle in 1992 and used by Hadfield on the Shuttle in 1995. The setup in the laboratory is in principle similar to that for a space mission [Stieber, McKay, Vukovich and Petriu]. A single video camera is used to image the robot workspace, which includes dedicated visual targets. The relative position, orientation and velocity between the robot "Payload" and its "Berth" to which it is to be manoeuvred, is determined by image processing.

Measurement of Position and Orientation by Vision System

The various points and associated coordinate frames used by the vision system are identified in Figure D.1, which also defines abbreviations for long names. The relative position and orientation of the various reference frames can be conveniently described by homogeneous coordinate transformations, defined by transformation matrices $\mathbf{T} \in \mathbb{R}^{4\times4}$ (see [Fu, Gonzales and Lee]). The transformation ${}^{A}_{B}\mathbf{T}$ transforms the coordinates of a point expressed in reference frame A into the coordinates in frame B. The inverse transformation for going from B to A is ${}^{B}_{A}\mathbf{T} = {}^{A}_{B}\mathbf{T}^{-1}$ and always exists.

Our goal is to determine the relative position and orientation between Berth and Payload in order to provide a guidance command to the robot. This transformation can be expressed in terms of a chain of homogeneous transformations:

$$ {}^{Berth}_{Payload}\mathbf{T} = {}^{Berth}_{Cam}\mathbf{T} \cdot {}^{Cam}_{PTarget}\mathbf{T} \cdot {}^{Ptarget}_{Payload}\mathbf{T} \qquad \text{(D.1)} $$

The transformation ${}^{Bert}_{Cam}\mathbf{T}$ is given by:

$$ {}^{Berth}_{Cam}\mathbf{T} = {}^{0}_{Berth}\mathbf{T}^{-1} \cdot {}^{0}_{CamB}\mathbf{T} \cdot {}^{CamB}_{PTU}\mathbf{T} \cdot {}^{PTU}_{CamH}\mathbf{T} \cdot {}^{CamH}_{Cam}\mathbf{T} \qquad \text{(D.2)} $$

The transformation ${}^{Cam}_{Ptarget}\mathbf{T}$ in (D.1) is determined by photogrammetric image processing as discussed in detail below, while the other transformations on the

right-hand side of (D.1) must be "known" a priori in order to determine the left-hand side. Transformations ${}^{Ptarget}_{Payload}\mathbf{T}$, ${}^{BTarget}_{Berth}\mathbf{T}$, ${}^{CamH}_{Cam}\mathbf{T}$ can be accurately measured "before flight" and are not subject to significant variations "in flight" because of the relatively small translations typically associated with these transformations. Although the transformations ${}^{0}_{CamB}\mathbf{T}$ and ${}^{0}_{Berth}\mathbf{T}$ can also be measured "before flight", thermal deformations and other effects can lead to variations "in flight" which can be significant in comparison to the accuracy of the SVS. Cameras are often mounted on pan-and-tilt units (PTUs) which provide a read-out of pan and tilt angles, but with insufficient accuracy for our purposes. Hence one has to assume that there is significant uncertainty associated with ${}^{PTU}_{CamH}\mathbf{T}$. The effect of all these errors can be reduced considerably by calibration using a stationary auxiliary Berthing Target. After photogrammetric measurement of ${}^{Cam}_{BTarget}\mathbf{T}$ we can use the following relationship to calibrate the estimate for ${}^{Berth}_{Cam}\mathbf{T}$ in (D.2):

$$ {}^{Berth}_{Cam}\mathbf{T} = {}^{Cam}_{BTarget}\mathbf{T}^{-1} \cdot {}^{BTarget}_{Berth}\mathbf{T}^{-1}. \tag{D.3} $$

Photogrammetric Image Processing

Figure D.2 shows the basic relations between the position of a target in the real world and its image on the CCD of an ideal camera with focal length f_e. It is well known [Fu, Gonzales and Lee] that the X, Y, Z coordinates of a particular target element j in real world ($\mathbf{W}$ frame) and its y, z photo-coordinates in the image plane ($\mathbf{P}$ frame) are related as follows:

$$ \frac{{}^{Cam}\mathbf{P}_y(j)}{f_e} = \frac{{}^{Cam}\mathbf{W}_Y(j)}{{}^{Cam}\mathbf{W}_X(j)} \tag{D.4} $$

$$ \frac{{}^{Cam}\mathbf{P}_z(j)}{f_e} = \frac{{}^{Cam}\mathbf{W}_Z(j)}{{}^{Cam}\mathbf{W}_X}(j) \tag{D.5} $$

Based on the a-priori knowledge of the location of target elements in the Payload Target reference frame, the 6 unknown parameters of the transformation ${}^{Cam}_{PTarget}\mathbf{T}$ can be uniquely determined from (D.4) and (D.5) iff the target array has 3 or more elements, i.e. $j = 1 \ldots k$, $k \geq 3$. The solution of these non-linear equations requires iterative numerical methods in most cases. The SVS applies small corrections to

(D.4) and (D.5) in order to compensate for optical imperfections of the camera/lens assembly which are determined in a one-time camera calibration process.

The centroid position of the target elements are interpolated to sub-pixel level to further increase the accuracy of the photogrammetric solution. Due to their symmetries, circular target elements permit very accurate and robust centroid determination and are therefore preferred target elements. However, the SVS is also able to track other target elements such as corners, intersections of lines and ends of lines.

As an example for photogrammetric image processing Figure D.3 shows the motion of one of the Payload Target elements in the camera image as the Payload moves through the workspace. For the same case Figure D.4 shows the time history of the Payload motion in the Berth frame, computed by solving (D.4), (D.5) and performing the transformation (D.1), (D.2).

Performance Characteristics of the Vision System

Very fast image processing is required in order to support the real-time control of a robotic system. The SVS as currently hosted on a 486 PC computer with C40 DSP boards is capable of processing, at a video frame rate of 30 Hz, the photogrammetric solutions and coordinate transformations for 2 target arrays with up to 10 elements each, using one or 2 cameras. The measurement accuracies achieved vary considerably with the distance between camera and target, the size and the accuracy of the targets, and the accuracy of the various calibration schemes. During preliminary tests in the laboratory the distance Camera-Berth was 1.83 m and planar target arrays with 4 circular dots of 42 mm diameter were used in ambient lighting conditions (Figure D.1). Figure D.5 shows the measurement of the an open-loop transient response of the robot with a flexible link of 1.28 m length. (The flexible link used during those tests had different physical parameters than the one used for the experiments described in Section 7.5.) The results confirm the ability of the SVS to track the Payload motion in spite of relatively high velocities and accelerations, and to resolve the small components of the motion along the Z-axis and about the Roll axis. When the Payload is

moved through the workspace in a single-joint robot motion, joint-angle encoder measurements can be compared with SVS measurements to estimate the absolute measurement accuracy achieved. Although the geared encoders are considered very accurate, small residual vibrations in the robot flexible structure, which have been identified in the power spectrum of the SVS measurements, introduce some "errors" into this comparison. Figure D.6 shows the difference of the Payload-Berth range measurements by the SVS and the encoder for 70 data points spread over the range of roughly -0.4 m to $+0.5$ m, and a least-squares fit to the data. All measurement differences are less than 10 mm over the entire range. A "systematic error" of about 10 mm/m is observed and attributed to imprecise calibration of the SVS during the preliminary test. The "random errors", which have a standard deviation of 2.3 mm from the regression line, are attributed in part to residual vibrations of the robot and partly to measurement noise in the SVS. The latter could be reduced by filtering the SVS measurements taken at 30 Hz. The robot oscillations could be reduced by more careful experimentation. In spite of their preliminary nature, these results provide confidence in the accuracy of the photogrammetric technique and its suitability for real-time robotics applications.

Target Design for Control Experiments

During the development of the laboratory facility the flexible link and the visual targets were updated from the original design discussed above. The target design used in the experiments discussed in Section 7.5 is shown in Figure C.7. The relatively large dark areas surrounding the circular target markings permit the tracking of fast motions and avoids that SVS tracking windows lock on to features in the image background during rapid repositioning of the target.

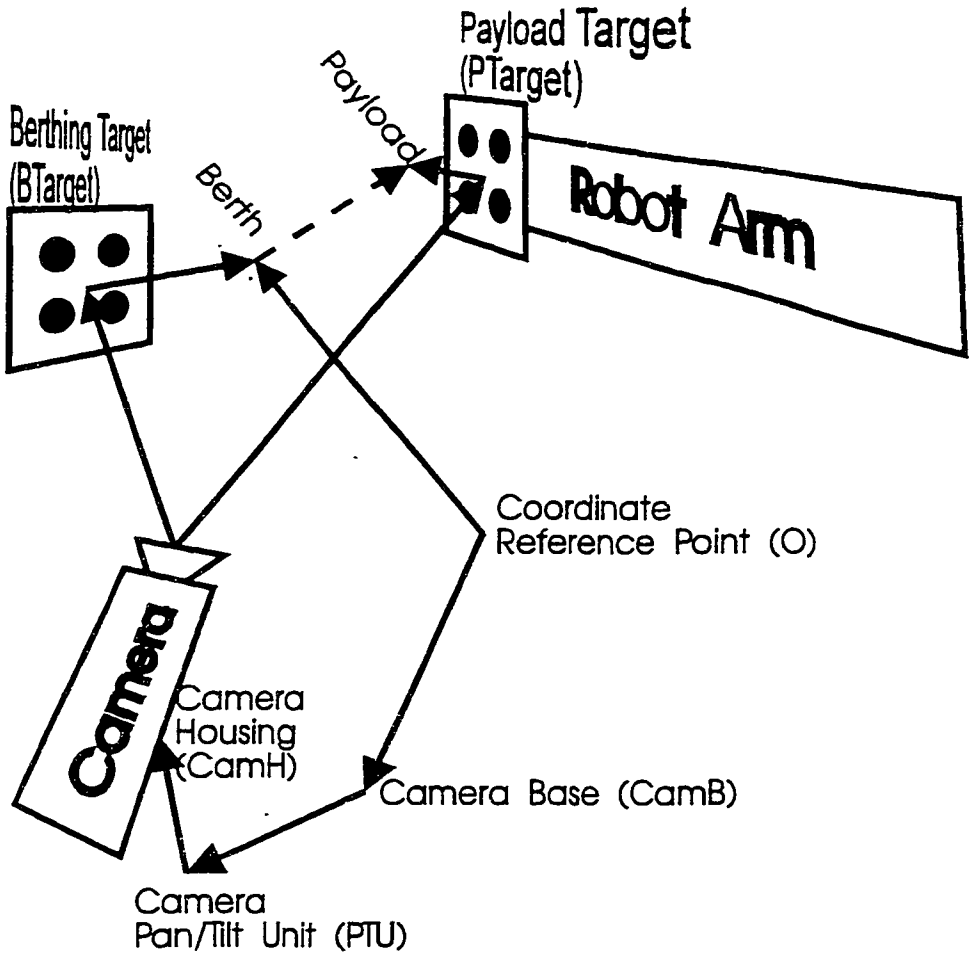

Figure D.1: Reference Frames used by the Vision System

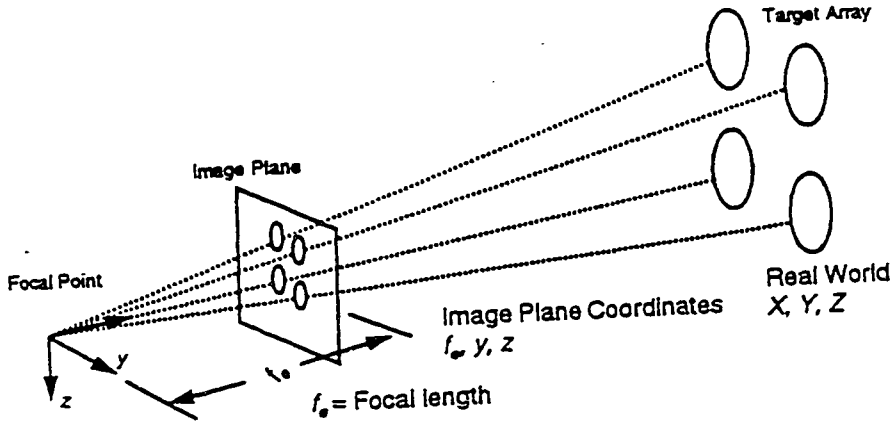

Figure D.2: Photogrammetric Relationships

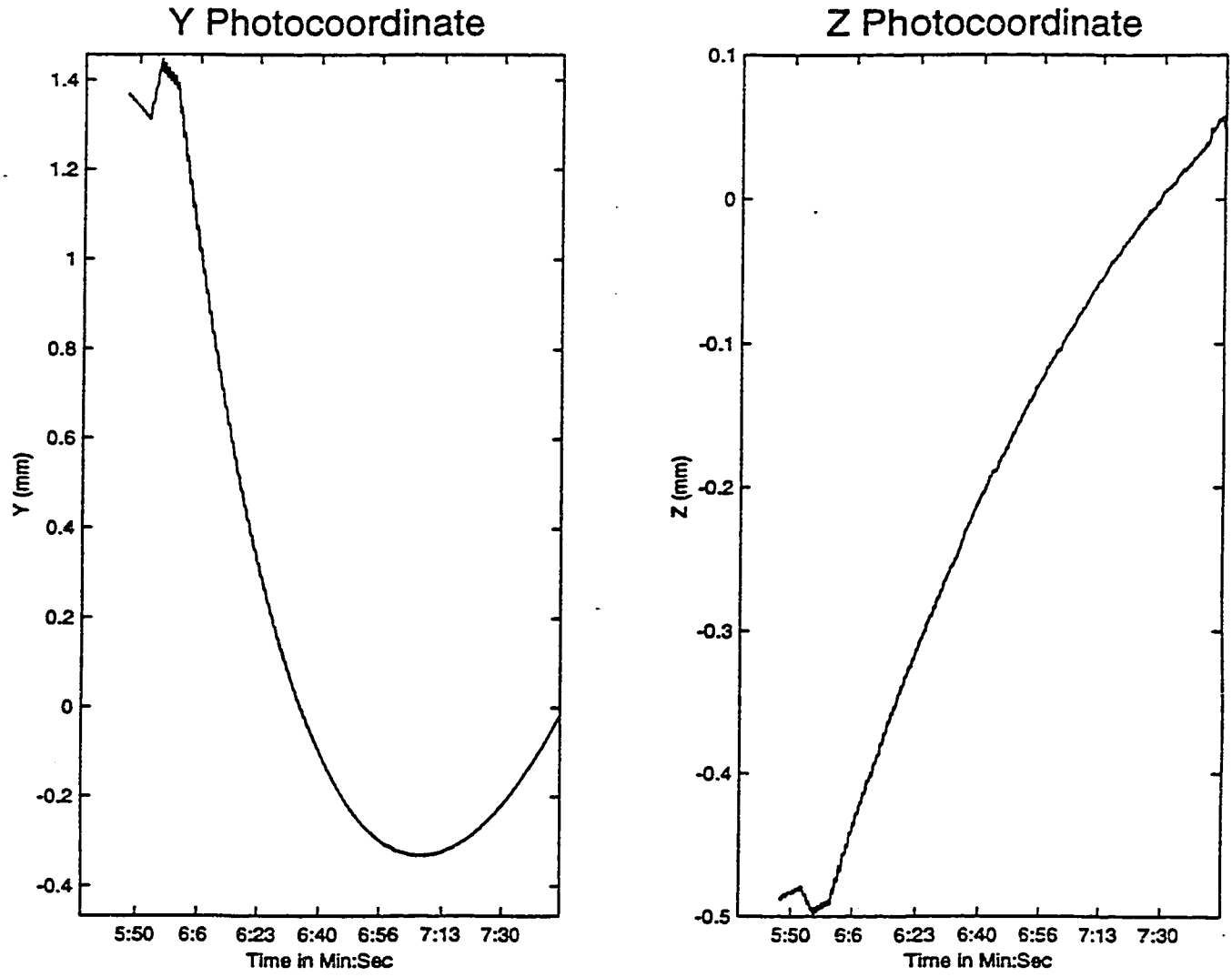

Figure D.3: Camera Image of Target Motion

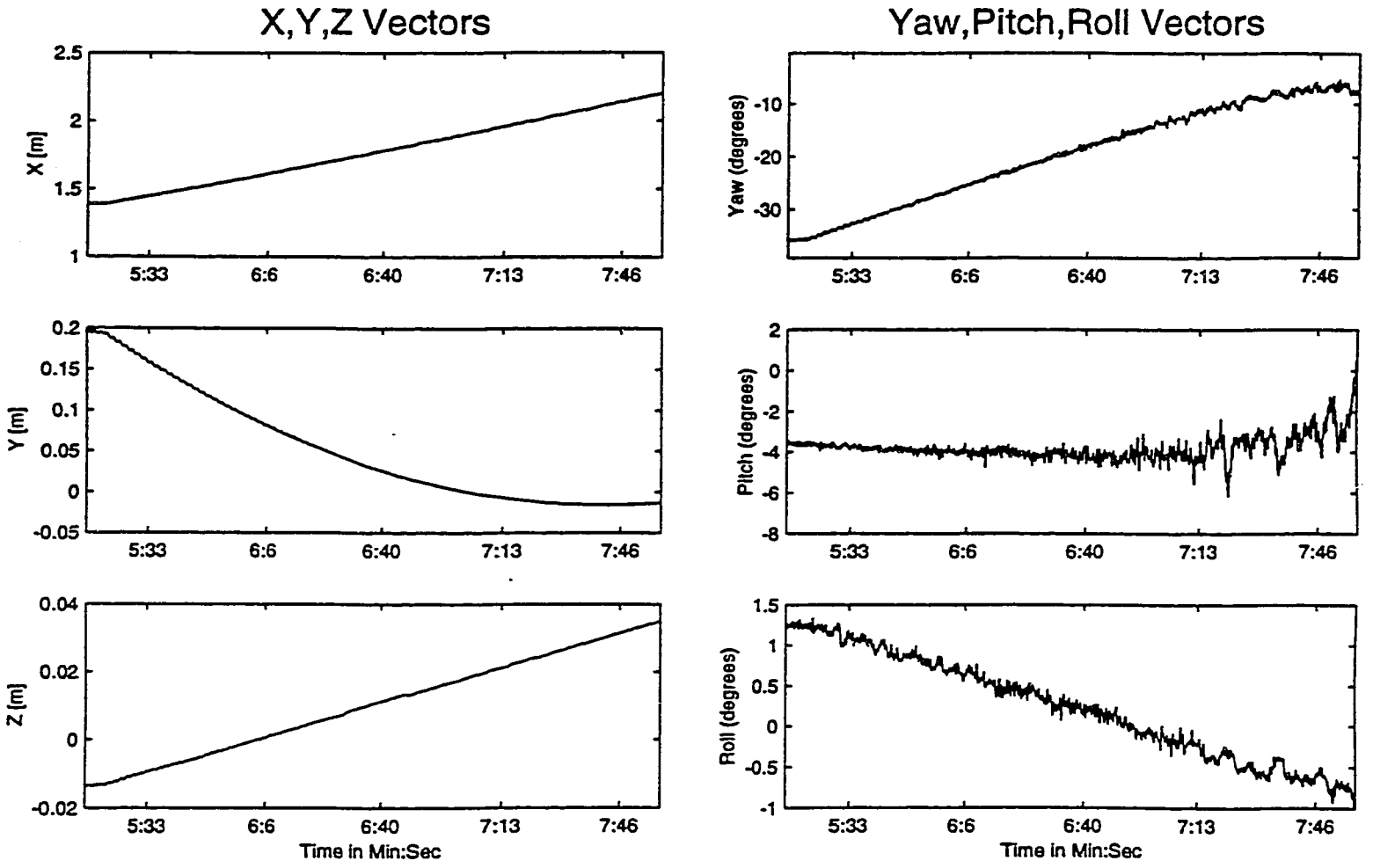

Figure D.4: Payload Motion Calculated by Vision System

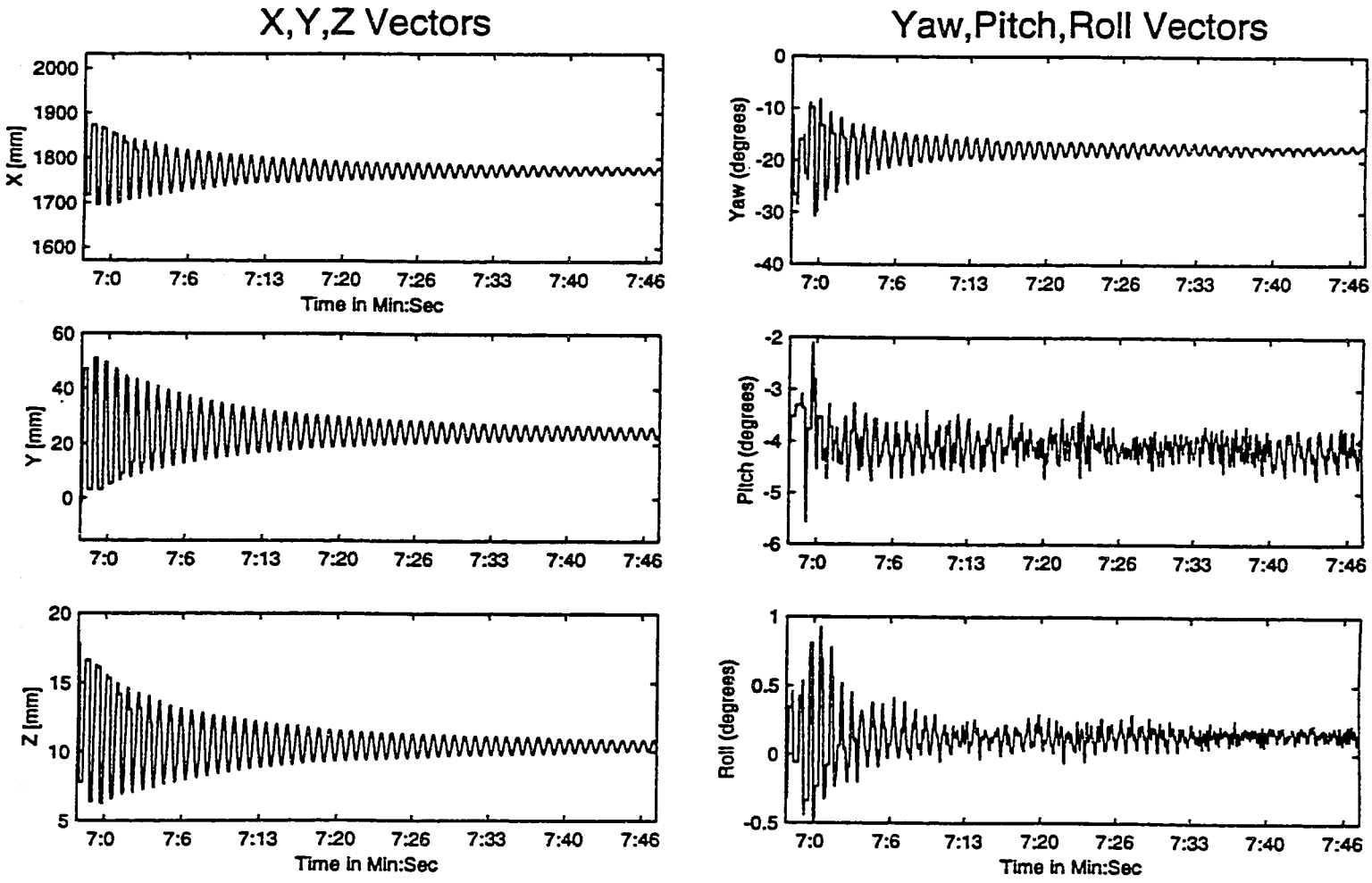

Figure D.5: Robot Oscillations Tracked by Vision System

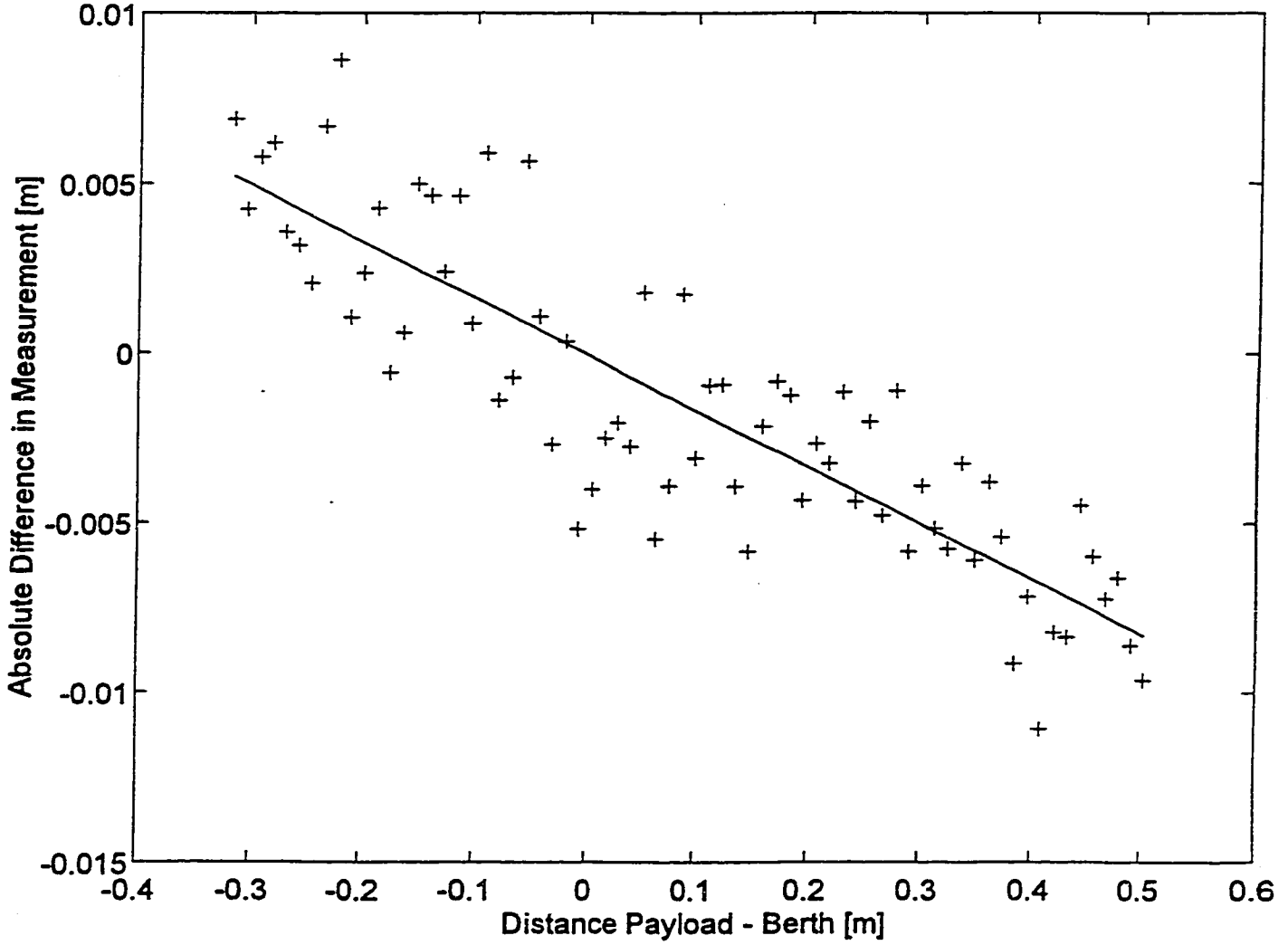

Figure D.6: Differences in SVS and Encoder Measurements

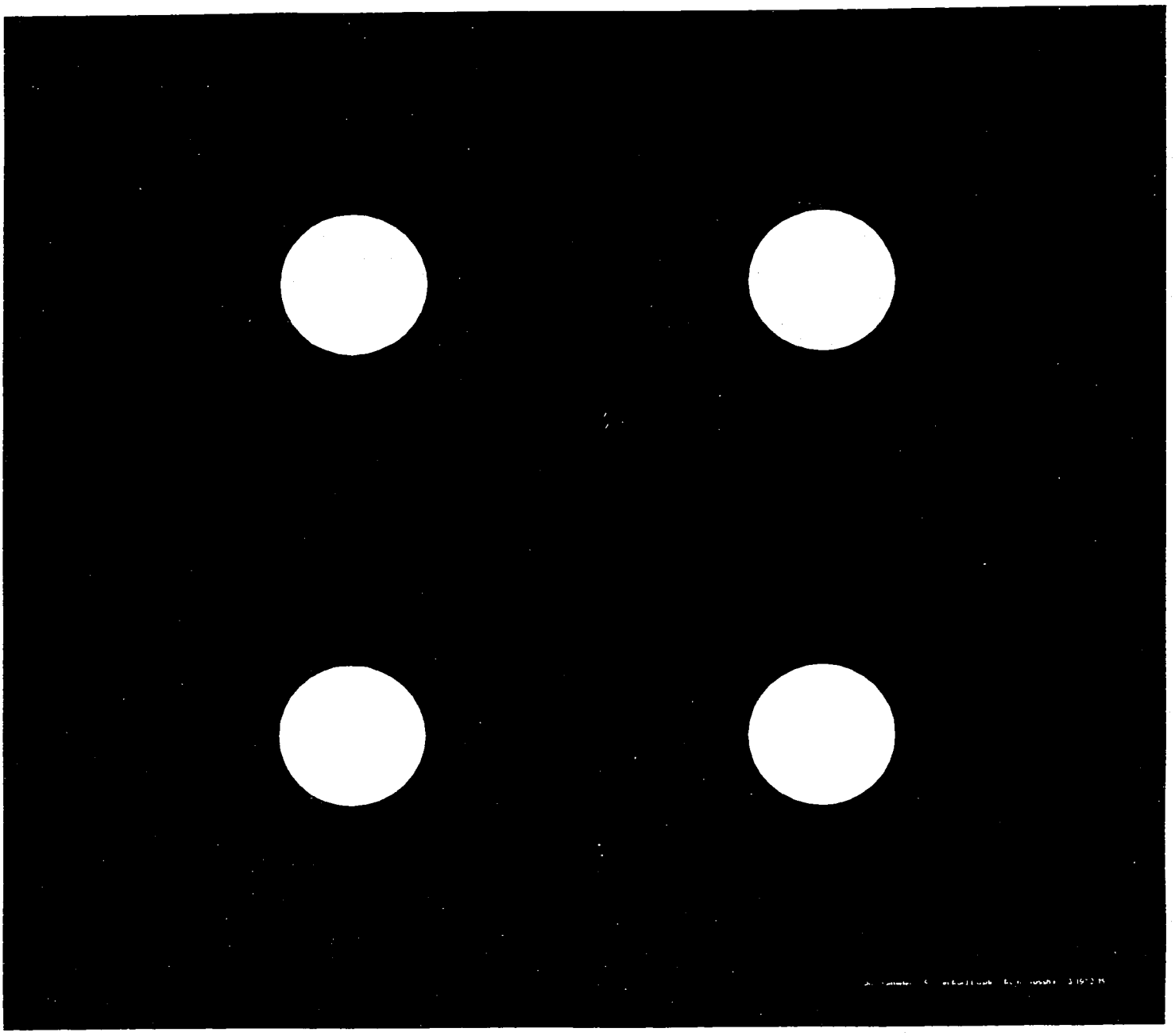

Figure D.7: Design of Visual Targets used in Tests (Reduced roughly 2:1)

APPENDIX E:
PARAMETERS FOR FLEXIBLE LINK SIMULATION

Table of Contents

E.1.1 Computation of Modal Parameters for Flexible Link without Payload

System parameters:

```
> MU:=.14;    L:=1.585;    RHO:=1.17;    KAPPA:=3.5;
```

$$\mu := .14$$

$$L := 1.585$$

$$\rho := 1.17$$

$$\kappa := 3.5$$

Definition of mode shape function phi(x) per Equation (3.4.33)

```
> PHI:=X ->A*(SIN(X*LAMBDA)+SIN(LAMBDA*L)/SINH(LAMBDA*L)*SINH(X*LAMBDA));
```

$$\phi := x \to a\left(\sin(x\,\lambda) + \frac{\sin(\lambda\,L)\,\sinh(x\,\lambda)}{\sinh(\lambda\,L)}\right)$$

Definition of mode shape function Y(x) without normalization factor, per Equation (3.4.33)

```
> Y:=X -> SIN(X*LAMBDA)+SIN(LAMBDA*L)/SINH(LAMBDA*L)*SINH(X*LAMBDA);
```

$$Y := x \to \sin(x\,\lambda) + \frac{\sin(\lambda\,L)\,\sinh(x\,\lambda)}{\sinh(\lambda\,L)}$$

Eigenvalue Problem per Equation (3.4.34)

```
> LAMBDA:='LAMBDA';
> COSH(LAMBDA*L)*SIN(LAMBDA*L)-COS(LAMBDA*L)*SINH(LAMBDA*L)+2*LAMBDA*MU/RHO*SIN(L
> AMBDA*L)*SINH(LAMBDA*L)=0;
```

$$\lambda := \lambda$$

$$\cosh(1.585\,\lambda)\sin(1.585\,\lambda) - \cos(1.585\,\lambda)\sinh(1.585\,\lambda) + .2393162394\,\lambda\sin(1.585\,\lambda)\sinh(1.585\,\lambda) = 0$$

Numerical solution of eigenvalue problem for the first 4 flexible modes

```
> LAMBDA:=FSOLVE(",LAMBDA=2..3);
```

$$\lambda := 2.341441385$$

$$\lambda := 4.254403148$$

$$\lambda := 6.187973946$$

$$\lambda := 8.134719526$$

Computation of modal frequencies per Equation (3.4.28), and their squared values for matrix (3.4.42)

```
> OMEGA:=EVALF(LAMBDA^2*SQRT(KAPPA/RHO));
```

$$\omega := 9.482168571$$

$$\omega := 31.30533634$$

$$\omega := 66.22745166$$

$$\omega := 114.4527570$$

```
> "^2;
```

89.91152081

980.0240834

4386.075353

13099.43358

Computation of normalization factor a per Equation (3.4.39), based on function Y(x)

```
> A:=SQRT(1/(MU*(Y(L)^2)+EVALF(INT (RHO*Y(X)^2, X=0..L))));
```

$$a := 1.016764355$$

$$a := 1.023384698$$

$$a := 1.027714851$$

$$a := 1.030499335$$

Check of modal frequency based on orthogonality condition (3.4.37)

```
> EVALF(SQRT(INT(KAPPA*DIFF(DIFF(PHI(X),X),X)^2, X=0..L)));
```

9.482168568

31.30533632

66.22745166

114.4527569

Computation of output matrix coefficients for tip sensors at by evaluation of mode shape function and its derivative at x= L per Equation (3.4.44)

```
> PHI(L);
```

-1.096658564

.9087395126

-.7684303737

```
                                    .6623118346
> D(PHI)(L);
                                   -3.290249406
                                    5.834308034
                                   -8.275845763
                                    10.63204910
```

Computation of input and output matrix coefficients for joint sensors and actuators by evaluation of the derivative of the mode shape function at x= 0 per Equations (3.4.43) and (3.4.44)

```
> D(PHI)(0);
                                    2.317878556
                                    4.358448631
                                    6.359211133
                                    8.382836608
```

Normalization factor a1 for the rigid-body mode per Equation (3.4.40) and derivative d1 per Equation (3.4.35)

```
> A1:=1/SQRT(RHO*L/3+MU);
                                    a1 := 1.148477339
> D1:=A1/L;
                                    d1 := .7245913811
```

Plot the rigid-body mode for 0<x<L

```
> PLOT(A1*X/L,X=0..L,TITLE='RIGID-BODY MODE SHAPE');PLOT(A1/L,X=0..L,
> TITLE='DERIVATIVE OF RIGID-BODY MODE SHAPE');
```

Plot the flexible mode shape function and its derivative for the first 4 flexible modes for 0<x<L

```
> PLOT(PHI(X),X=0..L,TITLE='MODE SHAPE');PLOT(DIFF(PHI(X),X),X=0..L, TITLE='DERIVATIVE
> OF MODE SHAPE');

>
```

Rigid-Body Mode Shape

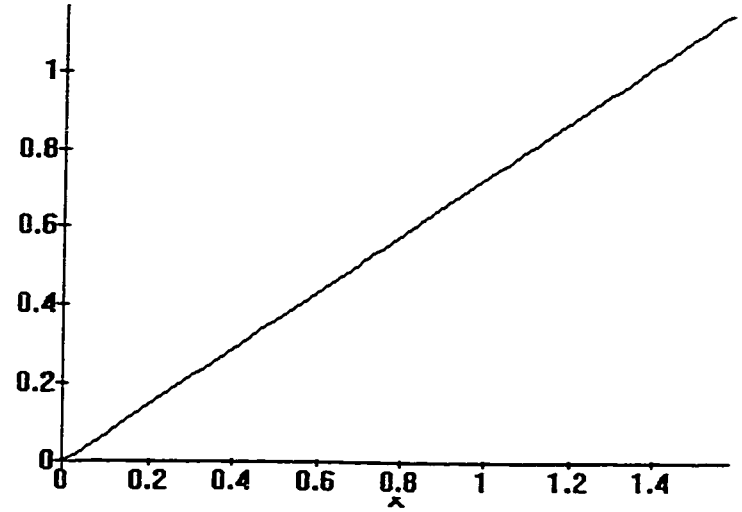

Derivative of Rigid-Body Mode Shape

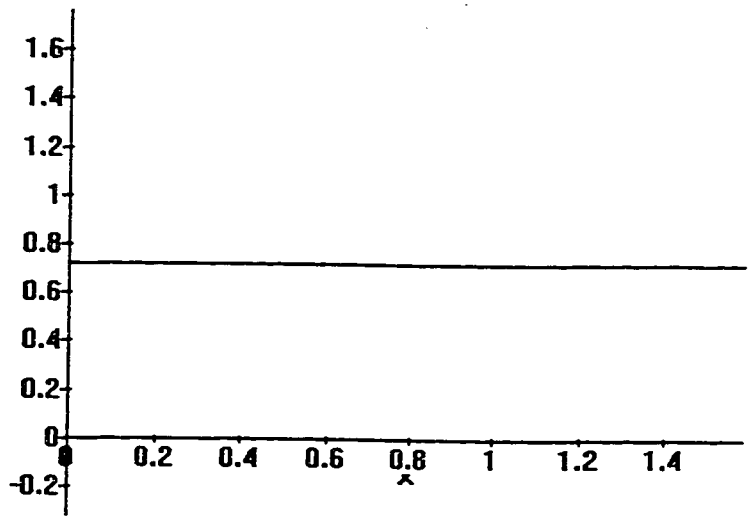

Mode Shape

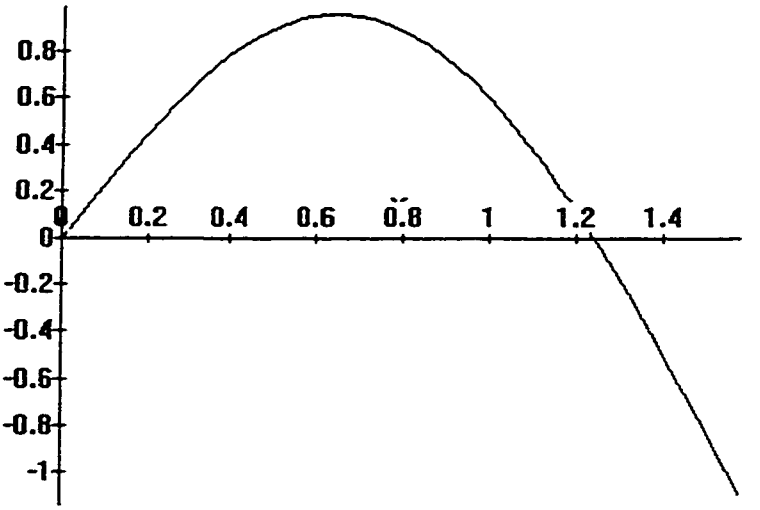

Derivative of Mode Shape

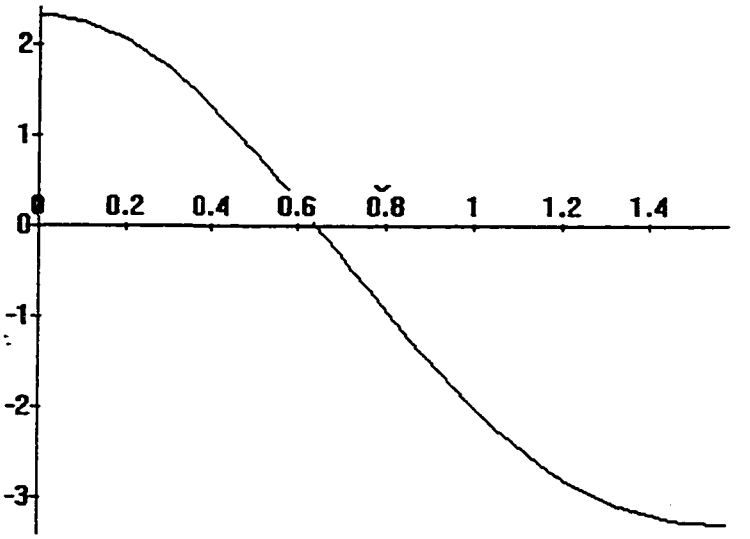

Mode Shape

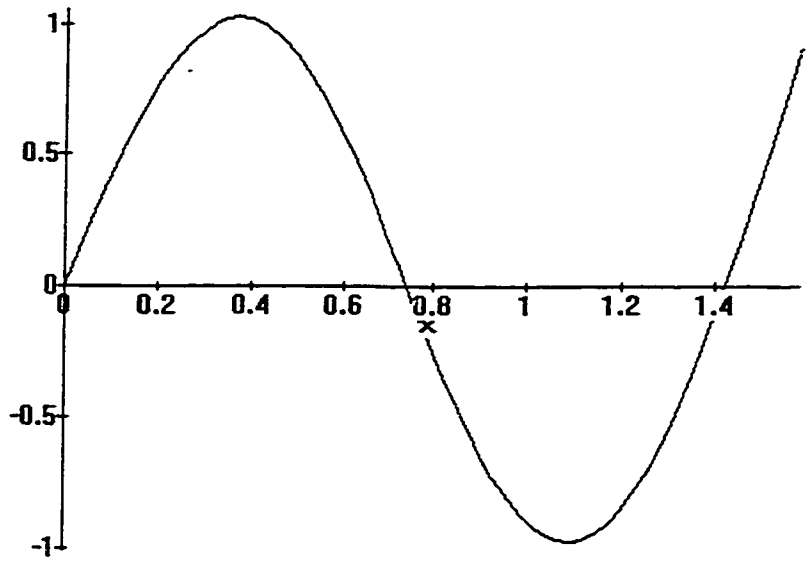

Derivative of Mode Shape

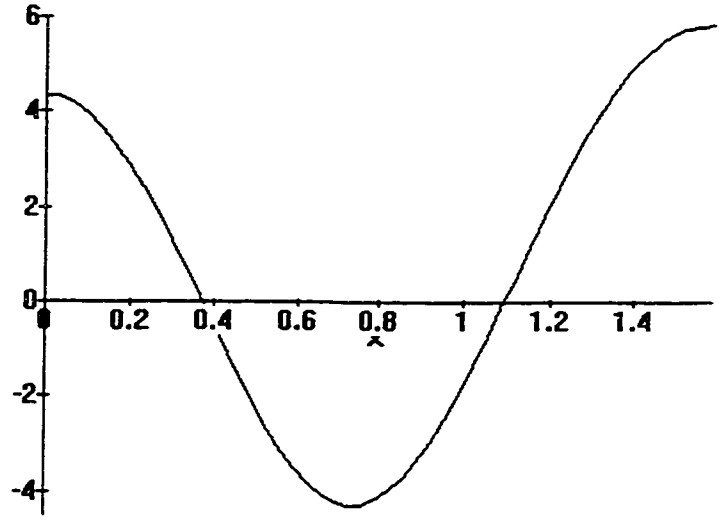

Mode Shape

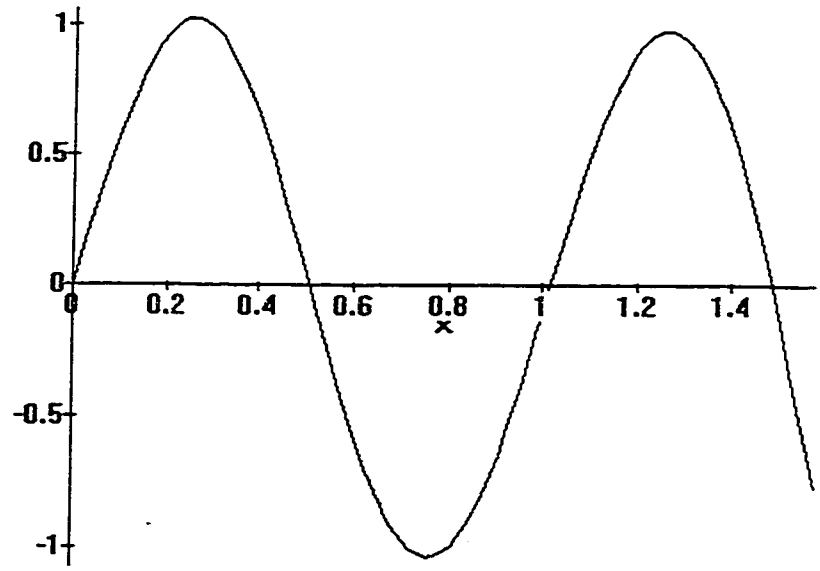

Derivative of Mode Shape

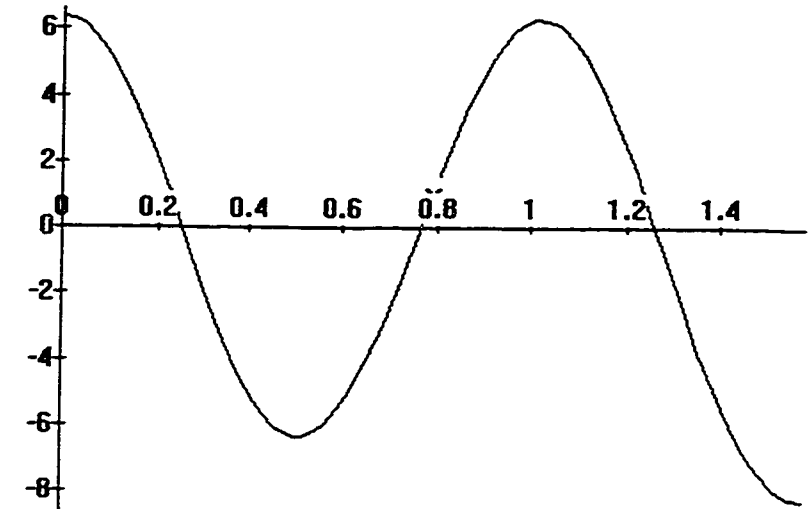

Mode Shape

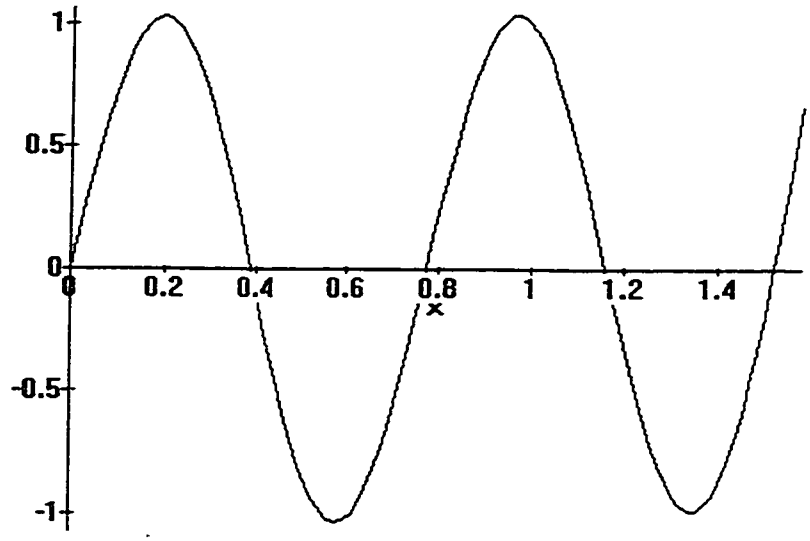

Derivative of Mode Shape

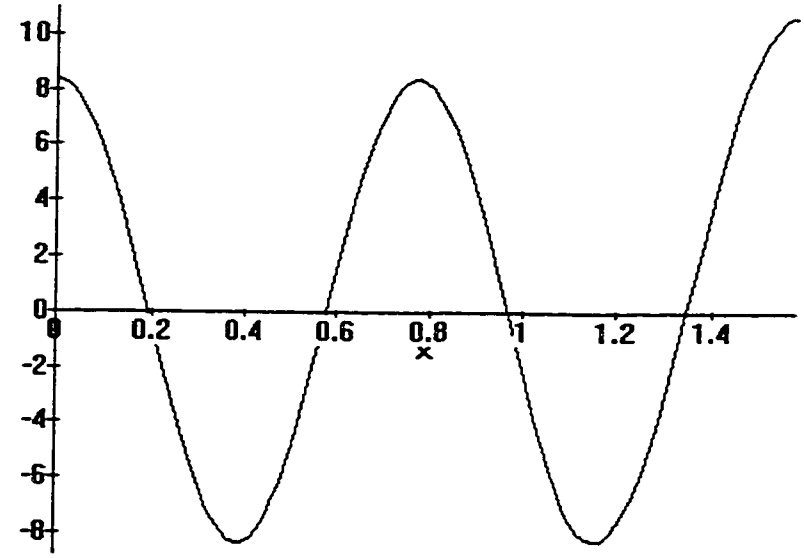

E.1.2 Computation of Modal Parameters for Flexible Link with 1.2 kg Payload

System parameters:

```
> MU:=1.2;    L:=1.585;    RHO:=1.17;    KAPPA:=3.5;
```

$$\mu := 1.2$$

$$L := 1.585$$

$$\rho := 1.17$$

$$\kappa := 3.5$$

Definition of mode shape function phi(x) per Equation (3.4.33)

```
> PHI:=X ->A*(SIN(X*LAMBDA)+SIN(LAMBDA*L)/SINH(LAMBDA*L)*SINH(X*LAMBDA));
```

$$\phi := x \to a\left(\sin(x\,\lambda) + \frac{\sin(\lambda\,L)\,\sinh(x\,\lambda)}{\sinh(\lambda\,L)}\right)$$

Definition of mode shape function Y(x) without normalization factor, per Equation (3.4.33)

```
> Y:=X -> SIN(X*LAMBDA)+SIN(LAMBDA*L)/SINH(LAMBDA*L)*SINH(X*LAMBDA);
```

$$Y := x \to \sin(x\,\lambda) + \frac{\sin(\lambda\,L)\,\sinh(x\,\lambda)}{\sinh(\lambda\,L)}$$

Eigenvalue Problem per Equation (3.4.34)

```
> LAMBDA:='LAMBDA';
> COSH(LAMBDA*L)*SIN(LAMBDA*L)-COS(LAMBDA*L)*SINH(LAMBDA*L)+2*LAMBDA*MU/RHO*SIN(L
> AMBDA*L)*SINH(LAMBDA*L)=0;
```

$$\lambda := \lambda$$

$$\cosh(1.585\,\lambda)\sin(1.585\,\lambda) - \cos(1.585\,\lambda)\sinh(1.585\,\lambda) + 2.051282052\,\lambda\sin(1.585\,\lambda)\sinh(1.585\,\lambda) = 0$$

Numerical solution of eigenvalue problem for the first 4 flexible modes

```
> LAMBDA:=FSOLVE(',LAMBDA=2..3);
```

$$\lambda := 2.099533121$$

$$\lambda := 4.031947601$$

$$\lambda := 5.993599558$$

$$\lambda := 7.964658899$$

Computation of modal frequencies per Equation (3.4.28), and their squared values for matrix (3.4.42)

```
> OMEGA:=EVALF(LAMBDA^2*SQRT(KAPPA/RHO));
```

$$\omega := 7.624064323$$

$$\omega := 28.11712102$$

$$\omega := 62.13217240$$

$$\omega := 109.7173864$$

```
> " ^2;
```

58.12635680

790.5724945

3860.406847

12037.90488

Computation of normalization factor a per Equation (3.4.39), based on function Y(x)

```
> A:=SQRT(1/(MU*(Y(L)^2)+EVALF(INT (RHO*Y(x)^2, x=0..L))));
```

$$a := 1.016303865$$

$$a := 1.030858450$$

$$a := 1.034742027$$

$$a := 1.036281223$$

Check of modal frequency based on orthogonality condition (3.4.37)

```
> EVALF(SQRT(INT(KAPPA*DIFF(DIFF(PHI(x),x),x)^2, x=0..L)));
```

7.624064325

28.11712103

62.13217244

109.7173864

Computation of output matrix coefficients for tip sensors at by evaluation of mode shape function and its derivative at x= L per Equation (3.4.44)

```
> PHI(L);
```

-.3762231539

.2211088083

-.1552254342

```
                                    .1193420165
> D(PHI)(L);
                                   -2.492858317
                                    4.578147997
                                   -6.649538480
                                    8.715191173
```

Computation of input and output matrix coefficients for joint sensors and actuators by evaluation of the derivative of the mode shape function at x= 0 per Equations (3.4.43) and (3.4.44)

```
> D(PHI)(0);
                                    2.105390989
                                    4.157862470
                                    6.201759706
                                    8.253629594
```

Normalization factor a1 for the rigid-body mode per Equation (3.4.40) and derivative d1 per Equation (3.4.35)

```
> A1:=1/SQRT(RHO*L/3+MU);
                                    a1 := .7416263382
> D1:=A1/L;
                                    d1 := .4679030525
```

Plot the rigid-body mode for 0<x<L

```
> PLOT(A1*X/L,X=0..L,TITLE='RIGID-BODY MODE SHAPE');PLOT(A1/L,X=0..L,
> TITLE='DERIVATIVE OF RIGID-BODY MODE SHAPE');
```

Plot the flexible mode shape function and its derivative for the first 4 flexible modes for 0<x<L

```
> PLOT(PHI(X),X=0..L,TITLE='MODE SHAPE');PLOT(DIFF(PHI(X),X),X=0..L, TITLE='DERIVATIVE
> OF MODE SHAPE');
```

```
>
```

Diagram of Rigid-Body Mode

>

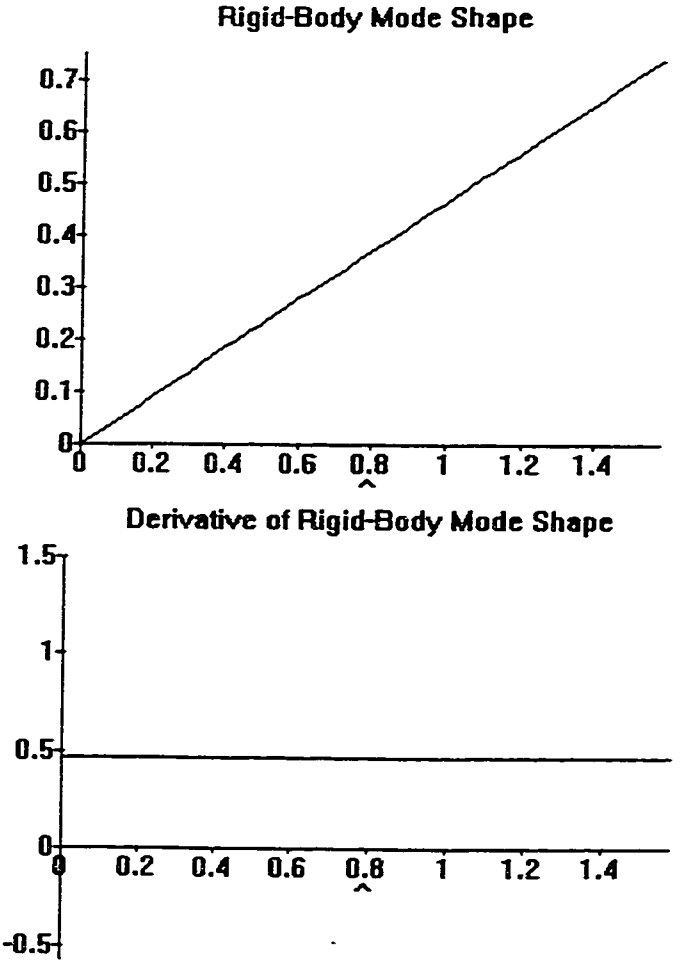

>

Diagram of 1st Flexible Mode

>

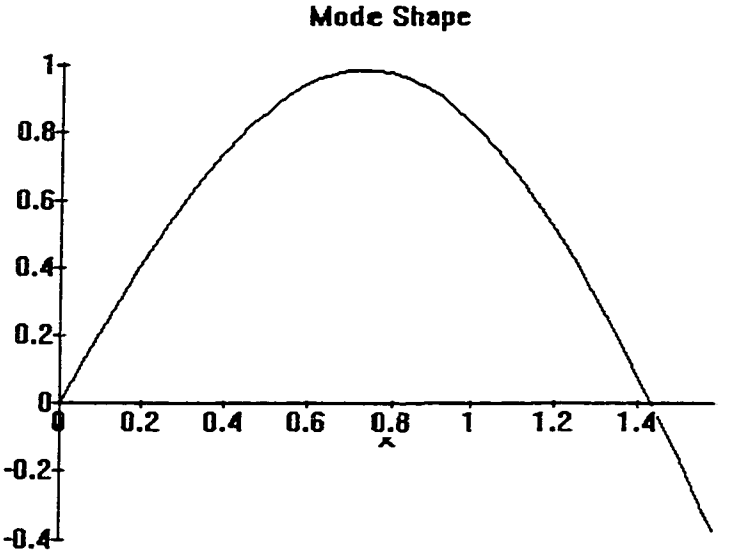

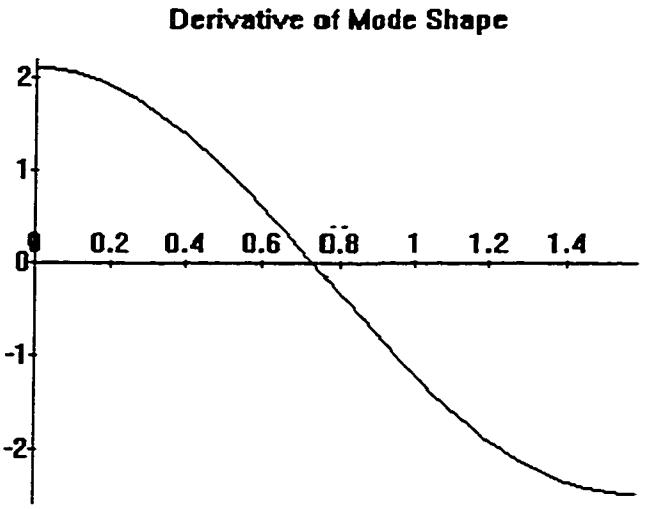

>

Diagram of 2nd Flexible Mode

>

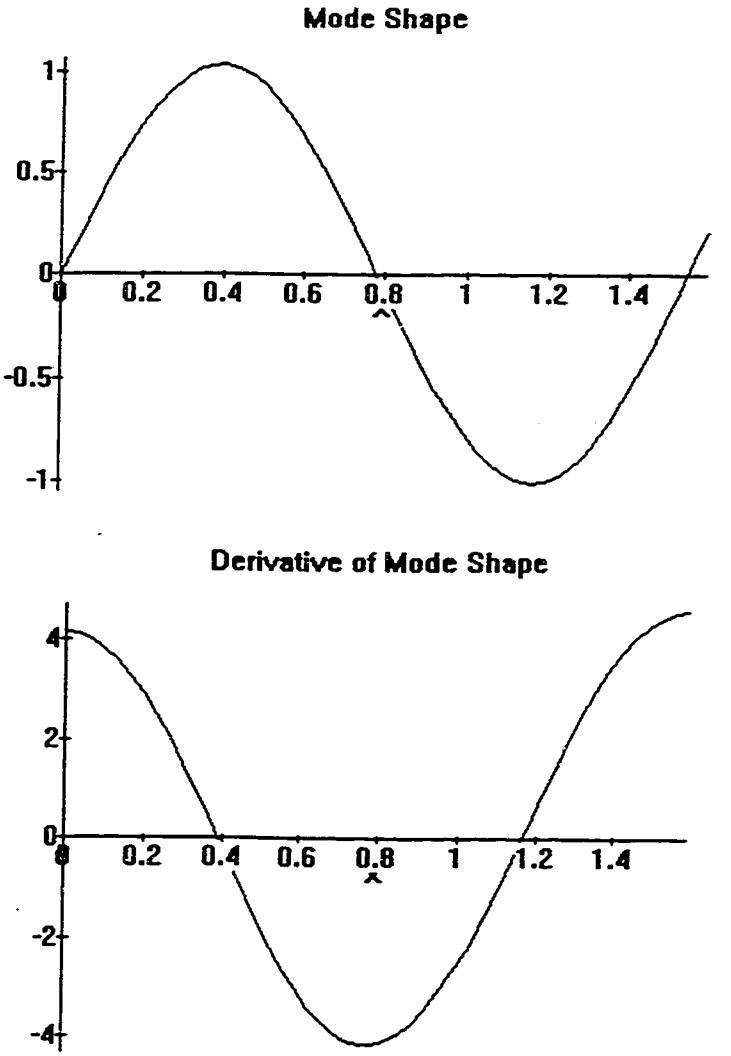

>

Diagram of 3rd Flexible Mode

>

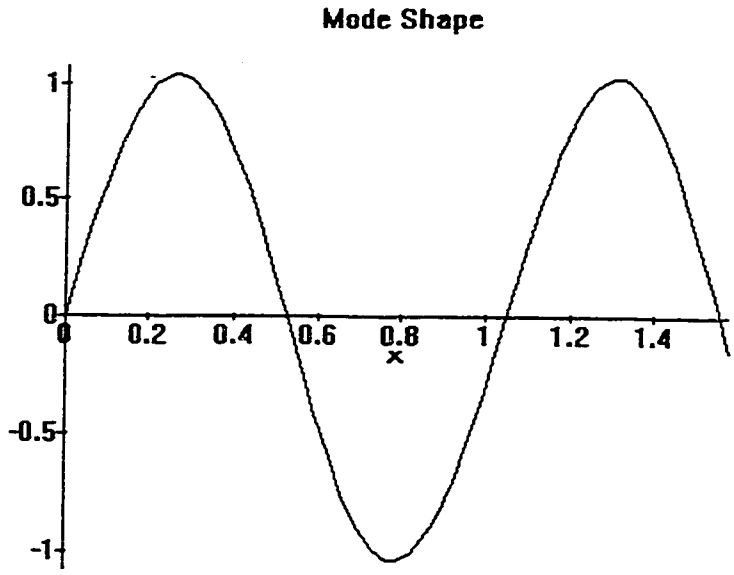

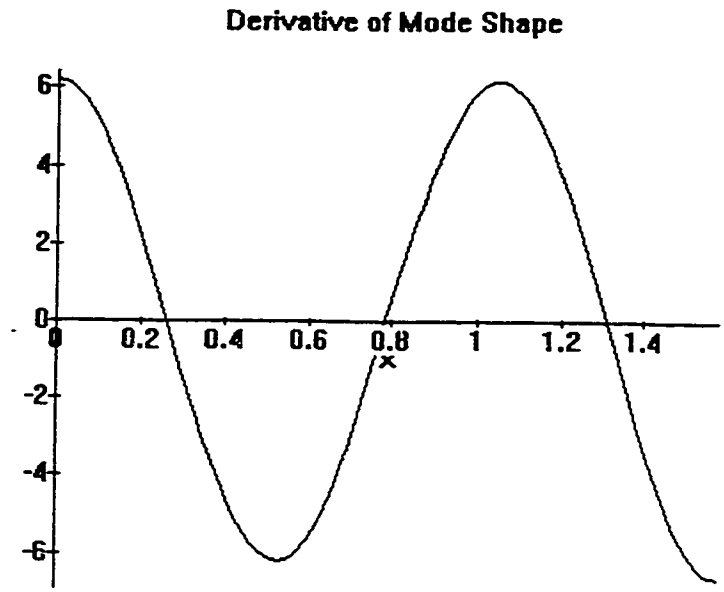

>

Diagram of 4th Flexible Mode

>

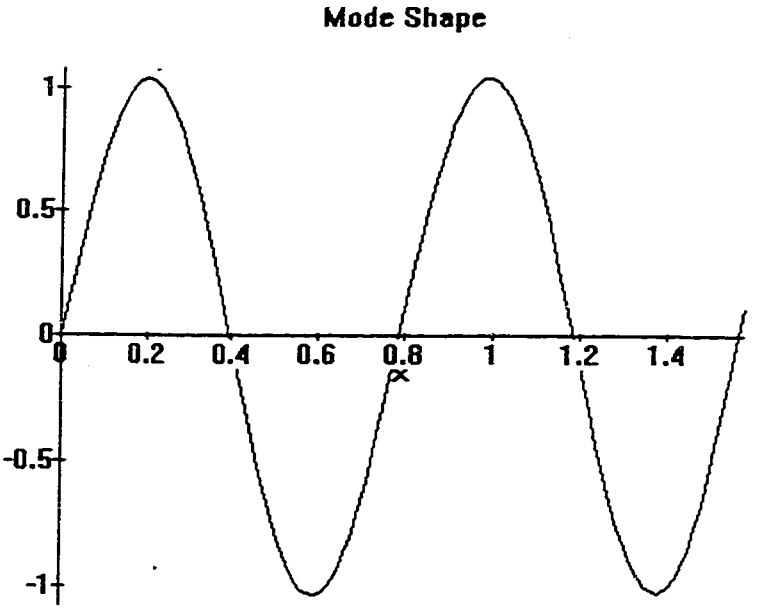

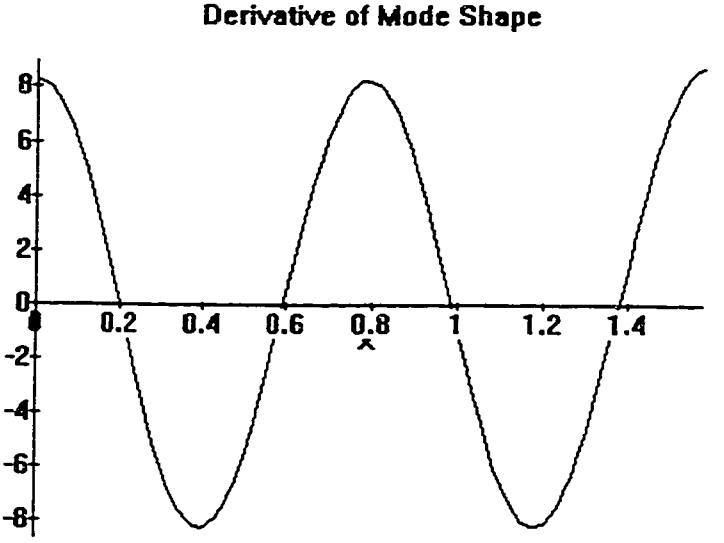

E.1.3 Computation of Modal Parameters for Flexible Link with 12 kg Payload

System parameters:

```
> MU:=12;     L:=1.585;     RHO:=1.17;     KAPPA:=3.5;
```

$$\mu := 12$$

$$L := 1.585$$

$$\rho := 1.17$$

$$\kappa := 3.5$$

Definition of mode shape function phi(x) per Equation (3.4.33)

```
> PHI:=X ->A*(SIN(X*LAMBDA)+SIN(LAMBDA*L)/SINH(LAMBDA*L)*SINH(X*LAMBDA));
```

$$\phi := x \rightarrow a\left(\sin(x\,\lambda) + \frac{\sin(\lambda\,L)\,\sinh(x\,\lambda)}{\sinh(\lambda\,L)}\right)$$

Definition of mode shape function Y(x) without normalization factor, per Equation (3.4.33)

```
> Y:=X -> SIN(X*LAMBDA)+SIN(LAMBDA*L)/SINH(LAMBDA*L)*SINH(X*LAMBDA);
```

$$Y := x \rightarrow \sin(x\,\lambda) + \frac{\sin(\lambda\,L)\,\sinh(x\,\lambda)}{\sinh(\lambda\,L)}$$

Eigenvalue Problem per Equation (3.4.34)

```
> LAMBDA:='LAMBDA';
> COSH(LAMBDA*L)*SIN(LAMBDA*L)-COS(LAMBDA*L)*SINH(LAMBDA*L)+2*LAMBDA*MU/RHO*SIN(L
> AMBDA*L)*SINH(LAMBDA*L)=0;
```

$$\lambda := \lambda$$

$$\cosh(1.585\,\lambda)\sin(1.585\,\lambda) - \cos(1.585\,\lambda)\sinh(1.585\,\lambda) + 20.51282052\,\lambda\sin(1.585\,\lambda)\sinh(1.585\,\lambda) = 0$$

Numerical solution of eigenvalue problem for the first 4 flexible modes

```
> LAMBDA:=FSOLVE(',LAMBDA=1..3);
```

$$\lambda := 1.997107107$$

$$\lambda := 3.971804357$$

$$\lambda := 5.951358130$$

$$\lambda := 7.932163320$$

Computation of modal frequencies per Equation (3.4.28), and their squared values for matrix (3.4.42)

```
> OMEGA:=EVALF(LAMBDA^2*SQRT(KAPPA/RHO));
```

$$\omega := 6.898327451$$

$$\omega := 27.28454948$$

$$\omega := 61.25947377$$

$$\omega := 108.8239252$$

```
> "^2;
```

47.58692162

744.4466403

3752.723127

11842.64670

Computation of normalization factor a per Equation (3.4.39), based on function Y(x)

```
> A:=SQRT(1/(MU*(Y(L)^2)+EVALF(INT (RHO*Y(X)^2, X=0..L))));
```

$$a := 1.034712315$$

$$a := 1.037515798$$

$$a := 1.038058930$$

$$a := 1.038251595$$

Check of modal frequency based on orthogonality condition (3.4.37)

```
> EVALF(SQRT(INT(KAPPA*DIFF(DIFF(PHI(X),X),X)^2, X=0..L)));
```

6.898327449

27.28454948

61.25947373

108.8239253

Computation of output matrix coefficients for tip sensors at by evaluation of mode shape function and its derivative at x= L per Equation (3.4.44)

```
> PHI(L);
```

-.04929340151

.02515830923

-.01686759778

```
                                    .01268371269
> D(PHI)(L);
                                    -2.115242703
                                    4.170469160
                                    -6.227849110
                                    8.285732222
```

Computation of input and output matrix coefficients for joint sensors and actuators by evaluation of the derivative of the mode shape function at x= 0 per Equations (3.4.43) and (3.4.44)

```
> D(PHI)(0);
                                    2.062269894
                                    4.120994121
                                    6.177852417
                                    8.235581568
```

Normalization factor a1 for the rigid-body mode per Equation (3.4.40) and derivative d1 per Equation (3.4.35)

```
> A1:=1/SQRT(RHO*L/3+MU);
                                    a1 := .2815153998
> D1:=A1/L;
                                    d1 := .1776122396
```

Plot the rigid-body mode for 0<x<L

```
> PLOT(A1*X/L,X=0..L,TITLE='RIGID-BODY MODE SHAPE');PLOT(A1/L,X=0..L,
> TITLE='DERIVATIVE OF RIGID-BODY MODE SHAPE');
```

Plot the flexible mode shape function and its derivative for the first 4 flexible modes for 0<x<L

```
> PLOT(PHI(X),X=0..L,TITLE='MODE SHAPE');PLOT(DIFF(PHI(X),X),X=0..L, TITLE='DERIVATIVE
> OF MODE SHAPE');
```

>

Diagram of Rigid-Body Mode

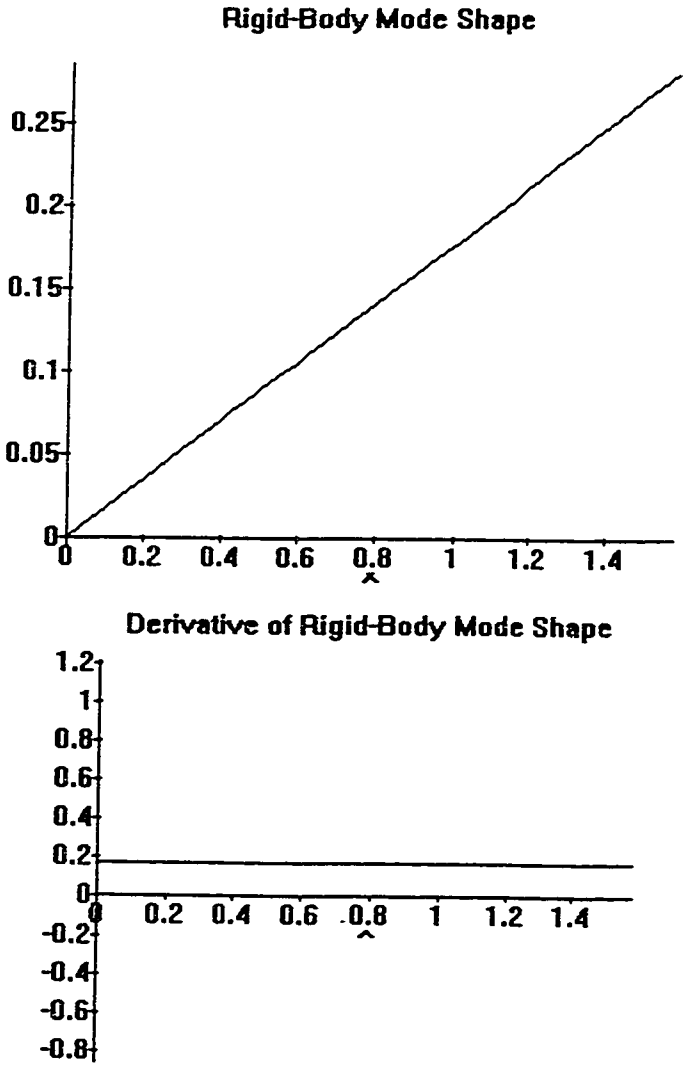

Diagram of 1st Flexible Mode

>

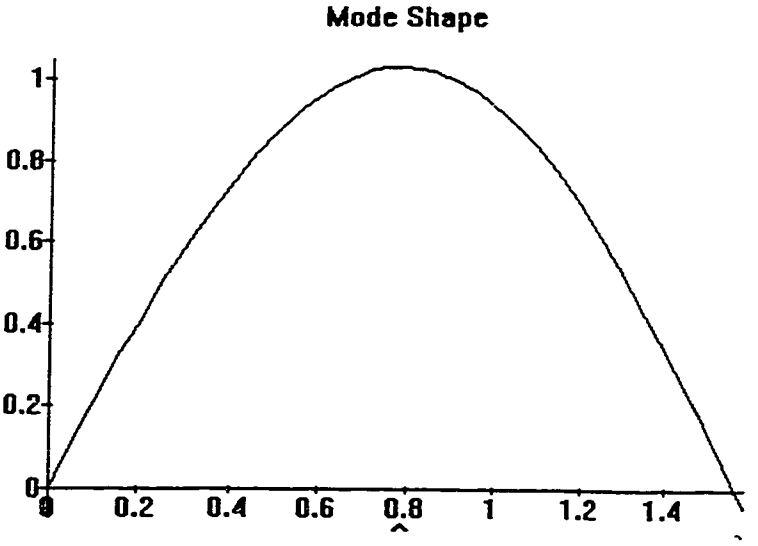

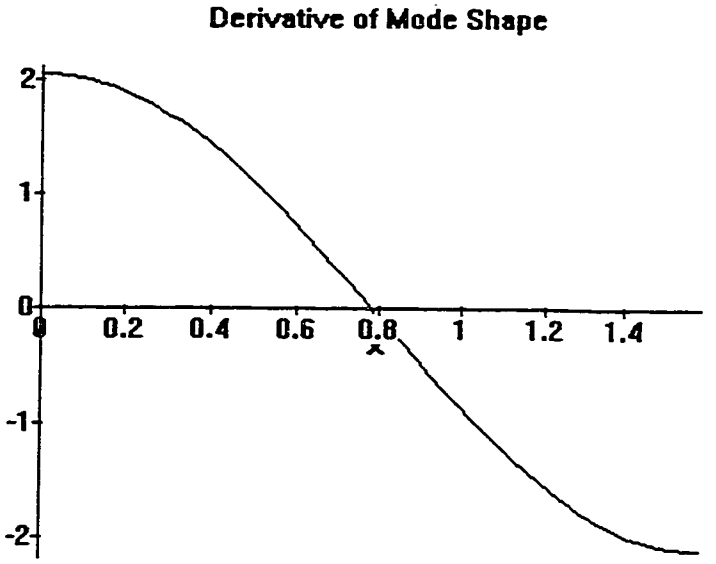

>

Diagram of 2nd Flexible Mode

>

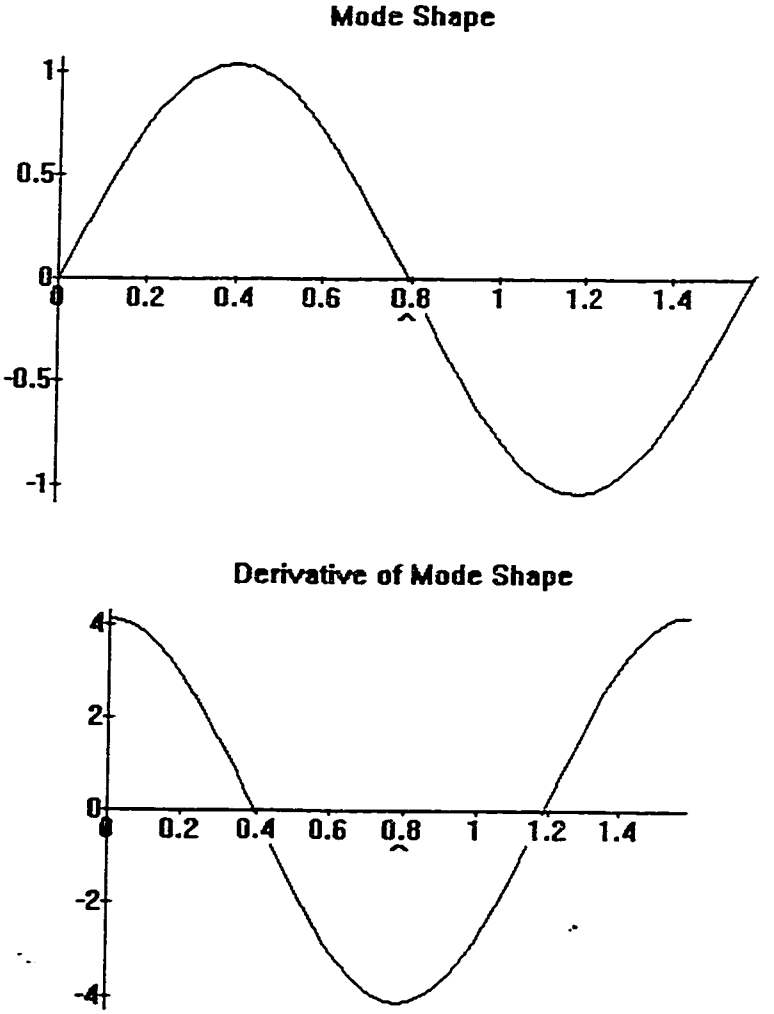

>

Diagram of 3rd Flexible Mode

>

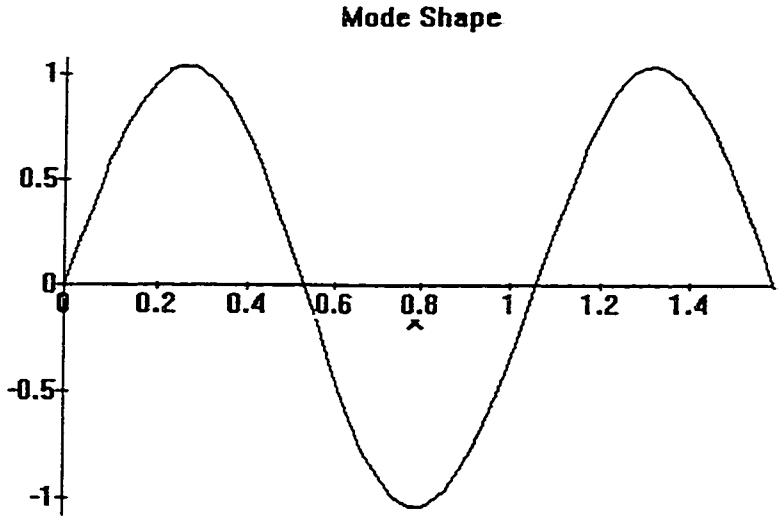

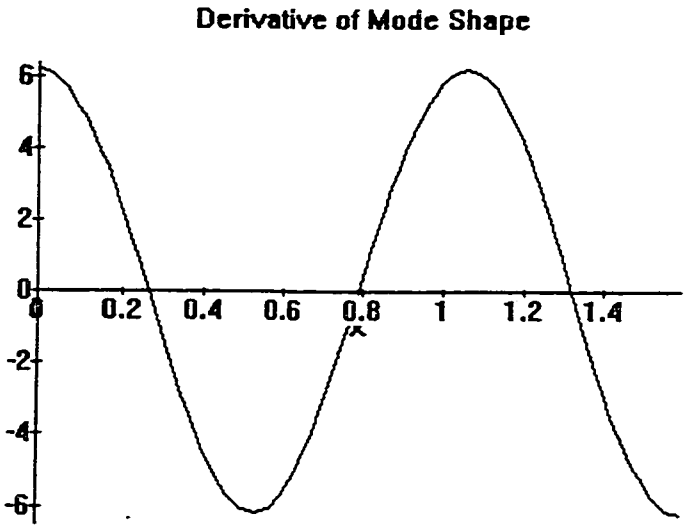

>

Diagram of 4th Flexible Mode

>

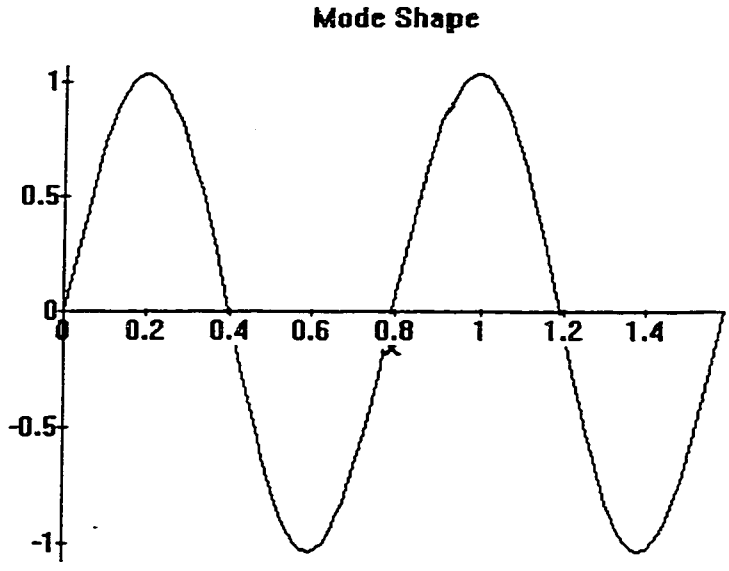

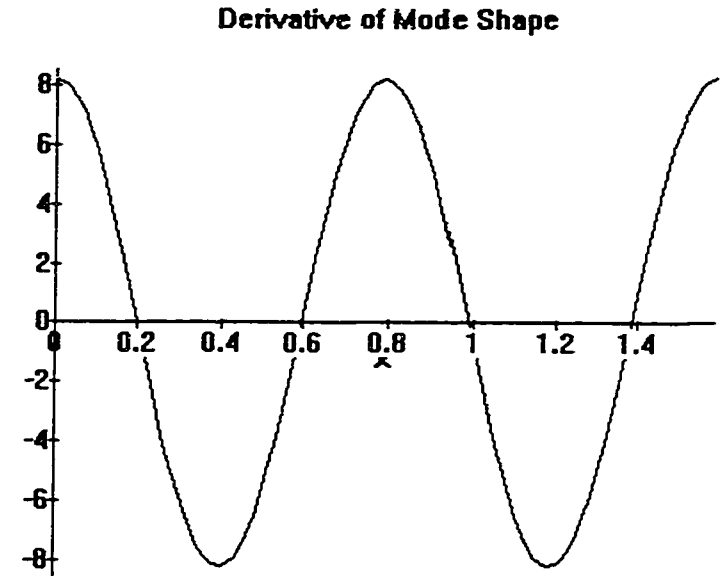

E.1.4 Computation of Modal Parameters for Flexible Link with 120 kg Payload

System parameters:

```
> MU:=120;     L:=1.585;     RHO:=1.17;     KAPPA:=3.5;
```

$$\mu := 120$$

$$L := 1.585$$

$$\rho := 1.17$$

$$\kappa := 3.5$$

Definition of mode shape function phi(x) per Equation (3.4.33)

```
> PHI:=X ->A*(SIN(X*LAMBDA)+SIN(LAMBDA*L)/SINH(LAMBDA*L)*SINH(X*LAMBDA));
```

$$\phi := x \rightarrow a\left(\sin(x\,\lambda) + \frac{\sin(\lambda\,L)\,\sinh(x\,\lambda)}{\sinh(\lambda\,L)}\right)$$

Definition of mode shape function Y(x) without normalization factor, per Equation (3.4.33)

```
> Y:=X -> SIN(X*LAMBDA)+SIN(LAMBDA*L)/SINH(LAMBDA*L)*SINH(X*LAMBDA);
```

$$Y := x \rightarrow \sin(x\,\lambda) + \frac{\sin(\lambda\,L)\,\sinh(x\,\lambda)}{\sinh(\lambda\,L)}$$

Eigenvalue Problem per Equation (3.4.34)

```
> LAMBDA:='LAMBDA';
> COSH(LAMBDA*L)*SIN(LAMBDA*L)-COS(LAMBDA*L)*SINH(LAMBDA*L)+2*LAMBDA*MU/RHO*SIN(L
> AMBDA*L)*SINH(LAMBDA*L)=0;
```

$$\lambda := \lambda$$

$$\cosh(1.585\,\lambda)\sin(1.585\,\lambda) - \cos(1.585\,\lambda)\sinh(1.585\,\lambda) + 205.1282052\,\lambda\sin(1.585\,\lambda)\sinh(1.585\,\lambda) = 0$$

Numerical solution of eigenvalue problem for the first 4 flexible modes

```
> LAMBDA:=FSOLVE(',LAMBDA=1..3);
```

$$\lambda := 1.983624116$$

$$\lambda := 3.964929544$$

$$\lambda := 5.946748937$$

$$\lambda := 7.928697219$$

Computation of modal frequencies per Equation (3.4.28), and their squared values for matrix (3.4.42)

```
> OMEGA:=EVALF(LAMBDA^2*SQRT(KAPPA/RHO));
```

$$\omega := 6.805497058$$

$$\omega := 27.19017734$$

$$\omega := 61.16462234$$

$$\omega := 108.7288408$$

```
> " ^2;
```

$$46.31479021$$

$$739.3057438$$

$$3741.111026$$

$$11821.96082$$

Computation of normalization factor a per Equation (3.4.39), based on function Y(x)

```
> A:=SQRT(1/(MU*(Y(L)^2)+EVALF(INT (RHO*Y(x)^2, x=0..L))));
```

$$a := 1.038098601$$

$$a := 1.038400905$$

$$a := 1.038457146$$

$$a := 1.038476858$$

Check of modal frequency based on orthogonality condition (3.4.37)

```
> EVALF(SQRT(INT(KAPPA*DIFF(DIFF(PHI(x),x),x)^2, x=0..L)));
```

$$6.805497059$$

$$27.19017734$$

$$61.16462231$$

$$108.7288408$$

Computation of output matrix coefficients for tip sensors at by evaluation of mode shape function and its derivative at x= L per Equation (3.4.44)

```
> PHI(L);
```

$$-.005089938527$$

$$.002550353145$$

$$-.001701209093$$

.001276237385

```
> D(PHI)(L);
```

-2.064258292

4.122239343

-6.180500189

8.238826471

Computation of input and output matrix coefficients for joint sensors and actuators by evaluation of the derivative of the mode shape function at x= 0 per Equations (3.4.43) and (3.4.44)

```
> D(PHI)(0);
```

2.058761367

4.117205287

6.175443113

8.233768611

Normalization factor a1 for the rigid-body mode per Equation (3.4.40) and derivative d1 per Equation (3.4.35)

```
> A1:=1/SQRT(RHO*L/3+MU);
```

$$a1 := .09105287607$$

```
> D1:=A1/L;
```

$$d1 := .05744660951$$

Plot the rigid-body mode for 0<x<L

```
> PLOT(A1*X/L,X=0..L,TITLE='RIGID-BODY MODE SHAPE');PLOT(A1/L,X=0..L,
> TITLE='DERIVATIVE OF RIGID-BODY MODE SHAPE');
```

Plot the flexible mode shape function and its derivative for the first 4 flexible modes for 0<x<L

```
> PLOT(PHI(X),X=0..L,TITLE='MODE SHAPE');PLOT(DIFF(PHI(X),X),X=0..L, TITLE='DERIVATIVE
> OF MODE SHAPE');
```

```
>
```

Diagram of Rigid-Body Mode

>

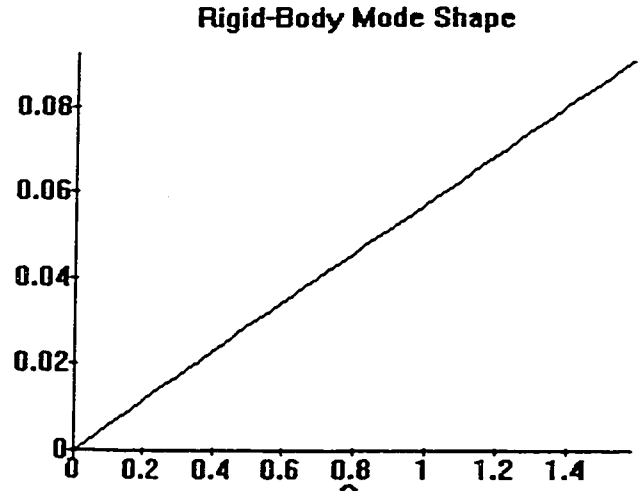

>

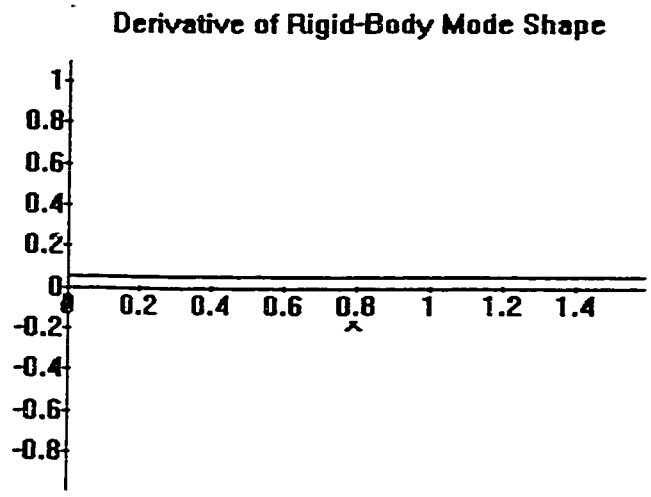

Diagram of 1st Flexible Mode

>

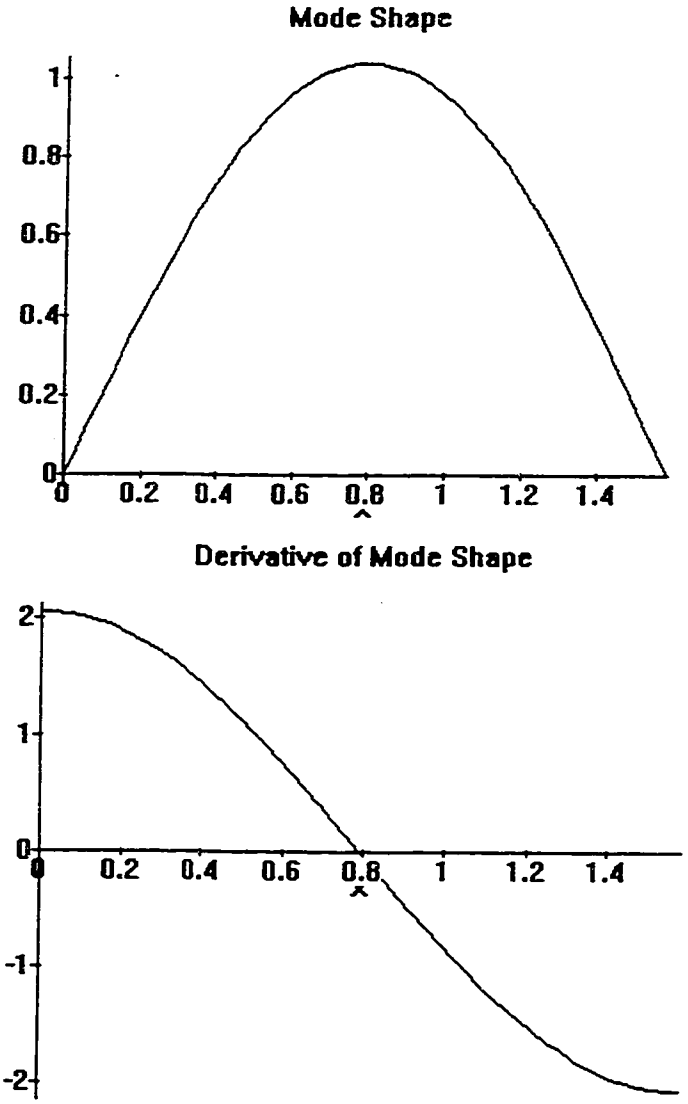

>

Diagram of 2nd Flexible Mode

>

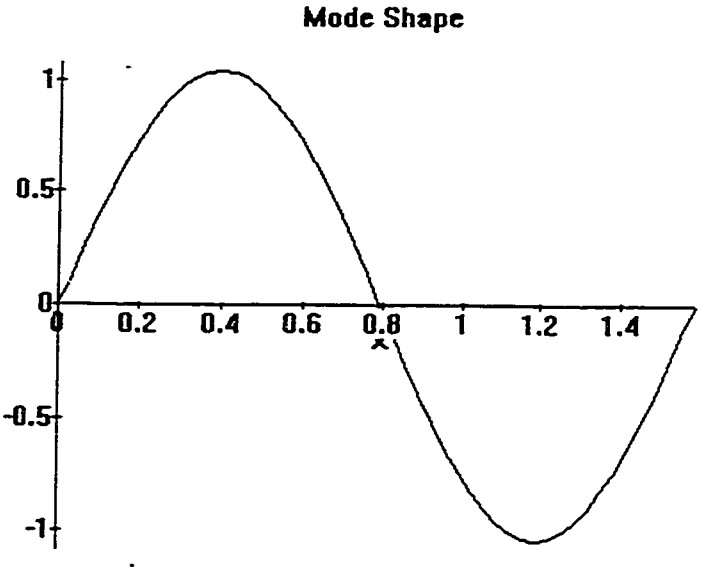

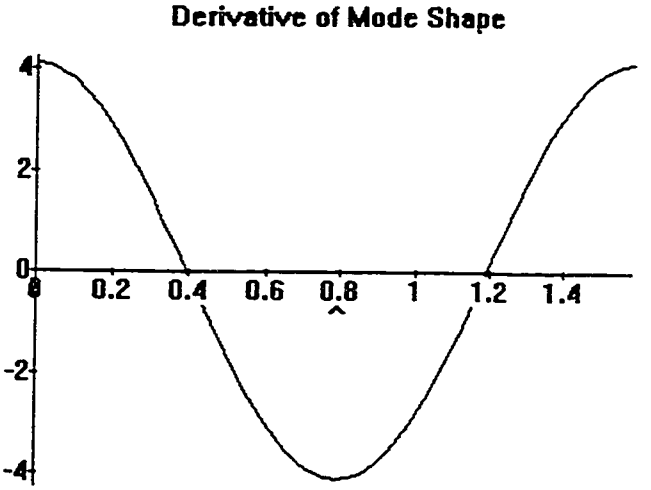

>

Diagram of 3rd Flexible Mode

>

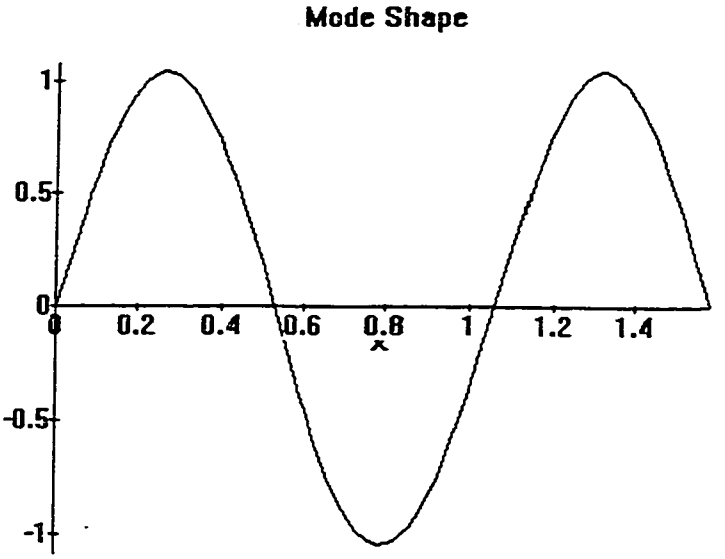

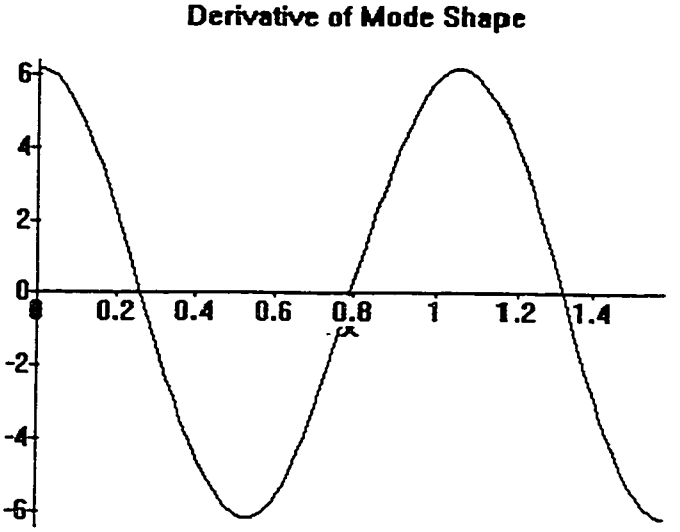

>

Diagram of 4th Flexible Mode

>

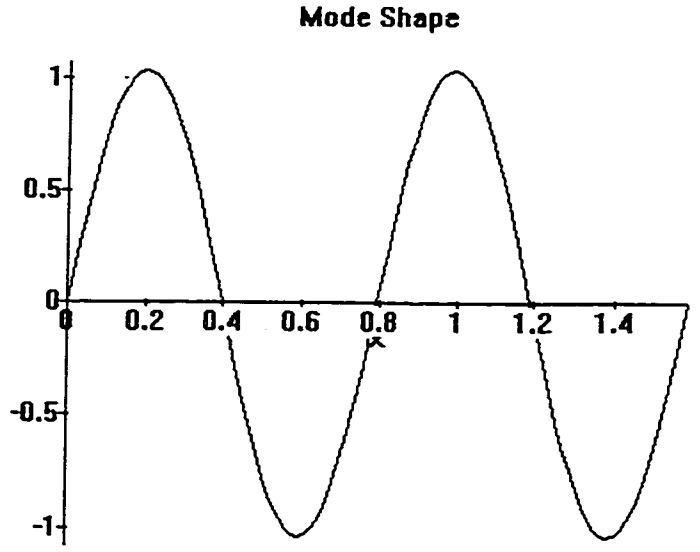

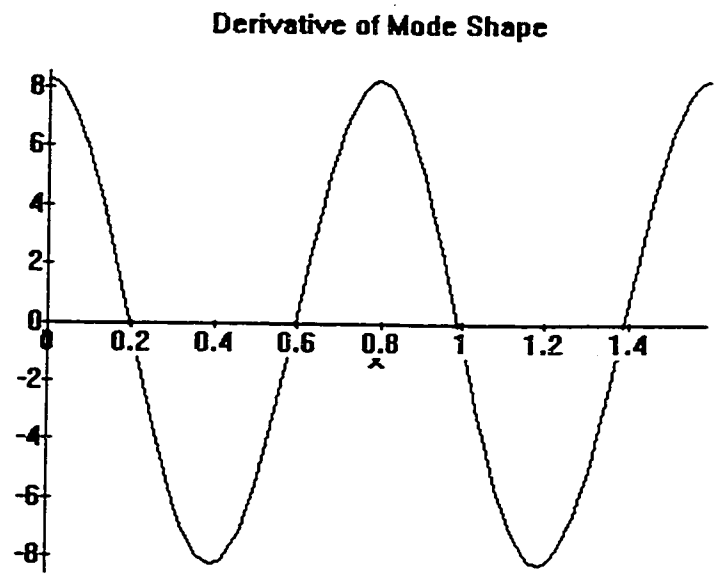

E.2 State-Space Matrices of Flexible Link

E.2.1 Model for Payload: 0.14 kg, 1 Flexible Mode

A linear state-space model of the flexible link per (3.2.18) with state vector $\mathbf{x} = [\mathbf{q} \quad \dot{\mathbf{q}}]^T$ can be expressed as follows:

$$\dot{\mathbf{x}} = \mathbf{A}\mathbf{x} + \mathbf{B}\mathbf{u}$$

$$\mathbf{y} = \mathbf{C}\mathbf{x}$$

For a payload mass of $\mu = 0.14$ kg and one flexible mode included in the model, the state-space matrices have the following coefficients:

$$\mathbf{A} = \begin{bmatrix} 0 & 0 & 1 & 0 \\ 0 & 0 & 0 & 1 \\ 0 & 0 & 0 & 0 \\ 0 & -89.911 & 0 & 0 \end{bmatrix}$$

$$\mathbf{B} = \begin{bmatrix} 0 \\ 0 \\ 0.725 \\ 2.318 \end{bmatrix}$$

$$\mathbf{C} = \begin{bmatrix} 1.148 & -1.097 & 0 & 0 \\ 0 & 0 & 1.148 & -1.097 \\ 0.725 & 2.318 & 0 & 0 \\ 0 & 0 & 0.725 & 2.318 \end{bmatrix}$$

E.2.2 Model for Payload: 0.14 kg, 2 Flexible Modes

A linear state-space model of the flexible link per (3.2.18) with state vector $\mathbf{x} = [\mathbf{q} \quad \dot{\mathbf{q}}]^T$ can be expressed as follows:

$$\dot{\mathbf{x}} = \mathbf{A}\mathbf{x} + \mathbf{B}\mathbf{u}$$

$$\mathbf{y} = \mathbf{C}\mathbf{x}$$

For a payload mass of $\mu = 0.14$ kg and two flexible modes included in the model, the state-space matrices have the following coefficients:

$$\mathbf{A} = \begin{bmatrix} 0 & 0 & 0 & 1 & 0 & 0 \\ 0 & 0 & 0 & 0 & 1 & 0 \\ 0 & 0 & 0 & 0 & 0 & 1 \\ 0 & 0 & 0 & 0 & 0 & 0 \\ 0 & -89.911 & 0 & 0 & 0 & 0 \\ 0 & 0 & -980.02 & 0 & 0 & 0 \end{bmatrix}$$

$$\mathbf{B} = \begin{bmatrix} 0 \\ 0 \\ 0 \\ 0.725 \\ 2.318 \\ 4.358 \end{bmatrix}$$

$$\mathbf{C} = \begin{bmatrix} 1.148 & -1.097 & 0.909 & 0 & 0 & 0 \\ 0 & 0 & 0 & 1.148 & -1.097 & 0.909 \\ 0.725 & 2.318 & 4.358 & & 0 & 0 \\ 0 & 0 & 0 & 0.725 & 2.318 & 4.358 \end{bmatrix}$$

E.2.3 Model for Payload: 0.14 kg, 3 Flexible Modes

A linear state-space model of the flexible link per (3.2.18) with state vector $\mathbf{x} = [\mathbf{q} \quad \dot{\mathbf{q}}]^T$ can be expressed as follows:

$$\dot{\mathbf{x}} = \mathbf{A}\mathbf{x} + \mathbf{B}\mathbf{u}$$

$$\mathbf{y} = \mathbf{C}\mathbf{x}$$

For a payload mass of $\mu = 0.14$ kg and three flexible modes included in the model, the state-space matrices have the following coefficients:

$$\mathbf{A} = \begin{bmatrix} 0 & 0 & 0 & 1 & 0 & 0 & 0 \\ 0 & 0 & 0 & 0 & 1 & 0 & 0 \\ 0 & 0 & 0 & 0 & 0 & 1 & 0 \\ 0 & 0 & 0 & 0 & 0 & 0 & 1 \\ 0 & 0 & 0 & 0 & 0 & 0 & 0 \\ 0 & -89.911 & 0 & 0 & 0 & 0 & 0 \\ 0 & 0 & -980.02 & 0 & 0 & 0 & 0 \\ 0 & 0 & 0 & -4386.1 & 0 & 0 & 0 \end{bmatrix}$$

$$\mathbf{B} = \begin{bmatrix} 0 \\ 0 \\ 0 \\ 0 \\ 0.725 \\ 2.318 \\ 4.358 \\ 6.359 \end{bmatrix}$$

$$\mathbf{C} = \begin{bmatrix} 1.148 & -1.097 & 0.909 & -0.768 & 0 & 0 & 0 & 0 \\ 0 & 0 & 0 & 0 & 1.148 & -1.097 & 0.909 & -0.768 \\ 0.725 & 2.318 & 4.358 & 6.359 & & 0 & 0 & 0 \\ 0 & 0 & 0 & 0 & 0.725 & 2.318 & 4.358 & 6.359 \end{bmatrix}$$

E.2.4 Model for Payload: 1.2 kg, 2 Flexible Modes

A linear state-space model of the flexible link per (3.2.18) with state vector $\mathbf{x} = [\mathbf{q} \quad \dot{\mathbf{q}}]^T$ can be expressed as follows:

$$\dot{\mathbf{x}} = \mathbf{A}\mathbf{x} + \mathbf{B}\mathbf{u}$$

$$\mathbf{y} = \mathbf{C}\mathbf{x}$$

For a payload mass of $\mu = 1.2$ kg and two flexible modes included in the model, the state-space matrices have the following coefficients:

$$\mathbf{A} = \begin{bmatrix} 0 & 0 & 0 & 1 & 0 & 0 \\ 0 & 0 & 0 & 0 & 1 & 0 \\ 0 & 0 & 0 & 0 & 0 & 1 \\ 0 & 0 & 0 & 0 & 0 & 0 \\ 0 & -58.127 & 0 & 0 & 0 & 0 \\ 0 & 0 & -790.57 & 0 & 0 & 0 \end{bmatrix}$$

$$\mathbf{B} = \begin{bmatrix} 0 \\ 0 \\ 0 \\ 0.468 \\ 2.105 \\ 4.158 \end{bmatrix}$$

$$\mathbf{C} = \begin{bmatrix} 0.742 & -0.376 & 0.221 & 0 & 0 & 0 \\ 0 & 0 & 0 & 0.742 & -0.376 & 0.221 \\ 0.468 & 2.105 & 4.158 & & 0 & 0 \\ 0 & 0 & 0 & 0.468 & 2.105 & 4.158 \end{bmatrix}$$

E.2.5 Model for Payload: 12 kg, 2 Flexible Modes

A linear state-space model of the flexible link per (3.2.18) with state vector $\mathbf{x} = [\mathbf{q} \quad \dot{\mathbf{q}}]^T$ can be expressed as follows:

$$\dot{\mathbf{x}} = \mathbf{A}\mathbf{x} + \mathbf{B}\mathbf{u}$$

$$\mathbf{y} = \mathbf{C}\mathbf{x}$$

For a payload mass of $\mu = 12$ kg and two flexible modes included in the model, the state-space matrices have the following coefficients:

$$\mathbf{A} = \begin{bmatrix} 0 & 0 & 0 & 1 & 0 & 0 \\ 0 & 0 & 0 & 0 & 1 & 0 \\ 0 & 0 & 0 & 0 & 0 & 1 \\ 0 & 0 & 0 & 0 & 0 & 0 \\ 0 & -47.587 & 0 & 0 & 0 & 0 \\ 0 & 0 & -744.45 & 0 & 0 & 0 \end{bmatrix}$$

$$\mathbf{B} = \begin{bmatrix} 0 \\ 0 \\ 0 \\ 0.178 \\ 2.062 \\ 4.121 \end{bmatrix}$$

$$\mathbf{C} = \begin{bmatrix} 0.2820 & -0.0493 & 0.0252 & 0 & 0 & 0 \\ 0 & 0 & 0 & 0.2820 & -0.0493 & 0.0252 \\ 0.1776 & 2.0622 & 4.121 & & 0 & 0 \\ 0 & 0 & 0 & 0.1776 & 2.0622 & 4.121 \end{bmatrix}$$

E.2.6 Model for Payload: 120 kg, 2 Flexible Modes

A linear state-space model of the flexible link per (3.2.18) with state vector $\mathbf{x} = [\mathbf{q} \quad \dot{\mathbf{q}}]^T$ can be expressed as follows:

$$\dot{\mathbf{x}} = \mathbf{A}\mathbf{x} + \mathbf{B}\mathbf{u}$$

$$\mathbf{y} = \mathbf{C}\mathbf{x}$$

For a payload mass of $\mu = 120$ kg and two flexible modes included in the model, the state-space matrices have the following coefficients:

$$\mathbf{A} = \begin{bmatrix} 0 & 0 & 0 & 1 & 0 & 0 \\ 0 & 0 & 0 & 0 & 1 & 0 \\ 0 & 0 & 0 & 0 & 0 & 1 \\ 0 & 0 & 0 & 0 & 0 & 0 \\ 0 & -46.31 & 0 & 0 & 0 & 0 \\ 0 & 0 & -739.3 & 0 & 0 & 0 \end{bmatrix}$$

$$\mathbf{B} = \begin{bmatrix} 0 \\ 0 \\ 0 \\ 0.0574 \\ 2.0588 \\ 4.1172 \end{bmatrix}$$

$$\mathbf{C} = \begin{bmatrix} 0.09105 & -0.00509 & 0.00255 & 0 & 0 & 0 \\ 0 & 0 & 0 & 0.09105 & -0.00509 & 0.00255 \\ 0.05744 & 2.05876 & 4.11721 & & 0 & 0 \\ 0 & 0 & 0 & 0.05744 & 2.05876 & 4.11721 \end{bmatrix}$$

E.3 Parameters for Model-based Control

E.3.1 Model-based Control Design with one Flexible Mode

The design process for model-based control design is outlined in Section 4.3. The matrices listed below are defined by equations (4.3.1) – (4.3.14). The design for the flexible link based on one flexible mode uses the following parameters:

$$\mathbf{A}_M = \begin{bmatrix} 0 & 0 & 1 & 0 \\ 0 & 0 & 0 & 1 \\ 0 & 0 & 0 & 0 \\ 0 & -89.911 & 0 & 0 \end{bmatrix}, \qquad \mathbf{B}_M = \begin{bmatrix} 0 \\ 0 \\ 0.725 \\ 2.318 \end{bmatrix}$$

$$\mathbf{C}_M = \begin{bmatrix} 1.148 & -1.097 & 0 & 0 \\ 0 & 0 & 1.148 & -1.097 \end{bmatrix}$$

$$\mathbf{Q} = \begin{bmatrix} 5 & 0 & 0 & 0 \\ 0 & 5 & 0 & 0 \\ 0 & 0 & 5 & 0 \\ 0 & 0 & 0 & 5 \end{bmatrix}, \qquad \mathbf{R} = 1$$

$$\mathbf{V}_1 = \begin{bmatrix} 5 & 0 & 0 & 0 \\ 0 & 5 & 0 & 0 \\ 0 & 0 & 5 & 0 \\ 0 & 0 & 0 & 5 \end{bmatrix}, \qquad \mathbf{V}_2 = \begin{bmatrix} 1 & 0 \\ 0 & 1 \end{bmatrix}$$

$$\mathbf{F} = [2.236 \quad 5.274 \quad 3.465 \quad 2.179]$$

$$\mathbf{K} = \begin{bmatrix} 2.541 & 0.942 \\ -0.332 & 1.609 \\ 1.018 & 1.991 \\ 1.688 & -14.46 \end{bmatrix}$$

E.3.2 Model-based Control Design with two Flexible Modes

The design process for model-based control design is outlined in Section 4.3. The matrices listed below are defined by equations (4.3.1) – (4.3.14). The design for the flexible link based on two flexible modes uses the following parameters:

$$\mathbf{A}_M = \begin{bmatrix} 0 & 0 & 0 & 1 & 0 & 0 \\ 0 & 0 & 0 & 0 & 1 & 0 \\ 0 & 0 & 0 & 0 & 0 & 1 \\ 0 & 0 & 0 & 0 & 0 & 0 \\ 0 & -89.911 & 0 & 0 & 0 & 0 \\ 0 & 0 & -980.02 & 0 & 0 & 0 \end{bmatrix}, \quad \mathbf{B}_M = \begin{bmatrix} 0 \\ 0 \\ 0 \\ 0.725 \\ 2.318 \\ 4.358 \end{bmatrix}$$

$$\mathbf{C_M} = \begin{bmatrix} 1.148 & -1.097 & 0.909 & 0 & 0 & 0 \\ 0 & 0 & 0 & 1.148 & -1.097 & 0.909 \end{bmatrix}$$

$$\mathbf{Q} = \begin{bmatrix} 5 & 0 & 0 & 0 & 0 & 0 \\ 0 & 5 & 0 & 0 & 0 & 0 \\ 0 & 0 & 5 & 0 & 0 & 0 \\ 0 & 0 & 0 & 5 & 0 & 0 \\ 0 & 0 & 0 & 0 & 5 & 0 \\ 0 & 0 & 0 & 0 & 0 & 5 \end{bmatrix}, \quad \mathbf{R} = 1$$

$$\mathbf{V}_1 = \begin{bmatrix} 5 & 0 & 0 & 0 & 0 & 0 \\ 0 & 5 & 0 & 0 & 0 & 0 \\ 0 & 0 & 5 & 0 & 0 & 0 \\ 0 & 0 & 0 & 5 & 0 & 0 \\ 0 & 0 & 0 & 0 & 5 & 0 \\ 0 & 0 & 0 & 0 & 0 & 5 \end{bmatrix}, \quad \mathbf{V}_2 = \begin{bmatrix} 1 & 0 \\ 0 & 1 \end{bmatrix}$$

$$\mathbf{F} = [2.236 \quad 3.214 \quad 17.30 \quad 3.486 \quad 2.223 \quad 2.168]$$

$$\mathbf{K} = \begin{bmatrix} 2.566 & 1.128 \\ -0.548 & 0.682 \\ 0.0857 & -1.861 \\ 1.139 & 1.924 \\ 2.035 & -19.53 \\ -0.242 & 38.77 \end{bmatrix}$$

APPENDIX F: LIST OF SYMBOLS

Lowercase Symbols

a_i, b_i, c_i, d_i constants of general mode shape function for beam

$\mathbf{a}$ task space coordinate or trajectory

b feedback variable

$\mathbf{b}$ feedback signal vector

$\mathbf{c}$ vector function of Coriolis, centrifugal and damping forces

$\mathbf{d}$ disturbances

$\mathbf{e}$ error vector or disturbance vector

$\mathbf{f}$ force vector

f force

$\mathbf{g}$ system state propagation function

$\mathbf{h}$ system output function

i integer index

j $\sqrt{-1}$, or integer index

k index for discrete time, or integer index

$\mathbf{k}$ vector function of forces due to potential energy

ℓ length of flexible link

l number of system inputs and hyperstability sensors

m function associated with measurement process

$\mathbf{m}$ vector function associated with measurement process

n number of modes included in system

p order of stiffness operator of flexible system

$\mathbf{q}$ vector of generalized coordinates

q_i generalized coordinate

$\mathbf{r}$ general spatial coordinate vector

s Laplace operator/complex frequency

t time

u system input (scalar)

$\mathbf{u}$ system input vector

v physical motion coordinate

$\mathbf{v}$ vector of physical motion; local abbreviation used in App. B.

w commanded motion/set point

$\mathbf{w}$ vector of commanded motion

x spatial position coordinate

$\mathbf{x}$ state vector; in App. A: vector of sensor/actuator locations.

$\mathbf{y}$ system output vector or vector of hyperstability sensor outputs

$\bar{\mathbf{y}}$ vector of hyperstability sensor outputs with measurement errors

y system output or output of hyperstability sensor; in App. D: photo coordinate

z performance sensor output; in App. D: photo coordinate

$\mathbf{z}$ vector of performance sensor output; in App. A and C.2: state vector

$\mathfrak{z}^{-1}$ shift operator of $\mathfrak{z}$-transform

Upper Case Symbols

$\mathbf{A}$ system matrix

$\mathbf{B}$ system input matrix

$\mathcal{B}_j$ operator defining constraints on boundary of distributed parameter system

$\mathbf{C}$ system output matrix

$\mathcal{C}$ sensor fusion and control operator

$\mathbf{C}_0$ damping matrix of linearized system

$\mathbf{D}$ system throughput matrix

$\mathcal{D}$ domain of distributed parameter system

E energy

F scalar feedback gain/function

$\mathbf{F}$ feedback gain matrix; local definition in App. C.2

$\mathcal{F}$ function describing kinematic constraints

G transfer function (frequency domain)

J performance index

$\mathbf{J}$ Jacobian matrix

$\mathbf{K}$ stiffness matrix

$\mathcal{K}$ stiffness operator

L Lagrangian function

$\mathbf{L}$ matrix in Kalman-Yakubovich Lemma

$\mathbf{M}$ mass matrix; local definition in App. C.2

$\mathcal{M}$ mass operator

$\mathbf{N}$ matrix in Kalman-Yakubovich Lemma

P mechanical power

$\mathbf{P}$ solution of Riccati equation; local definition in App. D

$\mathbf{Q}$ state weighting matrix

$\mathbf{R}$ input weighting matrix

$\mathbf{S}$ solution of Lyapunov equation

$S(\cdot)$ polynomial

$\mathcal{S}$ system, system operator

T kinetic energy

$\mathbf{T}$ local definitions in App. B, C.2 and D

$\mathbf{U}$ matrix defined in equation (B.17)

$U_T(s) = \mathcal{L} < u_T(t) >$

V Lyapunov function

$\mathbf{V}$ covariance matrix

W mechanical work

$\mathbf{W}$ 'world' reference frame in App. D

$W(s) = \mathcal{L} < w(t) >$

$Y(s) = \mathcal{L} < y(t) >$

$Z(s) = \mathcal{L} < z(t) >$

X, Y, Z 'world' coordinates in App. D

Greek Symbols

$\left.\begin{matrix}\alpha \\ \beta_0 \\ \beta_1 \\ \gamma \\ \xi\end{matrix}\right\}$ constants used in definition of hyperstability

η integral relationship associated with hyperstable system

ε error parameter for hyperstability sensor

ϕ_i shape function of mode i

$\boldsymbol{\phi}$ vector of mode shape functions

κ stiffness distribution

λ_i eigenvalue

μ tip mass

ν function appearing in η

φ function appearing in η

ϑ_i coefficient in digital sensor fusion and control algorithm

χ_i coefficient in digital sensor fusion and control algorithm

ψ elastic deformation

ρ mass distribution

σ combined system output vector

ω natural frequency

τ time

τ_i lag time constant

$\boldsymbol{\Gamma}$ robot forward kinematics

θ joint angle

Λ binary fusion logic variable

ζ real function based on logic variable Λ

$\boldsymbol{\Omega}$ matrix of natural frequencies

Other Symbols and Notation

∂	partial derivative
$\delta < \cdot >$	variation of $< \cdot >$
δ_{ij}	Kronecker delta
$< \cdot >^{(j)}$	$= \frac{\partial^j < \cdot >}{\partial x^j}$, spatial derivative of $< \cdot >$
$\mathcal{L} < \cdot >$	Laplace transform of $< \cdot >$
$\mathcal{E}(\cdot)$	expectation of $(\cdot)$
$\mathrm{cov}(\cdot)$	covariance of $(\cdot)$
$\mathbf{0}$	zero matrix
$\mathbf{I}$	identity matrix
$\mathbb{R}$	set of real numbers
$\mathbb{C}$	set of complex numbers
$\Re\{\cdot\}$	real part
${}^A_B\mathbf{T}$	homogeneous transformation from frame A to frame B
$< \cdot >^T$	transpose of matrix or vector $< \cdot >$
$< \cdot >^\dagger$	generalized right inverse of $< \cdot >$
$\lfloor \cdot \rfloor$	floor function (rounding down to nearest integer)

REFERENCES

Alberts, T.E., Book, W.J. and Dickerson, S.L., Experiments in Augmenting Active Control of a Flexible Structure with Passive Damping, *Proceedings of the 1986 AIAA Aerospace Sciences Meeting*, Reno, NV, January 6-9, 1986.

Alberts, T.E., Xia, H. and Chen, Y., "Dynamic analysis to evaluate viscoelastic passive damping augmentation for the Space Shuttle Remote Manipulator Systems," *ASME J. Dyn. Syst., Meas., Control,* vol. 114, no. 3, pp. 468-475, Sept. 1992.

Anderson, B.D.O. [.1], "The small gain theorem, the passivity theory and their equivalence", *J. Franklin Inst.* 293 (2), 105-115, Feb. 1972.

Anderson, B.D.O. [.2], "A System Theory Criterion for Positive-Real Matrices," *SIAM Journal of Control*, vol. 5, pp. 171-183, 1967.

Astrom, K.H., and Wittenmark, B., "On Self-Turning Regulators", *Automatica*, vol. 9, pp. 185-198, 1973.

Bailey, T., Hubbard, J.E., "Distributed Piezoelectric-Polymer Active Vibration Control of a Cantilevered Beam," *AIAA J. Guidance, Control, Dynamics*, vol. 8, no. 5, pp. 605-611, 1985.

Balas M. J., "Direct velocity feedback control of large space structures," *AIAA J. Guidance, Control and Dynamics* 2, pp. 252-253, 1979.

Barker, D.S., and Jacquot, R.G., "Spillover Minimization in the Control of Self-Adjoint Distributed Parameter Systems," *Journal of Astronautical Sciences*, vol. 34, no. 2, pp. 358-384, 1986.

Baruh H., K. Choe, "Sensor placement in structural control", *AIAA J. Guidance and Control*, 13, 3, 1990.

Bassett, D.A., Wojcik, Z.A., Zaguli, R.J., Stieber, M.E., "Ground Based Control of Robots Aboard Space Station," *44th International Astronautical Congress*, Graz, Austria, October, 1993.

Bayo, E., "Computed torque for the position control of open-chain flexible robots," in *Proc. 1988 IEEE Int. Conf. Robotics Automat.*, Philadelphia, PA, pp. 316-321, Apr. 25-29, 1988.

Benhabib, R.J., Iwens, R.P., and Jackson, R.L., "Stability of Large Space Structure Control Systems Using Positivity Concepts," *AIAA Journal of Guidance and Control*, vol. 4, no. 5, pp. 487-494, 1981.

Book, W.J., Maizza-Neto, O., and Whitney, D.E.,"Feedback control of two beam, two joint systems with distributed flexibility," *ASME J. Dyn. Syst., Meas., Contr.*, vol. 97, no. 4, pp. 424-431, 1975.

Bretthauer, G. and Opitz, H.P., "Stability of Fuzzy Systems – A Survey," *Proc. EUFIT '94*, 1994

Cannon, R.H., Jr., and Schmitz, E., "Initial experiments on the end-point control of a flexible one-link robot," *Int. J. Robotics Research*, vol. 3, no. 3, pp. 62-75, 1984.

Carusone, J., and D'Eleuterio, G.M.T., "Tracking control for end-effector position and orientation of structurally flexible manipulators," *J. Robotic Systems*, vol. 10, no. 6, pp. 847-870, 1993.

Carusone, J., Buchan, K.S., and D'Eleuterio, G.M.T., "Results in End Effector Tracking Control for Structurally Flexible Space Manipulators", *IEEE Trans. Robotics and Automation*, vol. 9, no. 5, pp. 553-558, Oct. 1993.

Chen, W.H., and Seinfeld, J.H.,"Optimal locations for process measurements" *Int. J. Control*, 21, 6, pp.1003-1014, 1975.

Choe K., H. Baruh, "Actuator placement in structural control," *AIAA J. Guidance, Control and Dynamics*, 15, 1, 1992.

D'Eleuterio, G.M.T. [.1], "Dynamics of an elastic multibody chain: Part C - Recursive dynamics," *Dynamics and Stability of Systems*, vol. 7, no. 2, 1992.

D'Eleuterio, G.M.T. [.2], Multibody dynamics for space station manipulators: survey of selected formulations, *Dynacon Enterprises Ltd. Report SS-1*, 1985.

DeLorenzo M., "Sensor and actuator selection for large space structure control", *AIAA J. Guidance, Control and Dynamics*, 13, 2, 1990.

Desoer, C.A., and Vidyasagar, M., *Feedback Systems: Input-Output Properties*, Academic Press, New York, 1975.

Devasia S., T. Meressi, B. Paden, E. Bayo, "Piezoelectric actuator design for vibration suppression: placement and sizing", *AIAA J. Guidance, Control and Dynamics*, 16, 1, 1993.

Fu, K.S., Gonzales, R.C., and Lee, C.S.G., *Robotics: Control, Sensing, Vision and Intelligence*, McGraw-Hill, 1987.

Geromel, J.C. and Gapski, P.B., "Synthesis of Positive Real H_2 Controllers," *IEEE Trans Automatic Control*, vol. 42, no. 7, pp. 988-992, July 1997.

Gevarter, W.B., "Basic relations for the control of flexible vehicles", *AIAA Journal*, vol. 8, no. 4, pp. 666-672, 1970.

Goldenberg, A.A., and Rakhsha, F., "Feedforward control of a single-link flexible robot," *Mechanism and Machine Theory*, vol. 21, no. 4, pp. 325-335, 1986.

Goldstein, E., *Classical Mechanics*, Addison-Wesley, 1960.

Hahn, W., *Stability of Motion*, Springer Verlag, New York, 1967.

Hughes, P.C., and Sincarsin, G.B., "Dynamics of an elastic multibody chain: Part B–Global dynamics," *Dynamics and Stability of Systems*, vol. 4, no. 3, pp. 227-244, 1989.

Hughes, P.C., "Space structure vibration modes: How many exist? Which ones are important?," *IEEE Con. Sys. Mag.*, pp. 22-28, Feb. 1987.

Joshi, S.M., *Control of Large Flexible Space Structures*, vol. 131, Lecture Notes in Control and Information Sciences, Springer-Verlag, Berlin, 1989.

Joshi, S.M., Maghami, P.G., and Kelkar, A.G., "Design of Dynamic Dissipative Compensators for Flexible Space Structures," *IEEE Transactions on Aerospace and Electronic Systems* (to be published).

Juang, J.-N., Wu, S.-C., Phan, M., and Longman, R.W., "Passive Dynamic Controllers for Nonlinear Mechanical Systems," *Journal of Guidance, Control and Dynamics*, vol. 16, no. 5, pp. 845-851, 1993.

Juang, J.-N., and Rodriguez, G., "Formulation and Application of Large Structure Actuator and Sensor Placements", *Proc. Second VPI&SU/AIAA Symp. Dynamics Control Large Flexible Spacecraft*, pp 247-262, 1979.

Junkins, J.L., and Kim, Y., *Introduction to Dynamics and Control of Flexible Structures*, AIAA, 1993.

Kailath, T., *Linear Systems*, Prentice Hall, Englewood Cliffs, 1980.

Kelkar, A.G., Joshi, S.M., and Alberts, T.E.[.1], Dissipative Controllers for Nonlinear Multibody Flexible Space Systems, *J. Guidance, Control and Dynamics*, vol. 18, no. 5, pp. 1044-1052, Sept-Oct 1995.

Kelkar, A.G., Joshi, S.M., and Alberts, T.E.[.2], "Passivity-Based Control of Nonlinear Flexible Multibody Systems," *IEEE Transactions on Automatic Control*, vol. 40, no. 5, pp. 910-914, 1995.

Kim Y., J. Junkins, "Measure of controllability for actuator placement", *AIAA J. Guidance, Control and Dynamics*, 14, 5, 1991.

Kwakernaak, H., and Sivan, R., *Linear Optimal Control Systems*, New York: Wiley-Interscience, 1972.

de Lafontaine, J., and Stieber, M.E., "Sensor/Actuator Selection and Placement for the Control of Elastic Continua," *Proc. IFAC Symp. Control of Distributed Parameter Systems*, Pasadena, 1986.

Lanczos, C., *The Variational Principles of Mechanics*, University of Toronto Press, Toronto, 1964.

Landau, I.D., *Adaptive Control*, Marcel Dekker, New York, 1979.

Lasalle, J. and Lefschetz, S., *Stability by Lyapunov's Direct Method with Applications*, Academic Press, New York, NY, 1961.

Likins, P.W., Analytical dynamics and non-rigid spacecraft simulation, *JPL Technical Report 32-1593*, 1974.

Lim K., "Method for optimal actuator and sensor placement for large flexible structures", *AIAA J. Guidance, Control and Dynamics*, 15, 1, 1992.

Lim T., "Actuator / sensor placement for modal parameter identification of flexible structures", *Int. J. Analytical and Experimental Modal Analysis*, vol. 8, no. 1, pp. 1-13, 1993.

MacLean, S.G., Pinkney, H.F.L., "Machine Vision in Space," *Canadian Aeronautics and Space Journal*, vol. 39, no. 2, June 1993.

McLaren, M.D., and Slater, G.L., "Robust Multivariables Control of Large Space Structures Using Positivity," *Journal of Guidance Control, and Dynamics*, vol. 10, no. 4, pp. 393-400, 1987.

Magee, D.P. and Book, W.J., "The application of input shaping to a system with varying parameters," in *Proc. 1992 ASME Japan-USA Symp. Flexible Automat.*, vol. 1, San Francisco, CA, July 13-15, 1992, pp. 519-526.

Maghami P., S.M. Joshi, "Sensor/actuator placement for flexible space structures", *IEEE Trans. Aerosp. Electronic Sys.*, 29, 2, 1993.

Marin, J.P. and Titli, A.,."Comparative Analysis of Stability Methods for Fuzzy Controllers," *Proc. EUFIT '94*, 1994

Meirovitch, L., *Analytical Methods in Vibration*, Macmillan Co., 1967.

Moudgal, V.G., Passino, K.M. and Yurkovich, S., "Rule-Based Control for a Flexible-Link Robot", *IEEE Trans. Control Systems Technology*, vol. 2, no. 4, pp. 392-403, 1994.

Moore, B.C., "Principal Component Analysis in Linear Systems: Controllability, Observability, and Model Reduction," *IEEE Transactions on Automatic Control*, vol. AC-26, no. 1, pp. 17-32, 1981.

Narendra, K.S. and Annaswamy, A.M., *Stable Adaptive Stystems*, Prentice Hall, Englewood Cliffs, N.J., 1989.

Nemir, D., Koivo, A.J., and Kashyap, R.L., "Control of gripper position of a compliant link using strain gauge measurements", *Proc. 25th Conference on Decision and Control*, Athens, Greece, Dec. 1986.

Norris G.A., R. E. Skelton, "Selection of dynamic sensors and actuators in the control of linear systems", *Trans. ASME*, 111, 1989.

Opdenacker, P., Jonckheere E.A., "LQG Balancing and Reduced LQG Compensation of Symmetric Passive Systems", *Int. J. Control*, vol. 41, no. 1, pp.73-109, 1985.

Piedboef, J.C., "Symbolic Modelling of Flexible Manipulators", *Proc. AAS/AIAA Astrodynamics Specialist Conference*, Halifax, Canada, 1995.

Popov, V.M. [.1], "The Solution of a New Stability Problem for Controlled Systems," *Automatic and Remote Control*, 24, pp.1-23, 1963.

Popov, V.M. [.2], *Hyperstability of Control Systems*, Springer-Verlag, 1973.

Ravindran, R., Doetsch, K., "Design Aspects of the Shuttle Remote Manipulator Control," *Proc. AIAA Guidance and Control Conference*, 1982.

Sandberg, I.W., Some results on the theory of physical systems governed by nonlinear functional equations, *Bell Sys. Tech. J.* 44, 871-898, May-June 1965.

Sepulveda A., L. Schmit, "Optimal placement of sensors in control augmented structural optimization", *Int. J. Num. Meth. Engrg*, 32, pp 1165-1187, 1991.

Schulz, G., and Heimbold G., "Dislocated Actuator/Sensor Positioning and Feedback Design foe Flexible Structures," *Journal of Guidance, Control and Dynamics*, vol. 6, no. 5, pp. 361-367, 1983.

Siciliano, B., Yuan, B.S., and Book, W.J., "Model reference adaptive control of a one link flexible arm," in *Proc. 1986 IEEE Conf. Decision and Control*, vol. 1, Athens, Greece, pp. 91-95, 1986.

Sincarsin, G.B., and Hughes, P.C., "Dynamics of an elastic multibody chain: Part A–Body motion equations," *Dynamics and Stability of Systems*, vol. 4. no. 3, pp.209-226, 1989.

Sincarsin, G.B., D'Eleuterio, G.M.T., and Hughes, P.C., "Dynamics of an elastic multibody chain Part D – Modelling of Joints," *Dynamics and Stability of Systems*, vol. 8, no. 2, 1993.

Singer, N.C. and Seering, W.P., "Preshaping command inputs to reduce system vibration," *ASME J. Dyn. Syst., Meas., Contr.*, vol. 112, no. 1, pp. 76-82, 1990.

Skelton, R.E. and Hughes, P.C., "Modal Cost Analysis for Linear Matrix-Second-Order Systems," *Trans. ASME, Journal of Dynamic Systems, Measurement, and Control*, vol. 102, pp. 151-158, Sept. 1980.

Skelton, R.E. and Chiu, D., "Optimal Selection of Inputs and Outputs in linear stochastic systems," *J. Astronautical Sciences*, vol. 31, no. 3, pp. 399-414, July-Sept. 1983.

Spector, V.A., and Flashner, H., "Modelling and Design Implications of Noncollocated Control in Flexible Systems," *Trans. ASME, J. Dynamic Systems, Measurement and Control*, vol. 112, pp. 186-193, June 1990.

Stieber, M.E., Trudel, C., Hunter, D., "Robotic Systems for the International Space Station." *IEEE International Conference on Robotics and Automation*, Alburquerque, NM, 1997.

Stieber, M.E., Laurenzio, D.A., Fung, P.T.K., "Control Systems Architecture of the Mobile Servicing System," *Proc. 42nd Congress of the International Astronautical Federation*, Montreal, Canada, October 1991.

Stieber, M.E., "Sensors, Actuators, and Hyperstability of Structures," *Proc. AIAA Conf. Guidance and Control*, August 1988.

Stieber, M.E., E. Petriu, G. Vukovich [.1], "Systematic Design of Instrumentation Architecture for Control of Mechanical Systems," *IEEE Trans. Instrumentation and Measurement*, Vol 45, No. 6, April 1996.

Stieber, M.E., M. McKay, G. Vukovich, E. Petriu, "Vision-Based Sensing and Control for Space Robotics Applications," *Proc. IEEE Conf. Instrumentation and Measurement*, Brussels, June 1996. (Submitted to *IEEE Trans. Instrumentation and Measurement)*

Stieber, M.E., G. Vukovich, E. Petriu, "Stability Aspects of Vision-Based Control for Space Robots," *Proc. IEEE Int. Conf. Robotics and Automation,* Albuquerque, NM., 1997

Stieber, M.E., Petriu, E., Vukovich, G.[.2], "Instrumentation and Data Fusion Architecture for Systems Control," *IEEE Trans. Instrumentation and Measurement*, Vol 47, No. 4, August 1998.

SPAR-SS-TM-1049-D, MSC MDST/NRT Model Description Report - SSRMS Version D, Spar Aerospace Ltd., 1994.

Suarez, D.A. and Lozano, R., Adaptive Control of Nonmimumum Phase Systems Subject to Unknown Bounded Disturbances, *IEEE Trans. Automatic Control*, vol. 41, no. 12, pp. 1830-1836, December 1996.

Timoshenko, S., *Vibration Problems in Engineering*, Princeton, N.J. 1955.

Trudel, C.P., Hunter, D.G., and Stieber, M.E., "Control and Operation of Space Manipulator Systems," *NATO AGARD Lecture Series 193, Advanced Guidance and Control Aspects in Robotics*, 1993.

Turan, L., Safonov, M.G., and Huang, C.H., "Synthesis of Positive Real Feedback Systems: A simple Derivation via Parrott's Theorem," *IEEE Trans Automatic Control*, vol. 42, no. 8, pp 1154-1161, August 1997.

Yang S. , Lee, Y., "Optimization of non-collocated sensor/actuator location and feedback gain in control systems", *Smart Mater. Struct.*, 2, 1993.

Wu, Y.W., Rice, R.B., and Juang, J.-N., "Sensor and Actuator Placement for Large Flexible Space Structures," *Proc. J. Automatic Control Conf.*, Denver, CO, pp. 230-238, 1979.

Zames, G., On the input-output stability of nonlinear time-varying feedback systems, Pt. I and II, *IEEE Trans. Automat. Contr.* AC-11 (2), 228-238, Apr. 1966 and (3), 465-477, July 1966.

Zuo, K. and Wang, D., "Closed loop shaped-input control of a class of manipulators with a single flexible link," in *Proc. 1992 IEEE Int. Conf. Robotics Automat.*, vol. 1, Nice, France, May 12- 14, pp. 782-787, 1992.

IMAGE EVALUATION
TEST TARGET (QA–3)

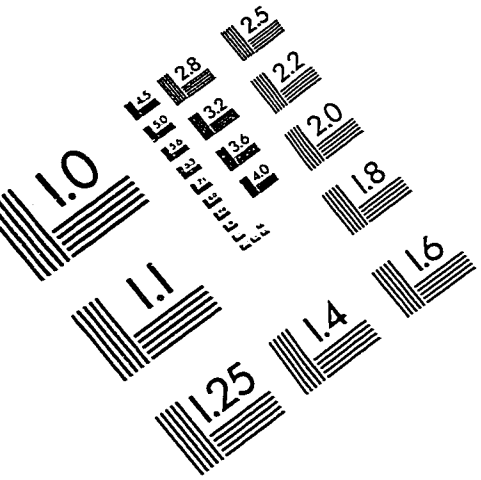

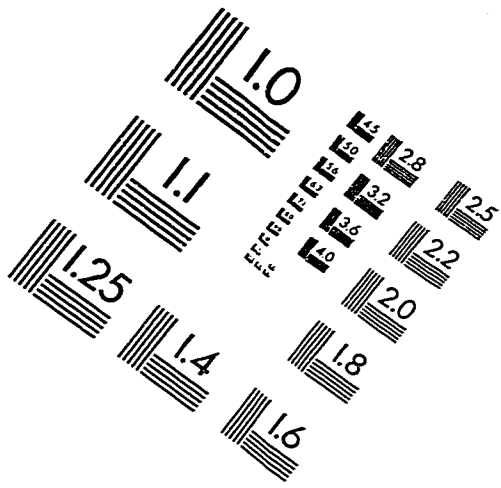

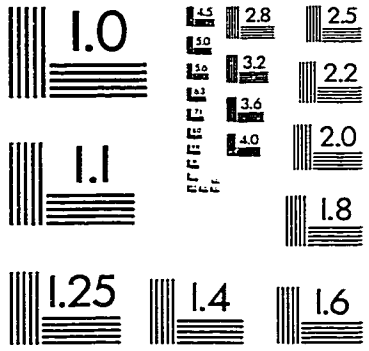

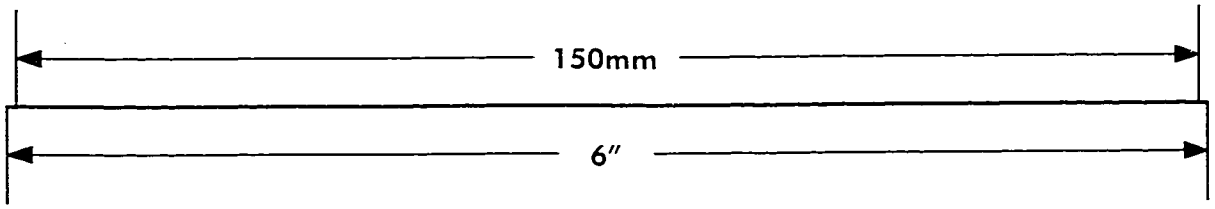

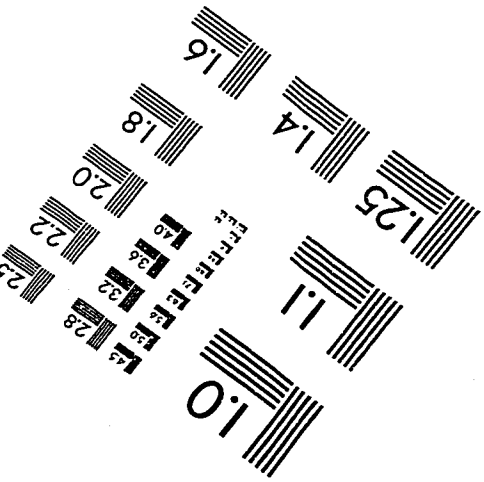

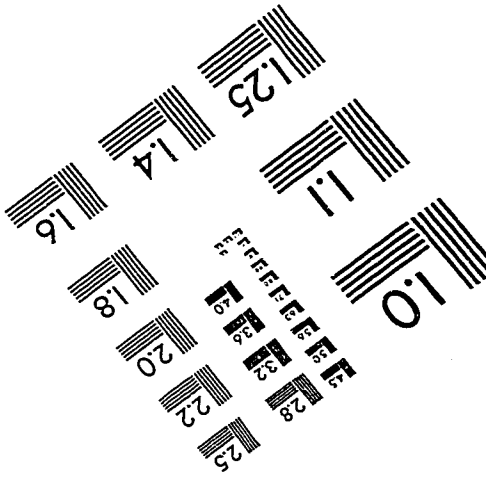

APPLIED IMAGE, Inc
1653 East Main Street
Rochester, NY 14609 USA
Phone: 716/482-0300
Fax: 716/288-5989